Sustainable Glider Tow Craft

Final Report
Design of MARCUS-T
Group 08

Delivery Date: Wednesday 26th June, 2024

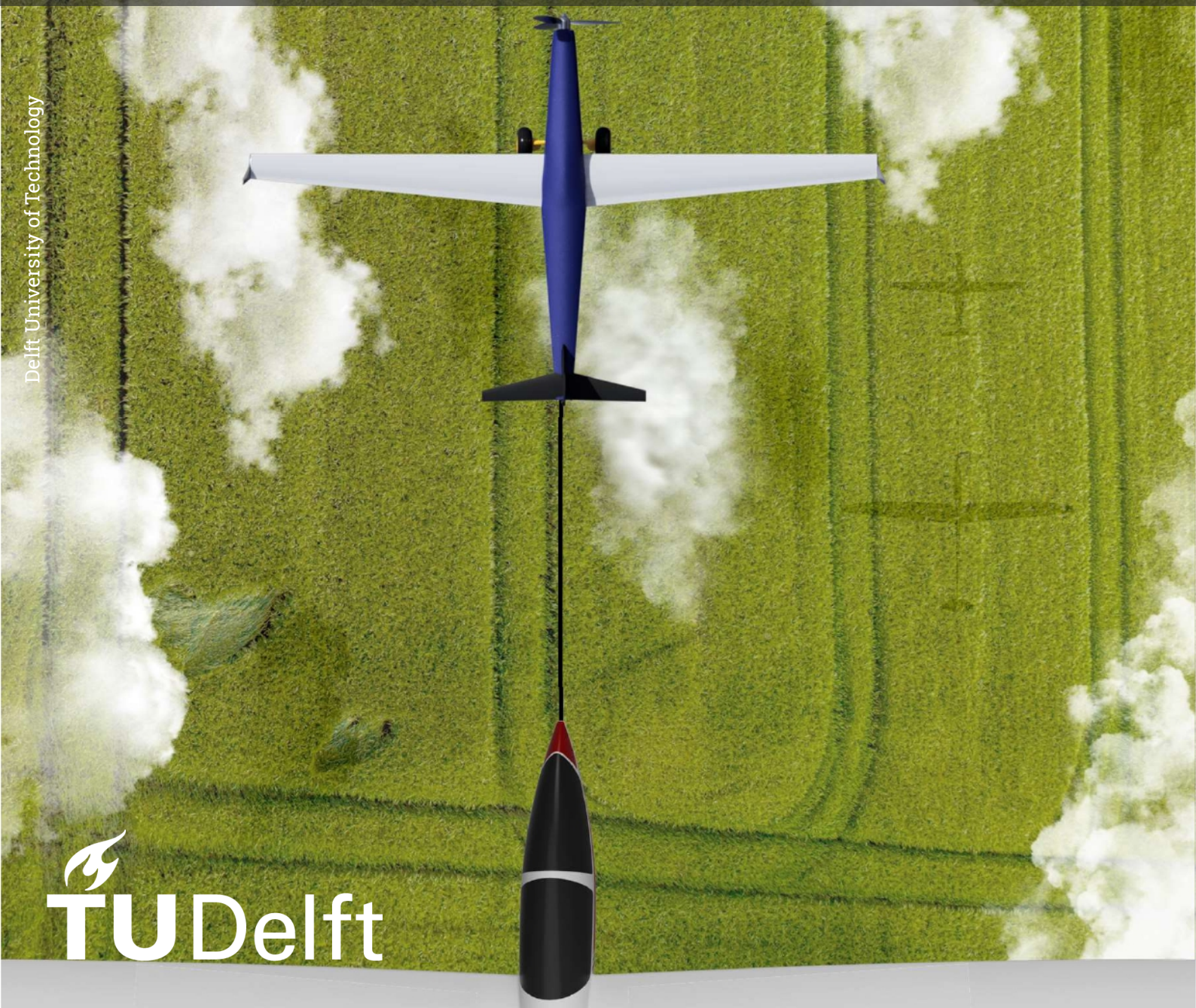

Delft University of Technology

TU Delft

[This page intentionally left blank]

Sustainable Glider Tow Craft

Final Report
Design of MARCUS-T
Group 08

by

Student Name	Student Number
Andreas Van Acker	5205107
Annika Plaggenborg	5073944
Christian Grunwald	5037662
Filip Nowosielski	5452406
Gerard Mendoza Ferrandis	5531357
Mees Werners	5048451
MianTao Zhao	5536650
Niels van Nieuwland	5283183
Stan Etman	5579996
Tamara van Santen	5490359

Delivery Date – Wednesday 26th June, 2024

Version Control

Version	Date	Author(s)	Description
1.0	19/06/2024	Everyone	First Draft
1.1	25/06/2024	Everyone	Final Report

Tutor: Ir. J.A. (Joris) Melkert
Coaches: Ir. J.S. (Josephine) Pockelé & Ir. M.R. (Maria Rosaria) Acquaviva
Date: Wednesday 26th June, 2024
Program: Aerospace Engineering
Course: Design Synthesis Exercise

TU Delft

Acknowledgement

We, Group 08, would like to express our sincere gratitude to the many experts, coaches, assistants, and peers who aided us in the process of creating this report, and supported us throughout the entirety of the Design Synthesis Exercise. We are deeply indebted to Ir. J.A. (Joris Antonius) Melkert, who is not only responsible for the exercise as a whole, but also our tutor. As our tutor his insight, experience, and knowledge were invaluable contributions to the report, we would like to thank him for his patience, feedback, and willingness to take time out of his busy schedule to assist and answer our many questions. We would also like to extend special thanks to our coaches Ir. J.S. (Josephine Siebert) Pockelé and Ir. M.R. (Maria Rosaria) Acquaviva. Their guidance and feedback was indispensable and much appreciated. A special thanks goes out to Marcus Basien, our 'client', for concieving the idea of autonomous glider tow craft. We are very grateful to Ir. Loek M. M. Boermans for his advice on aerodynamic aspects of the tow craft and providing us with his DU15-160/15 airfoil. We are also thankful for the organisation of the Dutch National Gliding Championships and Terlet Airfield for welcoming us to the national championships and presenting us with valuable insights into the sport, with special thanks to the various pilots who let us interview them. Additional thanks go out to the teaching assistants, staff of the Fellowship, and our fellow students who proofread our reports.

Executive Overview & Project Objective

by Annika, Everyone

Despite the increasing awareness of climate change and unpowered nature of the sport, sustainability has not traditionally been a major influence on gliding and has not been thoroughly explored. A significant contribution of the emissions affecting climate change stems from aviation and the industry is only expected to continue growing. The necessity of designing a sustainable glider tow craft is thus indisputable, and as such, the objective of this report is as follows.

Design a craft capable of towing a glider sustainably, minimising the environmental impact of the gliding sport.

The Motorised Automatic Return Craft Used for Sustainable Towing (*MARCUS-T*) is designed to fulfil this objective. Prior to this report, an initial set of design options fitting the mission profile were compiled. Eventually, this lead to a trade-off with the winning design looking much like the typical single-engined turboprop aircraft used for aerotow. However, *MARCUS-T* will be an electric and automatic aircraft, the latter explaining the lack of a pilot's cabin. The steps required to now reach a substantially preliminary design are outlined in this report, and as such, are summarised hereafter.

Mission Profile Structure

MARCUS-T is designed to operate in complex environments, exemplified by its operations at Hilversum Airport. As such, it necessitates a detailed description of the flight phases and operational scenarios.

Initially, three distinct taxiing profiles are described, namely the deployment taxi, taxi in, taxi out, and storage taxi. The take-off phase involves accelerating the tow craft to a lift-off speed and transitioning into a climb angle, ensuring a smooth ascent with the glider in tow. The climb phase is divided into two segments in order to reach 1,000 m in altitude. In the meantime, it avoids the circuit area as much as possible while towing the glider to its training area.

The descent phase offers four profiles: a steady descent, a dive, an unpowered glide, and a steep dive. Each profile is designed to return the tow craft to the circuit entry point while adhering to altitude restrictions and avoiding airfield activity zones. The mission profile also includes a circuit and go-around procedure. The landing phase completes the mission, following a precise approach, flare, and ground roll sequence to bring the craft to a stop.

Requirements

Previously, the requirements of stakeholders for *MARCUS-T* were set up, as well as those of the subsystems in the craft. Additionally, requirements flowing from CS-22 and CS-23 are also included. To ensure each requirement is accounted for, each department receives (a) requirement(s) relevant to their department. The departments are defined as "Structures, Materials, and Manufacturing", "Aerodynamics", "Software, Stability, and Control", "Power, Performance, and Propulsion", and "Airfield Performance, Operations, and Logistics". Each department holds their own responsibilities aside from the requirements they must fulfil. It is of high importance to have a good understanding of the interdependencies between the different departments to ensure a well-rounded design is reached in the end.

Design Methodology and Synthesis

With the responsibilities of each department known, their subsystem designs and design synthesis can be performed. This will be done by first describing the methodology used and thereafter the results that were obtained from this.

Structures, Materials, and Manufacturing

The Structures, Materials, and Manufacturing department (SMM) is responsible for calculating a Class II weight estimate of the craft. This estimate includes calculating the weight of all subsystems of the craft and determining the centre of gravity location. The subsystem masses are calculated using a variety of methods, mainly the USAF methods described by Roskam, the general aviation methods described by Raymer, and selecting sample components. The mass of the wing specifically is determined through a structural analysis which calculates the required geometry, material, and mass of the wing.

After the iterations, SMM also investigates and designs the fuselage and landing gear components, considering a variety of materials. The main results of the iterations for SMM are given in Table 1.

Table 1: Masses of the most noteworthy components.

Masses	Value	Unit
Maximum take-off mass	210	kg
Battery mass	43	kg
Fuselage mass	13	kg

Using these results, the wing, fuselage, and landing gear are designed. The material chosen for the fuselage frame and wing is Al6061-T6, and the material chosen for the landing gear structure is Al7075-T6. The wing, fuselage, and landing gear designs need further analysis to optimise their shape, material, and mass. The preliminary shape of the fuselage can be seen in Figure 1.

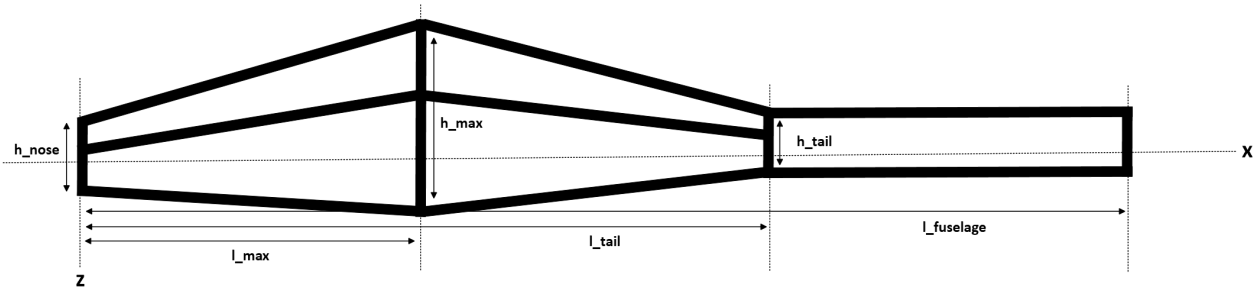

Figure 1: Fuselage side view.

Aerodynamics

The aerodynamic analysis of available airfoils lead to selection of the DU15-160/15 airfoil. Recommendations by Ir. Boermans suggest optimal flap hinge placement at 85% of the chord and the use of Mylar tape to seal gaps for enhanced efficiency. Pressure distributions on the wing at flap deflections of 0° and 20° indicate the transition from laminar to turbulent flow, guiding the placement of turbulator tape. Performance metrics such as the lift coefficient (C_l), lift-to-drag ratio ($\frac{C_L}{C_d}$), and pitching moment (C_m) vary significantly with flap settings (respectively at 0°, 20°, and 60°). Integration of high-lift devices (HLD) aims to improve lift and drag coefficients during critical flight phases. A drag estimation then outlines components contributing to total drag (C_D), including wing, fuselage, empennage, and flap drag coefficients. The addition of winglets for efficiency enhancement during climb phases is also explored. Furthermore, after a lift and drag analysis the craft is chosen to have airbrakes, in order to reduce its speed during a dive. Overall, the aerodynamic design aims to optimise performance during the climb phase, as this is the longest and most critical phase of the flight.

The design iteration lead to the planform design presented on Figure 2, along with the most important parameters.

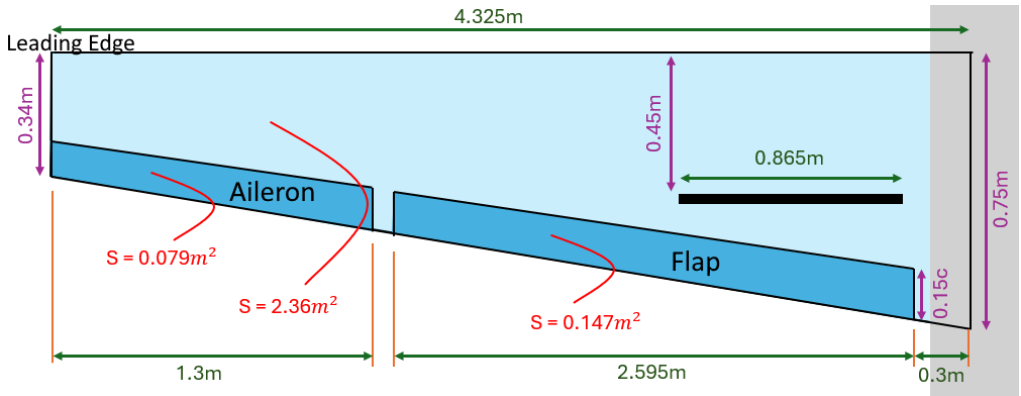

Figure 2: Wing planform.

Software, Stability, and Control

The Software, Stability, and Control department (SSC) is responsible for sizing the horizontal and vertical tailplane. This sizing takes into account longitudinal and lateral stability, along with the controllability of the craft. Additional forces due to towing are also taken into account in this sizing. The wing of the craft is positioned during this process, as this allows the surface area of the horizontal tailplane to be minimised.

Once the tailplane sizing and wing positioning are integrated with all other departments, a preliminary dynamic stability analysis is performed in which the eigenmotions of the craft are determined. This analysis is done for the craft both while attached to, and detached from the glider. Lastly, a preliminary sizing of control surfaces is also performed.

Airfield Performance

The Airfield Performance, Operations, and Logistics department is responsible for calculations surrounding the airfield performance of *MARCUS-T*. This includes taxi, take-off, and landing, the first two of which partially determine the battery mass. The taxi energy is calculated with an estimated weight and used as fixed value. Some values, like for instance the stall speed and lift-off speed, are also relevant and are based off of the Arcus-T. Calculations for the minimum thrust needed in order to meet the required maximum take-off distance of 500 m are then made and put into the final iteration loop. This is done to size the battery mass specifically for this thrust. The take-off distance is calculated for different values for the thrust using equations from Raymer. The minimum thrust giving a value for the take-off distance lower than 475 m is taken as limiting case and is used to calculate the battery mass needed. After the iteration loop, the landing distance is calculated, again using Raymer. A sanity check is done to ensure the distance was viable for normal runways. The results and important velocities are shown in Table 2.

Table 2: Airfield performance parameters of *MARCUS-T*.

Parameter	Value	Unit	Parameter	Value	Unit
Take-off velocity	30.6	m/s	Take-off thrust	2585	N
Climb velocity	36.1	m/s	Take-off distance	472	m
Clean stall velocity	20	m/s	Take-off time	45	s
Taxi energy	84	Wh	Taxi distance	1450	m
Stall velocity when landing	17.6	m/s	Landing distance	426	m

Power, Performance, & Propulsion

Based on the mission profile, a set of flight phases and legs are compiled to simplify calculations. The final mission is split up as follows: 1. Taxi, 2. Take-off, 3. Initial Climb (Climb 1), 4. Climb-Out (Climb 2), 5. Turning at 1,000 m, 6. Descent A, B, C, or D, 7. Circuit at 200 m, 8. Turning at 200 m, 9. Approach, 10. Landing, and lastly 11. Taxi. In the case of a go-around a go-around climb, circuit at 200 m, turning at 200 m, and approach are added before landing and taxi.

The in- and outputs are linked by several functions and methods. The battery mass is based on two calculation methods: First, the battery mass fraction method as proposed by Raymer is applied. Apart from that a ”power times time”-method is applied. This is based on calculating the power required for a certain leg and multiplying that power by the time of that leg. This yields a total energy required for the whole mission. Together with an energy density, the battery mass can be calculated. It is opted for the higher of the two values to be conservative. Onto the actual battery mass a reserve of two go-arounds is added. The maximum power is calculated by looking at the maximum of the required take-off power and the climb power. The take-off power is calculated using the disk actuator theory from the thrust needed for take-off. The climb power is calculated taking into account the climb rate, the drag and the weight of the tandem. The propeller is sized by a statistical relationship given by Raymer. As electric motors have the ability of also functioning as generator, energy recuperation during descent is also considered. An initial approach to calculating the order of magnitude is laid out. Lastly, as noise is directly related to the propeller and motor, also the noise level will be calculated.

Performing the iterations and combining the propulsion department with the other departments the final values for the preliminary design are obtained and are given as follows:

Table 3: Power and propulsion values.

Parameter	Value	Unit	Parameter	Value	Unit
Battery mass	43	kg	Max. Power required	62	kW
Max. climb power required	34	kW	Propeller efficiency	0.8	-
Battery efficiency	0.9	-	Battery-to shaft efficiency	0.8	-
Nominal mission energy	26	MJ	Total energy provided	36	MJ
Number of motors	1	-	Propeller diameter	1.54	m
Energy recuperated	6200	J	Power recuperated	63	W

Apart from that, several design choices are made. First, the battery type is chosen. It is strived to have the highest specific energy, i.e. the amount of energy a battery can store per kilogram. Yet, the battery type also has to be suited for airplane applications. Lithium-ion batteries are considered to be the most well-suited ones, as they offer a good energy density, have a reasonable long lifetime and are already used in aerospace applications. Under the Lithium-ion batteries, it is chosen to use Lithium-polymer batteries, which have the best performance of all Lithium-ion batteries for the design's considerations. Considering the number of motors, meaning the motor and propeller as a unit, it is argued that one motor is enough if a motor which is powerful enough can be found. An off-the-shelf motor is found, which fulfils the maximum power requirements as well as the continuous climb power requirement as listed in Table 3. The motor that is selected is the Rotex Electric REB 90, which provides a maximum power of 80kW and a continuous power of 60-70kW. For the selection of the propeller, it turns out that the propeller diameter is required to be 1.54 m, considering three blades are chosen for. This by itself offers already more ground clearance. However, a final design choice is not yet made. For the noise requirement, the noise of 93.5 dB is computed at a distance of 50 m during take-off.

MARCUS-T Description

After integration of the various systems a three-view of *MARCUS-T* was created. The result is shown in Figure 3.

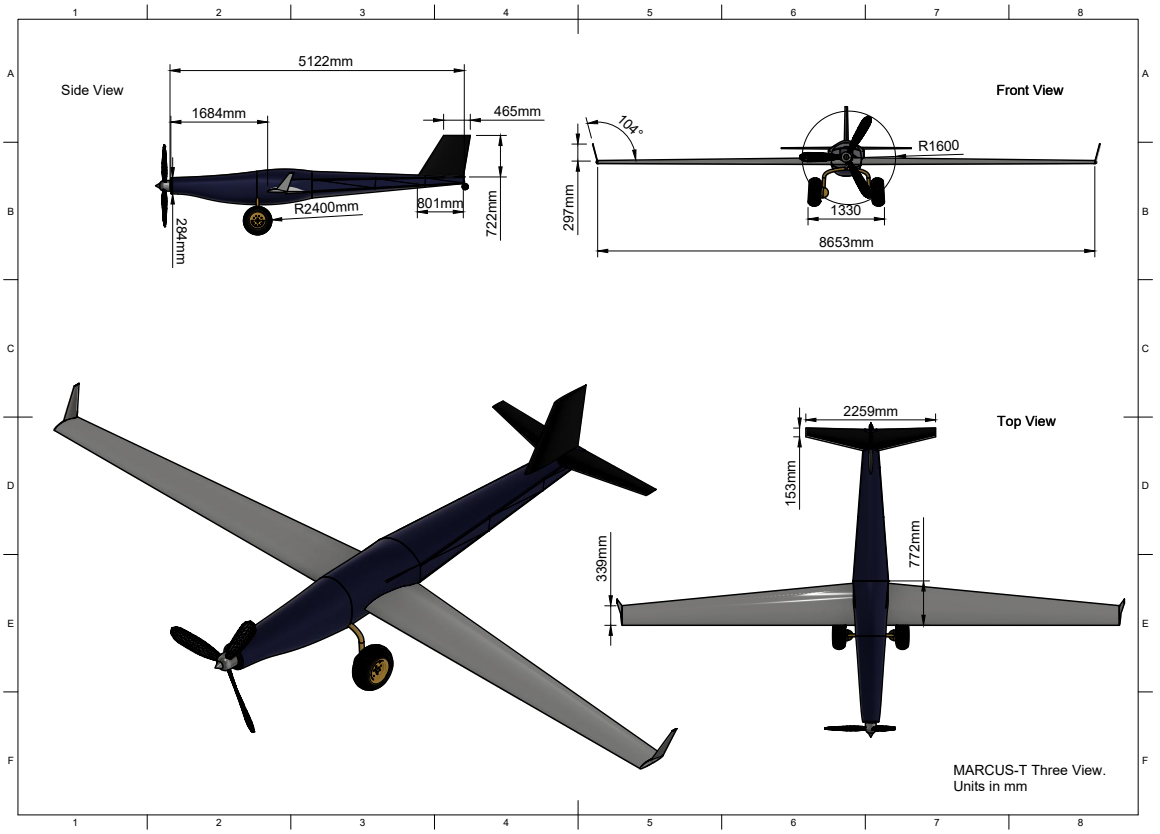

Figure 3: Three-view of *MARCUS-T*.

Logistics and Operations

The logistics and operations give an outline of the framework for operating and supporting *MARCUS-T*. Airfield logistics specifically describe the systems that are required to support *MARCUS-T* , including a battery charging system to ensure the availability of *MARCUS-T* on a day of flying. During a mission, the craft uses approximately 7,100 W·h (65% of its battery capacity) in 15 minutes time, necessitating three battery sets that will be charged throughout the day. In order to charge the battery system and *MARCUS-T* overnight, a new electrical infrastructure is laid out in the hangar. A control station integrated into existing gliding club trucks allows a licensed UAV pilot to monitor and control *MARCUS-T* and its systems remotely. Regular inspections ensure airworthiness, covering checks on the fuselage, landing gear, wings, control systems, and electrical systems, with more extensive inspections conducted periodically.

The ground operations include steps from removing the glider from the hangar, to battery swapping and pre-launch preparations. The latter ensure that all systems are checked and that the craft is ready for towing. Flight operations describe towing procedures in the air. Finally, procedures for emergencies are briefly described. This comprehensive approach establishes a baseline for the safe and efficient operation of *MARCUS-T*.

System Description and Risk Analysis

MARCUS-T has nine principal systems: the Flight Management System (FMS), Integrated Surveillance System (ISS), Electric Power System (EPS), Power Provision System (PPS), Flight Navigation System (FNS), Glider Coupling System (GCS), Radio Transmission System (RTS), Emergency Descent System (EDS), and the Aerodynamics and Structural System (ASS). ASS contains two subsystems, namely the Structural Health Monitoring System (SHMS) and the Flight Control System (FCS).

The FMS will act as the decision-making system of *MARCUS-T*. These decisions will be mainly informed by the ISS, FNS, GCS, RTS, and SHMS systems. The provision of power to the systems will be the responsibility of the PPS, and the propulsion will be provided by the EPS. The FCS will perform the control of the craft. In case of loss of control or similar emergencies, the EDS will activate.

The decision to have these systems stems both from requirements and risk analyses. Two risk analyses were performed, first a Specific Operations Risk Analysis (SORA), and second a Technical Risk Analysis (TRA). Through the SORA, the ground and airborne collision risks were minimised in order to comply with EU regulations on unmanned aerial systems. A Failure Mode Effect Criticality Analysis (FMECA) is used to assess the TRA. All risks are minimised to an acceptable level where they do not require constant monitoring.

Finally, a Reliability, Availability, Maintainability, and Safety (RAMS) analysis, informed by the TRA, concludes that the craft is safe, and has a reliability score of 99.8%, maintainability score of 100.0%, and availability score of 97.7%.

Market Analysis

The market analysis starts off with an overview of the tow craft market. Out of the 27 tow craft assumed to be purchased each year across Europe, a market share of 30% is assumed to be realistic. This results in an estimated 8 tow craft sold each year. The prediction of costs highly depends on the aircraft manufactured within the first five years of production. With 40 tow craft produced in the first five years, the total cost to produce a tow craft would reach EUR 437,669.51. With a 10% profit margin, the craft should be sold at EUR 558,029. As this conflicts with the requirement of the craft being sold at EUR 310,000, no return of investment can be expected by merely considering the purchase price. The total lifetime cost, however, is only at EUR 912,210, calculated assuming 30 years of operation where 700 flights are performed each year. The total cost per tow is EUR 29.01. This could make *MARCUS-T* an attractive choice for glider clubs, though the initial investment of EUR 310,000 is quite high. For the manufacturer, the lower lifetime cost allows for a higher selling price of EUR 496,870. This is similar to the highest lifetime cost encountered during previous market analyses. Considering this updated selling price of EUR 496,870, the break-even point would be achieved after selling the 49^{th} aircraft. Assuming linear selling behaviour during the first five years, the break-even point is therefore encountered after roughly 6.13 years. Future developments like the reduction in electricity prices and an increase in fuel prices for conventional tow craft could improve the financial performance of *MARCUS-T* even more. The development of new batteries in the future could also lead to an improvement of financial performance.

Future Outlook

With the design of *MARCUS-T* specified, the future outlook on the design can be described. This includes a post-DSE planning, manufacturing plan, and sustainability of *MARCUS-T*.

Post-DSE Planning

A plan is setup for the continued development of *MARCUS-T*. This process is divided into five stages, the design, certification, manufacturing, delivery, and operation phases. In addition to the development planning, a manufacturing assebly and integration (MAI) plan is developed along with a production philosphy designed to deliver 50 aircraft over 5 years. For maintenance and battery swapping, considerations must be made for hatches or disassembling opportunities. Specifically, for battery swapping, two hatches are required behind the trailing edge of the wing on either side of the fuselage to facilitate quick access and replacement. The structured and phased approach in the MAI plan ensures that the manufacturing process is efficient, with a focus on quality and adaptability to market demands, ultimately supporting the sustainable development of the *MARCUS-T* glider tow craft

Sustainability

During the design of *MARCUS-T* , there are multiple aspects of sustainability considered. As the goal of creating the craft was to make a sustainable glider tow craft. The carbon dioxide of *MARCUS-T* during operation is also compared to a current tow craft and a fuel power small automatic tow craft, to make sure the impact of *MARCUS-T* is smaller. *MARCUS-T* is more economically sustainable, because 70% of repairs can be performed locally, also 70% of the parts of *MARCUS-T* can be replaced. *MARCUS-T* is more social sustainable because having a UAV towing the glider is more safe for the tow pilot. Lastly for environmental sustainability, creating a UAV makes *MARCUS-T* much lighter so less energy is needed to get the craft into the air which produces fewer emissions. Because *MARCUS-T* is electrical it gives the opportunity to use green energy and the lithium polymer batteries used have a lower environmental impact than other batteries. The other materials used for *MARCUS-T* are aluminium 6061-T6 and ceconite which are recyclable and easy to repair.

Contents

Nomenclature

Abbreviations & Acronyms

ACAS	Airborne Collision and Avoidance System
ADR	Annex to Delegated Regulation (EU) 2019/945
ADS-B	Automatic Dependent Surveillance Broadcast
AERO	Aerodynamics
AFA	AI Flight Assistant
AI	Artificial Intelligence
AIP	Aeronautical Information Package
AIR	Annex to Implementing Regulation (EU) 2019/947
AMC	Acceptable Means of Compliance
AMSL	Above Mean Sea Level
AO	Airfield Operations
AoA	Angle of Attack
APDC	Attitude and Position Determination Computer
APOL	Airfield Performance, Operations, and Logistics
AR	Aspect Ratio
ARC	Air Risk Classification
ASS	Aerodynamic and Structural System
AT	Authorities
ATC	Air Traffic Control
ATSAW	Airborne Traffic Situational Awareness
BMF	Battery Mass Fraction
BP	Ballistic Parachute
BPDS	Ballistic Parachute Deployment System
BT	Battery
CAD	Computer-Aided Design
CAT	Catastrophic
CC	Cross Checking
CG	Centre of Gravity
CLT	Client
COM	Communication System
COTS	Components of the Shelf
CRDR	Cover Regulation to Delegated Regulation (EU) 2019/945
CRIR	Cover Regulation to Implementing Regulation (EU) 2019/947
CS	Computer, Probe, Sensor, and Antenna
CS-22	Certification Specifications Sailplanes and Powered Sailplanes
CST	Cost
CT	Motor and Propeller Controller
CV	Coefficent Variation
DAL	Development Assurance Level
Dep	Department
DMA	Data Management Application
DMS	Data Management System
DSE	Design Synthesis Exercise
eAIP	Electronic Aeronautical Information Package
EASA	European Aviation Safety Agency
EDS	Emergency Descent System
EHHV	Hilversum Airport
EM	Electric Motor
EOL	End Of Life
EOP	Emergency Operating Procedure
EPS	Electric Propulsion System
FAA	Federal Aviation Administration
FCA	Flight Control Application
FCS	Flight Control System
FDAU	Flight Data Acquisition Unit
FDRBNU	Flight Data Recorder and Backup Navigational Unit
FGA	Flight Guidance Application
FILIP	Feature Identification and Language Interpretation Platform
FMA	Flight Management Application
FMC	Flight Management Computer
FMEA	Failure Mode Effect Analysis
FMS	Flight Management System
FNS	Flight Navigation System
FPLS	Functional and Positional Lighting System
GAT	Ground Arresting System
GC	Glider Clubs
GCS	Glider Coupling System
GDC	Guidance System
GHS	Ground Handling System
GM	Guidance Material
GP	Glider Pilot
GRC	Ground Risk Classification

HAZ	Hazardous
HC	Hand Calculations
HLD	High-Lift Devices
HTP	Horizontal Tailplane
ILT	Inspectie Leefomgeving en Transport
IMU	Inertial Measurement Unit
ISA	International Standard Atmosphere
ISS	Integrated Surveillance System
L	Likely
L/G	Landing Gear
LCN	Logistics Control Number
LG	Landing Gear
LiPo	Lithium-Polymer
LOF	Lift-Off
LR	Local Residents
LT	Lights
LVNL	Luchtverkeersleiding Nederland
M	Medium
MAC	Mean Aerodynamic Chord
MAI	Manufacturing, Assembly, and Integration
MAJ	Major
ME	Main Wing and Empenage
MF	Manufacturers
MIN	Minor
MTBF	Mean Time between Failures
MTOM	Maximum Take-Off Mass
MTOW	Maxium Take-Off Weight
MTTR	Mean Time to Repair
NAV	Navigation System
NP	Neutral Point
NSE	No Safety Effect
OP	Operational Personnel
OPS	Operations
OSO	Operational Safety Objectives
PDCU	Power Distribution and Control Unit
PPP	Power, Performance and Propulsion
PPS	Power Provision System
PR	Propeller
PRO	Propulsion System
PWR	Power System
RAMS	Reliability, Availability, Maintainability, and Safety
REG	Regulation
ROC	Rate of Climb
RPM	Rounds per Minute
RTS	Radio Transmission System
SAIL	Specific Assurance Integrity Level
SBIS	Structural Break-up Indication Sensor
SHMS	Structural Health Monitoring System
SMM	Structures, Materials, and Manufacturing
SOP	Standard Operating Procedure
SPL	Sound Pressure Level
SSC	Software, Stability, and Control
STK	Stakeholder
STR	Structural System
SUS	Sustainability
SYS	System
TAS	True Airspeed
TAWS	Terrain Alert and Warning System
TEC	Technical
TF	Transformer and PDCU
TH	Tail Hook
TMS	Tension Monitoring System
TO	Take-Off
TRA	Technical Risk Assessment
U	Unlikely
UA	Unmanned Aircraft
UAS	Unmanned Aerial System
UAV	Unmanned Aerial Vehicle
USP	Unique Selling Point
UTM	Unmanned Traffic Management
VFR	Visual Flight Rules
VFR-RT	Visual Flight Rules - Radio Telephony
VI	Visual Inspection
VL	Very Likely
VTP	Vertical Tail Plane
VU	Very Unlikely

1

Introduction

by Annika

Gliders were the first heavier-than-air aircraft capable of transporting people. Since then, gliding has significantly taken off in popularity. Typically, the operations of the gliding sport include a glider being launched into the air via winch or aerotow. Due to important considerations such as the drop-off location and altitude, an aerotow tends to be preferred over a winch. Additionally, despite the increasing awareness of climate change and unpowered nature of the sport, sustainability has not traditionally been a major influence on gliding and has not been thoroughly explored. Aviation is a significant contributor, its emissions estimated to account for approximately 5 % of human-induced global warming [1]. Due to the expected continued growth of the industry, the necessity of designing a sustainable glider tow craft is indisputable.

The aim of this report is to design a craft capable of towing a glider sustainably, minimising the environmental impact of the gliding sport. The Motorised Automatic Return Craft Used for Sustainable Towing (*MARCUS-T*) is designed to fulfil this objective by employing an electric propulsion system and hot-swappable batteries. Furthermore, its mission entails receiving a drop-off location and altitude from the glider pilot after which the glider is released and the craft automatically flies back to base. *MARCUS-T* is designed to tow the heaviest gliders regulations will allow, at a maximum take-off mass of the glider of 850 kg. Naturally, the cost of the craft is a driving design requirement to ensure an average gliding club may afford at least one *MARCUS-T*.

In order for the design of *MARCUS-T* to flourish, an extensive design process was initiated, starting off with an exhaustive list of preliminary analyses. This included an initial sustainability development strategy, budget breakdown, and technical risk assessment [2]. Subsequently, a set of design options that fit the mission profile could be compiled, eventually leading to a handful of leftover options [3]. With these, a trade-off was performed, and at last, the winning design was selected.

The steps required to reach a finalised design are outlined in this report. Starting off, Chapter 2 covers a discussion with the client on the previously selected design, as well as any relevant aspects of the mission profile of *MARCUS-T*. Further requirements it must meet are thereafter stated in Chapter 3. Chapter 4 considers the tools created for the iterative process outlined in Chapter 5 which connects all departments. This process delivers a converged design that is verified and validated as described in Chapter 6. Chapter 7 then showcases the resultant values *MARCUS-T* is composed of alongside a three-view model. The logistics surrounding *MARCUS-T* during operation are laid out next in Chapter 8 to ensure it stays up and running. The hardware and software of *MARCUS-T* are illustrated subsequently in Chapter 9. A specific operations risk assessment (SORA), technical risk assessment (TRA), and reliability, availability, maintainability, and safety (RAMS) analysis are also performed to ensure its safety. Next, Chapter 10 presents an analysis on both technical and non-technical budgets, including an extensive sight into the cost budget by delving into a market analysis and investigating the return on investment (ROI). Chapter 11 concerns the plan of attack for future development of *MARCUS-T* , including a preliminary manufacturing, assembly, and integration (MAI) plan. A sustainable development strategy is also composed here, revisiting what has already been decided and conceptually designed, and discussing what is to be done in the future. The report closes off with a set of recommendations for *MARCUS-T* in future development, given alongside the conclusion in Chapter 13.

2

Mission Profile Structure

This chapter begins with an explanation of the design choice following a prior trade-off [3]. Next, the mission profile is considered, entailing all flight phases. Finally, an updated functional flow diagram and functional breakdown structure are described.

2.1. Final Design Choice

by Christian

This section discusses the change in final design option, coming from a trade-off performed previously [3]. Viable design options concerned a wide variety of automatic, electric tow craft for gliders. In the end, the trade-off showed a fixed nose-mounted design as shown in Figure 2.1 as most viable. However, the design option which will be designed in detail in this report is a different design. It will have the form as displayed in Figure 2.2. The final design that will be analysed in further detail, is a battery-driven drone which will tow a glider using the conventional towing method making use of a tow cable. The reason for the change in design are misgivings voiced by the client. In a conversation with the client, they stated, "Unless [the team] can prove that attaching the tow craft to the glider delivers aerodynamic benefits (...) the conventional tow option should be opted for." Furthermore, they expressed, "Another point of concern is the angle of incidence between glider and tow craft wings. This might be very limiting [when] adopting various gliders.". As the client was identified as a key-stakeholder [2, Fig. 3.1], they had the final say. Hence, the final design is now set as conventional tow craft.

Figure 2.1: The proposed design, the Nose Plane.

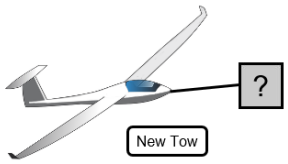

Figure 2.2: New design which is to be determined.

2.2. Mission Profile

by Mees, Christian

In this section, the mission profile the craft shall perform will be defined. It was decided that the craft should be able to perform its mission in a complex environment. For this reason, the flight phases are based on operations on Hilversum Airport, EHHV. However, it will apply to most airfields the craft will operate on. This airport is a relatively small but busy airport with 6 runways, a complicated airspace structure and both glider and motorised aircraft activity. The considered flight phases are taxi, take-off, climb, descent and landing. A cruise phase is not considered part of the mission. The whole mission shall be flown within a radius of 5 km around the airfield.

Taxi

There are four different profiles for taxiing, all shown in Figure 2.3.

1. **Deployment/Storage Taxi**: Taxi from the hangar to the designated battery swapping area in the vicinity of the tow launch area and back. This taxi profile will be unpowered. The craft is being towed by an external vehicle using a hook installed to the craft. From experience it is known that usually multiple (electric) carts pull the gliders to the starting area. Hence, electric carts are readily available. This taxi profile will not be automatic, as the craft is indirectly steered by the electric carts,
2. **Taxi Out**: Taxi from the designated battery swapping area to the start position at the launch area. The distance is assumed to be 50 m. Furthermore, the taxi profile is propeller-powered and steered remotely by a ground crew.

3. **Taxi In**: Taxi from landing to the designated battery swapping area. Additionally, the distance covered is assumed to be equal to the landing distance added to the 50 m, mentioned earlier. This profile is propeller-powered and remotely steered by ground crew.
4. **Bypass Taxi** Taxi from the runway directly to the start position. When the craft is in the Taxi In phase but the next mission could be performed with the current battery level, the craft will bypass the battery swap area and directly taxi to the launch area.

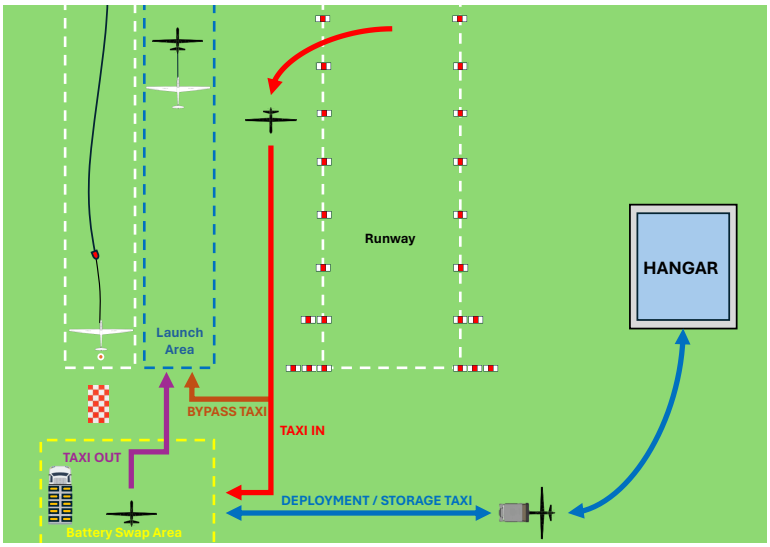

Figure 2.3: Generic ground chart for taxi profiles.

At the start and end of the day, the deployment taxi becomes relevant, whereas during operation the taxi in, taxi out and bypass taxi profiles alternate. A glider airfield is a dynamic environment and not easily predictable for an automated system. The general taxi speed for the taxi in and the taxi out phase is assumed to be walking pace, i.e. 5 km/h. Between the taxi in phase and the taxi out phase a turn-around is planned. This step is only required if the battery level has dropped below a certain threshold and needs to be swapped. Otherwise a bypass taxi is performed.

Take-Off[1]

The take-off starts from standstill. The tow craft and glider accelerate to a lift-off speed, V_{LOF}, from which the craft takes-off. It is probable that the glider is already airborne before the tow craft. At V_{LOF}, the craft takes off and goes through the transition phase (with radius, R_{TR}) and transitions to a climb angle, γ_c, of about 5 ° . After the transition, the combination will steadily climb until a screen height, h_s, of 15 m is reached. The take-off distance covered to clear a height of 15 m for the tandem may not exceed 500 m[4]. After clearing 15 m, the climb-out continues with a vertical speed of 3 m/s and a climb speed, V_c, of 130 km/h. A visual representation of this phase can be seen in Figure 2.4

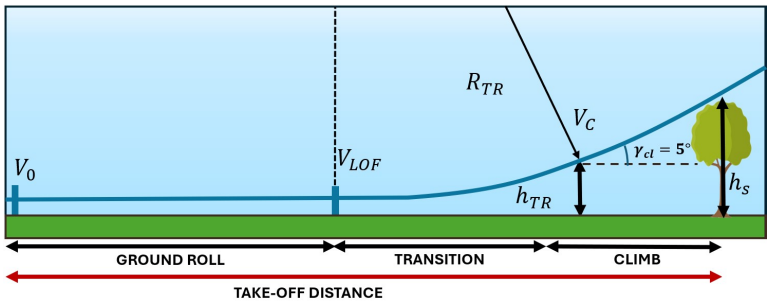

Figure 2.4: Take-off profile of the tow craft.

[1]The heights mentioned in this section are measured above ground level.

Climb

The overall climb is split into two phases. The first phase contains the initial climb-out with a vertical speed of 3 m/s at a climb out speed of 130 km/h, up to a height of 180 m. The second phase is performed at a speed of 130 km/h and a vertical speed of 2.5 m/s up to 1,000 m AMSL. Figure 2.5 shows the climb track for runway 36 at Hilversum Airport. The climb is laid out such that it does not enter the circuit area and will reach the glider training area at 1,000 m. Here, the glider will be dropped off and the tow craft will start its decent. While this chart is for Hilversum Airport, this profile can be used for most airfields.

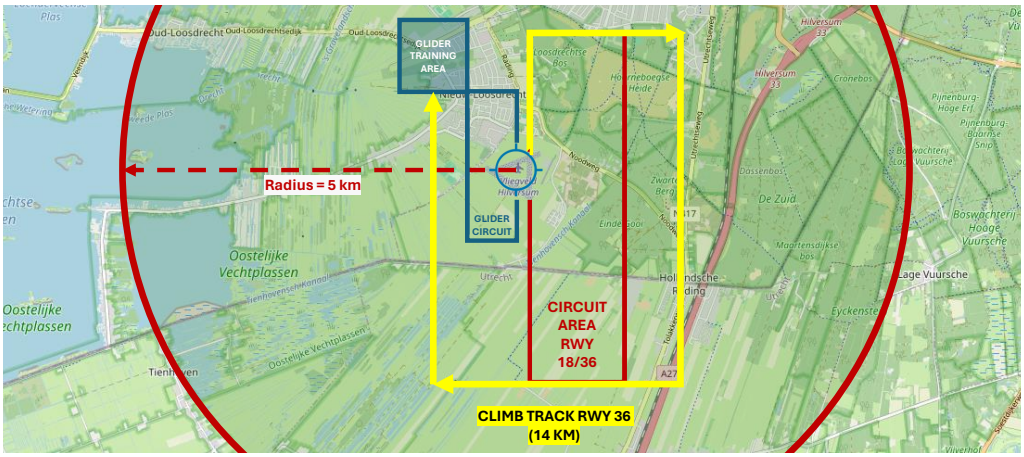

Figure 2.5: Climb track for runway 36 at Hilversum Airport .

Descent

After the tow craft drops the glider off in the glider training area, the tow craft will initiate its descent. Four possible descent profiles are considered. The first descent profile is the steady descent from the glider training area, visible in Figure 2.6. This descent profile will be a continuous descent from 1,000 m to the circuit entry point. Figure 2.6a shows the ground track of this descent profile. Figure 2.6b shows the side profile of this standard descent. The ground track distance is equal to 5,500 m and results into a required flight path angle of 8.3°. The tow craft will not fly over the circuit areas.

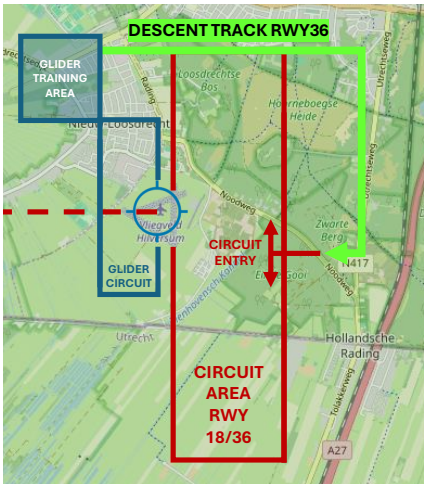

(a) Descent track for runway 36 at Hilversum Airport.

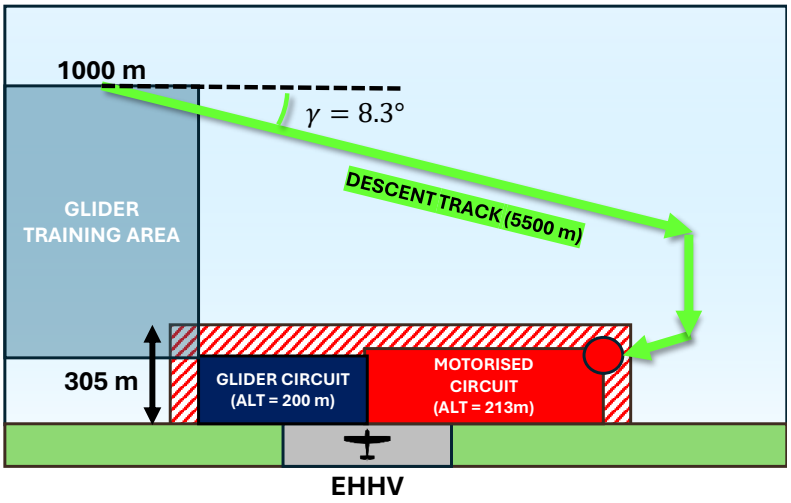

(b) Side profile of the descent track.

Figure 2.6: Standard descent profiles for runway 36 at Hilversum Airport.

The second descent profile is a dive profile, shown in Figure 2.7a. Instead of descending around the circuit as shown in Figure 2.6a, the tow craft will descend directly over the airfield. From the eAIP[2] , the circuit areas may not be overflown below an altitude of 1003 ft / 305.7 m AMSL . In Figure 2.7b, it is shown that the

[2] eaip.lvnl.nl [cited 04 June 2024]

tow craft will always be above this limit. Moreover, the tow craft should avoid flying overhead the aerodrome during glider or para-jumping activities as much as possible. Hence, the dive profile can only be performed when no winch launches and para-jumps are taking place. This should be coordinated with ATC and glider control. The ground track is 3,100 m and results into a required flight path angle of 14°.

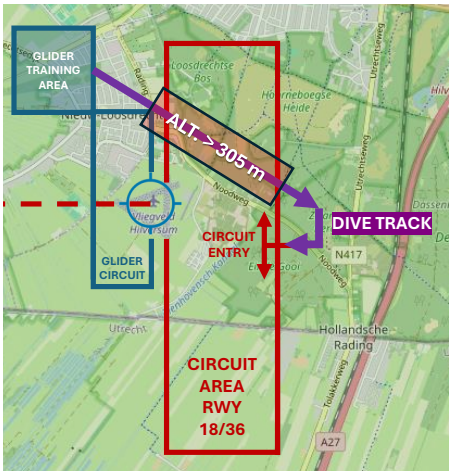

(a) Dive track for runway 36 at Hilversum Airport.

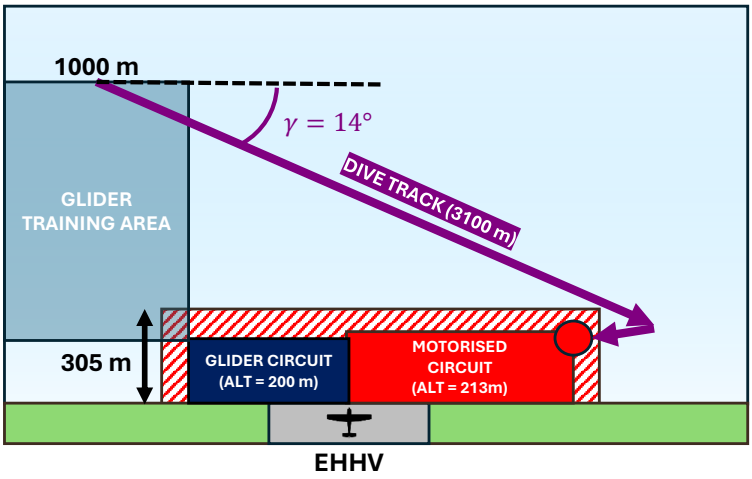

(b) Side profile of the dive track.

Figure 2.7: Dive profiles for runway 36 at Hilversum Airport.

The third descent profile is a special case descent. As specified in the introduction to this section, the vehicle shall stay within 5 km of the airfield. Emanating from the limiting case of being 5 km away from the airfield, as mentioned previous, an unpowered glide is planned. Once again, the tow craft should overfly the aerodrome at an altitude of at least 305 m. A flight path angle of 6° is required to cover the total ground track of 7,300 m. This can be achieved with a glide-ratio of at least 9.3. A higher glide-ratio of the craft is required in case of headwind components.

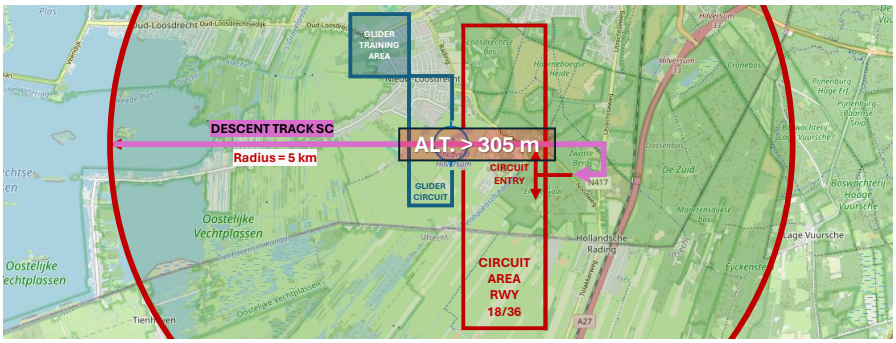

(a) Glide descent track for runway 36 at Hilversum Airport.

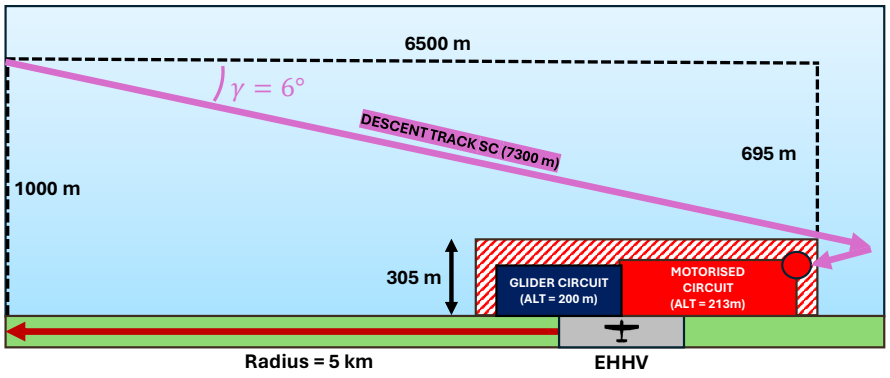

(b) Side profile of the special descent track for runway 36 at Hilversum Aiport.

Figure 2.8: Special case descent profiles for runway 36 at Hilversum Airport.

The fourth profile is the steep dive profile. As shown in Figure 2.9, the tow craft will drop the glider near the circuit entry point. After release, it will dive down with a flight path angle of 45° and then use its kinetic energy to cover the final horizontal distance to the circuit entry point.

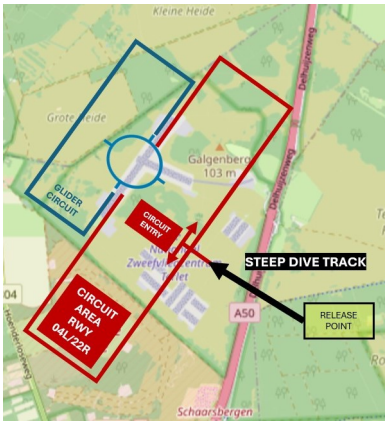

(a) Steep dive track for runway 22L at Terlet Airfield.

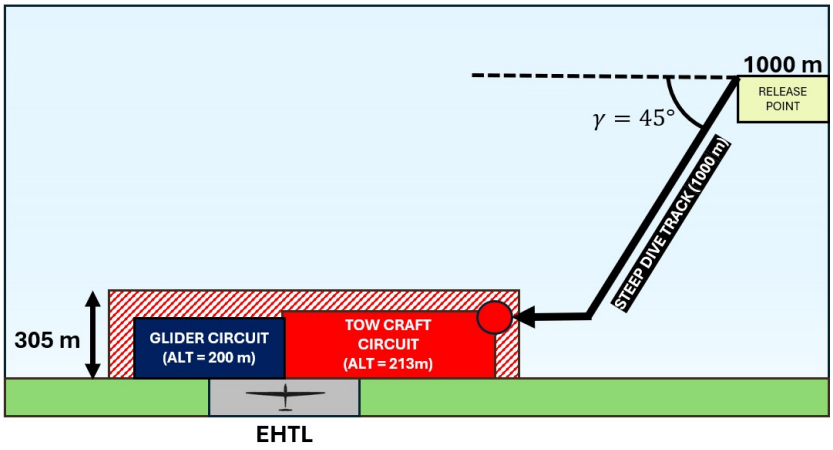

(b) Side profile of the steep dive.

Figure 2.9: Steep dive profiles for runway 22L at Terlet Airfield.

Circuit and Go-Around

When the tow craft reaches the circuit entry point at 213 m, it will fly along the landing pattern and continuously descend with a flight path angle of 3°. This is shown in Figure 2.10. A go-around procedure will be performed by flying to the published traffic pattern altitude accordingly.

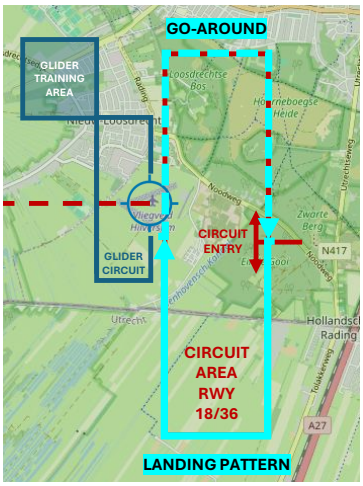

(a) Landing pattern ground track for runway 36 at Hilversum Airport.

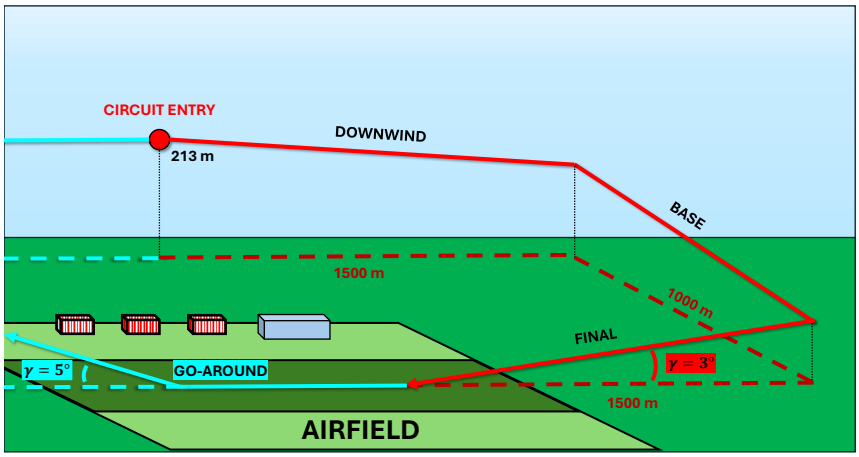

(b) Generalised landing side profile.

Figure 2.10: Landing pattern profiles for runway 36 at Hilversum Airport.

Landing

The landing operation begins with the approach phase, where the aircraft descends towards the runway at an approach speed, V_{APP}, along a flight path angle of 3°. The aircraft crosses the threshold at a screen height, h_s. As the aircraft continues its descent, the flare is initiated at a flare height, h_f. During this phase, the aircraft follows a curved path with a flare radius, R_f, reducing its descent rate. The landing is completed with the ground roll phase, where the aircraft touches down at a landing speed, V_{TD}, and decelerates to a complete stop. The total landing distance is the sum of the approach, flare, and ground roll phases.

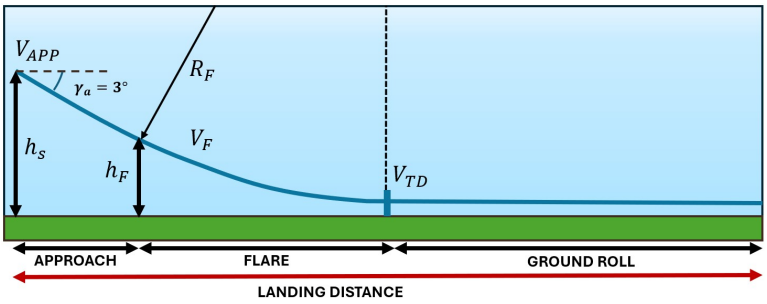

Figure 2.11: Landing profile of the tow-craft.

2.3. Functional Flow Diagram

by Annika, MianTao, Stan, Tamara, Mees

An updated functional flow diagram is created to aid the detailed design of craft. The functions of the craft are divided in a storage phase, four different taxi phases, a battery swapping phase, a starting phase, a launch phase, a release phase, a return phase and an end phase.

2.4. Functional Breakdown Structure

by Andreas, Filip, Gerard

To structure the functional flow diagram described in Section 2.3, a functional breakdown structure is created. This diagram groups the functional flow diagram in a structured way making it a useful overview of functions of craft.

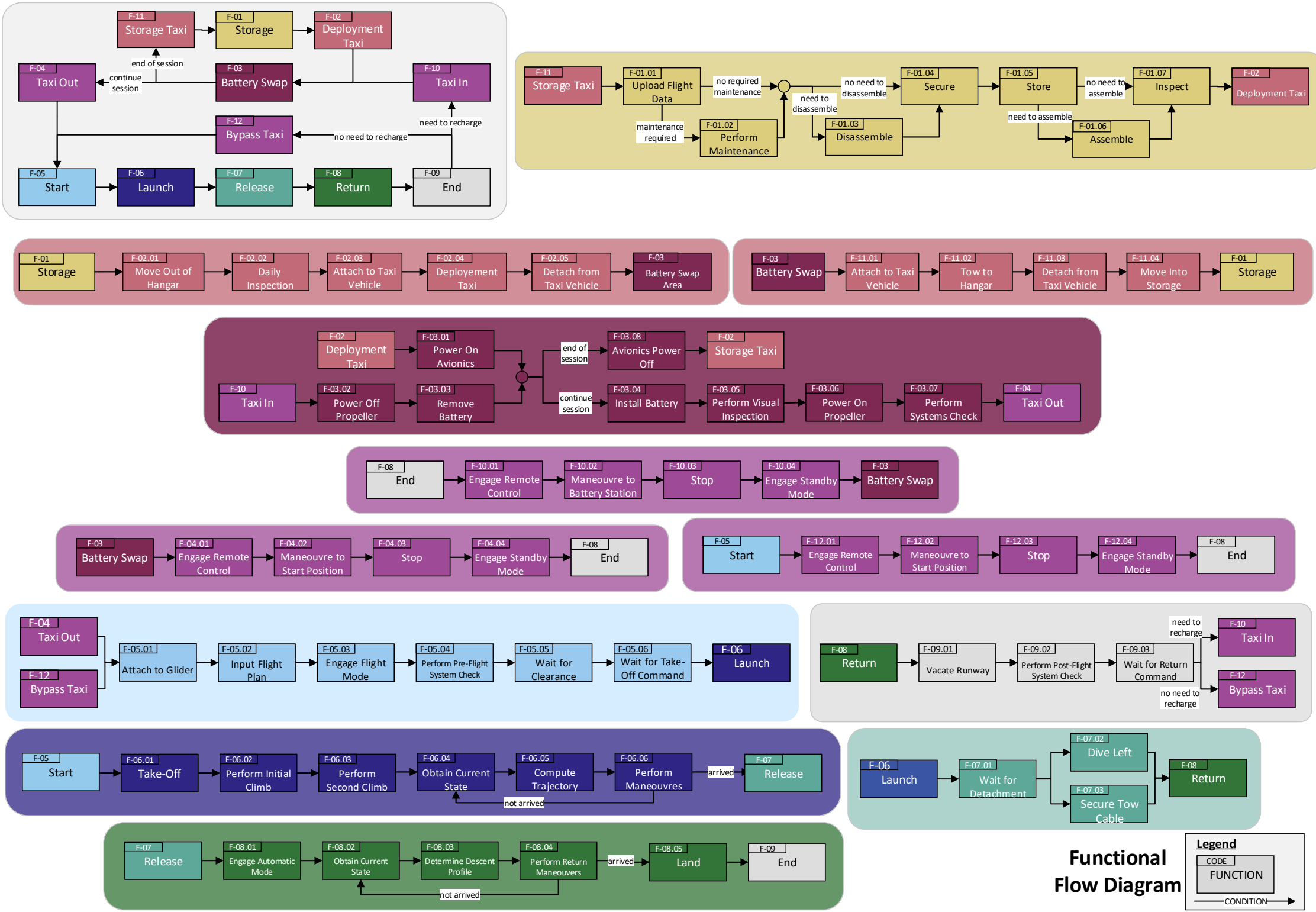
F-11 Storage Taxi
F-01 Storage
F-02 Deployment Taxi
F-04 Taxi Out
end of session
continue session
F-03 Battery Swap
F-10 Taxi In
F-12 Bypass Taxi
need to recharge
no need to recharge
F-05 Start
F-06 Launch
F-07 Release
F-08 Return
F-09 End
F-11 Storage Taxi
F-01.01 Upload Flight Data
no required maintenance
maintenance required
F-01.02 Perform Maintenance
need to disassemble
no need to disassemble
F-01.03 Disassemble
F-01.04 Secure
F-01.05 Store
no need to assemble
need to assemble
F-01.06 Assemble
F-01.07 Inspect
F-02 Deployment Taxi
F-01 Storage
F-02.01 Move Out of Hangar
F-02.02 Daily Inspection
F-02.03 Attach to Taxi Vehicle
F-02.04 Deployement Taxi
F-02.05 Detach from Taxi Vehicle
F-03 Battery Swap Area
F-03 Battery Swap
F-11.01 Attach to Taxi Vehicle
F-11.02 Tow to Hangar
F-11.03 Detach from Taxi Vehicle
F-11.04 Move Into Storage
F-01 Storage
F-02 Deployment Taxi
F-03.01 Power On Avionics
end of session
F-03.08 Avionics Power Off
F-02 Storage Taxi
F-10 Taxi In
F-03.02 Power Off Propeller
F-03.03 Remove Battery
continue session
F-03.04 Install Battery
F-03.05 Perform Visual Inspection
F-03.06 Power On Propeller
F-03.07 Perform Systems Check
F-04 Taxi Out
F-08 End
F-10.01 Engage Remote Control
F-10.02 Maneouvre to Battery Station
F-10.03 Stop
F-10.04 Engage Standby Mode
F-03 Battery Swap
F-03 Battery Swap
F-04.01 Engage Remote Control
F-04.02 Maneouvre to Start Position
F-04.03 Stop
F-04.04 Engage Standby Mode
F-08 End
F-05 Start
F-12.01 Engage Remote Control
F-12.02 Maneouvre to Start Position
F-12.03 Stop
F-12.04 Engage Standby Mode
F-08 End
F-04 Taxi Out
F-12 Bypass Taxi
F-05.01 Attach to Glider
F-05.02 Input Flight Plan
F-05.03 Engage Flight Mode
F-05.04 Perform Pre-Flight System Check
F-05.05 Wait for Clearance
F-05.06 Wait for Take-Off Command
F-06 Launch
F-08 Return
F-09.01 Vacate Runway
F-09.02 Perform Post-Flight System Check
F-09.03 Wait for Return Command
need to recharge
no need to recharge
F-10 Taxi In
F-12 Bypass Taxi
F-05 Start
F-06.01 Take-Off
F-06.02 Perform Initial Climb
F-06.03 Perform Second Climb
F-06.04 Obtain Current State
F-06.05 Compute Trajectory
F-06.06 Perform Maneouvres
arrived
not arrived
F-07 Release
F-06 Launch
F-07.01 Wait for Detachment
F-07.02 Dive Left
F-07.03 Secure Tow Cable
F-08 Return
F-07 Release
F-08.01 Engage Automatic Mode
F-08.02 Obtain Current State
F-08.03 Determine Descent Profile
F-08.04 Perform Return Maneouvers
arrived
not arrived
F-08.05 Land
F-09 End
Functional Flow Diagram
Legend
CODE
FUNCTION
CONDITION

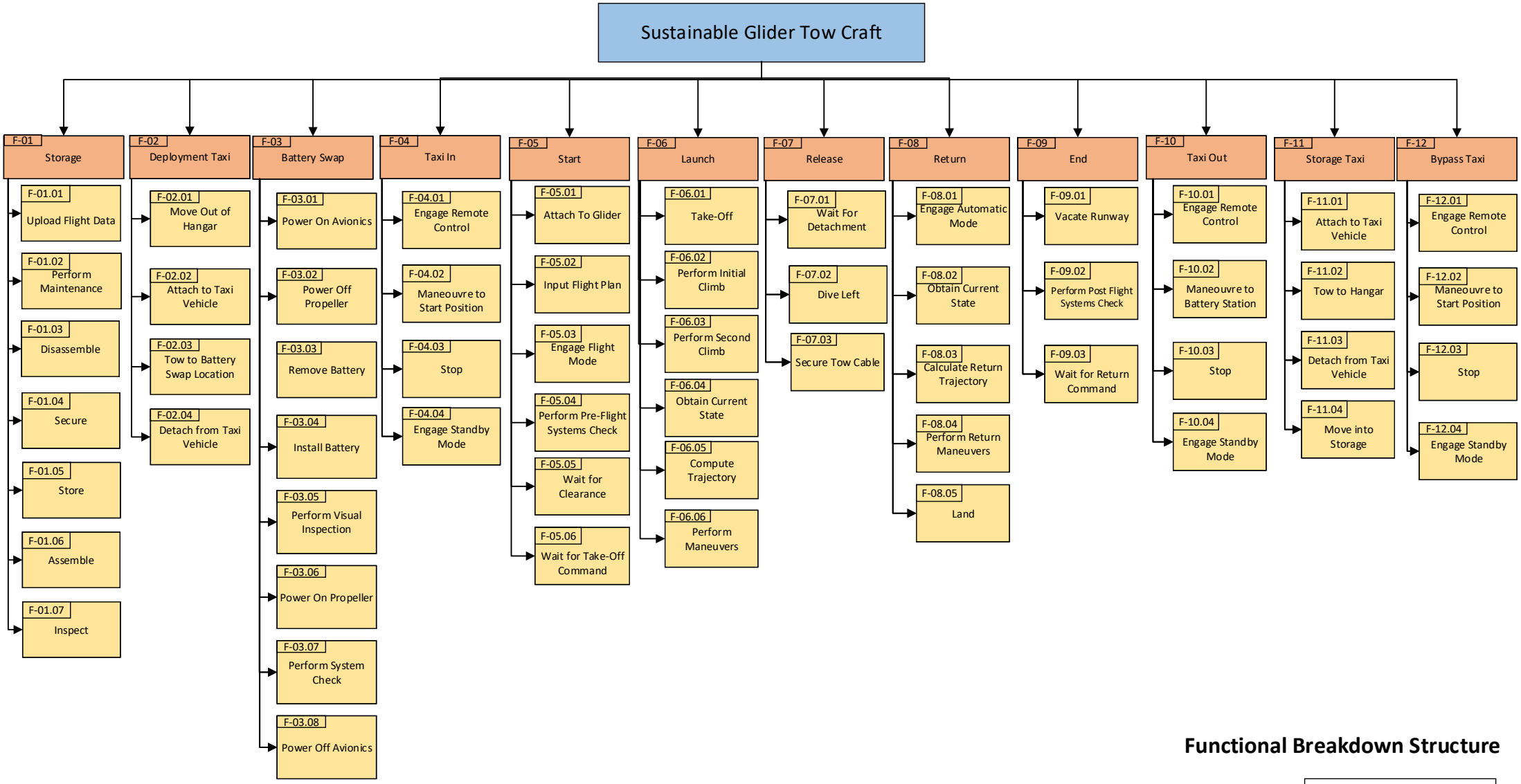
Sustainable Glider Tow Craft
F-01 Storage
F-01.01 Upload Flight Data
F-01.02 Perform Maintenance
F-01.03 Disassemble
F-01.04 Secure
F-01.05 Store
F-01.06 Assemble
F-01.07 Inspect
F-02 Deployment Taxi
F-02.01 Move Out of Hangar
F-02.02 Attach to Taxi Vehicle
F-02.03 Tow to Battery Swap Location
F-02.04 Detach from Taxi Vehicle
F-03 Battery Swap
F-03.01 Power On Avionics
F-03.02 Power Off Propeller
F-03.03 Remove Battery
F-03.04 Install Battery
F-03.05 Perform Visual Inspection
F-03.06 Power On Propeller
F-03.07 Perform System Check
F-03.08 Power Off Avionics
F-04 Taxi In
F-04.01 Engage Remote Control
F-04.02 Maneouvre to Start Position
F-04.03 Stop
F-04.04 Engage Standby Mode
F-05 Start
F-05.01 Attach To Glider
F-05.02 Input Flight Plan
F-05.03 Engage Flight Mode
F-05.04 Perform Pre-Flight Systems Check
F-05.05 Wait for Clearance
F-05.06 Wait for Take-Off Command
F-06 Launch
F-06.01 Take-Off
F-06.02 Perform Initial Climb
F-06.03 Perform Second Climb
F-06.04 Obtain Current State
F-06.05 Compute Trajectory
F-06.06 Perform Maneuvers
F-07 Release
F-07.01 Wait For Detachment
F-07.02 Dive Left
F-07.03 Secure Tow Cable
F-08 Return
F-08.01 Engage Automatic Mode
F-08.02 Obtain Current State
F-08.03 Calculate Return Trajectory
F-08.04 Perform Return Maneuvers
F-08.05 Land
F-09 End
F-09.01 Vacate Runway
F-09.02 Perform Post Flight Systems Check
F-09.03 Wait for Return Command
F-10 Taxi Out
F-10.01 Engage Remote Control
F-10.02 Maneouvre to Battery Station
F-10.03 Stop
F-10.04 Engage Standby Mode
F-11 Storage Taxi
F-11.01 Attach to Taxi Vehicle
F-11.02 Tow to Hangar
F-11.03 Detach from Taxi Vehicle
F-11.04 Move into Storage
F-12 Bypass Taxi
F-12.01 Engage Remote Control
F-12.02 Maneouvre to Start Position
F-12.03 Stop
F-12.04 Engage Standby Mode
Functional Breakdown Structure
Legend
First Level
F-X
Second Level Function X
F-X.x
Third Level Function X.x
F-X.x.x
Fourth Level Function X.x.x

3

Requirements

It is vital to have a clear overview of the relevant requirements for the rest of the design process of craft. The final responsibilities for these requirements will be split over five departments, namely Structures, Materials, and Manufacturing (SMM), Aerodynamics (AERO), Software, Stability, and Control (SSC), Power, Performance and Propulsion (PPP), and Airfield Performance, Operations, and Logistics (APOL). First, the stakeholders and their requirements are explained. Then a list of requirements and constraints is presented together with their responsible department, including those regarding certification specifications. Next, the responsibilities of each department are explained. Finally, interdependencies between the departments are shown in an N^2 chart.

3.1. Stakeholder Requirements

by Tamara, Everyone

Finding the stakeholders and their requirements is necessary before designing. The stakeholders and their abbreviation can be found in Table 3.1. The requirements of these stakeholders are shown in Table 3.2.

Table 3.1: Identified stakeholders and their abbreviations.

Stakeholder	Abbreviation	Stakeholder	Abbreviation
Client	CLT	Glider pilot	GP
Glider clubs	GC	Operational personnel	OP
Manufacturers	MF	Local residents	LR
Authorities	AT	Airfield operations	AO

Table 3.2: Stakeholder requirements.

Requirement Code	Description
STK-CLT-01	The tow craft shall be electrically powered with the help of battery packs.
STK-CLT-02	The battery pack shall be swappable.
STK-CLT-04	The tow craft shall be (remotely) piloted by the glider pilot followed by an automatic return to base.
STK-CLT-05	The return to base may be powered but may also be executed via a controlled parachute landing.
STK-CLT-06	The craft may be strapped onto the glider or execute the towing in any other way perceivable.
STK-CLT-09	The battery pack shall be large enough to complete at least one towing manoeuvre of an Arcus T at a MTOW of 850 kg.
STK-CLT-10	The tow craft shall meet the regulations certification requirements for glider launching.
STK-CLT-11	The costs shall be such that an average glider club can afford one or more of these crafts (Price €310,000).
STK-GP-01	The glider pilot shall be able to release at any time during the aerotow manoeuvre.
STK-GP-02	The tow craft shall behave in a predictable manner during emergency procedures as specified by authorities.
STK-GP-03	The glider pilot shall be able to determine the release location of the aerotow manoeuvre.
STK-GP-04	The glider pilot shall be able to determine the release altitude of the aerotow manoeuvre.
STK-GP-05	The tow craft shall be able to tow at least an Arcus T at a MTOW of 800 kg while complying with the other requirements.
STK-GP-07	The tow craft shall at least be able to perform a tow manoeuvre in VFR conditions.

Continued on next page

Requirement Code	Description
STK-GP-08	The tow craft shall not be the limiting factor in regards to atmospheric conditions.
STK-GP-09	The tow craft shall perform manoeuvres according to regulations
STK-GC-03	The tow craft shall have at least a similar performance/cost ratio as current tow aircraft.
STK-GC-04	The tow craft shall have a similar insurance cost to as current tow craft.
STK-GC-08	The tow craft shall at least have a similar block time as the current tow aircraft.
STK-GC-010	The tow craft shall fit in a hangar of at least 30m length x 15m width x 4m height.
STK-GC-11	The tow craft shall have a deploy time of 30 minutes.
STK-GC-12	The tow craft shall require no changes to the current glider designs .
STK-OP-01	The tow craft shall be easy to couple with the glider.
STK-OP-02	The tow craft shall be safe to be around during ground operations.
STK-OP-03	The tow craft shall be easy and intuitive to be operated by trained members.
STK-MF-01	There shall be no glider design changes needed to use the tow craft.
STK-MF-03	The tow craft shall be manufacturable using available techniques.
STK-MF-04	The tow craft shall be produced using sustainable manufacturing techniques.
STK-MF-05	The tow craft shall be produced using lean manufacturing techniques.
STK-MF-06	The manufacturing cost of the tow craft shall not exceed €200,000 .
STK-LR-03	The tow craft shall not exceed a noise level higher than specified in regulations
STK-LR-04	The tow craft shall not endanger the residents surrounding the airfield under any circumstances.
STK-AU-03	The tow craft shall adhere to the right of ways.
STK-AU-05	The tow craft shall perform manoeuvres according to regulations
STK-AU-06	The tow craft shall be able to detect other airspace users.
STK-AU-07	The tow craft shall be visible for all airspace users.
STK-AT-01	The tow craft shall comply with the regulations specified in regulations.
STK-AT-04	The tow craft shall comply with EASA, ILT and LVNL rules.
STK-AT-05	The tow craft shall comply with environmental rules according to regulations.
STK-AO-01	The tow craft shall not hinder any airfield operations.
STK-AO-04	The tow craft shall be visible to airfield users.

3.2. System Requirements and Constraints

by Everyone

A set of system requirements and constraints is necessary to ensure no qualities are forgotten when diving into the design process. Table 3.3 shows all of these, including revised requirements explained later [3, 2]. Furthermore, the responsible departments for meeting each requirement are specified.

Table 3.3: All requirements and constraints on the system.

Requirement Code	Requirement Description	Dep.
SYS-PWR-01	The power system shall have a maximum power of 80 kW.	PPP
SYS-PWR-02	The power system shall have a maximum voltage of 800 V.	PPP
SYS-PWR-03	The power system shall have a minimum power of 62 kW.	PPP
SYS-PWR-04	The power system shall have a minimum voltage of 400 V.	PPP
SYS-PWR-05	The power system shall be battery powered.	PPP
SYS-PWR-06	The battery shall have at least a capacity of 10 kWh.	PPP
SYS-PRO-01	The propulsion system shall provide a thrust of 2500 N.	PPP
SYS-PRO-02	The propulsion system shall be electric.	PPP
SYS-GHS-01	The maximum outer main gear wheel span shall be smaller than 15m	SMM

Continued on next page

Requirement Code	Requirement Description	Dep.
SYS-STR-01	The structure shall have a maximum length of 7.10 m when disassembled.	SMM
SYS-STR-02	The structure shall have a maximum width of 11.0 m when disassembled.	SMM
SYS-STR-03	The structure shall have a maximum height of 2.30 m when disassembled.	SMM
SYS-STR-04	The structure shall be manufacturable using existing techniques.	SMM
SYS-STR-05	The structure shall have lights according to relevant regulation.	SMM
SYS-STR-07	The wingspan shall be smaller than 80 m.	AERO
SYS-STR-08	The structure shall be able to withstand a maximum load factor of 5.	SMM
SYS-STR-09	The structure shall be able to withstand a minimum load factor of -2.5.	SMM
SYS-GCS-02	The coupling system shall resist a force of 16260 N.	SMM
SYS-GCS-03	The pilot shall be able to directly decouple at all stages of the operations.	SMM
SYS-GCS-04	The glider coupling system shall detect a decouple.	SMM
SYS-GCS-05	The glider coupling system shall communicate its status to the FMS.	SMM
SYS-FMS-01	The flight management system shall be programmed with an automatic mode.	SSC
SYS-FMS-02	The flight management system shall react to pilot input.	SSC
SYS-FMS-03	The flight management system shall have a database of the terrain.	SSC
SYS-FMS-04	The flight management system shall have a database with the locations of airfields.	SSC
SYS-FMS-05	The flight management system shall have two way communication with the communication system.	SSC
SYS-FMS-06	The flight management system shall have two way communication with the ground handling system.	SSC
SYS-FMS-07	The flight management system shall have two way communication with the guidance system.	SSC
SYS-FMS-08	The flight management system shall have two way communication with the navigation system.	SSC
SYS-FMS-09	The flight management system shall have two way communication with the flight control system.	SSC
SYS-FMS-10	The flight management system shall have two way communication with the power system.	SSC
SYS-FMS-11	The flight management system shall have two way communication with the propulsion system.	SSC
SYS-FMS-12	The flight management system shall have two way communication with the data monitoring system.	SSC
SYS-FMS-13	The flight management system shall have two way communication with the glider coupling system.	SSC
SYS-FMS-15	The flight management system shall be programmed with an emergency mode.	SSC
SYS-FMS-16	The flight management system shall provide flight envelope protection in Normal Law.	SSC
SYS-FMS-17	The flight management system shall be programmed with Alternate Law.	SSC
SYS-FMS-18	The flight management system shall have a database of the airspace.	SSC
SYS-FMS-19	The craft shall be equipped with ACAS.	SSC
SYS-FMS-20	The craft shall be equipped with FLARM.	SSC
SYS-FMS-22	The flight management system shall have a total system error of (18 - OMGWS)/2 m	SSC
SYS-COM-01	The craft shall have 2-way communication with the glider pilot with a bandwidth of 100 kbps.	APOL
SYS-COM-02	The craft shall have 2-way communication with the ground station with a bandwidth of 100 kbps.	APOL
SYS-COM-03	The craft shall have 2-way communication with the ATC.	APOL
SYS-COM-04	The craft shall have 2-way communication with other aircraft.	APOL

Continued on next page

Requirement Code	Requirement Description	Dep.
SYS-COM-05	The craft shall be equipped with ADS-B.	APOL
SYS-COM-06	The craft shall be equipped with a radio reflector.	APOL
SYS-GDC-01	The guidance system shall have an error of 5 m from the FMS flight plan.	SSC
SYS-GDC-02	The guidance system shall compute the flight path to the airfield.	SSC
SYS-NAV-03	The navigation system shall obtain the height above ground with an accuracy of at least 0.9 m.	SSC
SYS-NAV-04	The navigation system shall trace the glider's position.	SSC
SYS-FCS-01	The flight control system shall allow for external input.	SSC
SYS-FCS-02	The craft shall be statically stable.	SSC
CON-CST-05-R	The craft shall be insured for shipping.	APOL
CON-OPS-07-R	The users of the craft shall be trained on emergency procedures.	APOL
CON-OPS-08-R	The users of the craft shall be trained on SOP.	APOL
CON-OPS-09-R	The emergency procedures shall be documented.	APOL
CON-OPS-10-R	The SOPs shall be documented.	APOL
CON-OPS-11-R	The manufacturing plan shall be fool-proof.	SMM
CON-OPS-12-R	Batteries shall be replaced when their capacity drops below 80% of the initial capacity.	APOL
CON-OPS-13-R	Battery charging station shall have a fire suppression system.	APOL
CON-TEC-06-R	The craft shall have certified components of the shelf (COTS).	SMM
SYS-PWR-12-R	The craft shall contain an independent power source for avionics.	PPP
SYS-GHS-01-R	The landing gear shall be able to withstand the loads generated during landing at MTOW.	SMM
SYS-DMS-01-R	The craft shall have a display to show system errors.	APOL
SYS-DMS-02-R	The DMS shall be designed to prioritise false negatives.	SSC
SYS-DMS-03-R	The DMS shall be designed under fail-safe philosophy (redundancy).	SSC
SYS-DMS-04-R	The DMS shall keep track of maintenance tasks.	APOL
SYS-DMS-05-R	The DMS shall inform the operator of maintenance tasks that need to be performed.	APOL
SYS-FCS-05-R	The FCS shall be designed under fail-safe philosophy (redundancy).	SSC
SYS-FMS-21-R	The FMS shall be designed under fail-safe philosophy (redundancy).	SSC
SYS-GCS-06-R	The GCS shall use certified latches.	SMM
SYS-GCS-07-R	The GCS shall have release capabilities by both pilot and tow craft.	SMM
SYS-GCS-08-R	The GCS shall have a redundant release mechanism.	SMM
SYS-GCS-09-R	The GCS shall have an alternate independent quick-release mechanism.	APOL
SYS-NAV-05-R	The navigation system shall be designed under fail-safe philosophy (redundancy).	SSC
SYS-PWR-07-R	The batteries shall be contained in protective housing with at least an IP56W rating.	SMM
SYS-PWR-08-R	The power system shall be equipped with a fire suppression system.	APOL
SYS-PWR-09-R	The battery shall have a power indicator.	PPP
SYS-PWR-10-R	The battery shall charge from 20% to 85% in 0.5 h.	PPP
SYS-PWR-11-R	The batteries shall be certified according to MIL-STD-810G drop-test standard.	SMM
SYS-STR-07-R	The craft shall have access hatches to all maintainable systems.	APOL
CON-REG-01	The craft shall meet CS-UAS requirements.	APOL
CON-REG-02	The craft shall meet relevant EASA operational requirements.	APOL
CON-SUS-01	The peak noise emitted by the craft shall not exceed 100 dB when measured from 50 m.	PPP
CON-SUS-02	The batteries used by the craft shall be rechargeable.	PPP

Continued on next page

Requirement Code	Requirement Description	Dep.
CON-SUS-03	The lifetime equivalent CO2 emission of the craft shall be less than that of all existing tow craft normalised by the number of launches per lifetime.	APOL
CON-SUS-04	At least 70% of repairs preformed on the craft shall be locally	APOL
CON-SUS-05	At least 70% of components of the craft shall be replaceable	SMM
CON-SUS-06	At least 60% of the components of the craft shall be reusable/recyclable	SMM
CON-SUS-07	At least 60% by mass, of the craft, shall be recyclable.	SMM
CON-CST-01	The craft shall cost less than EUR 310,000 to purchase.	APOL
CON-CST-02	The total operational cost of the craft shall be less than EUR 252,000	APOL
CON-CST-03	The craft shall cost less than EUR 562,000 to EOL.	SMM
CON-CST-04	The craft shall cost less than EUR 310,000 to manufacture.	SMM
CON-OPS-01	The craft shall have swappable batteries.	SMM
CON-OPS-02	The craft shall have a turn-around time less than 20 minutes.	APOL
CON-OPS-03	The craft shall have a block time of less than 30 minutes.	APOL
CON-OPS-04	The craft shall have a deploy time of less than 40 minutes.	APOL
CON-OPS-05	The craft shall be connected to the glider in less than 5 minutes.	APOL
CON-OPS-06	The craft shall have a delivery time of less than 14 days.	APOL
CON-TEC-01	The craft shall have a total mission range of 30 km with a glider attached of 850 kg.	PPP
CON-TEC-02	The craft shall have an endurance of 30 minutes.	PPP
CON-TEC-03	The craft shall be able to tow a glider of 850 kg.	PPP
CON-TEC-04	The craft shall be compatible with current gliders.	APOL
CON-TEC-05	The craft shall have a minimum vertical tow speed of 2.5 m/s with a glider of 850 kg.	PPP
CON-TEC-06	The maximum take-off distance of the combination (MTOW) to clear a 15 m obstacle shall be 500 m.	PPP

As the final design is now chosen, some requirements are adjusted to better reflect the configuration of *MARCUS-T*. Namely, SYS-GDC-01, SYS-NAV-01, SYS-NAV-02, SYS-FCS-03, and SYS-FCS-04 have been replaced with SYS-FMS-22. Also, SYS-FMS-14 has been removed, as in the conventional configuration this requirement is no longer applicable. Furthermore, it has been decided to remove SYS-STR-06, as it is deemed redundant.

3.3. Certification Specifications

by Andreas, Gerard, Niels

This section considers two types of Certification Specifications, namely CS-UAS (also referred to as CS-Drone), CS-22. Any relevant requirements and constrains following from these specifications are repeated hereafter, including a reasoning on their relevance. These will be used as a primary reference in the design of the craft.

The craft shall fall under the “specific” UAS category, but this category is not very prescriptive. To increase the chances of getting certified and ensuring safety and airworthiness, the craft shall be designed to meet CS-22 requirements, excluding any pilot requirements, and a specific operations risk assessment (SORA) will be performed to minimize ground and air risks.

The craft will be classified as automatic, not autonomous, according to CS-UAS. The drone will not be allowed to be piloted remotely under normal circumstances, but in case of emergency, an accredited drone operator will need to be available to take control.

3.3.1. CS-UAS

CS-UAS contains 4 parts: “Cover Regulation to Implementing Regulation (EU) 2019/947”, “Annex to Implementing Regulation (EU) 2019/947”, “Cover Regulation to Delegated Regulation (EU) 2019/945”, and “Annex to Delegated Regulation (EU) 2019/945”. These will be referred to as CRIR, AIR, CRDR, and ADR, respectively [5]. The relevant articles are discussed in this section.

Base Requirements (CRIR) As defined in Article 2 of CRIR, *MARCUS-T* will not be considered as "autonomous", but will be considered "automatic". Furthermore, craft will fall under the "specific" category as per Article 3 and Article 6, because of *MARCUS-T* 's size, weight, and operational profile. This means the drone must comply with all "specific" regulation from CRIR, but also with some further requirements from AIR (Part B) and CRDR (Chapter 3).

The operations of *MARCUS-T* will have to follow some constraints. The UAS will have to be certified by authorities, and thus a Specific Operations Risk Assessment (SORA) will have to be performed. Furthermore, both the craft and the pilot will have to be registered if there is a need for pilot override.

Specific Requirements (AIR, CRDR) Chapter III (Article 40) of AIR specifies that *MARCUS-T* will have to be certified by proving compliance with EASA's Part 21 (Airworthiness and Environmental Certification), Part 26 (Additional Airworthiness Specifications) and Continuing Airworthiness specifications. The craft shall also have a unique serial number, and shall have a remote identification system. Part B of CRDR also provides the guidance material that needs to be used to apply for certification of the operations of the drone. It defines that a SORA is needed, but also defines responsibilities for the operator and the pilot of the craft, and states the scenarios that *MARCUS-T* shall comply with.

3.3.2. CS-22 Glider Restrictions

In CS-22 the Certification Specifications, Acceptable Means of Compliance and Guidance Material for Sailplanes and Powered Sailplanes can be found [4]. In this report the tow craft itself will be designed, but the requirements specified for gliders on tow should be taken into account as well. These constraints are mostly limiting the forces exerted on the glider, maximum and minimum speeds, and takeoff performance for self-launching gliders. Furthermore, in CS-22 the specifications on demonstrating acceptable means of compliance are laid out. In the following paragraphs the most important limitations can be found.

CS 22.151 In this section of CS-22 there are various limitations given on the aerotow itself. Most cover the safety demonstrations that need to be performed before certification. Some requirements are given on the controllability of the glider from the glider pilots perspective.

CS 22.335 (d) Specifies that the design aerotow speed, V_{tow}, must not be less than 125 km/h. V_{Tow} will be the maximum airspeed the glider is allowed to fly during the aerotow.

3.3.3. CS-22 Tow Craft Restrictions

If *MARCUS-T* can be designed such that it falls into the powered sailplane category as specified in CS 22.1, then it does not need to comply with the stricter CS-23 regulations. When this is done, the craft may be less difficult to certify under CS-UAS as it can be demonstrated to comply with another CS, although now having an automatic flight control system rather than a pilot. This would create another unique selling point (USP) as it, under this regulation, can operate from glider airfields as well. The following certification specifications would in this case be of great importance [4].

CS 22.1(a) Specifies the conditions under which a plane is considered a powered sailplane. The requirements in Equation 3.1 and Equation 3.2 need to be met.

$$\frac{MTOM}{b^2} \leq 3 \tag{3.1}$$

$$MTOM \leq 850\ [kg] \tag{3.2}$$

Furthermore the number of occupants should be no more than 2, which will not pose constraint for the automatic craft. CS 22.1 does mention 'spark- or compression-ignition' specifically, thus a special condition[1] must be obtained, such as was done with the AS34Me [6].

Appendix K In this appendix, specifications and references are made for aerotowing by powered sailplanes specifically. Here most of the important information (or the references to them) on the tow craft's constraints

[1] www.easa.europa.eu [cited 31 May 2024]

can be found. The various sub parts cover topics such as flight (Subpart B), structure (Subpart C), design and construction (Subpart D), powerplant installation (Subpart E), equipment (Subpart F), and operating limitations and information (Subpart G).

CS-22 also specifies the flight envelope. Both manoeuvring and gust loads are specified. Calculating the load requirements for craft, the most critical load factor is 5.3.

3.4. Department Responsibilities

The responsibilities for the requirements and constraints are divided over the five different departments. To ensure each department is aware which requirements they are responsible for, these are described hereafter.

3.4.1. Structures, Materials, and Manufacturing

by Andreas, Stan

The structures, materials, and manufacturing (SMM) department is responsible for sizing the main structure of the craft. This includes all SYS-STR requirements except SYS-STR-07. It also includes SYS-GHS-01 and SYS-GHS-01-R, which size the landing gear.

The SMM department is also responsible for the coupling system, and is thus responsible for all SYS-GCS requirements, and all SYS-GCS-R requirements except SYS-GCS-09-R. As part of the modular repair philosophy, SMM will also be responsible for requirements such as CON-TEC-06-R, CON-SUS-05, CON-SUS-06, and CON-SUS-07. Manufacturing and materials are also in the domain of SMM, therefore CON-OPS-11-R, CON-CST-03, and CON-CST-04 are also the responsibility of SMM. To account for the swappability and safety of the batteries, the SMM department will thus be responsible for meeting CON-OPS-01, SYS-PWR-07-R and SYS-PWR-11-R.

The SMM department will also focus on optimising the structures, material, and manufacturing of the design to minimise cost and mass.

3.4.2. Aerodynamics

by Filip

The aerodynamics department is responsible for designing the wing, part of the empennage, and the fuselage. The only relevant requirement for the aerodynamics (AERO) department is SYS-STR-07, which entails a requirement for a maximum wingspan of the craft of 80 m. This is the only requirement that the AERO department is constrained by. However, some other requirements must also be monitored by this department, namely ones linked to performance. This is due to the fact that the performance is directly linked to the lift and drag parameters of the craft, that are calculated by the AERO department.

3.4.3. Software, Stability, and Control

by Gerard, MianTao

The software, stability, and control (SSC) department is responsible for ensuring stability and controllability of the craft. To accomplish this, it sizes the both the horizontal and vertical stabilisers of the craft, as well as determining the position of the wing. To ensure grounded stability it also determines the location of the landing gear.

It shall also be in charge of designing the flight control software and flight managements software, therefore they they are in charge of all SYS-FMS and SYS-FCS requirements including SYS-FMS-21-R and SYS-FCS-05-R.

In addition, it is also responsible for the navigation and guidance systems, which determine the crafts state and its desired trajectory respectively. Therefore it is also responsible for SYS-GDC-02, both SYS-NAV requirements, and SYS-NAV-05-R. The requirements SYS-GDC-03, SYS-NAV-01 and SYS-NAV-02 have been replaced by SYS-FMS-22.

Finally it is responsible for designing the data management system, and therefore is responsible for SYS-DMS-02-R and SYS-DMS-03-R.

3.4.4. Airfield Performance, Operations, and Logistics

by Annika, Mees

The airfield performance, operations, and logistics (APOL) department ensures the design is feasible for operations in the end. For this, proper communication between each subsystem is crucial. SYS-COM-01

until and including SYS-COM-04 are therefore the responsibility of the APOL department. Furthermore, as surveillance is also relevant to the logistics of the mission, SYS-COM-05 and SYS-COM-06 are also assigned to the APOL department.

Next, more general operations regarding the craft during shipping are mentioned in CON-CST-05-R and CON-OPS-06. Emergency procedures are also a task of the APOL department, laid out in CON-OPS-07-R, CON-OPS-08-R, CON-OPS-09-R, CON-OPS-10-R, CON-OPS-13-R, SYS-PWR-08-R. The APOL department will also be in charge of ensuring a battery is replaced once its maximum capacity degrades below 80%, following CON-OPS-12-R. Furthermore, SYS-DMS-04-R, SYS-DMS-05-R, and SYS-STR-07-R are assigned to the APOL department due to their relation to maintenance of the craft. Then, SYS-DMS-01-R and SYS-GCS-09-R are relevant due to their focus on uncertainties, and in turn, safety procedures.

As mentioned previously, the APOL department will be responsible of ensuring all kinds of requirements are met in the end, following both CON-REG requirements. These focus on both the Certification Specification requirements and constraints as mentioned in Section 3.3, and the operational requirements as set by EASA. Next, the APOL department ensures the lifetime equivalent CO_2 emission of the craft stays within the bounds as mentioned in CON-SUS-03. Then, the APOL department is responsible for ensuring CON-SUS-04 is met, relating to the number of repairs performed locally on the craft. Following CON-CST-01 and CON-CST-02, not only the operational, but also the total cost of the craft shall be overseen by the APOL department. Next, the APOL department is in charge of ensuring the craft is compatible with gliders, following CON-TEC-04. Finally, the APOL department is responsible for ensuring the turn-around, block, deploy, and attachment time stay within their predetermined limits seen in CON-OPS-02, CON-OPS-03, CON-OPS-04, and CON-OPS-05.

3.4.5. Power, Performance, and Propulsion

by Annika, Christian

Naturally, the most important requirements relevant to the power, performance and propulsion (PPP) department are those with a code containing “PWR” and “PRO”. Specifically, all SYS-PWR requirements are considered, ranging from minimum and maximum power and voltage requirements to ensuring there is a battery of high enough capacity. Both SYS-PRO requirements and CON-SUS-02 are also extremely relevant, ensuring the electric propulsion system provides enough thrust.

Furthermore, there is a set of requirements on range and endurance in CON-TEC-01 and CON-TEC-02. Next, CON-TEC-03, CON-TEC-05, and CON-TEC-06 are requirements that naturally flow from the mission profile and existing typical requirements for tow craft. However, in case slight improvements or adjustments need to be made, it is the PPP department that is in charge of handling these requirements. Also, the PPP department is responsible for CON-SUS-01, ensuring that an adequate noise level is kept to while the propeller design ensues.

Finally, some requirements were revisited and revised. The PPP department will be in charge of ensuring a power indicator is present as per SYS-PWR-09-R. Next, SYS-PWR-10-R and SYS-PWR-12-R enunciate the importance of enough battery capacity for not only the engine, but also for other subsystems of the tow craft such as its avionics.

3.5. Department Interdependencies

by Everyone

Though it is now clear which requirements are the responsibility of each department, it should still be noted that requirements are not necessarily solely important to one department each. To show the in- and outputs of each department in relation to each other, a chart with interdependencies of the parameters is created in the shape of an N^2 chart as seen in Table 3.4. This N^2 chart will determine the communication between the different departments during the design process, including possible iterations.

Table 3.4: N^2 chart showing the interdependence's of all departments.

SMM	Weight, L/G Size	Weight	Weight, Battery Swap System, L/G Size	Weight, L/G Size	Manufacturing Cost
Fuselage Shape,Wing Size, Empennage, HLD, Airbrakes	AERO	Wing Size, AR, HLD, Empennage, Control Surfaces, Stability Derivatives, Lift Performance, Airbrakes	Lift and Drag Performance during Take-Off and Landing	Wing Size, AR, HLD, Empennage, Control Surfaces, Stability Derivatives, Lift and Drag Performance	
Wing Position, Dihedral, Control Surfaces, Hinge Moments, L/G Position	Wing Position, Empennage Volume, Sweep, Dihedral, Control Surface Volume	SSC		Software	Software
Mission Profile, Operational Procedures	Mission Profile, V_{tow}, $V_{landing}$, Sensor Volume	Mission Profile, Sensor Volume	APOL	Mission Profile, $N_{battery}$, Take-Off Thrust	$s_{Take-Off}$, $s_{Landing}$, Communications, Ground Storage, Operational Procedures
Battery Mass, N_{engine}, $N_{propeller}$, Propeller Size, Thrust	Battery Mass, N_{engine}, $N_{propeller}$, Propeller Size, Thrust	Thrust	Battery Capacity	PPP	Mission Energy Usage, Thrust, Climb Angle, RPM
Load Envelope, V_{stall}, V_{dive}, V_{ne}	Load Envelope, V_{stall}, V_{dive}	Load Envelope, V_{stall}, V_{dive}, V_{ne}	Load Envelope, V_{stall}, V_{dive}, V_{ne}	Load Envelope, V_{stall}, V_{dive}, V_{ne}	OTHER

4

Subsystem Design Methodology

This chapter will discuss the methodology used to design the subsystems of the five departments. These tools are used later on in the form of an iterative process to ensure a coherent design is reached.

4.1. Structures, Materials, and Manufacturing (SMM)

by Andreas, Stan

This section discusses the subsystem design for the Structures, Materials and Manufacturing (SMM) department. It is split up into a Class II Weight estimation, initial wing structure design, initial fuselage structure design, and initial landing gear design.

4.1.1. SMM Flow Diagram

The flow diagram for the SMM department can be seen in Figure 4.1. This diagram is split up into: inputs, subsystem design, and outputs. The subsystem design describes the major blocks the SMM department designs: a Class II Weight estimation, the wing structure design, the fuselage structure design, and the landing gear structure design.

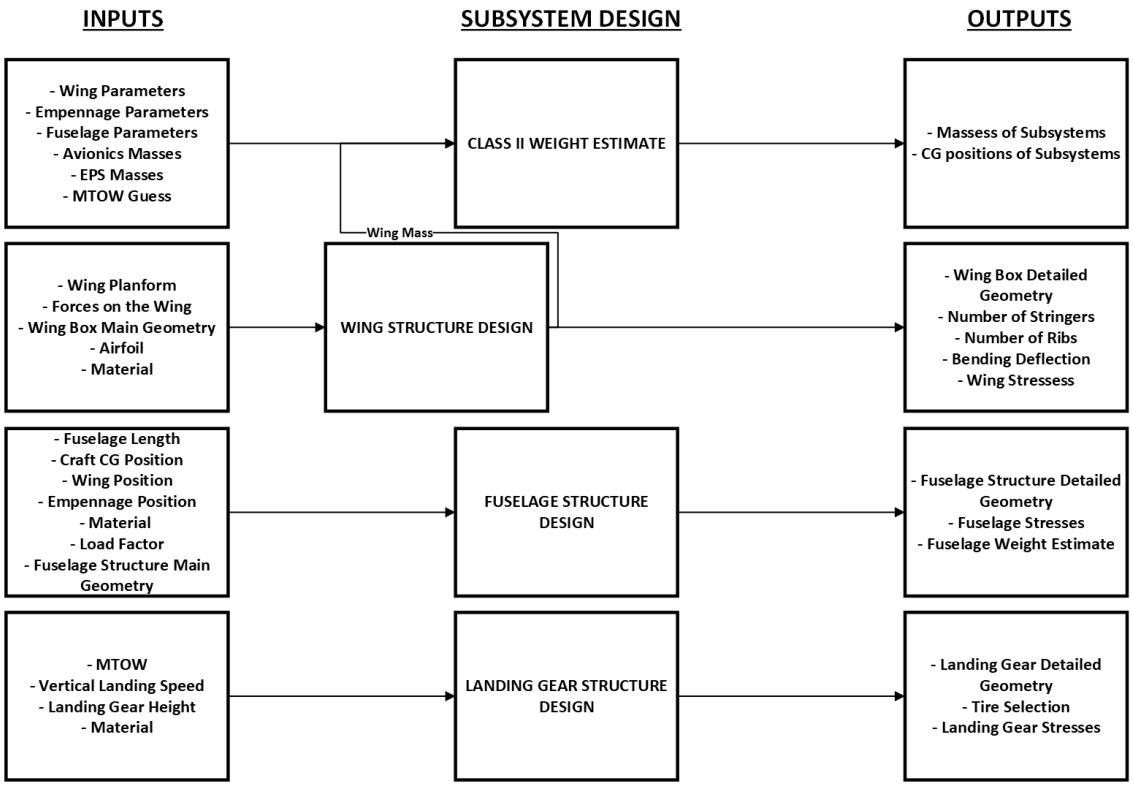

Figure 4.1: Flow diagram for the SMM department

4.1.2. Class II Weight Estimation

The Class II Weight estimation is used to get a second order preliminary number of the weights of several components in the craft. The maximum take-off weight of the craft is estimated using Equation 4.1.

$$W_{\mathrm{TO}} = W_E + W_{\mathrm{Bat}} \tag{4.1}$$

Here W_E is the empty weight of the craft, and W_{Bat} is the battery weight. W_E can be further divided into several groups as seen in Equation 4.2.

$$W_E = W_{\text{structure}} + W_{\text{PWR}} + W_{\text{FEQ}} \tag{4.2}$$

Here $W_{\text{structure}}$ is the structural weight, W_{PWR} is the weight from the propulsion group (without the batteries) and W_{FEQ} is the fixed equipment weight. The structural weight is specified as seen in Equation 4.3.

$$W_{\text{structure}} = W_W + W_{\text{emp}} + W_f + W_{\text{NG}} + W_{\text{MG}} \tag{4.3}$$

Here W_W is the wing weight, W_{emp} is the empennage weigth, W_f is the fuselage weight, W_{NG} is the nose gear weight and W_{MG} is the main gear weight. Note that imperial units are used where not specified.

Fuselage

Fuselage weight is estimated using an empirical formula from Roskam [7]. This equation relates fuselage length, width, and heigth, along with the design cruise speed and take off weight. Equation 4.4 shows the relation using imperial units.

$$W_f = 200 \left[\left(\frac{W_{\text{TO}} \cdot n_{\text{ult}}}{10^5} \right)^{0.286} \left(\frac{l_f}{10} \right)^{0.857} \left(\frac{w_f + h_f}{10} \right) \left(\frac{V_C}{100} \right)^{0.338} \right]^{1.1} \tag{4.4}$$

Here W_f is the weight of the fuselage, W_{TO} is the take off weight, n_{ult} is the maximum load factor given by CS-22, w_f , h_f, and l_f are maximum width, height, and length of the fuselage, and finally V_c is the cruise speed in KEAS.

Wing

The wing weight is estimated using an empirical formula as seen in Equation 4.5 [7].

$$W_W = 96.948 \left[\left(\frac{W_{\text{TO}} \cdot n_{\text{ult}}}{10^5} \right)^{0.65} \left(\frac{A}{\cos\left(\Lambda_{1/4}\right)} \right)^{0.57} \left(\frac{S}{100} \right)^{0.61} \left(\frac{1+\lambda}{2} \left(\frac{t}{c} \right)_m \right)^{0.36} \left(1 + \frac{V_H}{500} \right)^{0.5} \right]^{0.993} \tag{4.5}$$

In this equation: $\Lambda_{1/4}$ is the wing quarter chord sweep angle, A is the aspect ratio of the wing, S is the wing surface area in feet squared, λ is the wing aspect ratio, $\left(\frac{t}{c}\right)_m$ is the maximum thickness to chord ratio of the wing airfoil and V_H is the maximum level airspeed in KEAS.

Empennage

The empennage weight estimate consists of the horizontal and vertical tail surface as seen in Equation 4.6. These estimates are the USAF estimates compiled by Roskam, presented in Equation 4.7, Equation 4.8.

$$W_{emp} = W_h + W_v \tag{4.6}$$

$$W_h = \frac{3.184 W_{TO}^{0.887} \cdot S_h^{0.101} \cdot A_h^{0.138}}{174.04 t_{r_h}^{0.223}} \tag{4.7}$$

$$W_V = \frac{1.68 W_{TO}^{0.567} \cdot S_V^{1.249} \cdot A_V^{0.482}}{639.95 t_{r_V}^{0.747} \cdot \cos\left(\Lambda_{1/4_V}\right)^{0.882}} \tag{4.8}$$

In both cases, t_r is the thickness of the root of the vertical/horizontal tail. $\Lambda_{1/4_V}$ is the sweep at the quarter chord point of the vertical tailplane.

Landing Gear

The landing gear weight from Raymer is split into the nose and main gear and assumes a retractable gear. A reduction of 1.4 % in gear mass can be applied to correct for a non-retractable gear.

$$W_{\text{main landing gear}} = 0.095(N_l \cdot W_l)^{0.768} \left(\frac{L_m}{12}\right)^{0.409} \tag{4.9}$$

$$W_{\text{nose landing gear}} = 0.125(N_l \cdot W_l)^{0.566} \left(\frac{L_m}{12}\right)^{0.845} \tag{4.10}$$

Here, W_l is the landing design gross weight, which, in this case, is equal to the take off weight. N_l is the ultimate landing load factor ($n_{gear} \cdot 1.5$) and L_m is the length of main gear in meters.

Power and Propulsion

Estimating electric engine weights for aircraft presents problems due to the limited data available. Instead of sizing the propulsion system using empirical methods, a 'fixed' approach is taken; a set of off the shelf available motors and controllers are collected, along with their total mass. The calculated power required isused to select engines, and their actual mass is then added to the calculation.

The battery mass is estimated using Equation 4.11.

$$M_{\text{Bat}} = \frac{\left(\frac{P_{\text{Req}}}{\rho_{\text{Bat}}}\right)}{\eta_{\text{Bat}}} \cdot t \tag{4.11}$$

Here: P_{Req} is the required maximum power in Watts, ρ_{Bat} is the battery specific energy in watt hours per kilogram, t is the amount of time the battery is used, and η_{Bat} is the efficiency of the battery.

The propeller weight is estimated using the mass of existing propellers.

Fixed Equipment

The fixed equipment weight consists of the elements seen in Equation 4.12.

$$W_{\text{FEQ}} = W_{\text{fc}} + W_{\text{els}} + W_{\text{iae}} + W_{\text{ops}} + W_{\text{fti}} + W_{\text{aux}} + W_{\text{bal}} + W_{\text{pt}} + W_{\text{etc}} \tag{4.12}$$

Here: W_{fc} is the flight control system weight, W_{els} is the electrical system weight, W_{iae} is the instrumentation, avionics, and electronics system weight, W_{ops} is the weight of operational items , W_{fti} is the flight test instrument weight, W_{aux} is the auxiliary systems weight, W_{bal} is the ballast weight , W_{pt} is the paint weight, and W_{etc} is any additional weight not covered by other categories. For this analysis, it is assumed to be zero. These weights will be obtained using off-the-shelf components. Due to the early phase of the design, a technology factor of 1.3 is applied to the fixed empty weight to account for additional systems that may be required as the design progresses.

Instrumentation, Avionics, and Electronics

Existing empirical methods for estimating avionics mass only exist for significantly larger craft, thus these equations give significantly higher masses than would be expected for the tow craft. When using these methods, the avionics mass would make up half of the take-off mass. Instead it is decided to determine the mass by selecting off the shelf avionics and tallying up the mass. More detail on chosen avionics hardware is presented in Section 9.1. The total mass of the selected avionics components is 13 kg.

Auxiliary Systems

A ballistic parachute is included in the fixed equipment mass. An initial mass of 10 kg is used based on commercially available systems.

Flight Control System

The USAF method is once again used for estimating the weight of flight controls. This method does not account for more-electric aircraft with fully electric flight control systems, for this reason, this mass estimate will likely be higher than what is expected to be the true flight control system mass.

$$W_{\text{fc}} = 1.066 W_{\text{to}}^{0.626} \tag{4.13}$$

4.1.3. Wing Structure Design

For a more detailed analysis of the structure and weight of the wing, a wing box is designed and analysed for the load factors given by the requirements. Bending, shear, and thin sheet buckling are analysed. This is done by first specifying the wing box geometry, then assessing wing bending, and finally wing shear. The designed geometry is shown in Figure 4.2

Figure 4.2: Wing cross section.

Wing Box Geometry

A wing box structure is chosen for the structural analysis. Figure 4.3 shows the assumed wing box configuration. Here it is assumed that the front and rear spar have the same height, the top and bottom sheets have the same width, the number of stringers on top is the same as the number of stringers on the bottom and there are no stringers on the spars. The number of stringers is variable.

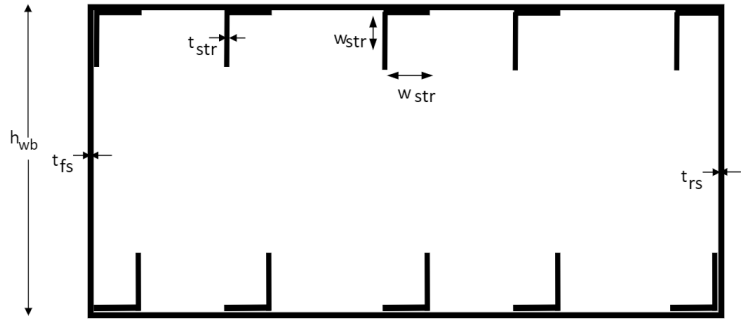

Figure 4.3: Geometry of the wing box.

In this figure, h_{wb} is the height of the wing box. w_{wb} is the width of the wing box, t_{fs} and t_{rs} are the thicknesses of the front and rear spar respectively. t_{ts} and t_{bs} are the thicknesses of the top and bottom sheet respectively, w_{str} is the width and height of a stringer. t_{str} is the thickness of a stringer, and n_{str} is the total number of stringers.

Several properties are obtained from this geometry. First of all the centroid can be found using Equation 4.14.

$$\bar{x} = \frac{\sum \tilde{x}_i \cdot A_i}{\sum A_i} \qquad \bar{z} = \frac{\sum \tilde{z}_i \cdot A_i}{\sum A_i} \tag{4.14}$$

Here: $\bar{x}$ and $\bar{z}$ are the coordinates of the centroid of the wing box, $\tilde{x}$ and $\tilde{z}$ are the local centroid coordinates of the separate parts which the wing box consists of, and A is the area of a certain part.

Secondly, the moment of inertia about both the x and z axis can be obtained using Equation 4.15.

$$I = \sum_i \bar{I}_i{}' + A_i \cdot d_i^2 \tag{4.15}$$

Here, $\bar{I}_i{}'$ is the local moment of inertia, A_i is the area, and d_i is the distance from the centroid to the desired part. The axis which the distance is relative to, depends on the required moment of inertia. The local moment of inertia can be obtained using Equation 4.16.

$$\bar{I}_i{}' = \frac{1}{12} w_i \cdot h_i^3 \tag{4.16}$$

Here, w_i and h_i are the width and height of the rectangle relative to the axis the moment of inertia is calculated around.

Besides geometrical properties, the mass of the wing box can be obtained by assuming that the cross sectional area of the wing box varies linearly with the span-wise location. This assumption is not entirely correct, but it is used as this is a preliminary wing box calculation. This yields Equation 4.17 is integrated to obtain the structural volume of the wing box.

$$A = A_{\text{rc}} - \frac{dA}{dy} y \tag{4.17}$$

Here A_{rc} is the cross sectional area of the wing box at the root of the wing, $\frac{dA}{dy}$ is the change in cross sectional area of the wing box with respect to the span, and y is the span-wise location. Multiplying the structural volume of the wing box by the density of the material used, results in the preliminary mass of the half wing.

Wing Bending

The wing box is analysed for bending moments around the x-axis. This analysis is done at the root of the wing. For this analysis, the wing box is treated as a beam with bending stress given by Equation 4.18.

$$\sigma = \frac{-M \cdot y}{I} \tag{4.18}$$

A visual interpretation is given in Figure 4.4.

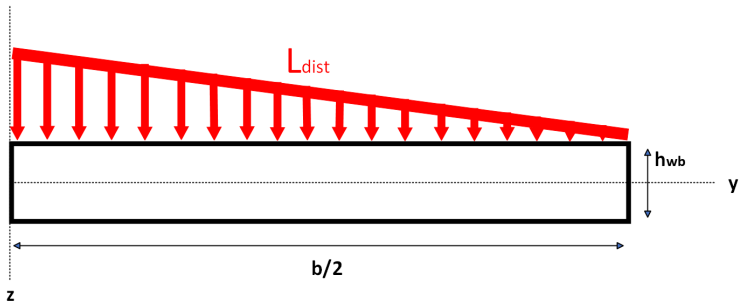

Figure 4.4: Wing simplification for wing box analysis.

Here, b is the wing span and the moment results from the distributed load L_{dist}. Note that the distributed load is given in the positive direction, where in reality the distributed lift force will be used which points in the opposite direction.

The wing is designed such that the bending stress at the top and bottom of the wing do not exceed yield strength, and that the top plate does not buckle. The main influence on bending moment resistance is coming from the stringers in the wing box as these have the largest contribution to the moment of inertia. A tool is created which iterates over several stringer thicknesses to find a minimum thickness which would result in compliance with the allowed yield stress of the wing box.

The buckling stress of the top plate is determined using Equation 4.19.

$$\sigma = \frac{\pi^2 E \cdot K_{\text{cr}}}{12(1-\nu_e^2)} \left(\frac{t}{b}\right)^2 \tag{4.19}$$

Here E is the modulus of elasticity, K_{cr} is the compressive buckling coefficient and is determined by fitting a cubic spline to the fully clamped buckling coefficient shown as line 'A' in Figure 4.5. $\frac{a}{b}$ is determined by the stringer and rib spacing. ν_e is the Poisson ratio, t is the thickness of the plate and b is the width of the plate. A tool is created that would automatically determine the rib and stringer placement to prevent buckling or yield failures. This tool iterates over several numbers of ribs to find a minimal amount which results in no buckling of the top sheet.

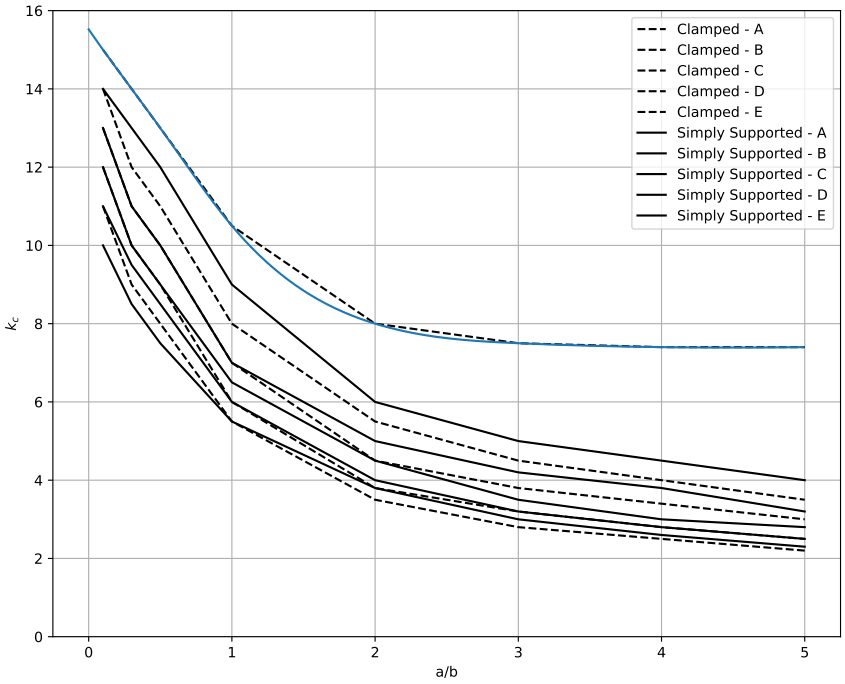

Figure 4.5: Compressive buckling coefficient for thin sheets.

Wing Shear

The torsion on the wing from the lifting force is also calculated using a boom-sheet simplification, with the stringers acting as booms, and the airfoil skin and spars acting as sheets that only carry shear. The shear flow in each sheet is calculated, giving the required thicknesses and stringer sizes. The method of wing structure analysis using boom simplification is based on the method from Megson [8]. The shear flow is calculated using Equation 4.20

$$q_s = \frac{-S_{y,w}}{I_{xx}} \sum_{r=1}^{n} B_r \cdot Y_r + q_{s,0} \tag{4.20}$$

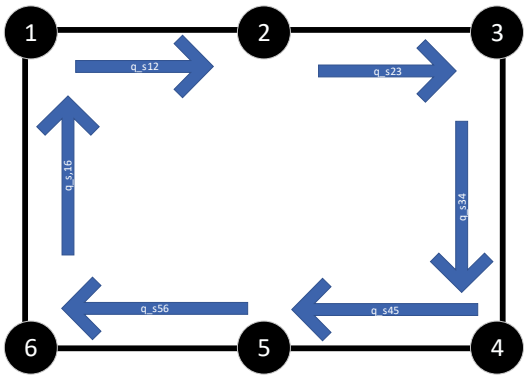

Figure 4.6: Boom-sheet simplification for shear flows.

The shear stress is calculated using Equation 4.21. The sheet thicknesses are iterated upon such that the shear strength is not exceeded.

$$\tau = \frac{q_s}{t} \tag{4.21}$$

τ is the shear stress in a plate, q_s is the shear flow in a plate, and t is the thickness of the plate.

4.1.4. Fuselage Structure Design

For the fuselage structure, two methods are considered, the more conventional "stringer-sheet" design, commonly used in pressurised aircraft, and a truss structure, commonly used in ultralights.

The stringer-sheet design consists of thin sheets, forming the skin of the aircraft, and stringers which carry the majority of the loads acting on the airframe. This design is very efficient, and would probably result in the lowest possible fuselage mass. Unfortunately, this method has significant manufacturing costs associated with it. Stringers require many flush rivets and precision machined parts. This increases the time and capital required for assembling the fuselage. A truss structure, more common on ultralight and older general aviation craft, is less efficient, but significantly cheaper to produce.

The design of the fuselage is done is several steps. First the layout of the truss structure is defined. This layout can be seen in Figure 4.7 and Figure 4.8.

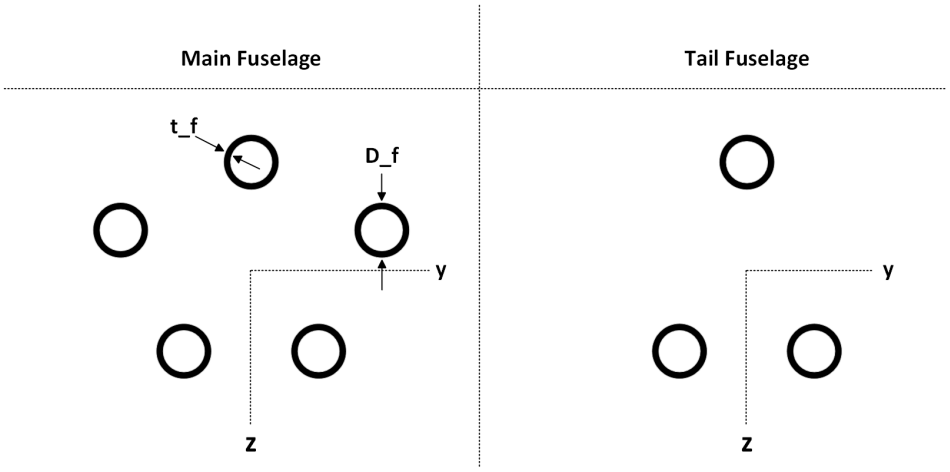

Figure 4.7: Fuselage cross section.

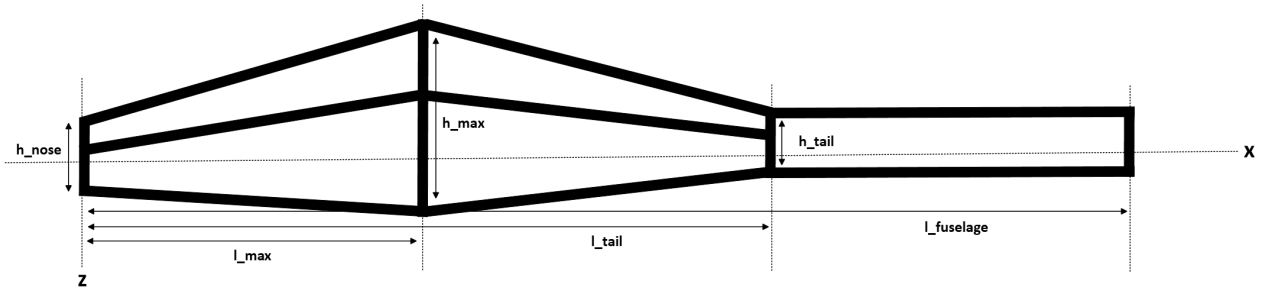

Figure 4.8: Fuselage side view.

Here t_f is the thickness of the tubes in the fuselage structure and D_f is the diameter of these tubes. h_{nose}, h_{max}, and h_{tail} are the nose, maximum, and tail fuselage heights respectively. l_{max}, l_{tail}, and l_{fuselage} are the distance to the maximum fuselage height, distance to the tail fuselage and total fuselage length respectively.

The main tubes presented in Figure 4.7 and Figure 4.8 will be connected to each other with multiple other trusses, however to simplify this analysis, they are left out. To size the tubes of the fuselage frame, the structure is analysed at maximum load factor of 5.3. This load case can be seen in Figure 4.9.

Here: L_w and L_h are the lift of the wing and horizontal tail respectively, in Newtons. M_{ac} is the moment

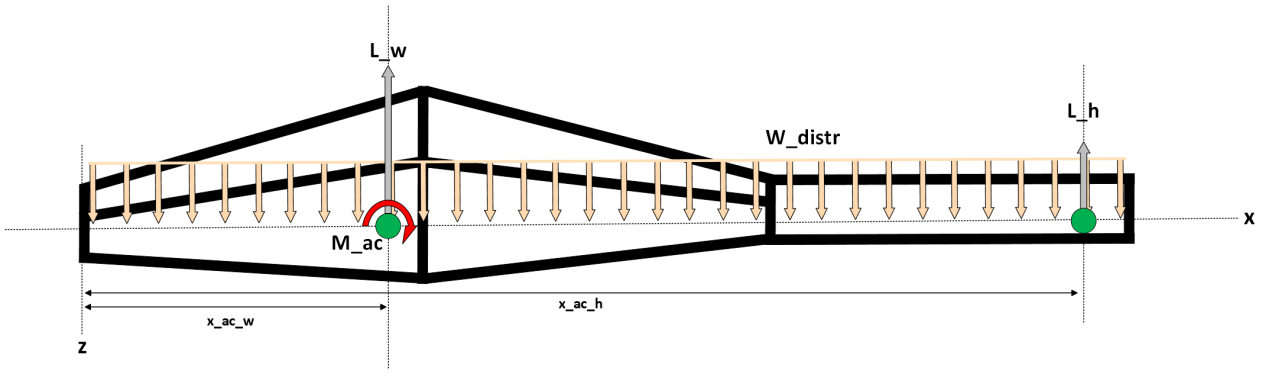

Figure 4.9: Aerodynamic forces on the fuselage

around the aerodynamic centre of the wing in Newton meters, W_{distr} is the distributed maximum take-off weight of the craft in Newtons. x_{ac_w} and x_{ac_h} are the distances to the aerodynamic centre of the wing and aerodynamic centre of the horizontal tail respectively.

The required moment of inertia is obtained using the same approach as seen in Subsection 4.1.3. The moment is obtained by making a moment diagram from Figure 4.9. This analysis will result in the minimum tube thickness needed to avoid yielding of the tubes.

4.1.5. Landing Gear Structure Design

For the sizing of the landing gear, the certification and specification requirements mention that the landing gear should be able to absorb 1.44 times the energy created by landing with a vertical speed of 1.77 m/s [9]. This kinetic energy is assumed to be fully converted to spring potential energy by the landing gear. This results in the energy relation as seen in Equation 4.22.

$$1.44\frac{1}{2}m \cdot V^2 = \frac{1}{2}k \cdot \delta^2 \tag{4.22}$$

Here, m is the mass of the moving object in kilograms, V is the vertical velocity of the moving object in meters per second, k is the spring stiffness of the landing gear system and δ is the axial deflection of the landing gear system.

The landing gear is simplified to the configuration as seen in Figure 4.10 and Figure 4.11, to obtain its spring stiffness.

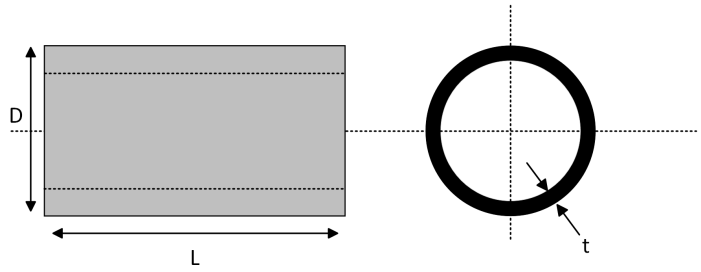

Figure 4.10: American projection of one cylinder in the landing gear.

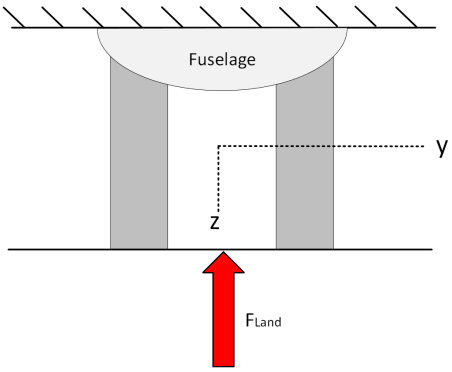

Figure 4.11: Force induced on the landing gear.

Here, L is the length of the landing gear, D is the diameter of the hollow cylinders and t is the thickness of the hollow cylinders. for such a system with two beams in parallel, the spring stiffness is given as seen in Equation 4.23 [10].

$$k = k_1 + k_2 = \frac{E_1 \cdot A_1}{L_1} + \frac{E_2 \cdot A_2}{L_2} = 2\frac{E \cdot A}{L} \tag{4.23}$$

Here: E is the modulus of elasticity of the material used and A is the cross sectional area of the hollow cylinder. It is assumed that the two cylinders are identical.

From Hooke's law, the deflection of the beam system is as seen in Equation 4.24.

$$\delta = \frac{F_{\text{land}} \cdot L}{A \cdot E} \tag{4.24}$$

Here, F_{land} is the force introduced from landing (also seen in Figure 4.11). Substituting Equation 4.23 and Equation 4.24 into Equation 4.22 and reordering the equation results in Equation 4.25.

$$F_{\text{land}} = \sqrt{\frac{1.44 \frac{1}{2} m \cdot V^2}{\frac{L}{A \cdot E}}} \tag{4.25}$$

With the landing force defined, the landing gear is now assumed to be as seen in Figure 4.12.

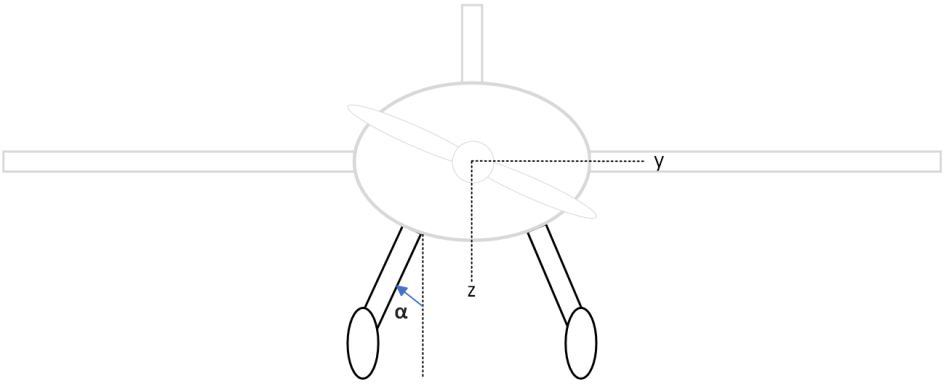

Figure 4.12: Landing gear under an angle.

In this visualisation the landing gear is put under an angle α to better simulate the outline of the real landing gear. The force on one of the cylinders in the landing gear is thus exposed to an axial force component and a lateral force component. The axial component is used in the analysis for buckling of the cylinder and the lateral component is used for bending of the cylinder.

The buckling force of a cylinder is given in Equation 4.26 [11].

$$F_{\text{buckl}} = 0.93A \cdot E \left(\frac{t}{r}\right)^{3/2} \left(\frac{r}{L}\right) \tag{4.26}$$

Here: t is the thickness of the cylinder in meters, and r is the radius of the cylinder in meters. Equating Equation 4.25 (this force is divided by two as the total force is split over the two landing gear cylinders) and Equation 4.26 will result in the minimum thickness required for buckling, with a specified radius of the cylinders.

Bending of the landing gear can be compared to the wing bending discussed in Subsection 4.1.3. The moment is caused by the lateral component of the force induced by landing. The yield stress of the material used will determine the minimum thickness of the landing gear cylinders.

The maximum of the two thicknesses presented will be used as the thickness of the landing gear cylinders.

4.2. Aerodynamics (AERO)

by Filip, Niels

The aerodynamic design of *MARCUS-T* is concerned with the loads exerted on the aircraft by the airflow around it. The main aspects that are considered in this section are the airfoil selection, the wing sizing and shaping, and the general configuration of the aircraft. These aspects should not be considered to be standalone, but rather part of the integrated design. The overview of steps taken to calculate the aerodynamical parameters in the iteration loop is presented in Figure 4.13.

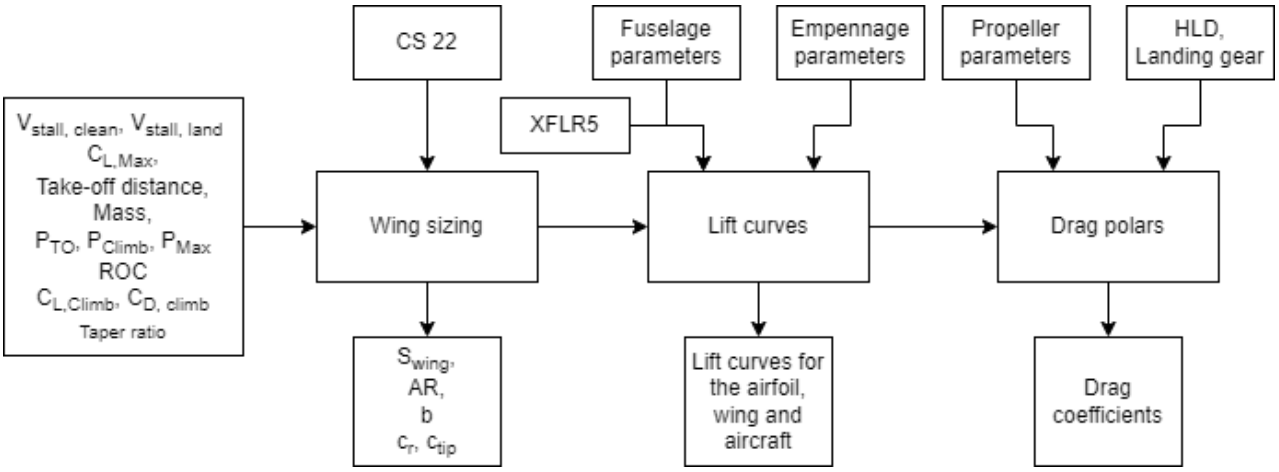

Figure 4.13: Flowchart of aerodynamical calculations.

4.2.1. Airfoil Selection

In this section the airfoil of the craft is selected. Choosing the right airfoil is essential for the performance of the final product. Therefore multiple parameters are taken into consideration such as aerodynamic performance, climb performance, weight, and cost.

The market study in the Baseline Report concluded that cost, and thus weight as they are closely linked together, is most limiting for the design [2]. Therefore, it is decided that a relatively thick airfoil should be selected, in the order of a thickness-to-chord ratio of 15-20%. This will reduce the design challenges for the structural integrity of the wings when high aspect ratios are applied. The high aspect ratio is needed to comply with the CS-22 requirement stated in Equation 3.1.

First the range of Reynolds numbers needs to be determined. This is done for the airspeed range between 60 km/h and 280 km/h (as specified in operations), the air density, ρ, of $1.225 kg/m^3$, for the chord lengths, c, specified in Table 5.3, and the dynamic viscosity, μ is 1.802×10^{-5} kgms.

$$Re = \frac{\rho \cdot V \cdot c}{\mu} \tag{4.27}$$

Then to determine Re_{min} and Re_{max} the lowest airspeed together with the smallest chord length, and the highest airspeed with the largest chord length were used. This resulted in $Re_{min} = 382,000$ and $Re_{max} = 4,000,000$. For slow aircraft, Raymer mentions the laminar airfoil Wortmann series in his book, which is further investigated as a possible airfoil choice [12]. The lower part of the specified Reynolds number range matches the airfoils from the Wortmann series best, the higher calculated range is only reached during the return dive flight where aerodynamic efficiency is not of high priority [13].

The tow craft is optimised for climb as this is the most important mission segment. To obtain a good climb performance, $C_L^{3/2}/C_D$ needs to be maximised [7]. This needs to be done for both the airfoil and the wing. From the Wortmann catalogue multiple airfoils, including the FX 66-17AII-182, FX 60-177, FX61-184, and the FX 66-S-196 V1, are analysed. The latter two having the best performance for the climb performance parameter. However, in the paper from Gooden it is mentioned that the FX 66-S-196 V1 airfoil is very sensitive to dust particles as shown in a windtunnel test [14]. This results in poor performance when the wing is subjected to bugs or dirt during normal operations. After consulting with aerodynamics expert Ir. Loek Boermans, it is decided to not use the Wortmann FX series airfoils. This decision is based on the high sensitivity to disturbances of those airfoils and the fact that research of this series was discontinued by professor Wortmann himself[1].

Ir. Loek Boermans recommends to use the DU15-160/15 airfoil he designed for the wing root of the EB29R Open Class glider. This airfoil has a thickness-to-chord ratio of 16%. It provides good climb characteristics, especially in turbulent conditions which are often experienced in the lower atmosphere with thermal activity.

[1] As specified by Ir. Loek Boermans.

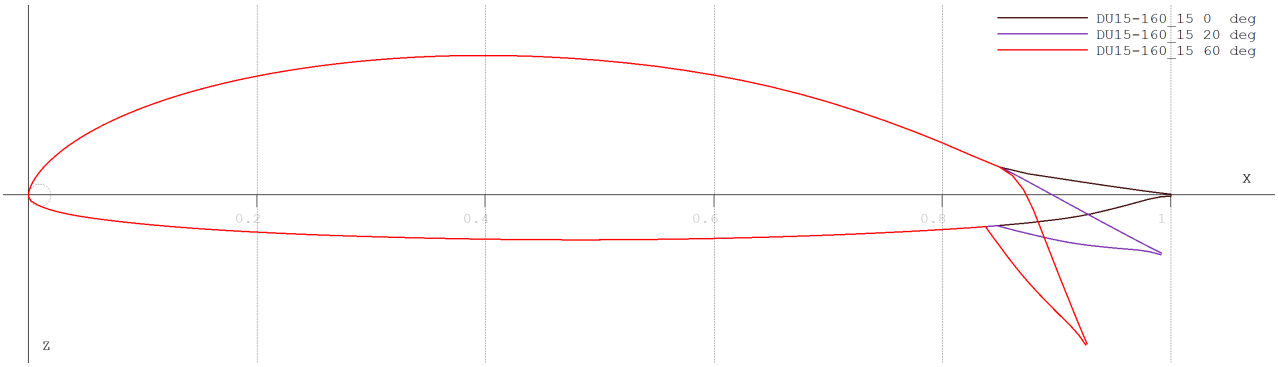

Figure 4.14: DU15-160/15 airfoil section, as designed by Ir. Loek Boermans, at 0, 20, and 60 degree flap deflection.

It should be noted that the flap deflections in Figure 4.14 are only illustrative and not the actual flap type used, that will be discussed in Subsection 4.2.2. The chord-wise location of the flap hinge is at 85% from the leading edge, as recommended by Ir. Boermans.

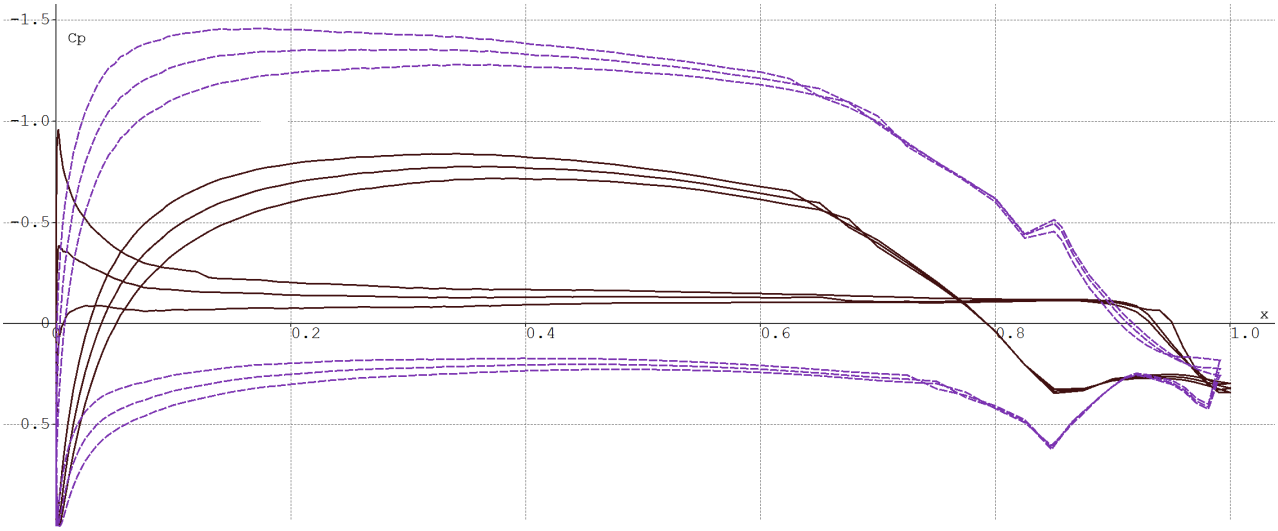

Figure 4.15: Pressure distribution at flap deflection of 0 degrees (black, continuous line) and 20 degrees (purple, dashed line). Ranging from an angle of attack of -1 to 1 degrees at Re = 3,000,000.

The airfoil is characterised by its high degree of laminar flow, which is up to 95% at a flap deflection of 0 degrees on the lower side. With a laminar flow on the upper side close to 83% at a flap deflection of 20 degrees as can be seen in Figure 4.15. To obtain these results in reality, the flap gap should be sealed using Mylar tape[2] such that it covers the gap during all flap deflection angles. Furthermore, zigzag tape is applied to force transition from laminar to turbulent flow, avoiding the added drag at low speeds, when separation bubbles might occur. According to Ir. Boermans the turbulator tape should be placed at 92% of the chord, on the underside of the airfoil. This can be confirmed when evaluating Figure 4.15. The separation location of the lower side of the airfoil is located at approximately 95% chord length. However, this is optimised for glider cruise flight. The tow craft is optimised for climb at a flap deflection of 20 degrees, as this is the flap deflection when the highest climb parameter can be achieved. Therefore, turbulator tape should be applied at the underside of the airfoil at 72% chord length, to avoid the transition occurring at 75% chord length during the climb phase condition.

[2]Pre-curved tape used to seal gaps between glider components to improve the airflow around them.

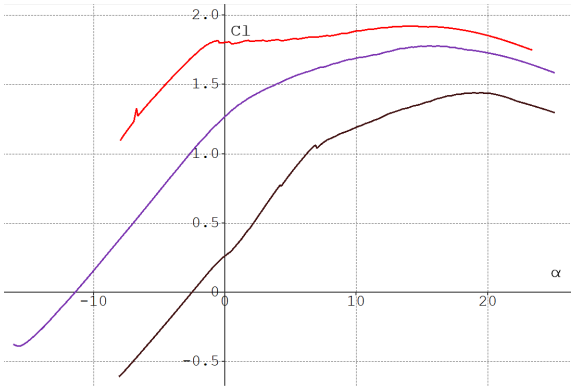

Figure 4.16: DU15-160/15 airfoil Cl-alpha curve for flaps setting of 0 (black), 20 (purple) and 60 (red) degrees at Re = 3,000,000.

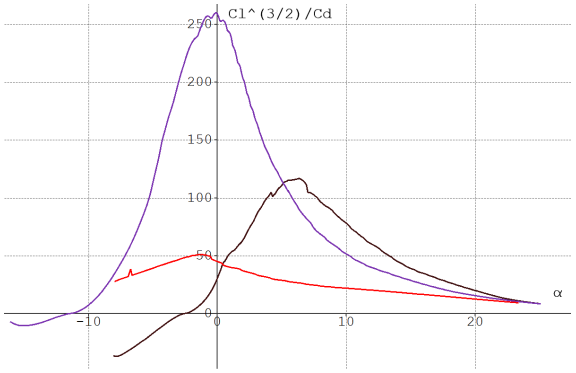

Figure 4.17: DU15-160/15 airfoil $C_l^{3/2}/C_d$-alpha curve for flaps setting of 0 (black), 20 (purple) and 60 (red) degrees at Re = 3,000,000.

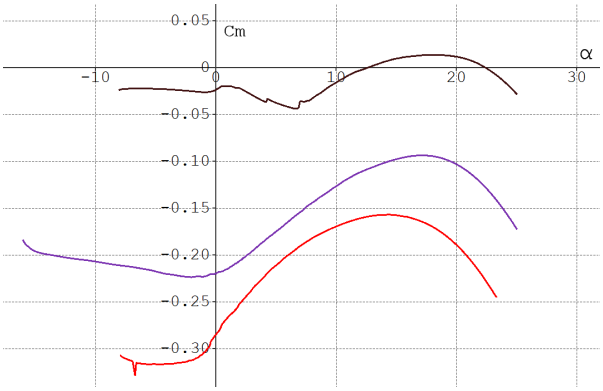

Figure 4.18: DU15-160/15 airfoil Cm-alpha curve for flaps setting of 0 (black), 20 (purple) and 60 (red) degrees at Re = 3,000,000.

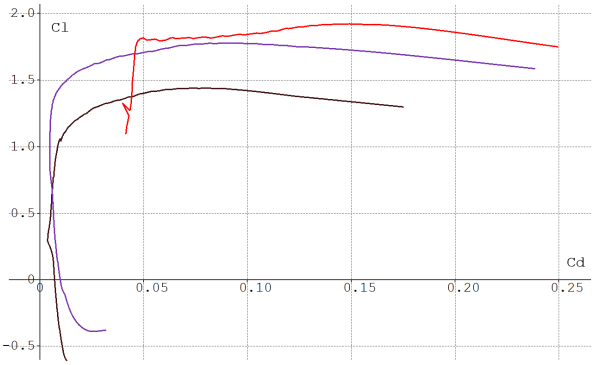

Figure 4.19: DU15-160/15 airfoil Cl-Cd curve for flaps setting of 0 (black), 20 (purple) and 60 (red) degrees at Re = 3,000,000.

The data from Figures 4.16, 4.17, 4.18, and 4.19 are obtained from an analysis with XFLR5. For the airfoil a maximum C_l value of 1.4 can be obtained. With a plain flap deflection of 20 degrees, a C_l of 1.7 is obtained. A (plain) flap deflection of 60 degrees gives a maximum lift coefficient that increases to 1.9. It should be noted that XFLR5 can only provide indicative values for maximum lift coefficients as viscous effects in flows are not well modelled. These become dominant in the stall regime especially for large flap deflections. The maximum lift coefficients of 1.40 and 1.77 are assumed to be sufficiently accurate for the Class II Aerodynamic Lift and Drag estimations. In Figure 4.17, the climb performance parameter, $c_l^{3/2}/c_d$, is shown. The best climb performance is obtained with a flap deflection of 20 degrees at -0.1 degrees angle of attack. Therefore it has been decided to use the airfoil only in its 20 degree flap deflection setting for the aerotow manoeuvre. The use of flaps is discussed in Subsection 4.2.2.

4.2.2. Wing Planform

The wing planform, together with the selected airfoil, has the most influence on the aerodynamic performance of the craft. In this subsection the configuration of the wing planform is discussed.

The wingspan, b, is in this case determined by the CS-22 requirement as given in Equation 3.1. When considering a margin of 0.2, the minimum wingspan is given with Equation 4.28.

$$b_{min} = \sqrt{\frac{MTOM}{2.8}} \tag{4.28}$$

$$AR = \frac{b^2}{S} \tag{4.29}$$

The aspect ratio is a function of both wingspan and surface area. The surface area, S, is obtained from the iterations performed in Chapter 5. This gives the aspect ratio as demonstrated in Equation 4.29.

According to Gudmundsson, using a taper ratio offers several benefits [15]. Of particular importance to this project are the reduced bending moments, improved aerodynamic efficiency by approximating the elliptical

lift distribution, and the geometric simplicity that facilitates easier manufacturing compared to an elliptical planform. Scholz's paper suggests an optimal taper ratio of 0.45, which is applied in this design [16]. The chord and tip length are found with Equation 4.30 and Equation 4.31, which result in a mean aerodynamic chord (MAC) as specified by Equation 4.32.

$$C_r = \frac{2 \cdot S}{b \cdot (1 + \lambda)} \tag{4.30}$$

$$C_t = C_r \cdot \lambda \tag{4.31}$$

$$MAC = \frac{2}{3} \cdot C_r \cdot \left(\frac{1 + \lambda + \lambda^2}{1 + \lambda} \right) \tag{4.32}$$

From a structural and operational standpoint, it is deemed that the tow craft will have problems with an aft centre of gravity. Therefore, Gudmundsson advises to use a straight leading edge and a swept trailing edge [15]. According to Raymer this is also beneficial for low speed flight, and in accordance with the historical trend line presented in his book [12, figure 4.20].

The pitching moment of the wing is found using Equation 4.33, assuming the leading edge sweep is zero [17]. A zero lift pitching moment of -0.22 for the airfoil with 20 degree flap deflection is obtained from Figure 4.18.

$$C_{m_{ac_w}} = C_{m_{0airfoil}} \cdot \left(\frac{AR}{AR + 2} \right) \tag{4.33}$$

High-Lift Devices

In order to enhance the overall performance of the tow craft, high lift devices (HLD) are used. During take-off they are used to increase the lift coefficient, and during landing they increase the lift and drag coefficients of the craft. As the craft will be optimised for the takeoff and climb phase, the 20 degree flap deflection airfoil as displayed in Figure 4.14, is chosen to be the standard, clean configuration, from now on. In this flap setting the airfoil obtains the maximum $C_l^{3/2}/C_d$, beneficial for climb performance. Apart from the takeoff and climb phase, there are no other flight phases in need of high C_L with relative low drag. The return flight phase requires high drag to allow for a steep dive without exceeding the maximum speed.

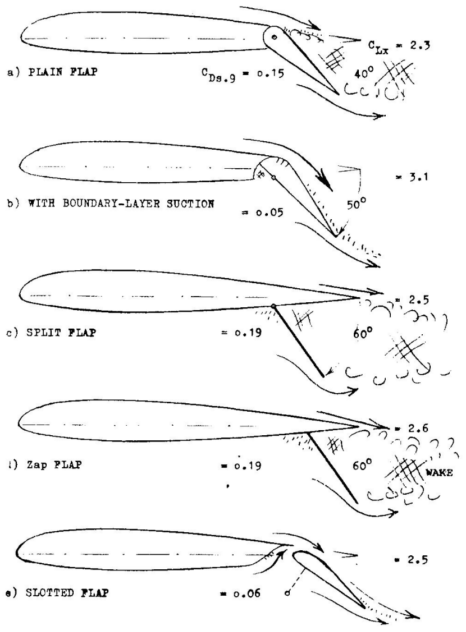

Figure 4.20: Types of trailing edge flaps [18].

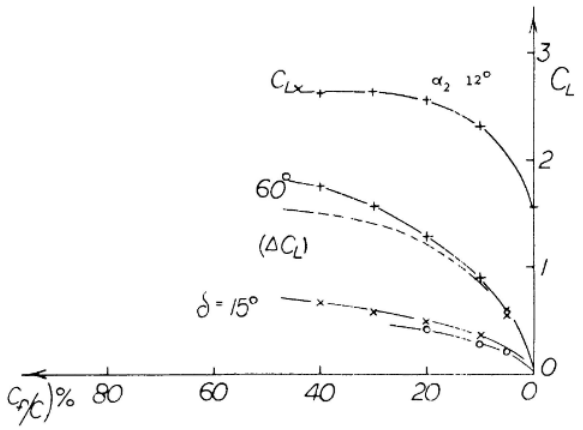

Figure 4.21: Lift increments for a split flap as a function of flap-chord ratio [18, p. 5-7, fig. 7].

After considerations of multiple flap types from Figure 4.20, it is decided to use a split flap for the return and landing phase. This type of flap allows for large increases in drag coefficient at large deflection angles while maintaining a simple and cheap design. This is favourable for the dive phase of the mission profile. A large

increase in drag coefficient would allow to leave out the dive breaks, reducing complexity further. Furthermore, it has the advantage of not creating a very large pitching moment [18].

For the selected airfoil, a flap chord to wing chord ratio ($\frac{c_f}{c}$) of 0.15 should be used. The airfoil has specifically been designed for this ratio. Although being designed for a plain flap, the split flap can be integrated in this part of the airfoil. Furthermore, after iterations performed in Chapter 5, it has been decided that the flaps should cover 60% of the wingspan. This span leaves space for the aileron on the tip of the wing and provides a sufficient increase in lift coefficient during take-off and landing.

During take-off, the airfoil stays as it is (fixed at its 20 degree nominal deflection). For the return dive and landing, the drag is increased significantly by deflecting the flap by 40 degrees with respect to the nominal airfoil chord line. This deflections provides sufficient gains in both lift coefficient and drag coefficient for the determined mission profile.

With the sizes of the HLD fixed, it is possible to estimate the performance of the proposed flaps. The first step is to get the increase in lift coefficient of a flap covering the entire wingspan. This is done using Figure 4.21. It can be seen that a ΔC_{L_f} of 0.8 for a deflection of 40° can be obtained. Here, the f subscript refers to a flap on the entire wingspan.

The second step is to scale down the ΔC_{L_f} to a flap that does not cover the entire wingspan. This can be one using Equation 4.34 [18, p. 5-15, eq. 24].

$$\frac{\Delta C_L}{\Delta C_{L_f}} \approx 1.25 \frac{b_f}{b} \tag{4.34}$$

With b_f the span of the flaps and b the wingspan. The method for calculating the drag coefficient caused by flap deflection can be found in Subsection 4.2.4. The HLD parameters are presented in Table 5.4a.

The increase in pitching moment coefficient caused by the flap deflection is calculated at a maximum flap deflection of 40 degrees, resulting in a $\Delta C_{L,40}$ of 0.6. From Roskam, the pitching moment derivative for a split flap is found to be -0.275 [19, table 9.4]. The increase in pitching moment coefficient is then found with Equation 4.35.

$$\Delta C_{m/4} = \frac{\Delta C_{m/4}}{\Delta C_L} \cdot \Delta C_L \tag{4.35}$$

Ailerons

The next step of sizing is adding the ailerons to the wing. For the same reason as for the HLD sizing, it is decided that the ailerons should span 15% of the wing's chord. Furthermore, they span 20% of the wingspan. This will allow to easily fit the flaps and ailerons on the wing, leaving a gap between them. Furthermore, a plain flap is used for the aileron, as it allows for upward and downward deflections.

4.2.3. Lift

In order to evaluate the tow craft's performance, it is necessary to find its lift curve. In order to do so, the lift of the whole wing and of the entire aircraft must be calculated. This is achieved by transforming the airfoil's lift curve, based on data described in Subsection 4.2.1, to a lift curve of the wing, and afterwards, to that of the entire aircraft. This subsection presents the method used to obtain the lift curves [19, pages 245-288].

Wing Zero-Lift Angle of Attack ($\alpha_{0_{L,wing}}$) The zero-lift angle of attack of a wing depends on the twist distribution along the wingspan. Furthermore, a Mach number correction factor is added. Equation 4.36 presents the method to calculate the wing's zero lift angle of attack (AoA) [19, sec. 8.1.3.1].

$$\alpha_{0_{L,wing}} = \left[\alpha_{0_l} + \left(\frac{\Delta\alpha_0}{\epsilon_t}\right)\epsilon_t\right] \cdot \left[\frac{\alpha_{0_{L,atM}}}{\alpha_{0_{L,AtM=0.3}}}\right] \tag{4.36}$$

With $\frac{\Delta\alpha_0}{\epsilon_t}$ being the change in wing zero-lift AoA per degree of wing twist, ϵ_t the wing twist angle, and $\frac{\alpha_{0_{L,atM}}}{\alpha_{0_{L,AtM=0.3}}}$ the Mach correction factor.

Since no wing twist is applied, and, as the tow velocity is small, the Mach correction factor is equal to one. The wing's zero-lift angle of attack is equal to the airfoil's zero-lift angle of attack.

Wing Lift Curve Slope ($C_{L_{\alpha},wing}$) The lift curve slope of a wing is mostly affected by the aspect ratio of the wing, the sweep, airfoil, and the velocity of the craft. This slope will always be lower than the slope of the airfoil due to the 3D flow losses. Equation 4.37 presents the method to calculate the wing's lift curve slope [19, eq. 8.22].

$$\frac{2\pi AR}{2+\left[\left(\frac{AR\cdot\beta}{k}\right)^2\cdot\left(1+tan^2(\Lambda_{c/2})/\beta^2\right)+4\right]^{1/2}} \tag{4.37}$$

With AR being the aspect ratio of the wing, β the Prandtl-Glauert compressibility correction, k the lift curve slope corrected for air compressibility, and $\Lambda_{c/2}$ the half chord sweep.

Wing Linear Range Angle of Attack (α^*_w) In preliminary design, this value can be assumed to be equal to the airfoil's one [19, subsec: 8.1.3.3].

Wing Maximum Lift Coefficient ($C_{L_{\mathbf{max,wing}}}$) and Angle of Attack for Maximum Lift ($\alpha_{C_{L,max,w}}$) These values result from the spanwise lift distribution calculated by a computer program. To do so, a wing planform, based on estimated sizing values, is modelled in XFLR5 and analysed. The program is able to produce a lift curve, from which the required values can be read [19, subsec: 8.1.3.4].

Aircraft Zero-Lift Angle of Attack ($\alpha_{0_{L,A}}$) This value is obtained by dividing the zero-angle-of-attack lift coefficient by the lift curve slope [19, eq. 8.31].

Aircraft Zero-Angle-of-Attack Lift Coefficient ($C_{L_{0,A}}$) This variable depends on the aircraft's lift curve slope and the horizontal tail parameters. The method to calculate this value is presented in Equation 4.38 [19, sec. 8.1.5.2].

$$C_{L_{0,A}} = C_{L_{0,wf}} + C_{L_{\alpha,h}}\cdot\eta_h\cdot\frac{S_h}{S}\cdot(-\alpha_{0_{L,h}}-\epsilon_{0_h}) \tag{4.38}$$

With $C_{L_{0,wf}}$ being the zero-angle-of-attack lift coefficient of the wing-fuselage combination, $C_{L_{\alpha,h}}$ the lift curve slope of the horizontal tail, η_h the ratio of dynamic pressures between the horizontal tail and the wing, S_h the horizontal tail area, S the wing area, and ϵ_{0_h} the tail incidence angle.

Aircraft Lift Curve Slope ($C_{L_{\alpha},A}$) This value depends on the wing lift curve slope, the fuselage sizing, horizontal tail airfoil and sizing, and on the downwash gradient ϵ. The relevant relation is presented in Equation 4.39 [19, sec. 8.1.5.3].

$$C_{L_{\alpha},A} = C_{L_{\alpha},wf} + C_{L_{\alpha},h}\cdot\eta_h\cdot\frac{S_h}{S}\cdot(1-d\epsilon/d\alpha) \tag{4.39}$$

With $C_{L_{\alpha},wf}$ being the wing-fuselage lift curve slope defined in [19, sec. 8.1.5.3], $C_{L_{\alpha},h}$ the lift curve slope of the horizontal tail, and $d\epsilon/d\alpha$ the downwash gradient at the horizontal tail.

Aircraft Linear Range of Angle of Attack (α^*_A) To estimate this value it is necessary to subtract the wing incidence angle from the wing's linear range AoA (α^*_w) [19, eq. 8.49].

Aircraft Maximum Lift Coefficient ($C_{L_{\mathbf{max,A}}}$) and Angle of Attack for Maximum Lift ($\alpha_{C_{L,max,A}}$) The AoA for maximum lift of the aircraft is found by subtracting the wing's incidence angle from the wing's AoA for maximum lift, as presented in Equation 4.40 [19, sec. 8.1.5.5].

$$\alpha_{C_{L,max,A}} = \alpha_{C_{L,max,wing}} - i_w \tag{4.40}$$

With i_w being the wing incidence angle. Furthermore, the aircraft's maximum lift coefficient can be calculated using Equation 4.41 [19, sec. 8.1.5.5].

$$C_{L_{\mathrm{max,A}}} = C_{L_{\mathrm{max,wing}}} + C_{L_{\alpha},h}\cdot\frac{S_h}{S}\cdot\left[\alpha_{C_{L,max,A}}\cdot(1-d\epsilon/d\alpha)-\epsilon_{0,h}+i_h\right] \tag{4.41}$$

Having calculated these values, it is possible to plot the lift curves. The final results are presented in Table 5.5 and the plots are shown in Figure 5.7.

4.2.4. Drag

This subsection presents the Class II Drag estimation for the tow craft. First, the different drag coefficient components are calculated, and then by summing them, the total drag acting on the craft may be computed. Equation 4.42 presents the different components that must be summed to compute the total drag of the craft. All calculations are done for the subsonic speed region [19, eq. 4.4].

$$C_D = C_{D_{\text{wing}}} + C_{D_{\text{fus}}} + C_{D_{\text{emp}}} + C_{D_{\text{np}}} + C_{D_{\text{flap}}} + C_{D_{\text{gear}}} + C_{D_{\text{cw}}} + C_{D_{\text{store}}} + C_{D_{\text{trim}}} + C_{D_{\text{int}}} + C_{D_{\text{misc}}} \quad (4.42)$$

Wing Drag Coefficient ($C_{D_{\text{wing}}}$) The wing drag coefficient can be divided into two parts: the zero-lift drag and the lift induced drag. This drag coefficient depends on the wing's profile and flight conditions, namely the velocity and altitude [19, sec. 4.2.1].

Fuselage Drag Coefficient ($C_{D_{\text{fus}}}$) The fuselage drag coefficient is divided into the fuselage zero-lift drag coefficient and the drag coefficient due to lift. This depends mainly on the fuselage geometry and the angle of attack the craft is flying at [19, sec. 4.3.1].

Empennage Drag Coefficient ($C_{D_{\text{emp}}}$) The empennage drag coefficients are calculated for the vertical and horizontal stabilisers, and then summed together. Furthermore, each drag coefficient can be divided in two components: the zero-lift drag coefficient and the lift-induced one. As, for drag calculations, no sideslip is assumed, the vertical tail will not have the lift-induced drag coefficient [19, sec. 4.4.1].

Nacelle-Pylon Drag Coefficient ($C_{D_{\text{np}}}$) The nacelle and pylon drag coefficients are not applicable to the tow craft as the engines are not placed on the wings, therefore no pylons are needed. However, it is possible to calculate the drag the stopped or windmilling propeller would generate [19, sec. 4.5.3].

Flap Drag Coefficient ($C_{D_{\text{flap}}}$) The flap drag coefficient increment can be calculated for deployed flaps. This depends on the flap and wing geometries [19, sec. 4.6].

Gear Drag Coefficient ($C_{D_{\text{gear}}}$) The landing gear drag coefficient depends on the tire size and the fairing used around it. Furthermore, the strut configuration used to attach the main landing gear to the fuselage.

Canopy/Windshield Drag Coefficient ($C_{D_{\text{flap}}}$) As the craft is unmanned, no canopy or windshield is needed, therefore this drag component is zero.

Store Drag Coefficient ($C_{D_{\text{store}}}$) No external storage areas are needed, therefore this component is zero.

Trim Drag Coefficient ($C_{D_{\text{trim}}}$) The trim drag is caused by the fact that the aircraft has to be trimmed for stable flight [19, sec. 4.10].

Interference Drag Coefficient ($C_{D_{\text{int}}}$) This drag component accounts for the drag caused by integrating components together [19, sec. 4.11].

Miscellaneous Drag Coefficient ($C_{D_{\text{misc}}}$) This drag accounts for, among others, the spoilers and surface roughness of the skin [19, sec. 4.12].

4.2.5. Winglet Design

Aircraft are equipped with winglets for various reasons, most importantly to improve aerodynamic efficiency at higher lift coefficients as can be seen in Figure 4.22. Although it could be argued that winglets improve the aesthetics of aircraft significantly as well. As both are important for the design of *MARCUS-T* , the winglet design is considered in this section.

There are many types of wingtip designs possible, from rounded edges to full on blended winglets. A trade-off needs to be made between the flight regime optimisation and manufacturability. As the winglet adds skin friction drag and interference drag, it is not optimal for all flight regimes. At certain lift coefficients, when designed correctly, the winglets do decrease the overall drag. This is done by giving the winglet an angle of attack with respect to the incoming flow, and thus it has to produce lift. This lift vector approximately points towards the nose of the aircraft due to the vortex over the wing tip, actually producing a small amount of thrust. The aerodynamic force generated results in a vortex that is superimposed on the existing wingtip vortex, moving the combination further outward. This increases the effective wingspan, and thus aspect ratio of the wing.

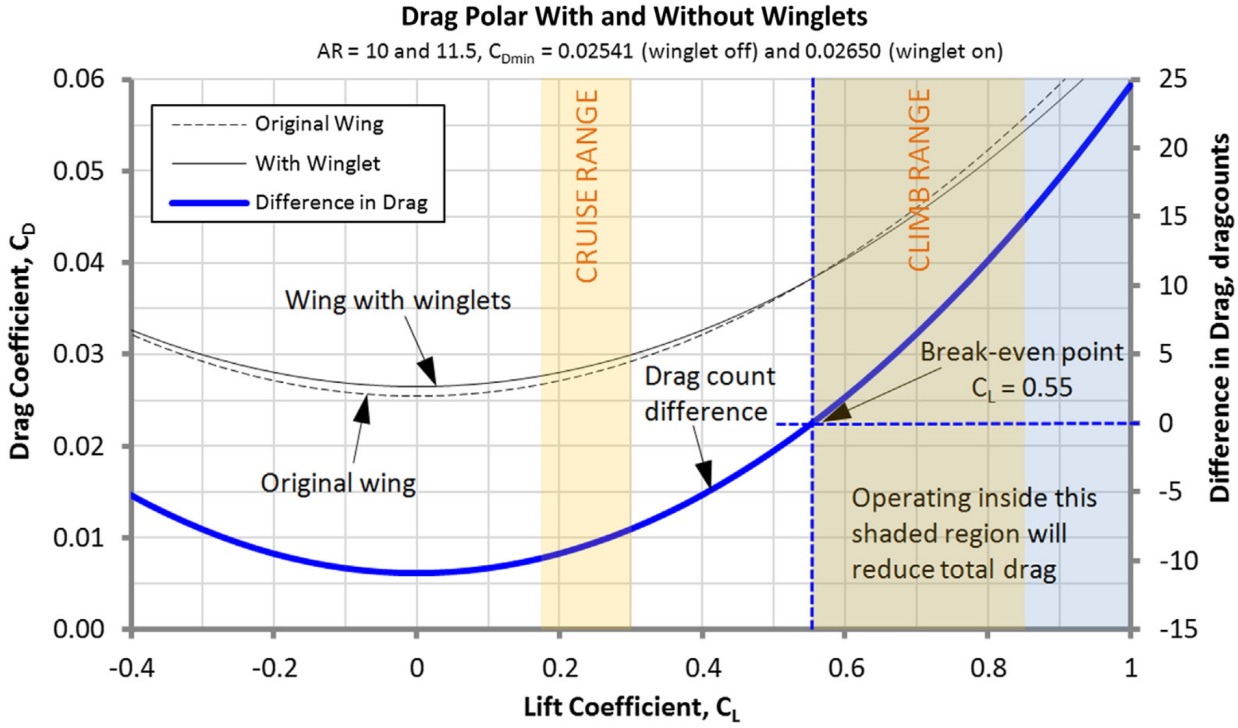

Figure 4.22: Case study on the influence of winglets on the drag polar by Gudmundsson [15].

The preliminary sizing of the winglet is done using a method presented by Gudmundsson [15]. The Whitcomb winglet configuration is used in this stage of the design as presented in figure 4.23.

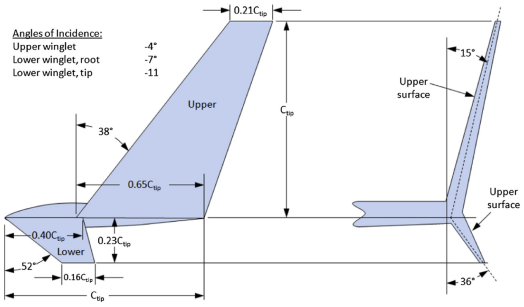

Figure 4.23: General layout of the Withcomb winglet [15].

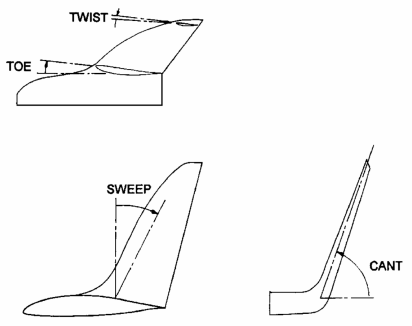

Figure 4.24: Definition of the toe angle [20].

According to Maughmer, the winglet can only be optimised for one flight condition [20]. This will be done for the climb phase of the tow craft. The parameter of the winglet that predominantly governs for which phase the winglet performs optimally, is the toe angle, as defined in Figure 4.24. Changing this angle, increases or decreases the aerodynamic winglet loading. In practise, the toe angle is determined such that the winglet and wing stall at the same time when the wing angle of attack is increased. As this is difficult to determine, a toe angle of one degree is used as it was demonstrated to be most beneficial for low speed flight (climb) regime for the Discus 2 [20, figure 11]. The sweep angle, as well as the cant angle, are taken from Figure 4.23. The winglet twist angle is set at 2.6 degrees [20]. According to Raymer, the airfoil at the tip needs to have a camber higher than that of the wing airfoil at the tip to ensure sufficient side force production. The wing root airfoil has a camber of 4.19%, which is decreasing towards the wingtip. Therefore the PSU 94-097 airfoil proposed by Maughmer for the winglet is used and displayed in Figure 4.25 [20][3]. This airfoil has a t/c ratio of 9.8%, and a maximum camber of 4%.

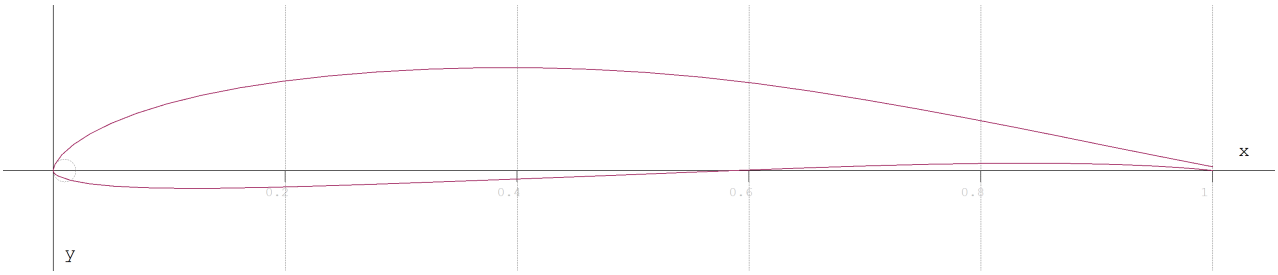

Figure 4.25: PSU 94-097 winglet airfoil section.

Due to the relatively narrow wheelbase and relatively large wingspan, the lower winglet is not used. Computing the values according to Figure 4.23, the final winglet size is presented in Table 5.7. Although, it should be noted that according to Maughmer it is easier to make overall performance worse rather than better when designing a winglet. Therefore, careful thought should be put into the design and the phase for which it is optimised. Assuming the winglet is correctly designed, the performance increase can be modelled as an increase in effective aspect ratio by Equation 4.43 [15].

$$\Delta AR = 1.9\frac{h}{b} \cdot AR \tag{4.43}$$

4.3. Software, Stability, and Control (SSC)

by Gerard, MianTao

SSC is responsible for both ensuring the stability and controllability of the craft, as well as the integration of hardware and software elements. This section mainly focuses on the former. To do this, first the vertical and horizontal stabiliser are sized for different flight conditions. A state space model is also developed for analysis of the dynamic stability of the final design. The software and hardware responsibilities of SSC are left for once the final design has been frozen.

4.3.1. Empennage Sizing

The tail is designed to provide longitudinal and lateral stability. The tail is composed of two surfaces: a vertical tailplane (VTP) and a horizontal tailplane (HTP). The code logic to obtain the minimum tail volume for the vertical and horizontal stabilisers is presented in Figure 4.27 and Figure 4.26, respectively.

[3] airfoiltools.com [cited 12 June 2024].

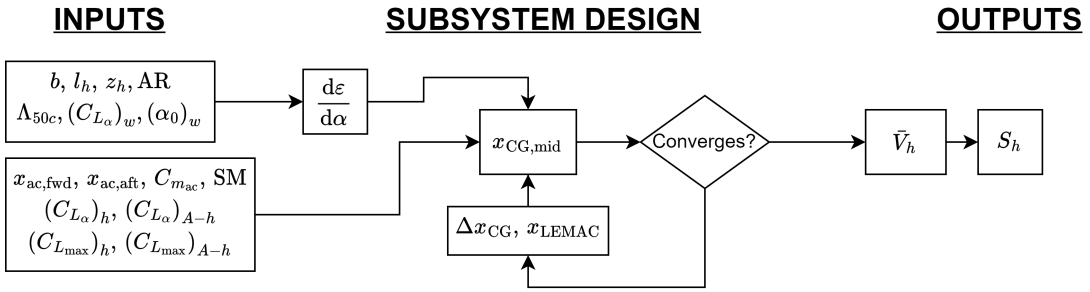

Figure 4.26: Horizontal tail sizing code.

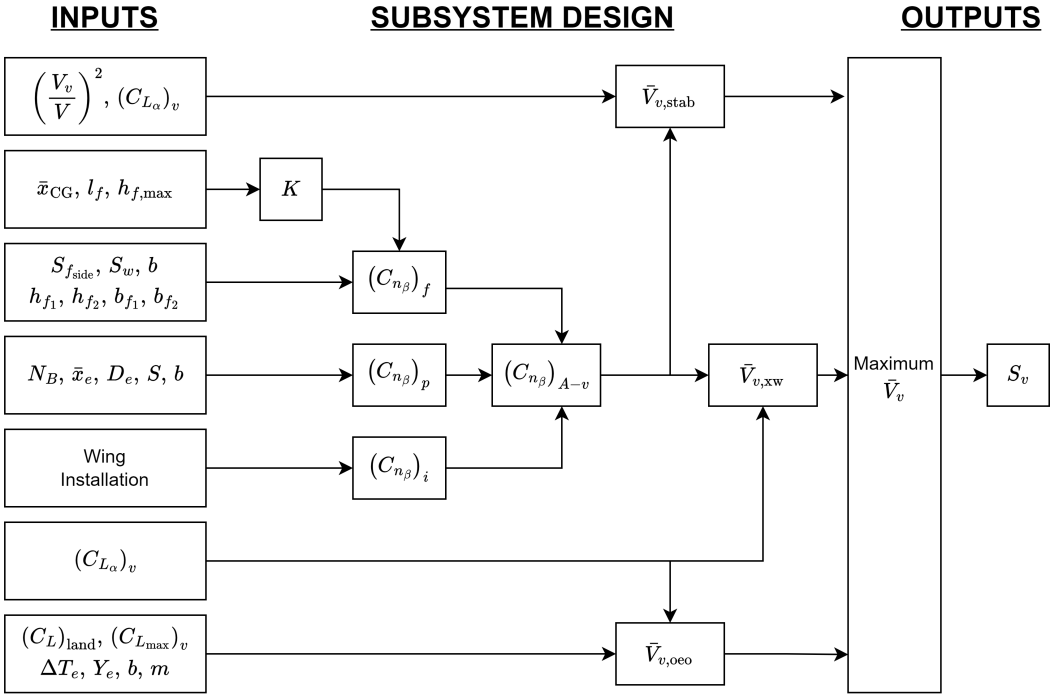

Figure 4.27: Vertical tail sizing code.

Vertical Tailpane

Torenbeek's method for vertical sizing has been chosen with some modifications to simplify the preliminary design [21]. This method is implemented according to Figure 4.27. Three conditions were considered the most important for the sizing for the vertical tail: attaining directional stability, compensating a one-engine-out situation, and resisting crosswind.

The directional stability of the craft must follow $C_{n_\beta} > 0$, also known as "weathervane stability". This inequality is detailed in Equation 4.44 [21, Eq. 9.62].

$$C_{n_\beta} = \left(C_{n_\beta}\right)_{A-v} + C_{Y_{v_\alpha}} \cdot \frac{S_v \cdot l_v}{S \cdot b} \cdot \left(1 - \frac{d\sigma_v}{d\beta}\right) \cdot \left(\frac{V_v}{V}\right)^2 > 0 \tag{4.44}$$

Here $\left(C_{n_\beta}\right)_{A-v}$ is the weathervane stability of the aircraft without the vertical tail plane (VTP), $C_{y_{v_\alpha}}$ is the lift slope of the VTP, S_v is the surface area of the VTP, S is the surface area of the wing, l_v is the tail length of the VTP, b is the wingspan, $\frac{d\sigma_v}{d\beta}$ is the sidewash gradient on the VTP, and $\left(\frac{V_v}{V}\right)$ is the speed ratio of the airspeed at the VTP with respect to the freestream.

The minimum required VTP volume is obtained by solving for the VTP volume in the inequality, leading to Equation 4.45 [21, Eq. 9.63].

$$\bar{V}_v := \frac{S_v \cdot l_v}{S \cdot b} \geq \frac{-\left(C_{n_{\beta_f}} + C_{n_{\beta_p}} + C_{n_{\beta_i}}\right)}{C_{Y_{v_\alpha}} \cdot \left(\frac{V_v}{V}\right)^2} \tag{4.45}$$

$\left(C_{n_\beta}\right)_{A-v}$ is divided into three contributions: fuselage ($C_{n_{\beta_f}}$), propeller ($C_{n_{\beta_p}}$), and wing installation ($C_{n_{\beta_i}}$) contributions. The influence of the sidewash is aggregated into the installation contribution. The equations for the fuselage, propeller, and wing installation contributions are given by Equation 4.46 [21, Eq. 9.64/65], Equation 4.47 [21, Eq. 9.66], and Equation 4.48 [21, Eq. 9.67], respectively.

$$C_{n_{\beta_f}} = -\left(0.3 \cdot \frac{l_{\text{cg}}}{l_f} + 0.75 \cdot \frac{h_{f_{\max}}}{l_f} - 0.105\right) \cdot \frac{S_{\text{fs}} \cdot l_f}{S \cdot b} \cdot \sqrt{\frac{h_{f_1}}{h_{f_2}}} \cdot \sqrt[3]{\frac{b_{f_2}}{b_{f_1}}} \tag{4.46}$$

$$C_{n_{\beta_p}} = -0.053 \cdot N_b \cdot \sum \frac{l_p \cdot D_p^2}{S \cdot c} \tag{4.47}$$

$$C_{n_{\beta_i}} = \begin{cases} -0.017 & \text{High Wing} \\ +0.012 & \text{Mid Wing} \\ +0.024 & \text{Low Wing} \end{cases} \tag{4.48}$$

Here l_{cg} is the lever arm from the VTP, l_f is the fuselage length, and h_f and b_f are the height and width of the fuselage at a certain point, respectively. The subscripts indicate if the h_f and b_f values are the maximum (max), at a quarter of the fuselage length from the nose (1) or at a quarter of the fuselage length from the back (2). N_b is the number of blades per propeller, D_p is the propeller diameter, and l_p is the distance from the propeller's plane to the CG location. Note that the semi-empirical relation in Equation 4.46 is only valid for ratios of $l_f / h_{f_{\max}} \geq 3.5$ and thus a check must be performed before using it.

This analysis yields a lower bound for the VTP volume for lateral directional stability. However, the engine-out condition might be more constraining and thus must also be analysed. To do this, Torenbeek provides Equation 4.49 [21, Eq. 9.59].

$$\left(\frac{V_v}{V}\right)^2 \cdot C_{Y_{v_\alpha}} \cdot \frac{S_v}{S} = \frac{C_L \cdot \frac{Y_e}{l_v} \cdot \frac{\Delta T_e}{W} + \beta \cdot \left(C_{n_\beta}\right)_{A-v} \cdot \frac{b}{l_v}}{\tau_v \cdot \delta_r - (\beta - \sigma_v)} \tag{4.49}$$

Here ΔT_e is the thrust asymmetry caused by the inoperative engine, Y_e is the lateral distance from the inoperative engine to the fuselage centerline, W is the weight of the aircraft, β is the sideslip angle, τ_v is the change in zero-lift angle per degree of control deflection of the rudder, δ_r is the rudder deflection, and σ_v is the VTP sidewash angle.

This equation can be simplified for more practical use, resulting in Equation 4.50.

$$\bar{V}_v = \left(\frac{(C_L)_{\max}}{(C_{Y_v})_{\max}} \cdot \frac{Y_e}{b} \cdot \frac{\Delta T_e}{W} + \frac{1}{C_{Y_{v_\beta}}} \cdot \left(C_{n_\beta}\right)_{A-v}\right) \cdot \left(\frac{V_v}{V}\right)^{-2} \tag{4.50}$$

Here a replacement has been made as $(C_{Y_v})_{\max} = \left(C_{Y_{v_\alpha}}\right) \cdot \beta_{\max}$. Note that here $(C_L)_{\max}$ is used account for the most crucial phase of flight: landing. In the case there are more than two engines, the Y_e and ΔT_e would be the worst-case scenario. $\left(C_{n_\beta}\right)_{A-v}$ is be calculated using Equation 4.46, Equation 4.47, and Equation 4.48. The VTP wing profile is NACA 0009, thus the parameters $(C_{Y_v})_{\max}$ and $C_{Y_{v_\alpha}}$ are known, as they are equivalent to $(C_L)_{\max}$ and C_{L_α}.

Finally, according to Torenbeek, in order to size the VTP for crosswind, ΔT_e just has to be set to 0 in Equation 4.50 [21, Eq. 9.68].

Horizontal Taiplane and Wing Position

For an aircraft to be flyable it must both be controllable and statically stable in the longitudinal direction under nominal flight conditions. In this context controllable means that it is possible to trim the aircraft for zero moment, whereas statically stable means that the aircraft has a nose-down response to increasing angle

of attack. The latter condition indicates that small deviations in angle of attack automatically produce a counteracting moment, restoring the original orientation of the aircraft. Though aerodynamically unstable craft can still be made stable with electronic systems, aerodynamic stability is preferred as it less prone to failure.

Both lateral stability and lateral controllability are attained by sizing the horizontal stabiliser of the aircraft, however the wing can also be positioned to minimise the size of the stabiliser. The method used for this is based on F. Oliviero [22].

In this method first the distance between the most forward and most aft position of the CG is computed in an aircraft loading diagram for an initial wing position. A scissor plot is generated for both controllability and stability. For this scissor plot and CG range, the optimal tail volume and CG position is then computed. For the normalised CG position, the lengthwise position of the wing along the fuselage can be determined, for which a new loading diagram can be computed. This process is repeated until it converges upon the final wing position and tail volume ratio. The implementation of this process is illustrated in Figure 4.26.

4.3.2. Empennage Sizing for Towing Force

In addition to the aerodynamic forces on the tow craft, a towing force F_{tow} is also applied, causing moments to the tow craft which can impact the controllability of the craft. To ensure the aircraft is controllable under all nominal conditions additional tail size is required to compensate for these moments. The additional size required for the HTP ($\Delta S_{h,\text{tow}}$) and VTP ($\Delta S_{v,\text{tow}}$) can be computed by equating the lift force the surfaces need to produce to balance the component of the towing force in their direction. This results in Equation 4.51 and Equation 4.52.

$$\Delta S_{h,\text{tow}} = \frac{F_{\text{tow}} \cdot \sin \tau_y}{\frac{1}{2}\rho \left(V_{\text{min,tow}} \frac{V_h}{V}\right)^2 \cdot (C_{L_h})_{\max}} \quad (4.51) \qquad \Delta S_{v,\text{tow}} = \frac{F_{\text{tow}} \cdot \sin \tau_z}{\frac{1}{2}\rho \left(V_{\text{min,tow}} \frac{V_v}{V}\right)^2 \cdot (C_{Y_v})_{\max}} \quad (4.52)$$

Here τ_y and τ_z are the maximum angles of the glider with respect to the xy and xz plane of the body of the tow craft respectively. Common values for these are $\tau_y = 30°$ and $\tau_z = 20°$ [23]. $V_{\text{min,tow}}$ is the minimum airspeed at which aerotow is performed. $(C_{L_h})_{\max}$ is the maximum achievable lift coefficient of the of the HTP used for determining controllability, as specified in [22].

4.3.3. State-Space Model

To analyse the dynamic stability properties of the aircraft, a state space model of the glider tow craft is constructed. This state space model is based on a linearised model given by in 't Veld [24], which decouples symmetrical and asymmetrical motions of an aircraft. The complete system of equations for this state space model is provided in Appendix A.

This model will be used for the dynamic analysis of the detached glider tow craft. To analyse the stability of the tow craft during the towing operation, the model is expanded to account for an additional towing force parameter. This towing force has been modelled as acting parallel to the x-axis of the vehicle-carried Earth-normal frame of reference in order to simplify the model. This assumption is realistic as, generally, glider pilots are trained to stay at the same altitude as the tow craft[4]. Therefore the error introduced by this simplification will be low, as long as changes in angles stay small. In addition, the force is assumed to be constant over time in both magnitude and direction. This assumption is not completely valid, as the force on the tow cable generally varies with a frequency of about 0.5 Hz [23]. The effect of this assumption affects the eigenmodes of the tow craft differently. For short period oscillation and aperiodic roll this effect is not significant, however it can cause inaccuracies when analysing phugoid and Dutch roll.

To account for the constant direction of the towing force, the state vector of the asymmetrical state space vector is expanded with a yaw angle state (ψ), which represents the angle of the body of the aircraft projected on the local horizontal plane. The convention used can be seen in Figure 4.28.

[4] www.gliding.world [cited 07 June 2024]

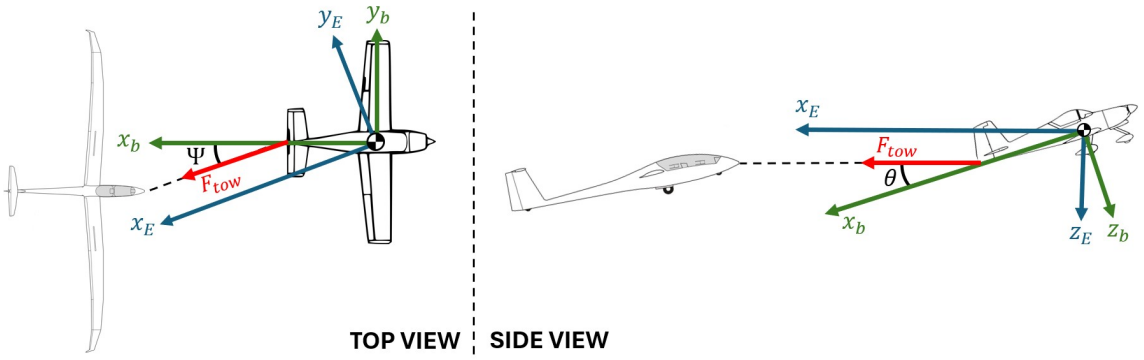

Figure 4.28: Simplified representation of the angles used to decompose the force between frames.

The tow force can expressed in the body-fixed reference frame by applying a set of transformations, resulting in Equation 4.53. Applying a similar logic to obtain the moment contributions results in Equation 4.54

$$F_{\text{tow}}|_b = \mathbb{T}_{bE} \cdot F_{\text{tow}}|_E = \mathbb{T}_x(\varphi) \cdot \mathbb{T}_y(\theta) \cdot \mathbb{T}_z(\psi) \cdot \begin{bmatrix} F_{\text{tow}} \\ 0 \\ 0 \end{bmatrix}_E = -F_{\text{tow}} \cdot \begin{bmatrix} \cos(\theta) \cdot \cos(\psi) \\ \sin(\varphi) \cdot \sin(\theta) \cdot \cos(\psi) - \cos(\varphi) \cdot \sin(\psi) \\ \cos(\varphi) \cdot \sin(\theta) \cdot \cos(\psi) + \sin(\varphi) \cdot \sin(\psi) \end{bmatrix} \tag{4.53}$$

$$M_{\text{tow}}|_b = F_{\text{tow}}|_b \times \begin{bmatrix} l_h \\ 0 \\ 0 \end{bmatrix} = -F_{\text{tow}} \cdot l_h \cdot \begin{bmatrix} 0 \\ \cos(\varphi) \cdot \sin(\theta) \cdot \cos(\psi) + \sin(\varphi) \cdot \sin(\psi) \\ -\sin(\varphi) \cdot \sin(\theta) \cdot \cos(\psi) + \cos(\varphi) \cdot \sin(\psi) \end{bmatrix} \tag{4.54}$$

Linearising Equation 4.53 and Equation 4.54 about the equilibrium state ($\Delta\vec{x}$), and assuming decoupling of lateral and longitudinal forces, results in Equation 4.55 being added to the standard linearised model provided by in 't Veld [24].

$$\vec{F}\left(\Delta\vec{x}\right)_{\text{extra,tow}}\Big|_0 = \begin{bmatrix} F_{\text{tow}} \cdot \sin\left(\theta_0\right) \cdot \Delta\theta \\ -F_{\text{tow}} \cdot \sin\left(\theta_0\right) \cdot \Delta\varphi + F_{\text{tow}} \cdot \Delta\psi \\ -F_{\text{tow}} \cdot \cos\left(\theta_0\right) \cdot \Delta\theta \end{bmatrix} \tag{4.55a}$$

$$\vec{M}\left(\Delta\vec{x}\right)_{\text{extra,tow}}\Big|_0 = \begin{bmatrix} 0 \\ -F_{\text{tow}} \cdot l_h \cdot \cos\left(\theta_0\right) \Delta\theta \\ -F_{\text{tow}} \cdot l_h \Delta\psi + F_{\text{tow}} \cdot l_h \cdot \sin\left(\theta_0\right) \Delta\phi \end{bmatrix} \tag{4.55b}$$

The forces are normalised by $1/2 \cdot \rho \cdot V^2 \cdot S$. Symmetrical moments are normalised by $1/2 \cdot \rho \cdot V^2 \cdot S \cdot \bar{c}$ and asymmetrical moments by $1/2 \cdot \rho \cdot V^2 \cdot S \cdot b$. For simplicity of the model, the definition in Equation 4.56 is used, such that the only addition to the symmetrical and asymmetrical models is given in Equation 4.57, resulting in $\mathbb{P} \cdot \dot{\vec{x}} = (\mathbb{Q} + \mathbb{Q}_{\text{extra,tow}}) \cdot \vec{x} + \mathbb{R} \cdot \vec{u}$.

$$C_{f_0} = \frac{F_{\text{tow}}}{\frac{1}{2} \cdot \rho \cdot V^2 \cdot S} \tag{4.56}$$

$$\left(\mathbb{Q}_{\text{extra,tow}}\right)_{\text{sym}} = \begin{bmatrix} 0 & 0 & -C_{f_0} \cdot \sin\left(\theta_0\right) & 0 \\ 0 & 0 & C_{f_0} \cdot \cos\left(\theta_0\right) & 0 \\ 0 & 0 & 0 & 0 \\ 0 & 0 & C_{f_0} \cdot \cos\left(\theta_0\right) \cdot \frac{l_h}{\bar{c}} & 0 \end{bmatrix} \tag{4.57a}$$

$$\left(\mathbb{Q}_{\text{extra,tow}}\right)_{\text{asym}} = \begin{bmatrix} 0 & C_{f_0} \cdot \sin\left(\theta_0\right) & 0 & 0 & -C_{f_0} \\ 0 & 0 & 0 & 0 & 0 \\ 0 & 0 & 0 & 0 & 0 \\ 0 & C_{f_0} \cdot \frac{l_h}{b} & 0 & 0 & C_{f_0} \cdot \sin\left(\theta_0\right) \cdot \frac{l_h}{b} \\ 0 & 0 & 0 & 0 & 0 \end{bmatrix} \tag{4.57b}$$

Furthermore, it must be noted that Equation 4.55a introduces a new state (ψ). Thus, an extra kinematic insight is added into the model: $D_c \cdot \psi = \frac{r \cdot b}{2V}$. The full model can be found in Appendix A.

4.3.4. Preliminary Decisions

To limit the design space, several preliminary decisions are made about the design parameters. Firstly both the horizontal and vertical tailplane have been chosen to have a NACA0009 airfoil as it is symmetric and offers low drag. In addition the vertical tailplane has been chosen to have aspect ratio of 2 whereas the horizontal tailplane was chosen to have an aspect ratio of 5. The lower aspect ratio for the horizontal tailplane is chosen such that the main wing stalls after the horizontal tailplane. This ensures the aircraft can be recovered during high angles of attack. Additionally, both surfaces are designed to be untapered as the effect of their induced drag is not significant and both tailplanes have a moderate to low aspect ratio.

4.4. Airfield Performance (APOL)

by Mees, Tamara

A responsibility of the APOL department is to ensure *MARCUS-T* has the required airfield performance. A take-off and landing distance tool is created to determine the required thrust to meet the take-off requirement from CS-22 and determine the landing distance [4]. Before the calculations are explained, a flow diagram is shown so that the relations of the inputs and outputs can be seen. After that it is explained what variables are chosen to be fixed and to which value they are fixed.

4.4.1. Flow Diagram for Ground Operations

In Figure 4.29 the ground operations flow diagram is shown.

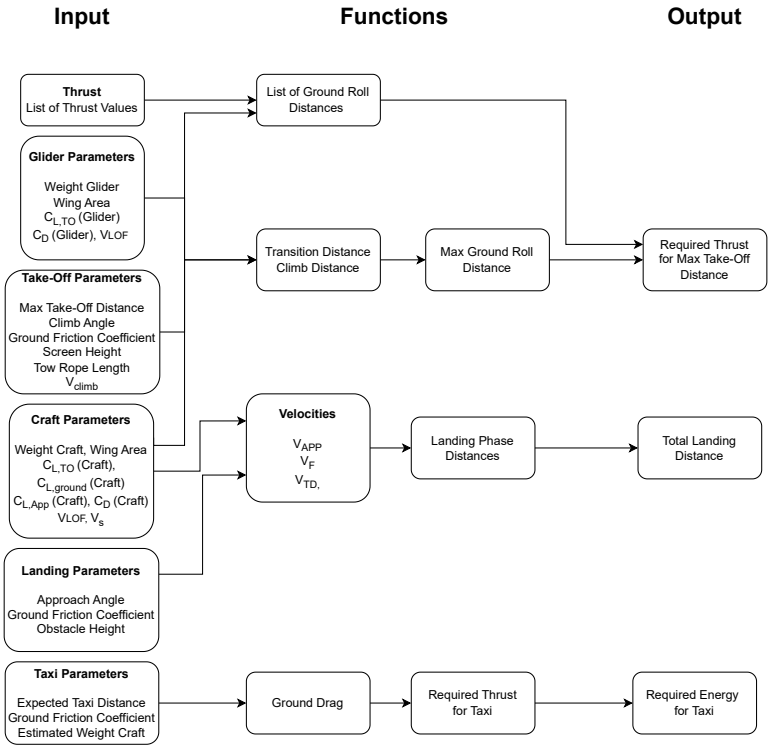

Figure 4.29: Flow diagram for the APOL department.

4.4.2. Fixed Values

The fixed values follow from the requirements and the mission profile.

The CS-22 requirement states that the maximum take-off distance of the tow craft and the glider should be lower than 500 m [4]. This is under the conditions that there is no wind, both crafts are at maximum take-off

weights, and they take-off at 0 m above sea level on a hard dry surface. A hard dry concrete runway has a ground friction coefficient of 0.03 [12]. For the thrust determination, a maximum take-off distance of 475 m is assumed. Moreover, it is assumed that during take-off, a tow cable of 60 m is used[5]. The take-off and stall velocity of *MARCUS-T* is chosen to be 110 km/h and 72 km/h. These values are based on the velocities of the Arcus-M (the heaviest glider *MARCUS-T* is designed to tow). The climb rate and velocity at climb are stated in Chapter 2 and are 3 m/s and 130 km/h respectively. This results in a climb angle of 5°.

4.4.3. Taxi

The energy needed for a taxi needs to be calculated. It is chosen to calculate this value ones and fix it during the iteration process. The energy to taxi to craft can be calculated with Equation 4.59. The derivation of this formula can be seen in Equation 4.58.

$$\begin{aligned} E_{taxi} &= P_{taxi} \cdot t_{taxi} \\ P_{taxi} = F_{taxi} \cdot V_{taxi} &= \mu \cdot W \cdot V_{taxi} \\ t_{taxi} &= \frac{s_{taxi}}{V_{taxi}} \end{aligned} \tag{4.58}$$

$$E_{taxi} = \mu \cdot W \cdot s_{taxi} \tag{4.59}$$

E is the energy needed for the taxi in joules. μ is the ground friction coefficient, W is the weight of *MARCUS-T* and s_{taxi} is the taxi distance. The energy needed is not dependent on the speed. The ground friction coefficient is 0.1, the preliminary weight is 450 kg, the runway taxi distance is 600 m, the estimated landing distance of 500 m plus two times 50 m for the taxi to and from the battery swap area. Then the energy required assumed for the taxi is 300,000 J.

4.4.4. Take-Off Distance Tool

As shown in Figure 4.30, the total take-off distance consists of the ground roll, the transition phase, and the climb phase. The total take-off distance is determined using Equation 4.60.

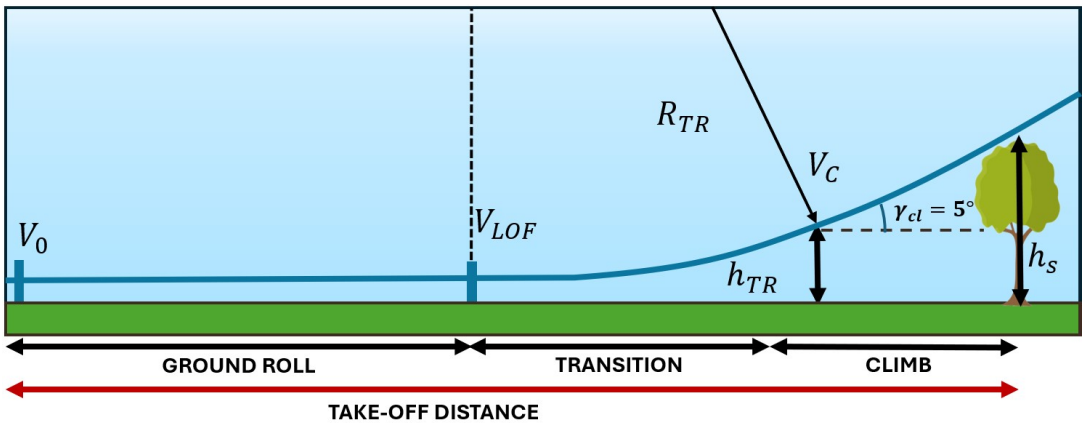

Figure 4.30: Profile used to determine the take-off distance.

$$s_{TO} = s_{GR} + s_{TR} + s_C \tag{4.60}$$

Take-Off Ground Roll

The free body diagram, visible in Figure 4.31, is created in order to establish the equation of motion, Equation 4.61.

[5] www.tost.de [cited 13 June 2024]

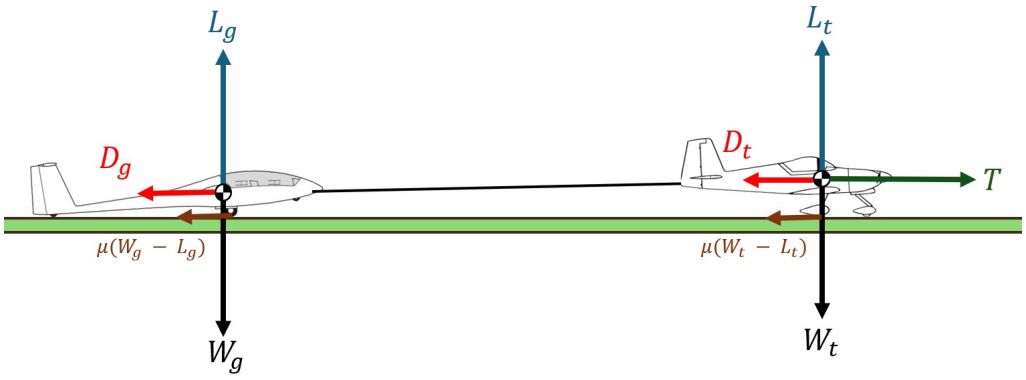

Figure 4.31: Free body diagram of the tow craft and glider during the take-off roll.

$$(m_t + m_g) \cdot \frac{dV}{dt} = T - D_t - \mu \cdot (W_t - L_t) - D_g - \mu \cdot (W_g - L_g) \tag{4.61}$$

Rewriting Equation 4.61 as a function for acceleration results in Equation 4.62.

$$a_c = \frac{g}{W_t + W_g} \cdot [T - D_t - \mu \cdot (W_t - L_t) - D_g - \mu \cdot (W_g - L_g)] \tag{4.62}$$

Where the thrust, T, is determined by Equation 4.63. With a being the thrust coefficient. The aerodynamic drag of the tow craft and the glider, D_t and D_g respectively, can be determined by Equation 4.64. The lift of the tow craft and the glider, L_t and L_g respectively, can be determined by Equation 4.65.

$$T = T_0 - a \cdot V^2 \tag{4.63}$$

$$D = \left(C_{D_0} + \frac{C_L^2}{\pi \cdot AR \cdot e} \right) \frac{1}{2} \cdot \rho \cdot V^2 \cdot S \tag{4.64}$$

$$L = C_L \cdot \frac{1}{2} \cdot \rho \cdot V^2 \cdot S \tag{4.65}$$

Then, according to Raymer, the covered ground roll distance can be calculated by using Equation 4.66 [12].

$$s_{GR} = \int_{V_0}^{V_{LOF}} \frac{V}{a_c} dV \tag{4.66}$$

This integral is solved using numerical integration. When the lift-off speed, V_{LOF}, is reached, the glider and tow craft leave the ground, and the next phase begins.

Transition and Climb

This next phase is the transition phase. During this phase, the tow craft and glider transition to the required climb angle, γ_{cl}. The transition radius, R_{TR}, is determined using Equation 4.68. The transition load factor, n_{TR}, is set at 1.2. According to Raymer, combining Equation 4.67 and Equation 4.68 results into the equation for the horizontal transition distance, Equation 4.69 [12].

$$\sin(\gamma_{cl}) = \frac{T - D_t - D_g}{W_{tot}} \tag{4.67}$$

$$R_{TR} = \frac{V_{TR}^2}{g(n_{TR} - 1)} \tag{4.68}$$

$$s_{TR} = \frac{V_{TR}^2}{g(n-1)} \cdot \frac{T - D_t - D_g}{W_{tot}} \tag{4.69}$$

The vertical distance covered during this transition phase is determined by Equation 4.70.

$$h_{TR} = \frac{V_{TR}^2}{g(n-1)} \cdot [1 - cos(\gamma_{cl})] \tag{4.70}$$

If $h_{TR} \geq h_s$, then the total take-off distance is equal to the sum of s_{GR} and s_{TR}. If this is not the case, the distance covered during the climb to 15 m should be calculated using Equation 4.71.

$$s_C = \frac{h_s - h_{TR}}{tan(\gamma_{cl})} \tag{4.71}$$

According to constrained CON-TEC-06, the combination of glider and tow craft should clear a 15 m obstacle within a take-off distance of 500 m. In order to determine the thrust required the transition and climb distance are calculated first. These distances and the rope length are subtracted from 475 m, to get the maximum ground roll distance allowed. Because the climb angle is already known, the needed climb thrust is calculated with Equation 4.67. The ground roll distance is calculated for a list of thrusts, with a minimum thrust being the climb thrust and a maximum thrust of 5,000 N. The thrust can be plotted against the total take-off distance so the lowest thrust that complies with the maximum allowed take-off distance, can be easily found. This thrust is used in further calculations.

4.4.5. Landing Distance Tool

The landing can be modelled in the same way as the take-off, but reversed. Figure 4.32 shows that the landing consists of the approach, flare, and ground roll phases. The total landing distance is determined by Equation 4.72. In this subsection, the individual phases are worked out.

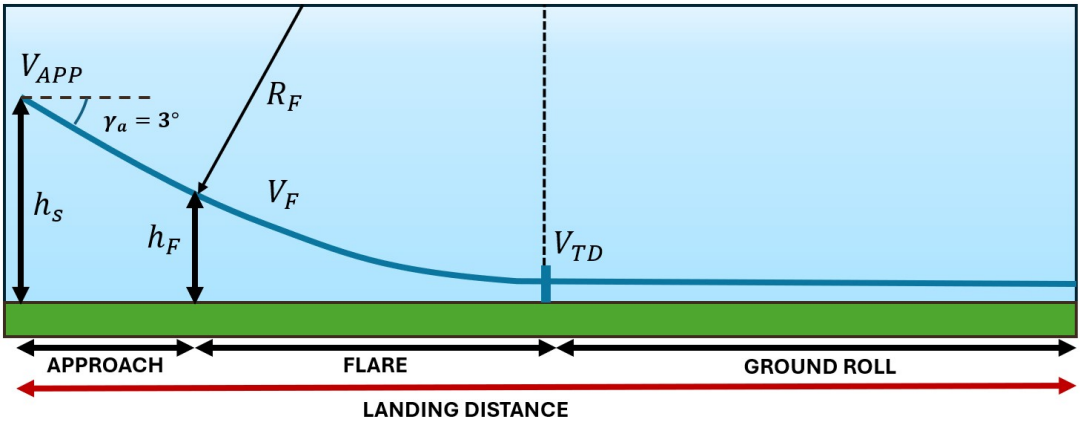

Figure 4.32: Profile used to determine the landing distance.

$$s_{LDG} = s_{APP} + s_F + s_{GR,ldg} \tag{4.72}$$

Approach and Flare

The approach begins with clearing the screen height with an approach velocity, V_{APP}. From the mission profile an approach angle, γ_a, of 3° is chosen. In order to determine the approach distance, s_{APP}, Equation 4.73 is used. To calculate the flare height, h_F, Equation 4.70 isused, with using the flare velocity, V_F.

$$s_{APP} = \frac{h_s - h_F}{tan(\gamma_a)} = \frac{h_s - \frac{V_F^2}{g \cdot (n-1)} \cdot (1 - cos(\gamma_a))}{tan(\gamma_a)} \tag{4.73}$$

In order to decrease the rate of descent, the craft will start its flare at flare height. The horizontal distance covered during this flare phase is determined by Equation 4.74.

$$s_F = \frac{V_F^2}{g \cdot (n-1)} \cdot sin(\gamma_a) \tag{4.74}$$

Landing Ground Roll

The tow craft will touch down at the touch-down velocity, V_{TD}. The throttle will be idle, resulting into zero thrust. To determine the deceleration during the ground roll, Equation 4.62 can be rewritten into Equation 4.75. In order to simulate braking during the ground roll, a braking coefficient, μ_B, is included.

$$d_t = \frac{g}{W_t} \cdot [-D_t - (\mu + \mu_B) \cdot (W_t - L_t)] \tag{4.75}$$

The ground roll distance can then be determined using Equation 4.76. This integral is once again solved with a numerical integration algorithm.

$$s_{GR,ldg} = \int_{V_{TD}}^{0} \frac{V}{d_t} dV \tag{4.76}$$

4.5. Power, Performance, and Propulsion (PPP)

by Annika, Christian

In this section, the power, performance, and propulsion (PPP) subsystem of *MARCUS-T* is specified. This entails not only a flow diagram to show inputs and outputs but also what is required to complete each stage of the mission. Further, also the requirements must be taken into account. These requirements come from both set parameters in Chapter 3, as well as information on power, performance, and propulsion as found in CS-22 [4]. Certain design choices are considered, namely those on the amount of blades the propeller has and the battery type that is used. Notably, energy recuperation is also touched upon. Lastly, it is important to note that the size of engine is dependent on not just the PPP subsystem, but all others as well. This part will therefore only be sized later on, when all subsystems have successfully been integrated into a complete system.

Literature on electric aircraft is limited and hence, regressional relationships or other sizing methods that rely on databases of existing aircraft are rare as well. The commonly-used Breguet equations cannot be applied either, as the mass does not change throughout flight for an electric aircraft. Research does suggest a derivation for the range equation, being a grounded method to validate the subsystem at a later point in development [12]. A similar version for the endurance of electric aircraft could be derived, but is not deemed necessary to the mission profile and thus not currently considered.

Besides this, there are still methods remaining for performing preliminary sizing, especially when it comes to the battery and propeller of the craft. Raymer has a lot of information on the battery sizing process and is therefore consulted multiple times in this section [12, Ch. 20].

4.5.1. Flow Diagram for the PPP-department

The flow diagram for the PPP department can be seen in Figure 4.33. This diagram is split up into: inputs, subsystem design, and outputs. The subsystem design describes the major blocks the PPP department designs: a battery mass fraction (BMF) calculation, the battery type and its specific energy, recuperation capabilities for a reserve, and design of both the propeller and motor.

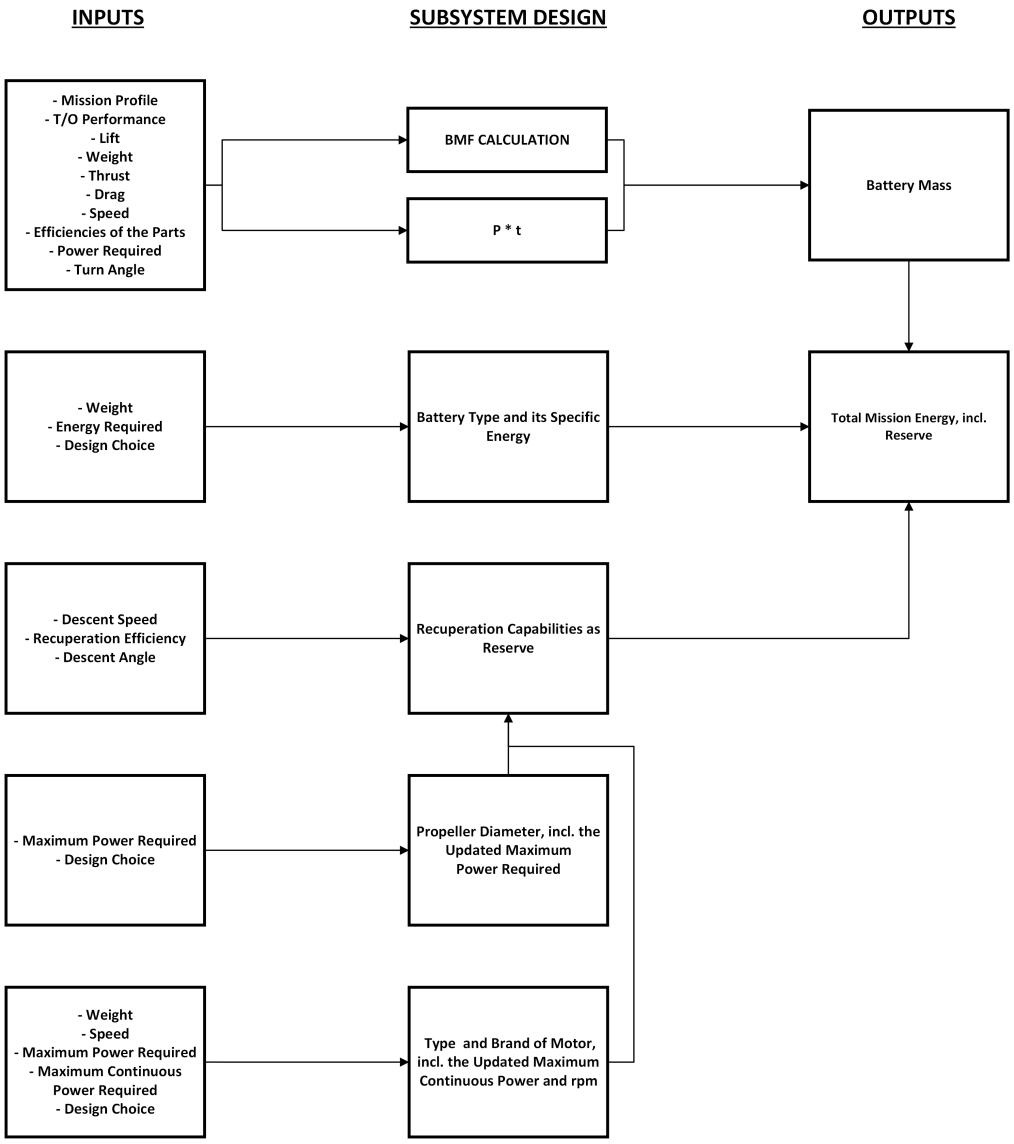

Figure 4.33: Flow diagram for the PPP department.

4.5.2. Mission Stages

To make sure the mission can be flown as intended and explained in Chapter 2, this forms the basis for what the tow craft should be capable of. For this, the whole mission is split up into different phases of constant parameters such that the power and propulsion parameters can be evaluated conservatively. As the mission is already introduced in Chapter 2, in the following only the most relevant parameters that are used in the calculations for power and propulsion are listed:

During a nominal mission the following stages occur:

- **Taxi**
- **Initial Climb (Climb 1)**
  - Glider attached,
  - From h_0 =15 m to h_1 =180 m,
  - γ: +5°,
  - ROC: 3m/s,
  - TAS: 130km/h,
  - Power setting: 100% of maximum power.
- **Climb-Out (Climb 2)**
  - Glider attached,
  - From h_1 = 180 m to h_2 = 1,000 m,
  - γ: +4°,
  - ROC: 2.5m/s,
  - TAS: 130km/h,
  - Power setting: 85% of maximum power.
- **Turning**
  - Glider attached,
  - Sustain 1,000 m during four turns of 90°,
  - TAS: 130km/h,
  - ϕ: 60°.

- **Descent A**
  - Glider detached,
  - Unpowered with potential recuperation,
  - From 1,000 m to 200 m,
  - TAS_{max}: 280 km/h,
  - γ: -6°.
- **Descent B**
  - Glider detached,
  - Unpowered with potential recuperation,
  - From 1,000 m to 200 m,
  - TAS_{max}: 280 km/h,
  - γ: -8.3°.
- **Descent C**
  - Glider detached,
  - Unpowered with potential recuperation,
  - From 1,000 m to 200 m,
  - TAS_{max}: 280 km/h,
  - γ: -14°.
- **Descent D**
  - Glider detached,
  - Unpowered with potential recuperation,
  - From 1,000 m to 200 m,
  - TAS_{max}: 280 km/h,
  - γ: -45°.
- **Circuit**
  - Glider detached,
  - Sustain 200 m,
  - TAS: 130 km/h,
  - Range: 8,000 m.
- **Approach**
  - Glider detached,
  - Unpowered,
  - From 200 m to 15 m,
  - γ: -3°.
- **Go-Around Climb**
  - Glider detached,
  - From 15 m to 200 m,
  - TAS: 130 km/h,
  - γ: +5°,
  - Power setting: 100%.

With the nominal procedures set, one last mission stage must be mentioned, which deals with a one-engine-out situation. As it is not yet known how many engines the design will have, this must still be considered, even if the design ends up having one engine. Therefore, the most constraining situation is an engine failure at 15 m, with the glider attached. A design decision is made that, the tow craft should be able to tow the glider up to a height of 200 m with one engine out, if applicable. This was chosen to give the glider enough room to manoeuvre itself out of the emergency situation. However, a lower vertical speed is allowed in this special situation, and thrust reduction is not necessary during the climb-out. In short, the following holds in case of engine failure:

With an attached glider, the tow craft is supposed to be able to climb on one engine inoperative from a height of 15 m to the circuit altitude of 200 m. Hereby, γ is not further specified. Climb-out is just performed at the highest possible power setting.

- Glider attached,
- Number of engines operative: N-1,
- From 15 m to 200 m,
- γ: as high as possible,
- Power setting: 100% of maximum power.

If the craft ends up having only one engine and this fails, then the craft is supposed to glide back. For more information on emergency procedures, the reader is referred to Subsection 8.2.3.

With the segments all defined, it is important to recall how to order and structure them in a way that reflects the mission in a correct manner. The mission starts with the taxi phase as laid out in Section 2.2. After the taxi to the starting position, the take-off is performed, which ends at an altitude of 15 m. From here, the aerial part of the mission begins in the following order, with the parameters per leg as described before.

1. (Taxi)[6]
2. (Take-off)
3. Initial Climb (Climb 1),
4. Climb-Out (Climb 2),
5. Turning,
6. Descent A, B, C, or D,
7. Circuit,
8. Turning at 200 m,
9. Approach.
10. (Landing)
11. (Taxi)

[6]The legs (in parentheses) form part of a nominal mission but their underlying calculations follow from considerations made in Section 2.2.

The reader may have noted that the turning phases are not integrated into the climb or into the circuit itself, while that is how Section 2.2 describes it. It is separated from each other, to ease analysis. However, it is made sure, that the turning yields the most conservative values in power consumption, such that underestimation of energy consumption is prohibited.

In the case of a go-around the following stages are added. First a go-around climb will be performed, which was specified before. At 200 m a circuit together with the belonging turns is flowsn. After that an approach is performed.

During the calculation of what the craft should be able to perform, the go-around is considered to be flown twice. This acts as reserve to the nominal mission profile, as laid out previously.

Lastly, for clarity, the following stages occurs in case an engine failure occurs.

1. Initial Climb (Climb 1) to 200 m (the circuit altitude),
2. Circuit,
3. Turning at 200 m,
4. Approach.

4.5.3. Battery Mass Calculations

One of the most important outputs of the PPP subsystem is the total battery mass required to make *MARCUS-T* perform its intended mission. For the battery mass, two different approaches are considered: the first way is to use Raymer's method of battery mass fractions for electric aircraft [12]. The second way is to calculate the battery mass using a simple "power times time" approach in which a certain power setting is multiplied by its applied time to get the consumed energy during that leg. The higher of the two will be considered most critical. The first approach of using battery mass fractions is laid out first.

Battery Mass Fraction

Raymer provides the following formulas in his book [12]:

$$BMF_{tot_{req}} = \frac{W_{bat_{tot_{req}}}}{W_{tot}} = \sum BMF \tag{4.77}$$

This sum can be multiplied by the total craft mass and this yields the total battery mass.

Furthermore, the following formulas are presented by Raymer: Equation 4.78 calculates the battery mass fraction (BMF) of the climb stage.

$$BMF_{\text{climb}} = \frac{\Delta h}{V_v \cdot E_{\text{sb}} \cdot \eta_{\text{b2s}}} \cdot \frac{P_{\text{used}}}{m_{\text{tot}}} \tag{4.78}$$

Here Δh stands for the altitude difference, V_v for the vertical speed, E_{sb} for the specific energy of the battery, η_{b2s} for the battery-to-shaft efficiency, P_{used} for the average power applied during that flight stage, and m_{tot} for the total mass of both the craft and glider. This formula can be used for the climb 1 and climb 2 segments of the mission, as well as the go-around climb, which resembles climb 1, mostly.

P_{used} is calculated with the basic formula for climb:

$$P_{\text{climb}} = ROC \cdot W + D \cdot V_{\text{TAS}} \tag{4.79}$$

V_v stands again for the vertical speed, W is the weight of the glider and the tow craft combined, D is the drag during that flight phase and V_{tas} is the true airspeed.

Equation 4.80 is used to obtain the BMF during steady flight.

$$BMF_{\text{steady}} = \frac{R \cdot g_0}{E_{\text{sb}} \cdot \eta_{b2s} \cdot \eta_p \cdot \left(\frac{L}{D}\right)_{\text{straight}}} \tag{4.80}$$

Here R stands for the range, g_0 for the gravitational acceleration at sea level, η_p for the propeller efficiency, $\left(\frac{L}{D}\right)_{\text{cruise}}$ for the glide ratio during cruise flight and E_{sb} the energy mass density. This formula can be used for all circuit segments during the mission.

For turning flight, Equation 4.80 is adjusted slightly, using a small detour, as can be seen in Equation 4.81. R is replaced by R_{turn} and the lift-to-drag ratio $\left(\frac{L}{D}\right)_{\text{cruise}}$ is replaced by $\left(\frac{L}{D}\right)_{\text{turn}}$. Specifically, the range for the turn will be replaced by relating the flight speed to the turn time for four 90° turns. This approach can be used for all the phases that are labeled as turning phases.

$$R_{turn} = v_{TAS} \cdot t_{turn} = V_{TAS} \cdot 4 \cdot \frac{\pi \cdot V_{TAS}}{2 \cdot g \cdot \sqrt{\frac{1}{cos(\phi)^2} - 1}} \tag{4.81}$$

Adding all battery mass fractions, the battery mass can be calculated. The descent phases are not taken into consideration as they are not powered.

Energy-per-Phase Method

A different approach to calculate the battery mass is the following: The total energy required for the mission can be obtained by adding up the energy consumed by the motor per engine phase as seen in Equation 4.82

$$E_{tot} = \sum P_{prop_i} \cdot t_i \tag{4.82}$$

Here P is the power setting per flight phase, and t is the time that this flight phase takes. This energy sum can be used to calculate the battery mass with the help of the energy density E_{sb} of the battery as seen in Equation 4.83.

$$W_{bat_{req}} = \frac{E_{tot}}{E_{sb} \cdot \eta_{tot}} \tag{4.83}$$

For the climb phase, Equation 4.79 is used. The time is calculated using the simple relation $t = \frac{\Delta h}{ROC}$.

The power setting for steady flight is given by Equation 4.84.

$$P_{prop} = D_{cruise} \cdot V_{tas} \tag{4.84}$$

Again the time is calculated using $t = \frac{R}{V_{tas}}$.

For turning flight again an adaption of the steady flight formula is used in Equation 4.85.

$$P_{prop} = D_{turn} \cdot V_{tas} \tag{4.85}$$

The time for the turn is calculated using the second part of Equation 4.81.

Again, descents and glides are not powered and hence do not influence the power calculations.

4.5.4. Engine Failure

Engine failure is, as was previously mentioned, analysed when occuring at 15 m altitude. The tow craft is supposed to then climb out at a non-constant ROC and/or γ. This value will namely be determined by the power that is available. The power thus limits the ROC. For engine out Equation 4.86:

$$D_{tot} = D_{TO} + D_{failure} \tag{4.86}$$

D_{nom} is the nominal drag the craft experiences. $D_{failure}$ is the extra drag that the craft experiences due to the failure. Typically, rudder deflections and windmilling propellers create this type of drag. For the rudder deflections mainly the yaw moment which needs to be compensated for, is important. The extra drag due to the windmilling is depending on the ability for it to feather. Although, an exact order of magnitude for $D_{failure}$ is not known, it is assumed that it will have the same order as the nominal drag during take-off, D_{TO}.

4.5.5. Taxi and Take-Off

The taxi and the take-off phases are pre-calculated phases and are added to the methods mentioned above. The energy that is added is given by:

$$m_{bat_{ground}} = \frac{E_{taxi} + E_{TO}}{E_{sb}} \tag{4.87}$$

Here, E_{taxi} is the energy spent on taxiing, E_{TO} is the energy spent on take-off and E_{sb} is the specific energy of the chosen battery type. E_{taxi} is a set value based on the speed of the taxi and the distance, as well as the force required to taxi at that speed. E_{TO} is calculated as seen in Equation 4.88

$$E_{TO} = P_{TO} \cdot t_{TO} = T_{TO} \cdot V_{TO} \cdot t_{TO} \tag{4.88}$$

4.5.6. Sizing for Power

The calculation concerning the maximum power, the parameter which drives the size of the motor, is based on the following considerations: The maximum power will either be required during take-off or climb. For the take-off, the following two formulas, Equation 4.89 and Equation 4.90, are considered.

$$P_{req} = \frac{1}{\eta} \cdot T_{TO} \cdot V_{TO} \tag{4.89}$$

The next formula that is considered is the climb power formula, Equation 4.79. It yields the power needed to sustain the speed and the climb rate. Climb segment 1 is considered most relevant and determining here. The last consideration is the power that must be applied to get the tow craft and the glider into motion during take-off. As the craft is standing still, the forward velocity is zero and hence Equation 4.89 will not yield meaningful results. Hence, other ways of solving for required power during standstill are considered. It is found that the disk actuator theory can be applied for a first, rather rough estimate. For a "statically thrusting propeller $V_0 = 0$", Equation 4.90 holds [25, p.492].

$$P_s = \sqrt{\frac{T_s^3}{2\rho A}} \tag{4.90}$$

Here T is the take-off thrust and A is the disk area, spanned by the propeller.

Determining the maximum of the three will be the limiting factor and hence is one requirement for sizing the motor. These are the considerations taken in mind for the maximum power situations. However, also the maximum continuous power setting must be kept in mind to not overexert the engine, and cause too high power loading. This is data, which is usually given by the manufacturer. However, it must be kept in mind when choosing the motor.

4.5.7. Propeller Sizing

For the sizing of the propeller, a statistical relationship is used which is described in Raymer and Gudmundsson [12, 15]. This, considering the fact that the tow craft shares a big similarity with the Pipistrel Velis Electro aircraft is the basis for the propeller sizing and propeller selection. Raymer proposes the following statistical relationship, shown in Equation 4.91, to size the propeller for an initial design.

$$D_{prop} = k \cdot \sqrt[4]{P_{shaft}} \tag{4.91}$$

Here P stands for the brake horsepower of the engine and k is dependent on the number of blades in the propeller. A value of 0.56 is used in the case of two blades, and 0.52 otherwise.

4.5.8. Energy Recuperation

A drag $D_{descent}$ will be present on the propeller during any of the four descent stages as the craft glides at a maximum flight speed of 280 km/h to the next stage. The value of this parameter is undetermined so far. To ensure the drag stays high enough that the maximum airspeed is not exceeded, the drag is turned into energy with the purpose of recuperation.

The gliding stage falls between an altitude of 1,000 m and 200 m. For safety reasons, recuperation is not accounted for below 200 m in altitude. To calculate the braking drag, the windmilling drag coefficient due to a

propeller $C_{D_{\text{wmprop}}}$ is used, see Subsection 4.2.4 [19]. For clarity, it is hereafter repeated in Equation 4.92.

$$\Delta C_{D_{\text{prop}}} = 33 \cdot \frac{1}{\bar{q} \cdot S} \cdot \frac{SHP_{\text{rated}}}{U_1} \tag{4.92}$$

Here, SHP_{rated} stands for the maximum rated shaft horsepower of the engine in the flight condition at hand, and U_1 stands for the steady state flight speed.

Next, Equation 4.93 can be set up.

$$D_{\text{prop}} = \Delta C_{D_{\text{prop}}} \cdot \frac{1}{2} \cdot \rho \cdot V_d^2 \cdot A_{\text{prop}} \tag{4.93}$$

Here, V_d stands for the descent flight speed, and A_{prop} can be calculated using $\pi \cdot \frac{d^2}{4}$.

Furthermore, the energy and power recuperated can be calculated using Equation 4.94 and Equation 4.95.

$$E_{\text{recup}} = D_{\text{prop}} \cdot s \cdot \eta_{\text{recup}} \tag{4.94}$$

$$P_{\text{recup}} = D_{\text{prop}} \cdot V_{\text{descent}} \cdot \eta_{\text{recup}} \tag{4.95}$$

The distance s can be found from the 6° flight path angle and difference in altitude of 800 m. s then turns out to be equal to $\frac{800}{\sin 6 \cdot \frac{\pi}{180}}$. η_{recup} is estimated to be approximately 10 % [26].

4.5.9. Noise

by Tamara

Noise is also an important factor to take into account for the PPP department. The main contributor to the noise is the propeller of the engine. To calculate the noise level the propeller creates, an empirical equation is used. The equation can be seen in Equation 4.96, here the SPL is the maximum sound pressure level in decibels. It is calculated using the brake power (P_{br}) of the engine in watts, the diameter (D) of the propeller in meters, the tip Mach number (M_t), the number of blades (B), and the number of propellers (N_p) [27].

$$SPL_{1,max} = 83.4 + 15.3 \log P_{br} - 20 \log D + 38.5 M_t - 3\,(B - 2) + 10 \log N_p \tag{4.96}$$

The tip Mach number is calculated with the propeller diameter(D), the rotational speed of the propeller(n_p) in rpm and the speed of sound (a) as shown in Equation 4.97 [27].

$$M_t = \frac{\pi \cdot D}{a} \frac{n_p}{60} \tag{4.97}$$

To get the maximum sound pressure on another distance Equation 4.98 can be used. The subscript s denotes the distance that the sound pressure is measured in decibels.

$$SPL_s = SPL_1 - 20 \log s \tag{4.98}$$

5
Design Synthesis

All of the subsystem design methods are integrated together in an iterative process, this process, and the results, are discussed in this chapter.

5.1. Iteration

by Filip, MianTao

Due to the inter-dependencies of subsystems and parameters of the tow craft, an iterative loop is required to develop a feasible designs. This allows all departments to converge upon a coherent and optimised design. Several tools from each department described in Chapter 4 have been integrated into an iteration loop. The structure of this loop is presented on Figure 5.1.

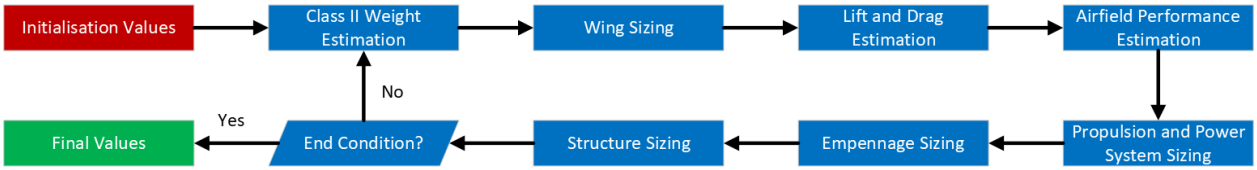

Figure 5.1: Design iteration loop.

The loop ends after a specified amount of iterations has been performed or when the relative change in every variable is smaller than 0.03% between two iterations. This number has been demonstrated to indicate convergence in initial testing of the loop and is not a measure for the accuracy of the method. If the loop breaks due to the maximum number of iterations, there is a large probability that the design does not converge. This means that the design is not viable for the specified initial values, requirements, and constants. In this case these values need to be adjusted. Furthermore, the design methodology can also be adjusted to produce a viable design. In addition early divergence of the iteration loop may also occur, causing the program to crash. This can be caused by a highly unfeasible design, but may also be caused by errors in the design methodology or errors in their implementation and integration. In this case the methods should be reevaluated to find possible errors overseen in the verification and validation.

A final iteration loop was performed which converged after 48 iterations. This yielded a viable design which will be discussed and designed in more detail in Sections 5.2 to 5.6.

5.2. Structures, Materials and Manufacturing (SMM)

by Andreas, Stan

The core of the iteration process is the weight estimate of the craft. It is therefore essential that these values are analysed criticaly, weaknesses in the process are identified, and conclusions about the design iteration are made. This section will interpret the results of the various SMM tools and present recommendations for further study.

5.2.1. Results and Iterations

The results from the iteration presented in Section 5.1 for the SMM department are shown in Table 5.1a, Table 5.1b, Table 5.2a, and Table 5.2b.

Due to time constraints, the actual values for the landing gear mass and fuselage mass are not included in the iteration (the actual wing mass is included). The values included in the iteration are obtained from the Class II Weight estimation presented in Subsection 4.1.2.

Table 5.1: Final results for fuselage and landing gear design.

(a) Final results for the fuselage.

Fuselage	Value	Unit
Nose Height	0.30	m
Maximum Height	0.50	m
Longitudinal Distance to Maximum Height	0.23	m
Tail height	0.25	m
Longitudinal Distance to Tail Fuselage	3.3	m
Nose Distance to Mid Tube	0.20	m
Tube Radius	0.01	m
Tube Thickness	$6.8 \cdot 10^{-4}$	m
Truss Frame Material	AL 6061 T6	-
Total Length	5.1	m

(b) Final results for the landing gear.

Landing Gear	Value	Unit
Strut Length	1.1	m
Strut Angle	20	deg
Strut Radius	0.05	m
Strut Thickness	0.011	m
Strut Material	AL 7075 T6	-
Tire Width	0.1	m
Tire Diameter	0.25	m

Table 5.2: Final results for the wing structure and masses of different components.

(a) Final results for the masses of the different components in the craft

Masses	Value	Unit
Max Take-Off Mass	210	kg
Wing Mass	40	kg
Electrical Motor Mass	30	kg
Empennage Mass	7	kg
Landing Gear Mass	12	kg
Fixed Equipment Mass	65	kg
Battery Mass	43	kg
Fuselage Mass	13	kg

(b) Final results for the wing structure design

Wing	Value	Unit
Wing Box Height	0.12	m
Wing Box Width	0.37	m
Number of Stringers	16	-
Stringer Width	0.2	m
Stringer Thickness	0.001	m
Spar Thickness	0.001	m
Wing box material	AL6061T6	-
Number of Ribs	4	-
Sheet Thickness	0.001	m

5.2.2. Wing Design

The wing design is found using the approach discussed in Subsection 4.1.3. The results can be seen in Table 5.2b

Geometry and Loads

After iterations, the wing design is limited by the minimum material thicknesses that is practical to manufacture and assemble. A limit of one millimetre is set for the skin thickness and stringer thickness. Sheet buckling is identified as the most limiting load case studied, requiring at least 14 stringers to ensure that the critical buckling stress is higher than the design stress. 16 stringers are selected as the more weight efficient configuration. A minimum of two ribs are required.

With the numbers specified in Table 5.2b, the wing bending deflection seen under the maximum load factor of 5.3 can be seen in Figure 5.2.

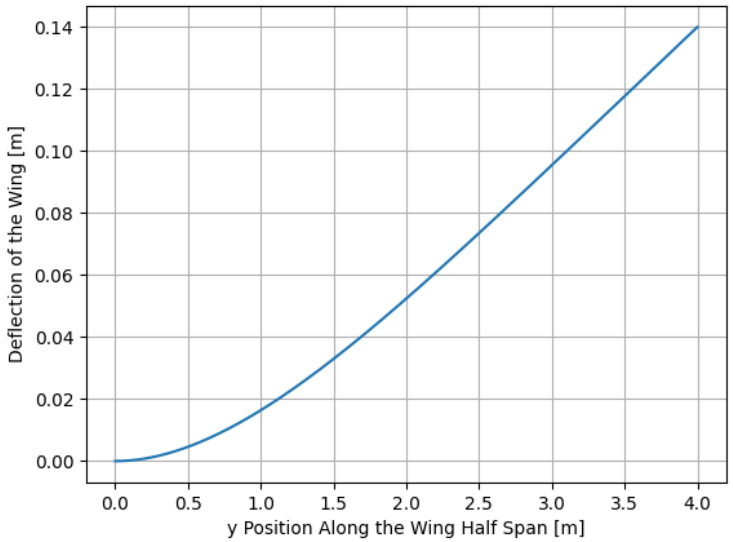

Figure 5.2: Wing bending deflection due to maximum aerodynamic loads.

Material Selection

The wing is tested with several materials, the best material being the 6061-T6. Using this material, the wing has a mass of 39.7 kg. This material is both widely available, relatively affordable, light. durable, and corrosion resistant. The wing has to be riveted, as they are too thin to reliably weld. Al 6061-T6 has ideal properties for forming the panels shaped around the airfoil, and for riveting.

The wing mass of *MARCUS-T* can be compared to the Bede BD5B wing mass. The wing surface area of the Bede BD5B is 4.4 m^2 and has a wing mass of 39.4 kg [7]. The wing surface area of *MARCUS-T* is 4.7 m^2 and has a mass of 39.5 kg. These numbers are comparable and the slightly lower fraction of the wing mass over wing surface area of *MARCUS-T* is due to the fact that the ribs and rivets have not been taken into account when calculating the wing mass.

Recommendations and Future Design

The wingbox assumes the number of stringers throughout the span, with thicknesses being scaled with the chord length. This results in a uniform decrease in area along the span, and stringers, sheets, and spars with a 0.45 mm thickness at the tip. The weight is re-calculated preventing sheet thicknesses from dropping below the minimum value of 1 mm, which results in a small increase in mass of 1 kg.

In the real wing, more ribs are expected such that the complex airfoil shape is maintained throughout the span. The stringer thicknesses are kept constant, but the number of stringers reduce along the span. More analysis needs to be performed for an optimal design.

No analysis was done for flutter or loading in other directions. This is important analysis that needs to be done before the design can be finalised. Flutter is unlikely to be an issue on the main wing due to the zero leading edge sweep, but the high aspect horizontal tailplane, and the thin fuselage leading to the tail, may pose higher risk of flutter. Additionally, more analysis needs to be done calculating stress throughout the whole span of the wing. Due to time constraints, the analysis was focused at the root, where the forces are the highest. However, as the chord decreases, the moments of inertia decreases, increasing the bending stresses along the span, complicating the analysis. A preliminary Finite Element Analysis analysis shows that this is the case. The design is strong enough at the root, but near the tip, the stress in a stringer exceeds its yield strength.

5.2.3. Fuselage Design

The results for the fuselage design can be found in Table 5.1a. These results are found using the method described in Subsection 4.1.4. This subsection presents an analysis on the design of the fuselage structure.

Geometry and Loads

The load case chosen to be assessed is the case of a steady horizontal coordinated turn with a load factor of 5.3 [9] (as seen in Figure 4.9). This load case results in the moment diagram seen in Figure 5.3.

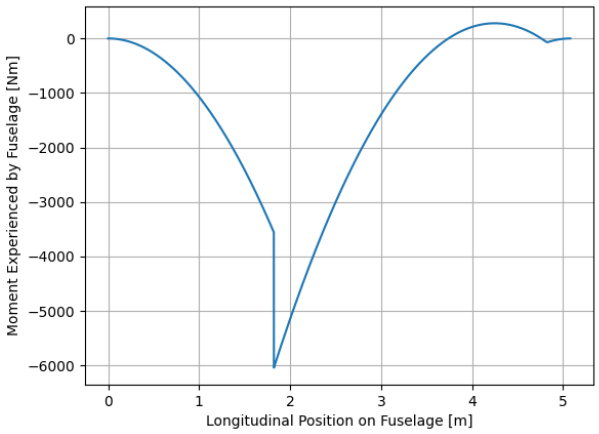

Figure 5.3: Moments experienced by the craft fuselage during steady, horizontal coordinated flight with a load factor of 5.3.

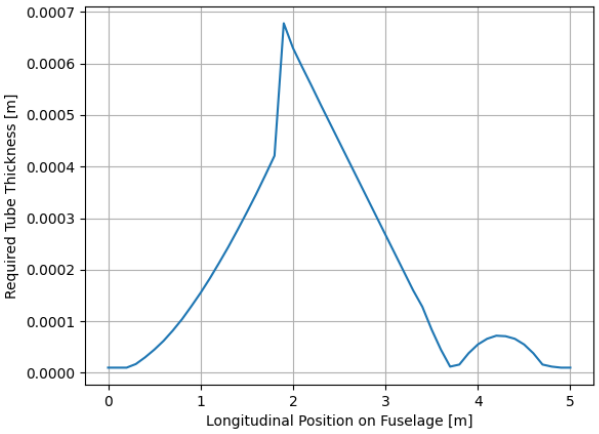

Figure 5.4: Cylinder thickness required for fuselage truss structure.

As expected, the first 1.8 meters (up until the aerodynamic centre of the wing) experience only the distributed load, resulting in a quadratic form of the moment diagram. The moment around the aerodynamic centre is then applied resulting in a step down in the moment diagram as this is a negative moment with the coordinate frame chosen. The lift force of the wing results in a steep positive slope which decreases with x position on the fuselage. Finally, there is one more change in the moment diagram at the aerodynamic centre of the tail where the tail lift force is applied.

The resulting required thickness of the cylinders, can be seen in Figure 5.4.

The maximum required thickness can be found around 1.8 meters on the x-axis. The maximum required thickness will be used for the whole fuselage structure. As can be seen in Table 5.1a, the required fuselage tube thickness is 0.68 mm. This is a very small thickness and it can thus be concluded that the bending moments, induced by aerodynamic loads, will not be the limiting cases for the fuselage structure. Instead, in further analysis, it is recommended to calculate the thickness required during other loading cases as for instance: the landing loads induced by the landing gear, or torsional loads induced by aerodynamic forces.

Structure Material Choice

The material choice for the fuselage truss structure has an influence on several aspects. The material has to be weldable, as the truss structure will be welded during production. The material has to be light and at the same time strong enough to cope with any loads induced in the fuselage. The material is preferred to be cheap to minimise the craft cost. Finally, the material has to be recyclable for sustainability reasons. The material chosen is aluminium 6061 T6. This aluminium is light weight compared to other commonly used metals in the aerospace industry and is the aluminium alloy which has the best weldability [12]. Also, recycling aluminium 6061 T6 results in almost no changes in its mechanical properties, making it very desirable from a sustainability point of view [28]. Aluminium 6061 T6 has been used throughout this analysis.

At this stage Ceconite, or similar modern skin canvas materials, are selected as the skin material for the fuselage. These are very light, cheap to purchase, and easy to assemble, keeping manufacturing costs down. However, further research has to be performed into the skin material used.

The mass of the fuselage, as seen in Table 5.2a, is 13.3 kg. To see if this number makes sense, the fuselage mass is compared to the Bede BD5B (with a maximum take-off mass of 473 kg), which has a fuselage mass of 40 kg [7]. Linearly decreasing this maximum take-off mass and fuselage mass down to the point where the maximum take-off mass matches that of *MARCUS-T* , results in a fuselage mass of 18 kg. The slightly smaller fuselage mass of *MARCUS-T* can be explained by noting that the skin has not been included in the fuselage mass yet.

Recommendations and Future Design

The fuselage design still has room for improvement. There are several loading cases which still have to be analysed resulting in larger thicknesses for the tubes in the fuselage truss structure. Also, buckling of the fuselage tubes has to be analysed. The assumption made that the weight of the fuselage is distributed uniformly should be changed to a more reliable distribution, for more reliable moments. Furthermore, a detailed trade off for skin materials has to be performed to find an optimal skin material. The fuselage geometry which has been used throughout the analysis has to be optimised, as this geometry is arbitrarily chosen. The current fuselage volume is significantly larger than required for all the necessary systems, this gives room for future requirements, but also an opportunity to further shrink the size of the craft. Finally, a more in depth material study has to be performed to find the most optimal material, also considering composite materials. This should be done for both the wing structure and wing skin.

5.2.4. Landing Gear Design

The landing gear is designed according to the method described in Subsection 4.1.5. Results can be found in Table 5.1b. This subsection presents an analysis on the design of the landing gear.

Geometry and Loads

The length of the landing gear is determined by taking the propeller radius and adding the required propeller ground clearance as specified by CS-23 [9]. The propeller ground clearance is set at 0.23 m for a plane with a tail landing gear and the propeller radius is 0.77 m. The total landing gear height being thus at least 1 m. With a landing gear angle of 20°, the cylinder length should be at least 1.06 m and is set at 1.1 m.

Iterations are performed between the force created on the landing gear by landing with a vertical speed of 1.77 m/s, the buckling force of a hollow cylinder, and the yield stress of the landing gear approached by bending. This results in a minimum thickness for buckling of 0.0039 m and for bending of 0.0083 m. The bending yield stress is thus the limiting case, and will thus be used as the minimum cylinder thickness of the landing gear.

Structure Material Choice

The material chosen for the landing gear depends on multiple aspects. The material has to be stiff and strong such that it can handle the landing loads without buckling or failing due to surpassing the yield stress. It is preferred to have a cheap material which is easy to form into the shape of a hollow cylinder. Moreover, the landing gear is optimised for low mass. Using Aluminium 6061-T6 for instance would lead to having a landing gear mass of 26.8 kg, while using titanium 6AL-4V results in having a landing gear mass of 12.2 kg. The two materials which lead to the lowest mass are found to be titanium 6AL-4V and aluminium 7075 T6. Titanium having a mass of 11.6 kg and aluminium a mass of 17.3 kg. As titanium has a price almost ten times as high as aluminium, aluminium 7075 T6 will be used for the landing gear hollow cylinders. This material has been used throughout the analysis.

The mass of the landing gear presented in Table 5.1b is the mass as specified by the Class II Weight estimations. This is because the mass estimation presented earlier in this analysis, is not included in the iteration loop due to time constraints. However the Class II Weight estimation does provide a reason for the calculated mass to be correct. Also comparing the mass values obtained to the mass of the landing gear of the Bede BD5B, being 14.4 kg, ensures that the numbers do make sense [7].

Wheel Design

As part of the landing gear design, the 8.5 inch goodyear tubeless tire 856T61-1[1] is selected as the main wheel tire. This is an initial selection, done in lieu of a formal trade off due to time constraints. This tire is common in general aviation and should easily handle the unpaved runways common in gliding clubs. A wheel fairing is also placed around the main gear. Referring to Figure 5.5, type A has been selected [19].

[1] www.aircraftspruce.com [cited 17 June 2024]

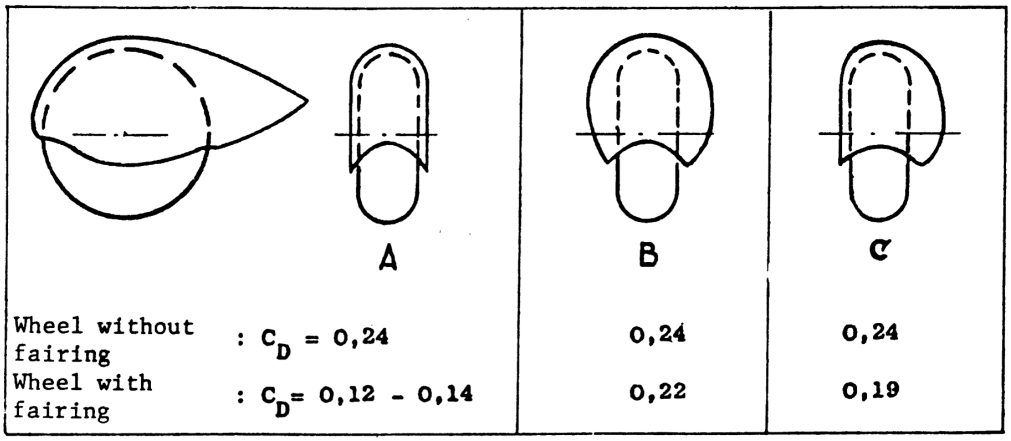

Figure 5.5: Wheel fairing options.

Recommendations and Future Design

The landing gear calculations and analysis are based on preliminary assumptions and simplifications. This results in having an over simplified model of the landing gear. This analysis thus has to be performed in further detail using an appropriate mass spring system, which also included any dampeners or springs. The result being a differential equation rather than the quadratic equation presented in Subsection 4.1.5. Oscillations will thus take place and these have to be taken into account when sizing the landing gear. Besides this are the tires now assumed to be fully rigid and transferring the full load to the landing gear struts. However, the tires will absorb some part of the landing energy because of the inflation they have.

5.3. Aerodynamics (AERO)

by Filip, Niels

This section presents the aerodynamic results of the iteration. To begin with, the wing planform sizing is described, followed by the lift and drag performance.

5.3.1. Wing Planform Design

Using the methodology described in Section 4.2, a wing planform is obtained. The relevant parameters are presented in Table 5.3.

Table 5.3: Wing planform parameters.

Parameter	Symbol	Value	Unit
Airfoil	-	DU15-160/15	-
Wing surface area	S	4.72	m^2
Wingspan	b	8.65	m
Aspect ratio	AR	15.6	-
Root chord length	c_r	0.75	m
Tip chord length	c_t	0.34	m
Taper ratio	λ	0.45	-
Wing LE sweep angle	Λ_{LE}	0	deg
Maximum wing loading	W/S	44.5	kg/m^2

The results of the wing planform sizing are in-line with the expectations based on the determined weight. The highest wing loading that the tow craft achieves is comparable to typical gliders and motor gliders [29] [3]. Furthermore, the aspect ratio that follows from the wing area and the wingspan (determined based on CS requirements), is in the expected order of magnitude. As mentioned before, the sweep angle of the leading edge of the wing is zero to move the CG of the wing to the front for improved stability.

Dimensions of the high lift devices and ailerons are also calculated and presented in Table 5.4. The HLD will be deployed for landing to increase the lift coefficient and, therefore, decrease the stall speed of the craft.

Furthermore, there is a possibility of deploying them during the dive descent to significantly increase the drag coefficient of the craft. Due to their large drag coefficient when deployed, there is no need for additional airbrakes (simplifying the design) to slow down the tow craft during this manoeuvre. However, this is revised in Figure 5.3.3.

Table 5.4: High lift device and ailerons parameters.

(a) HLD parameters.

Parameter	Symbol	Value	Unit
Flap-chord ratio	$\frac{c_f}{c}$	0.15	-
Flap span ratio	$\frac{b_f}{b}$	0.6	-
Flap span	b_f	5.19	m
Flap area	S_f	0.294	m^2
ΔC_L at 40° deflection	$\Delta C_{L,40}$	0.525	-

(b) Ailerons parameters.

Parameter	Symbol	Value	Unit
Aileron-chord ratio	$\frac{c_a}{c}$	0.15	-
Aileron-span ratio	$\frac{b_a}{b}$	0.25	-
Aileron span	b_a	2.16	m
Aileron area	S_a	0.158	m^2

The aileron's flap-chord ratio is a pre-determined value, as the chosen airfoil was designed for a flap-depth of 15%. Furthermore, it has been decided to fix the flap-span ratio to 60%, calculate the performance of the flap, and adjust this value if needed. In Section 5.5 it is shown that this flap sizing meets the requirements for landing performance. Using the wing planform's sizing and the previously mentioned flap dimensions, the span of the HLD and their surface area can be found. Those values can be found in Table 5.4a.

Combining all parameters described in this section, it is possible to make a top view of the wing planform. This can be seen on Figure 5.6, along with the most important dimensions.

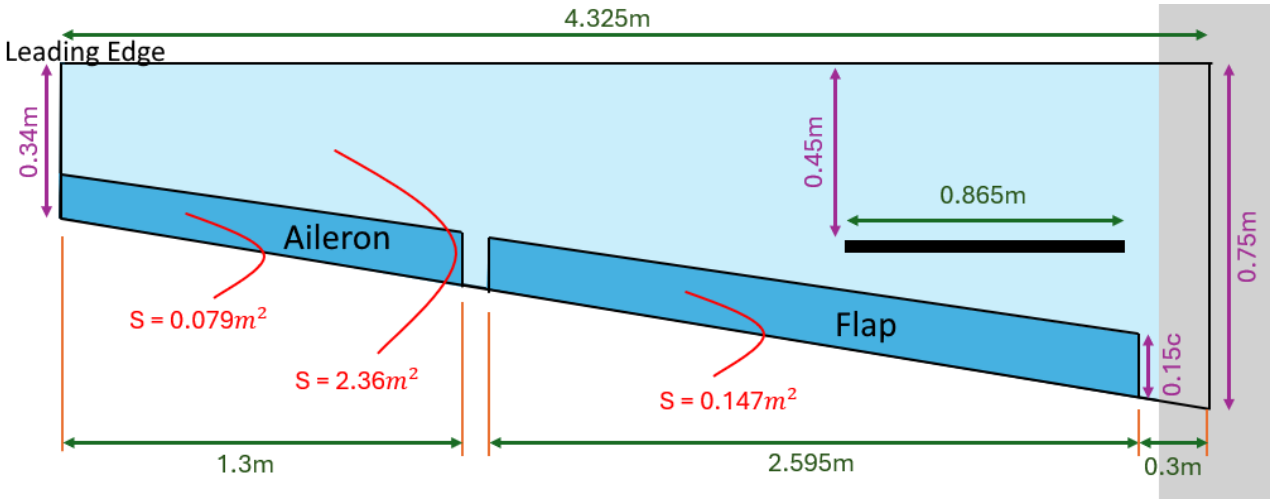

Figure 5.6: Wing planform top-view (not to scale).

5.3.2. Lift Performance

The iteration loop allows to calculate the final lift performance of the craft. The different values of the lift curves for the airfoil, wing, and aircraft are presented in Table 5.5. The resulting lift curves from those values are presented in Figure 5.7. This figure also includes the airfoil's lift curve that was found using XFLR5.

Table 5.5: Lift curve parameters calculated for *MARCUS-T* at Re=2,000,000.

Parameter	Symbol	Airfoil	Wing	Aircraft	Unit
Lift curve slope	C_{L_α}	0.1114	0.1124	0.1203	1/deg
Maximum lift coefficient	$C_{L_{\max}}$	1.775	1.66	1.76	-
Maximum lift coefficient AoA	$\alpha_{C_{L,max}}$	15.6	13	13	deg
End of linear region AoA	α^*	2	2	2	deg
Zero lift AoA	α_0	-11.4	-11.4	-11.4	deg

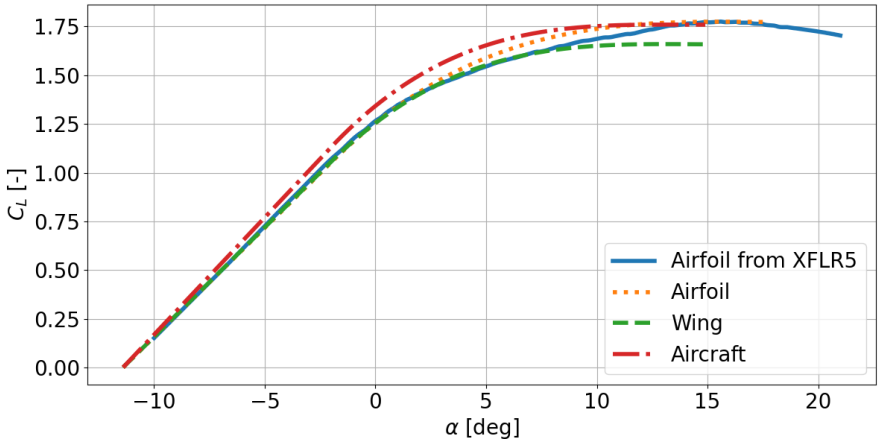

Figure 5.7: Lift curves at Re=2,000,000.

The wing's lift performance is in line with expectations. Since the wing has no twist and the craft flies in the low-speed region, the zero-lift angles of attack for both the airfoil and the wing are the same. Furthermore, the highest lift coefficient obtained by the wing is lower than that of the airfoil. This reduction is caused by the wingtip vortices and induced drag, which lower the overall lifting performance of the wing. Wings are less efficient in generating lift than a theoretical, infinite wing. Additionally, the maximum lift coefficient of the entire aircraft is higher than that of the wing alone. This is correct, as the fuselage itself creates lift, and the horizontal tail adds some lifting force to the craft. Due to the assumptions used, the AoAs for the ends of the linear regions (α^*) are the same for all three curves. In addition, since a symmetrical airfoil is used for the vertical stabiliser and the wing's incidence angle is zero, the zero-lift AoAs are also the same.

A interesting thing to note is that the lift curve slope for the airfoil, found with XFLR5, is slightly higher than the theoretical maximum slope from the thin airfoil theory. This may be caused by the fact that the thin airfoil theory assumes no viscous effects and XFLR5 plots the lift curves for a given Reynolds number. Therefore, the slopes plotted by the program may deviate from the theoretical maximum. Also, thin airfoil theory might start to break down for the 15% thick airfoil used.

5.3.3. Drag Components

In Table 5.6 a breakdown of the different drag components, as calculated in Subsection 4.2.4, is given. The drag coefficients are computed at 130 km/h, the towing airspeed.

Table 5.6: Drag breakdown during towing.

Component	Zero-lift drag coefficient	Induced drag coefficient	Total drag coefficient	Percentage of total drag [%]
Wings	0.0076	0.0072	0.0148	51
Fuselage	0.005	0.0002	0.0052	18
Horizontal tail	0.001	0.0001	0.0011	4
Vertical tail	0.001	0	0.001	3
Gear	0.007	0	0.007	24
TOTAL	**0.0216**	**0.0075**	**0.0291**	**100**
Windmilling propeller drag	0.012	0	0.012	-
Stopped propeller drag	0.003	0	0.003	-
Flaps 40° drag	0.008	0.009	0.017	-

Computing the C_D over the C_L range, the C_L - C_D curve is computed for the tow craft and presented in Figure 5.8. This curve is validated using the curves plotted in Figure 5.9. Here the drag polars are found for various older gliders. When comparing the tow craft, which falls under the powered sailplane category, to these gliders one can see that the tow craft's drag polar is shifted to the right with 0.01 C_D. This is expected as the gliders presented do not have a large landing gear extended and no large propeller causing additional drag. This validates the Class II Drag estimation performed in Subsection 4.2.4.

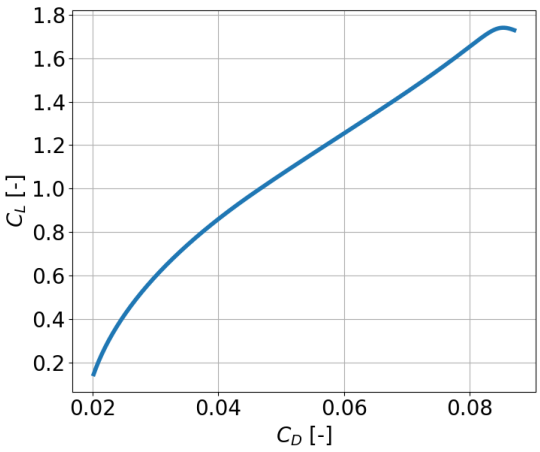

Figure 5.8: Drag polar for the tow craft.

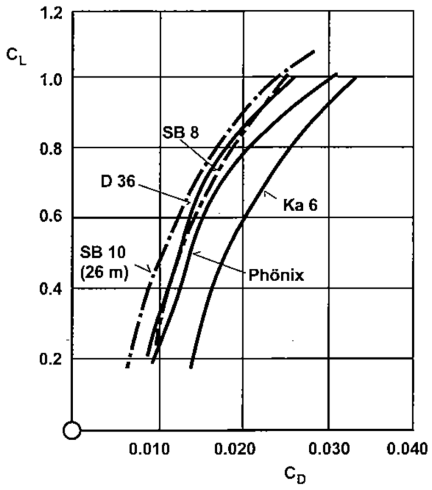

Figure 5.9: Calculated drag polars of existing gliders by Thomas [30].

Climb Performance

The optimal climb performance is reached when the sink speed is minimised. As stated in Subsection 4.2.1, the minimum sink rate is obtained when $\frac{C_L^{\frac{3}{2}}}{C_D}$ is maximised. Figure 5.10 is computed with the C_L of the wing, and the C_D of the whole aircraft. The optimal climb performance is thus obtained at an angle of attack of 4 degrees.

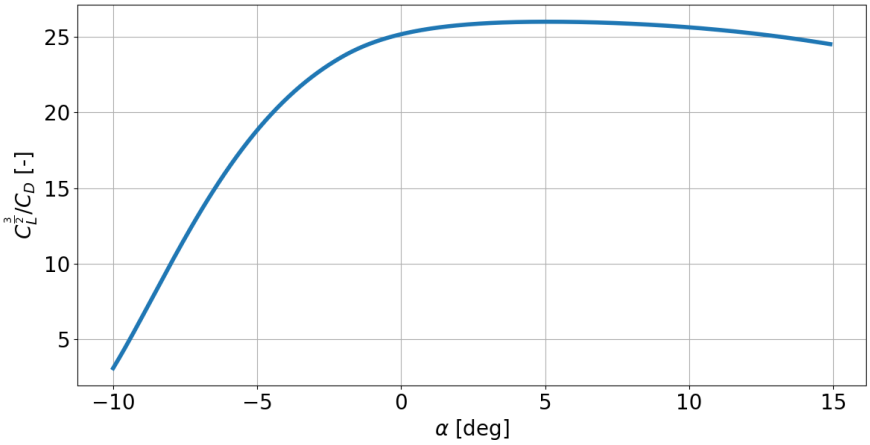

Figure 5.10: $\frac{C_L^{\frac{3}{2}}}{C_D}$ curve for *MARCUS-T*.

Return Flight

After calculating the drag components it is necessary to check if the total drag is high enough for the dive descent profile. The total drag coefficient, assuming a windmilling propeller and a 40° flap defection is 0.046. The required drag can be calculated using Equation 5.1.

$$c_{D_{dive,req}} = \frac{W \cdot cos(\gamma)}{0.5\rho \cdot v_{dive}^2 \cdot S} = 0.085 \tag{5.1}$$

It can be seen that the drag generated by the craft in its current configuration is too small for the dive manoeuvre; the additional drag coefficient should be at least 0.039. Therefore, it is necessary to create additional drag during this phase of flight. This can be either achieved by modifying the HLD or by adding an airbrake on the wings. Increasing the flap depth is not possible as the selected airfoil has been optimised for a

flap-chord ratio of 15% and this is already used to the full extend. There is a possibility to increase the span of the flaps, however doing so would decrease the space available for ailerons. For this reason it is decided to add an airbrake to the wing.

The size of the airbrake can be estimated using Roskam's method. It is decided to use a flat plate that extends upwards from the wing as seen on Figure 5.11 and is placed at 60% of the wing's chord. The drag coefficient of an airbrake can be calculated using Equation 5.2 [19, eq. 4.85].

Figure 5.11: Flat-plate airbrake at 0.6c.

$$c_{D_{airbrake}} = c_{D_{sp}} \cdot \frac{S_{airbrake}}{S} \tag{5.2}$$

With $c_{D_{sp}}$ being the specific drag coefficient for an airbrake type at a certain location and $S_{airbrake}$ the area of the airbrake.

The specific drag coefficient for the selected airbrake is 1.60 [19, fig. 4.76]. Furthermore, it is decided that the airbrakes should span 20% of the wingspan. By rewriting Equation 5.2, and filling in the previously mentioned values, it is possible to determine that the airbrake should have a height of 6.5 cm.

5.3.4. Winglet Parameters

From Subsection 4.2.5, the winglet parameters are computed and can be found in Table 5.7. These are based on the Whitcomb winglet as specified in Figure 4.23. A render of the actual winglet is presented in Figure 5.12.

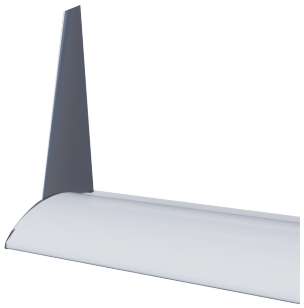

Figure 5.12: *MARCUS-T* winglet render.

Table 5.7: Winglet design parameters.

Parameter	Symbol	Value	Unit
Airfoil	-	PSU 94-097	-
Winglet tip chord	c_{wt}	0.071	m
Winglet root chord	c_{wr}	0.22	m
Winglet height	h_w	0.339	m
Winglet sweep angle	$\Lambda_{winglet}$	38	deg
Winglet twist angle	$\epsilon_{winglet}$	2.6	deg
Winglet toe angle	$\Gamma_{winglet}$	1	deg
Winglet cant angle	$\Theta_{winglet}$	75	deg
Increase in aspect ratio	ΔAR	1.16	-

Recommendations

It is discovered at a late stage that with a positive flap deflection at high speeds, the lower side of the airfoil will cause issues. This happens because the transition point moves rapidly forward when decreasing the angle of attack. According to Ir. Boermans, a laminar separation bubble will form at the nose which bursts when the angle of attack is decreased past a certain critical value. The rapid forward movement of the transition point can be observed in Figure 5.13. The transition point can be seen moving from approximately 0.68c to 0.55c to 0.21c when decreasing the angle of attack.

This phenomenon should be further investigated at a later stage. It could possibly be solved by including a 0 degree flap deflection (the original airfoil presented in Figure 4.14) for the return flight and increasing the airbrake size. The flaps will then only be used for takeoff, climb and landing.

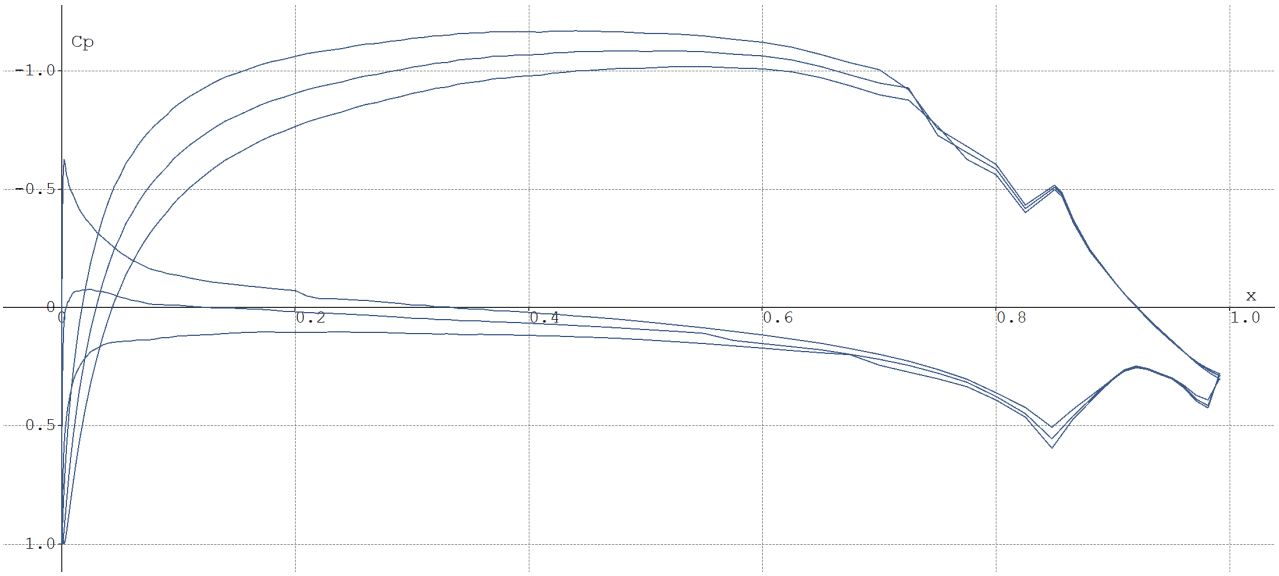

Figure 5.13: Pressure distribution at flap deflection of 20 degrees (nominal airfoil). At an angle of attack of -2.5 (lower curve), -3.8 (middle curve) and -5 (upper curve) degrees at Re = 3,000,000.

5.4. Software, Stability and Control (SSC)

by Gerard, MianTao

In this section stability and control related results are presented. These results are explained and checked for their validity through calculations. Sizing of the control surface is also performed, as well as a preliminary stability analysis. Finally recommendations are given for future development.

Hardware, software and data handling diagrams are not found in this section and are instead in Section 9.1.

5.4.1. Static Stability Check

The resultant stability is checked by locating the resultant neutral point and the CG excursion range. Relevant final values used for this check are found in Table 5.8.

Table 5.8: Values used for the verification of the stability of *MARCUS-T*.

x_{CG}		$\bar{x}_{\text{ac}_w}$		$C_{L_{w,\max}}$	$C_{L_{h,\max}}$	x_{LEMAC}	l_h	$\bar{c}$	$C_{m_{\text{ac}}}$	S_h/S	$(V_h/V)^2$
Forward	Aft	Forward	Aft								
1.80 m	1.93 m	0.22	0.28	2.288	1.450	1.70	3	0.57	-0.25	0.09	0.85

The location of the neutral point (NP) can be approximated using Equation 5.3.

$$x_{\text{NP}} = \frac{C_{L_{w,\max}} \cdot x_{\text{ac}_w} + C_{L_{h,\max}} \cdot x_{\text{ac}_h} \cdot \frac{S_h}{S} \cdot \left(\frac{V_h}{V}\right)^2}{C_{L_{w,\max}} + C_{L_{h,\max}} \cdot \frac{S_h}{S} \cdot \left(\frac{V_h}{V}\right)^2} \tag{5.3}$$

Here, the distance to the aerodynamic centres can be computed using Equation 5.4.

$$x_{\text{ac}_w} = \bar{x}_{\text{ac}_w} \cdot \bar{c} + x_{\text{LEMAC}} \tag{5.4a}$$

$$x_{\text{ac}_h} = x_{\text{ac}_w} + l_h \tag{5.4b}$$

This is calculated for the most forward and aft situations, which yields the results in Table 5.9.

Table 5.9: Parameters used for the static stability analysis.

$x_{\text{CG,aft}}$		$x_{\text{CG,fwd}}$		$x_{\text{NP,aft}}$		$x_{\text{NP,fwd}}$		$C_{m_{\text{ac}}}$
1.93 m	$0.40\bar{c}$	1.80 m	$0.17\bar{c}$	2.00 m	$0.52\bar{c}$	1.97 m	$0.47\bar{c}$	-0.25

For all neutral point positions and CG locations, the NP is behind the CG. Thus, as $C_{m,\text{ac}} < 0$, it is concluded that the aircraft is longitudinally stable at all times ($\forall\, x_{\text{CG}},\ C_{m_\alpha} < 0$).

Controllability of the craft is checked by evaluating the sum of moments around the aft CG of the craft, and by computing the required lift coefficient of the horizontal tailplane C_{L_h} for the equilibrium using Equation 5.5.

$$C_{L_h} = \frac{S \cdot (C_{m_{\text{ac}}} \cdot \bar{c} + C_L \cdot (x_{\text{CG}} - x_{\text{ac}}))}{S_h \cdot l_h} - \frac{F_{\text{tow}}}{S_h \cdot l_h} \tag{5.5}$$

This yields a lift coefficient of -1.44 which is almost identical to the maximum negative lift coefficient of the HTP of -1.45.

Lateral stability is checked by computing the derivative of the coefficient of yaw with respect to sideslip C_{n_β} using Equation 4.44. This yields $C_{n_\beta} = 0.11$, which is higher than typical values which range from 0.04 to 0.1 and higher than the target value of 0.07 [21]. This is due to the method used adding additional tail surface area to counteract towing forces. However, this is only necessary for a tail design which is limited by controllability and not stability. Therefore the current vertical tail has an excessive tail area. Recalculation using Equation 4.45 reveals it can be sized down in the future by almost 30%.

5.4.2. Control Surface Sizing

Once the final empennage surface areas are obtained, the elevator and rudder sizes are determined. To do this, statistical values are used from Roskam [19, Tab. 9.2/9.3]. The elevator-to-HTP area ratio (S_e/S_h), rudder-to-VTP area ratio (S_r/S_v), rudder hinge location as a percentage of the VTP chord ($\%c_h$), and the elevator hinge location as a percentage of the HTP chord ($\%c_v$) are averaged, resulting in the values on Table 5.10.

Table 5.10: Average statistical values for rudder and elevator sizing.

$(S_r/S_v)_{\text{avg}}$	$(S_e/S_h)_{\text{avg}}$	$(\%c_v)_{\text{avg}}$	$(\%c_h)_{\text{avg}}$
0.24	0.26	0.695	0.690

This results in the dimensions for the rudder and elevator in Table 5.11. These values assume the control surfaces to be quadrilateral.

Table 5.11: Final dimensions for the elevator and rudder control surfaces.

$S_e[m^2]$	$c_e[m]$	$b_e[m]$	$S_r[m^2]$	$c_r[m]$	$b_r[m]$
0.110	0.0903	1.22	0.0878	0.130	0.678

5.4.3. Preliminary Dynamic Stability Analysis

To analyse the dynamic stability of the craft, the final dimensions of the design are used to obtain a preliminary set of stability derivatives using the DATCOM method presented in Appendix B. This method is described by Roskam, and is based on statistical data [19]. The following assumptions are made during the process.

- The stability derivatives obtained from the statistical DATCOM method are representative,
- When needed, sea level conditions are used,
- When needed, the maximum speed of the craft are used,
- The stability derivatives are assumed to be constant. Thus, when needed, the initial angle of attack is used,
- The center of gravity of the craft is aligned with the centerline of the fuselage,
- The aerodynamic centers of lifting surfaces are located at their quarter-chord points.

Recall that DATCOM is based on military and transport aircraft. *MARCUS-T* is a small electric unmanned aircraft, thus the derivatives obtained from DATCOM are only considered a preliminary estimate. The equations used to compute the derivatives can be found in Appendix B. The resulting derivatives are summarised in Table 5.12.

Table 5.12: *MARCUS-T* 's preliminary stability derivatives, rounded to three significant figures.

(a) Lateral.

C	$\frac{d}{d\beta}$	$\frac{d}{d\dot{\beta}}$	$\frac{d}{dp}$	$\frac{d}{dr}$
C_Y	-0.354	0.335	0	0.221
C_l	-0.0134	n/a	-0.186	0.450
C_n	0.100	0.116	-0.233	-0.315

(b) Longitudinal.

C	0	$\frac{d}{du}$	$\frac{d}{d\alpha}$	$\frac{d}{d\dot{\alpha}}$	$\frac{d}{dq}$
C_X	0	0	1.49	0	0
C_Z	-0.284	-0.0301	-6.90	-1.39	-6.25
C_m	n/a	0	-0.482	-6.71	-0.606

When looking at the signs of the lateral stability derivatives in Table 5.12a, these are the ones expected for a conventional-configuration craft. This is also the case for the signs of the longitudinal stability derivatives in Table 5.12b.

Using the state-space model, the resulting eigenmodes for no towing force and a maximum expected towing force of 320 N can be found in Table 5.13 and Table 5.14, respectively.

Table 5.13: Resulting eigenvectors using no towing force and the DATCOM stability derivatives.

Mode	Non-Dimensional Eigenvalue	Normalised Eigenvector	Main Contributions	Behaviour
Longitudinal 1	-0.70+0j	$[0.2, 0.7, 0.1, 0.0]^T$	α	Convergent Non-Oscillatory
Longitudinal 2	-0.34+0j	$[0.2, 0.3, 0.5, 0.0]^T$	θ	Convergent Non-Oscillatory
Longitudinal 3	0.00018+0.011j	$[0.8, 0.0, 0.2, 0.0]^T$	u	Divergent Oscillatory
Lateral 1	0+0j	$[0.0, 0.0, 0.0, 0.0, 1.0]^T$	ψ	Convergent Non-Oscillatory
Lateral 2	0.19+0j	$[0.2, 0.5, 0.0, 0.0, 0.3]^T$	ϕ	Divergent Non-Oscillatory
Lateral 3	-0.40+0j	$[0.4, 0.4, 0.1, 0.0, 0.1]^T$	β, ϕ	Convergent Non-Oscillatory
Lateral 4	-0.78+1.02j	$[0.2, 0.3, 0.2, 0.1, 0.2]^T$	ϕ	Convergent Oscillatory

Table 5.14: Resulting eigenvectors using the maximum towing force and the DATCOM stability derivatives.

Mode	Non-Dimensional Eigenvalue	Normalised Eigenvector	Main Contributions	Behaviour
Longitudinal 1	-0.73+0j	$[0.2, 0.8, 0.1, 0.0]^T$	α	Convergent Non-Oscillatory
Longitudinal 2	-0.15+0.32j	$[0.2, 0.3, 0.6, 0.0]^T$	θ	Convergent Oscillatory
Longitudinal 3	-0.0011+0j	$[1.0, 0.0, 0.0, 0.0]^T$	u	Convergent Non-Oscillatory
Lateral 1	0.010+0j	$[0.2, 0.1, 0.0, 0.0, 0.8]^T$	ψ	Divergent Non-Oscillatory
Lateral 2	-0.77+1.04j	$[0.2, 0.3, 0.2, 0.1, 0.2]^T$	ϕ	Convergent Oscillatory
Lateral 3	-0.41+0j	$[0.4, 0.4, 0.1, 0.0, 0.1]^T$	β, ϕ	Convergent Non-Oscillatory
Lateral 4	0.18+0j	$[0.2, 0.4, 0.0, 0.0, 0.3]^T$	ϕ	Divergent Non-Oscillatory

Here the eigenvectors in Table 5.13 and Table 5.13 show the fractional contribution to each state.

While *MARCUS-T* is statically stable in all configurations, as well as controllable, the state-space model shows the craft to not be dynamically stable. There is a divergent longitudinal mode, and a divergent lateral mode with no tow force.

When looking at the maximum tow force being added, it causes the divergent longitudinal mode to converge. However, the dormant lateral mode dominant in yaw engages, which adds a divergent lateral mode.

It makes sense that the craft has a divergent spiral (Lateral Mode 2) and convergent dutch roll (Lateral Mode 4). For both to be convergent, the Spiral Stability ($E = C_{n_\beta} \cdot C_{l_r} - C_{l_\beta} \cdot C_{n_r}$) and Routh's Discriminant (R) must both be positive respectively [24]. However, $E < 0$ for *MARCUS-T* , placing it in the region of spiral instability. This means that $\left|C_{n_\beta} \cdot C_{l_r}\right| > \left|C_{l_\beta} \cdot C_{n_r}\right|$. The two parameters that the designer can alter are the weathervane stabilty (C_{n_β}) and the effective dihedral (C_{l_β}) [24]. In the case of the design of *MARCUS-T* , C_{n_β} is fixed by design, being limited by a minimum VTP surface area. Thus, only the effective dihedral can be altered to make $E > 0$. To do this a dihedral of $\Gamma = 6°$ is chosen. The updated non-dimensional spiral eigenvalue for no towing force is thus $\lambda_c \simeq -0.00624 + 0j$.

For the phugoid (Longitudinal Mode 3), according to a simplified model provided by in 't Velt, the convergence criterion is $C_{X_u} < 0$ [24]. This makes sense, as for this criterion to be valid, the drag increases as velocity increases, subsequently resulting in a velocity decrease again. This parameter is proportional to the slope of the $C_D - M$ graph at the Mach number of *MARCUS-T* (Appendix B). This derivative was not computed and assumed to be 0. Thus, it is recommended to evaluate this derivative to provide a more accurate estimation of C_{X_u}.

If the craft is still found to be unstable once more accurate analysis has been performed, any dynamic instabilities of the craft can be mitigated by designing a controller.

5.4.4. Recommendations

From this analysis, the following recommendations are proposed:

- Improving the accuracy of the stability derivatives using an alternative method to DATCOM. It is recommended that this is done using software such as AVL[2], which can simulate the aerodynamics of the craft and produce stability derivatives and eigenmodes,
- Develop a PID controller for the craft that can keep it within the dynamic stability envelope,
- Compute $C_{X_u} = \frac{\partial C_D}{\partial M} M$ such that the phugoid eigenmotion can be analysed accurately,
- Further investigate the effects of dihedral, wing twist, fuselage length, and different size empennage in the dynamic stability. Currently aerodynamics assumed several values for simplicity, but it is known that increasing dihedral can improve the lateral stability of the craft. This analysis was out-of-scope for this stage of design,
- The effect of the winglets has not been included in the stability analysis of the craft,
- Model the coupled dynamics of the towcraft-glider system. Currently, the force model is very simplified, and does not account for the motion of the glider over time. Thus, force is considered to be constant, and no eigenmotions result from the coupled-dynamics,
- Ensuring the control surfaces allow for the desired manoeuvrability. Currently statistical methods have been used, and as no manoeuvre requirements have been set, this method is appropriate for the current design scope. However, if further design stages decide on manoeuvre parameters, they may need to be reconsidered,
- Analyse the effect of a freely dangling tow cable on stability, as this also adds drag to the rear of the craft, which is stabilising, but also moves the effective combined CG of the system backwards, which is destabilising. In addition it may also influence controllability of the craft,

5.5. Airfield Performance (APOL)

by Mees, Tamara

The results of the iteration are used to analyse the airfield performance of *MARCUS-T*. This section presents the take-off and landing performance results.

5.5.1. Take-Off

After iteration, the final take-off distance is calculated to be 472.3 m, which is below the maximum allowable distance of 500 m. These results, along with other take-off parameters, are detailed in Figure 5.15.

[2] web.mit.edu [cited 18 June 2026].

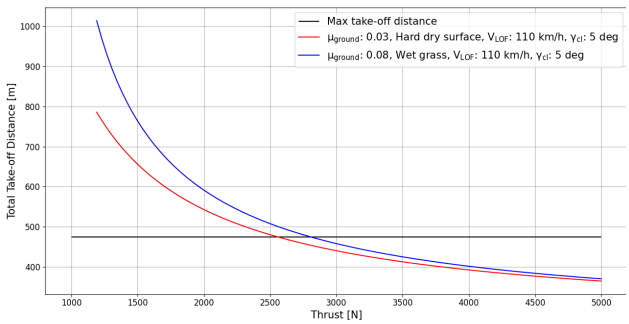

Figure 5.14: Take-off thrust result plot for hard dry surface and wet grass.

Parameter	Value	Unit
Take-off velocity	30.6	m/s
Stall velocity clean	20	m/s
Take-off max CL	1.76	-
Thrust coefficient	0.01	-
Take-off distance	472	m
Rope length	60	m
Ground roll distance	212	m
Transition distance	58	m
Climb distance	143	m
Take-off thrust	2,585	N
Take-off time	45	s
Taxi energy	300,000	J

Table 5.15: *MARCUS-T* take-off parameters.

The take-off thrust of 2,585 N is within the expected range. This thrust requirement is comparable to the Arcus-M during self-launch[3]. In contrast, the Aviat Husky requires more take-off power, which is understandable given its larger weight and lower aerodynamic characteristics [31]. Figure 5.14 shows the relationship between the thrust required per take-off distance. The relation is shown for taking of dry concrete and wet grass surfaces. Although the take-off requirement specifies a dry concrete surface, *MARCUS-T* will predominantly take-off from grass. Therefore, the take-off distance on wet grass has also been calculated, assuming a ground friction coefficient of 0.08 [12]. The take-off distance is 498 m, which is favourable as it allows *MARCUS-T* and a glider to take-off within 500 m on wet grass.

5.5.2. Landing

The landing distance calculation is performed separately from the iteration loop since it does not drive the design. These calculations are performed to verify that *MARCUS-T* will have a reasonable landing distance. The landing distance is reasonable, knowing that no braking is applied here. The results are summarised in Table 5.16.

Table 5.16: *MARCUS-T* landing parameters.

Parameter	Value	Unit
Approach velocity	22.2	m/s
Stall velocity landing	17.6	m/s
Ground CL	0.5	-
Landing max CL	2.29	-
Landing distance	426	m
Approach distance	161	m
Flare distance	22	m
Ground roll distance	243	m

5.5.3. Taxi

The total energy accounted for taxi was 300,000 J. This was based on an initial mass estimate for *MARCUS-T* [3]. This turned out to be more than twice the mass as the final mass of *MARCUS-T*. For this reason, a new taxi distance of *MARCUS-T* can be calculated. The new possible allocated taxi distance is 1,450 m on wet grass. Therefore, the deployment taxi could be powered instead of unpowered or the battery size could be decreased.

[3] www.schempp-hirth.com [cited 17 June 2024]

5.5.4. Recommendations

For further design phases, several recommendations are proposed:

- Currently, no explicit safety factors are applied to take-off and landing distances. It is recommended to use a safety factor of 1.33 to ensure adequate runway length for take-off[4]. Further investigation into standard safety factors for tow crafts or aircraft is advised.
- In future design phases, the stall and lift-off velocities should be calculated rather than approximated based. This will result in a more accurate determination of the take-off distance.
- Taxi energy is currently a fixed value. Including this calculation in the iteration process could reduce the battery mass.
- To better analyse the take-off power, the take-off time should be calculated rather than estimated. This will provide a more precise understanding of the power requirements for take-off.

5.6. Power, Performance, and Propulsion (PPP)

by Annika, Christian

In this section, the findings of the power, performance and propulsion (PPP) department are shown for their corresponding subsystem regarding the design loop. They will be explained and critically examined. Furthermore, final design choices on the motor and propeller that are not directly resulting from the iteration are reasoned and explained. To conclude this section, recommendations are given on how to proceed during future development.

5.6.1. Iterative Outcomes

Using the approach as laid out in Section 4.5, the power, performance, and propulsion parameters and relating design methodology are incorporated into the iteration loop of the design. The results from this are displayed in Table 5.17.

Table 5.17: Power, performance, and propulsion parameters as resulting from the design iterations.

Parameter	Value	Unit
Battery Mass	43	kg
Max. Power Required	62	kW
Max. Climb Power Required	34	kW
Nominal Mission Energy	25.55	MJ
Total Energy Provided	35.80	MJ
Propeller Diameter	1.54	m
Energy Recuperated	6200	J
Power Recuperated	63	W

Note that a propeller efficiency of 0.8 and battery-to-shaft efficiency of also 0.8 are taken from Raymer as typical results [12]. Normally, efficiencies are subject to several parameters that change during the flight, like ρ or flight speed. However, for the initial sizing it is deemed appropriate to use those values proposed by Raymer as a first estimate. Also note that the energy and power recuperated are noticably low. It is recommended to look into different propellers in the future for a potential increase in recuperation efficiency and efficacy.

5.6.2. Design Choices

Several design choices had to be made to finalise the design of the PPP subsystem. Hereafter the choices for the battery, motor and the propeller shall be mentioned and explained.

Choice of Battery

For the battery sizing solely Raymer's approach on electric aircraft design is used, as mentioned previously [12, Ch. 20]. Most importantly, a choice must be made on the battery type used in the craft. For electric vehicles,

[4] www.caa.co.uk [cited 17 June 2024]

high safety and energy density are preferred, along with a long cycle life[5]. There is a set of four potential candidates, lithium-ion (Li-ion), lithium-polymer (LiPo), lithium-sulfur (Li-S), and lithium-iron-phosphate (LiFePO4) batteries. Though Li-S batteries are very powerful in terms of the energy density they can provide, there are still a number of key points that must be improved upon before these can be taken as serious contender for battery type of *MARCUS-T* [32]. Some of these include increasing the power density of the cells, reducing their self-discharging tendencies, or increasing their lifetime.

This leads to using Li-ion, LiPo, or LiFePO4 batteries. For electric aircraft specifically, LiPo batteries are commonly used, though LiFePO4 shows a lot of potential with their longer cycle life[6,7]. The preference for LiPo batteries results mainly from their lightweight design. Though the extra sustainability and safety from LiFePO4 batteries would be convenient, LiPo batteries are significantly cheaper. Additionally, they do not suffer from a high self-discharge rate as was seen before with Li-S batteries. Hence, Lithium-polymer batteries are chosen[8].

Choice of Motor

In the following, reasoning is presented on why it is decided to opt for one engine. Apart from that, the motor shall be selected. To minimise operational costs, the approach is to ensure the number of motors[9] is as low as possible. This results from less motors requiring less maintenance and less spare parts. As the craft is meant to be operated by gliding clubs, the operation and maintenance should be as easy and straightforward as possible. Also, less motors result in less weight. Furthermore, having two or more motors result in further requirements on the vertical tail, as differential thrust during an engine failure needs to be counteracted. The event of an engine failure is very rare when using an electric motor as they are very reliable, more reliable than piston engines [12]. This is also a reason, why it is considered justifiable to opt for one engine, if the maximum required power allows for it.

Since a maximum required power is established as outcome of the iteration, this can be used for the motor selection. Also the continuous power must be kept in mind. As off-the-shelf products are supposed to form an essential part of all used parts for the whole craft, an already existing motor is used. Research identified two possible solutions, firstly considering an off-the-shelf model, the Rotex Electric REB 90. Its characteristics are displayed in Table 5.18. A second option is requesting the manufacturer of the Pipistrel Velis Electro engine to re-size the engine, requesting a stronger variant as the current E-811 engine does not fulfil the maximum take-off power needed for the tow craft. However, the required continuous thrust needed is achieved (Compare Table 5.17 with the E-811 engine: max. power: 57.6 kW, max. continuous power: 49.2 kW) [33].

From those two options, it is decided that having a motor that is available off-the-shelf will allow for faster market entrance. Hence, the choice falls onto the overpowered Rotex Electric REB 90 motor, see Table 5.18:

Table 5.18: Data of the Rotex Electric REB90 motor.

Parameter	Value	Unit
Type	Brushless electric motor	-
Max. power	80	kW
Max. continuous power	60-70	kW
Operating voltage	400-800	V
Cooling	Liquid/air cooled	-
Rotational speed	1800-2400	rpm
Mass of motor	23	kg
Mass of motor + controller	31	kg
Torque	300	Nm
Diameter	0.27	m

Note: The mass of 23 kg is not entirely representative of the system, as a gearbox is added to that as well as an engine controller, which is usually 15-35% of the motor weight [12]. This increases the actual motor mass to

[5] www.renonpower.com [cited 4 June 2024]
[6] www.renonpower.com [cited 4 June 2024]
[7] www.maxamps.com [cited 4 June 2024]
[8] thundersaidenergy.com [cited 17 June 2024]
[9] Motor refers to the combination of electric motor, gearbox and controller.

31 kg. It is not considered a disadvantage that the motor is overpowered as it allows for enough margin within the total propulsive considerations. Apart, from that an overpowered engine allows the design to operate at higher altitudes than sea level and still achieve the required climb rates. Also, since gliding is predominantly a summer activity it also helps to have contingencies in power as warmer air is less dense and hence more power is required compared to colder weather, where the air is denser.

Choice of Propeller

Just like for the motor, an off-the-shelf propeller is aimed for. This is because a new design of a propeller generally is expensive and time-consuming. Using an existing propeller eliminates these challenges and can allow earlier market entry. Also, using already existing propellers ensures that many propeller parameters are known to the aircraft manufacturer and can be directly used for further design stages. Due to the propeller and engine being intertwined in the design process, the precise configuration of the propeller will be left to a later date as well. However, there are already some decisions that can be made on the design of the propeller for the craft: It is decided that the propeller should have three blades. Although, this from theory is considered less optimal, it allows for a smaller diameter of the propeller for the same power, as visualised by Equation 4.91. More blades will decrease the overall propeller diameter. As grass runways are often present on glider airfields, ground clearance is an important design requirement. Technically, any ground clearance can be achieved by sizing the landing gear accordingly. However, this has negative consequences on the drag and performance as a non-retractable landing gear, as considered in this design, will create large amounts of drag. This might even reduce the benefit of having less blades on the propeller. Apart from that, the power loading must be considered as well. The more blades present, the lower the power loading. This means that the power the propeller produces can be forwarded more evenly to the air stream. Considering Table 5.17, the diameter of 1.54 m implies a ground clearance of 25 cm. Considering off-the-shelf products are ideally used, potential propellers are considered. It should be kept in mind that the motor and the propeller need to be attuned to each other. However, the exact fine tuning between motor and propeller are considered beyond the scope of an initial design. One design that is looked into is that of the Pipistrel Velis Electro, which is considered a reasonably well suited comparison, although its power output requirement are lower as that of *MARCUS-T*. The Pipistrel Velis Electro propeller has a diameter of 1.64 m, and hence would lead to a ground clearance of only 15 cm if everything else is considered constant. This is an issue that further analysis should be done on as 15 cm could be considered too small to keep enough clearance, especially in higher grass. Looking at requirements in CS-25, which in this case also hold for CS-23, a ground clearance of 22.85 cm is required[10]. This means that in order to use the Pipistrel Velis Electro propeller, a design adaptation would have to be made. This consideration could be discussed with the manufacturer. However, as with the Pipistrel motor, a new design even with minor changes, may take a long time. However, this could be worth the hassle as the propeller is designed for a light-weight electric motor with recuperation capabilities[11,12]. To make use of those advantages, a re-design of the landing gear should be conducted. Otherwise, off-the-shelf propellers for electric aircraft are available. However, more research on the compatibility with the proposed motor in Subsection 5.6.2 has to be made.

Noise

With the sized propeller the noise is calculated. The propeller this size is estimated to produce around 93.5 dB at a distance of 50 m. This means that the noise requirement of maximum 100 dB at 50 m is met.

5.6.3. Recommendations

In the following, recommendations shall be laid out which can help improve the design:

1. The performance is only calculated based on many pre-specified values, e.g. the climb angles and pattern altitudes. In the real world those can differ, which will inevitably change the performance characteristics of the craft. Therefore, a more dynamic mission profile, with more allowance for changing values should be considered.
2. It should be considered that the tow craft and its take-off performance are calculated for ISA (International Standard Atmosphere) conditions at an altitude of 0 m. If the airport is situated at higher elevations, the tow craft's performance will decrease, making higher power outputs necessary in case the same

[10] www.law.cornell.edu [cited 17 June 2024]
[11] www.pipistrel-aircraft.com [cited 17 June 2024]
[12] www.pilootenvliegtuig.nl [cited 17 June 2024]

performance output as in ISA and ground level is required. Therefore, the performance for different weather conditions and airport elevations should be reconsidered.

3. During climb the speed has been considered to be constant, while a climb at constant true airspeed (TAS) is an accelerated flight and not constant. Therefore, the change of properties with ρ should be reconsidered.
4. Engine recuperation was not considered as it was not possible to implement it in the given time frame[13]. Therefore, engine recuperation and its feasibility should be considered, investigated and traded against added benefit and weight improvements.
5. The P-factor, that is the aerodynamic effect of a moving propeller, should be considered when designing the rudder. It will have to be adjusted for, especially during phases of high power settings and high rotational speeds of the propeller. This is the case during take-off. With a glider attached it has to be made sure that ground controlability is given, even at low speeds where the rudder is less effective. Therefore, the P-factor should be considered for the sizing of the rudder.
6. The power requirement stems from the mission profile. However, it turns out that the chosen motor can deliver a higher continuous power than required for a climb rate of 3m/s. Therefore, a higher climb rate could be achieved. This in turn could make the mission shorter, reducing the turn-around time and the energy consumption as the higher power is applied over a shorter time. Therefore, a sensitivity analysis on the climb power setting and the increase in climb rate should be considered against an increase in climb rate and therefore time savings. Battery wear and risk should also be analysed.
7. One large assumption of the mission profile is to split up the straight legs and the turning legs. This is allowed but is prone to over- or even underestimations yielding imprecise results. Therefore, it should be considered to make a combined analysis. This especially holds for the turning climbing flight phases.
8. During the whole design process it is assumed that the efficiencies remain constant at the values presented in Table 5.17. However, it is well-understood that the efficiency of propellers change with speed and altitude, as well as for the transmission from the battery to the shaft. Associated with the propeller efficiency, also the design decision of a constant-speed or constant-pitch propeller must be made. Following Gudmundsson the proposed design should be fitted with a constant-pitch propeller [15]. Therefore, further investigation should be done on whether a constant-pitch propeller is the best choice for the propeller and which propeller setting should be used for which flight phase. Apart from that, all calculations should be performed with changing efficiencies.
9. As the battery, the motor and propeller are delicate parts of an aircraft, they must work together perfectly. This means that the battery must provide the correct voltage to the motor for the required torque such that the propeller can deliver the required amount of thrust. This is not straightforwardly calculated and manufacturer details on the parts must be collected, compared and evaluated. Furthermore, it must be decided how well the parts can perform together. Therefore, it is advised that the battery, the motor, the controller and the propeller are aligned so they can function flawlessly with each other.
10. Since the values regarding recuperation have proven to be quite low, it is recommended to look further into propellers with better a recuperative efficiency and efficacy. This could also be helped by looking into propellers that focus less on climb performance.

[13] An initial methodology was set up in Subsection 4.5.8.

6

Method Verification and Validation

To ensure the results obtained from the tools are correct, a verification of the tools must be performed. Verification of tools can be separated into verification of mathematical models and verification of their implementation in code. Mathematical models are expected to be verified as all sources used for mathematical formulas have been peer reviewed. Furthermore, all assumptions that are used are presented and verified. This includes checking for the validity of small angle approximations and other linearisations by inspecting final results.

Code is verified in multiple steps. Firstly, unit tests are performed to check whether every function works correctly. Secondly, sub-systems tests are performed for modules of code, these sub-system tests are designed to both inspect the validity of all used individual functions in the module and how they are integrated together. One test will be designed for every tool. Finally, system tests are performed to verify the correct integration and compatibility of all modules.

6.1. Unit Tests

by MianTao, Everyone

All performed unit tests are presented in Table D.1, in which they are sorted by department. These tests are intended to verify individual functions. Tests can be performed either by hand calculations (HC), comparison and cross checking with alternative methods (CC), or visual inspection (VI). As can be seen in Table D.1, all tests are passed, which indicates the functions are implemented correctly. In addition, almost all functions have been tested, which means a high coverage of calculations is ensured. The reported code coverage by Coverage.py[1] is only 66% however. This is due to there being several legacy, output, and plotting functions that are not tested. In addition not all tests are implemented in code, which means they are not registered by Coverage.py.

6.2. Subsystem Tests

by MianTao

Subsystem tests are performed on modules of code. Such tests are done by reverse engineering code to check for correct convergence using verified functions and performing end-to-end tests using hand calculated values or comparison with existing models. Finally, sensibility checks are also performed as well by inspecting results for any obvious errors. All modules used in the design method are verified in subsystem tests, ensuring complete coverage.

Almost all subsystem tests are passed, except for the tests performed on the asymmetrical state space model for control and stability discussed in Subsection 4.3.3. A comparison is made with an implementation given by In 't Veld [24]. Using given stability characteristics for the Cessna 500 Citation I, the computed eigenmodes differ from those provided by in 't Veld. However, they are in the same order of magnitude and are similar when comparing among themselves, with all eigenvalues consistently differing in magnitude by only about 50%. It is notable that the model yields an unstable spiral for the Citation, whereas both the model provided by in 't Veld and other models show it to have a stable spiral [24, 34]. As a result of this all code for the module has been rewritten, tested, and inspected in detail. This still yielded identical results however. Therefore, it is believed that the stability derivatives given by in 't Veld for the Cessna 500 Citation I are incorrect, leading to the model developing an incorrect unstable spiral.

6.3. System Tests

by MianTao

Finally, system tests are performed on the entire iteration loop. Firstly an end-to-end test is performed. This test catches any obvious errors in integration which may cause the program to crash or diverge early on. Secondly, the convergence of the iteration loop is tested. To ensure that the loop actually converges, the final

[1] Coverage.py is a Python tool that measures the coverage of a Python program as the percentage of statements that have been executed. It is commonly used to determine the coverage of testing. From coverage.readthedocs.io [cited 19 June 2024]

values are used as initial values for the loop once more. For converged final values and a correct implementation, the method should then converge after a single iteration.

Intermediate unconverged values are also logged in a separate file. These values are inspected to perform sensibility checks and to examine how the iteration loop converges. In addition they can be used to determine the source of error or unviability of initial values in case the loop does not converge. To ensure iterated design parameters are actually changed throughout the loop, all constant non-iterated values are also logged. Nonsensical and extreme initial values are also used to ensure the design loop does not converge for those, such that no nonsensical designs are produced. Finally, after actual initial values are used for the design sensibility checks are performed on all final converged values, which are discussed in Chapter 5.

6.4. Verification Coverage and Confidence

by MianTao

As can be observed in Table D.1, full coverage of unit tests is ensured, with key functions having multiple tests to ensure correctness. In addition a variation of unit tests is used, with a primary focus on hand calculations. This provides high confidence for the correct working of all individual functions.

Subsystem tests are also performed on all modules of code, with multiple verification methods performed per module. However, there is a noticeable lack of any extreme and nonsensical value testing. To account for this, modules and individual functions have checks for unacceptable conditions and raise exceptions when these are encountered. This means that most modules have high confidence for correct functioning. The exception from this is the previously discussed asymmetrical state space model. Though it is the belief of the team that the reason for the failure of the test is incorrect input and output data, confidence in the working of this specific module is still low. The model may still be used qualitatively to analyse influence of the tow craft on stability, but numbers from the model will not be used directly. All results derived from the dynamic model are to be verified by alternative methods in the future.

6.5. Uncertainty Analysis

by MianTao

To analyse the sensitivity of the method to small differences in inputs, an uncertainty analysis is performed. This is done using a Monte Carlo experiment[2]. For an initial analysis each input value is multiplied by a random variable $X \sim U(0.99, 1.01)$, where $U(a, b)$ denotes a random uniform distribution between a and b. A limited sample size of 50 is used due to computational constraints.

The randomised inputs are subsequently used by the method and intermediate results are documented at 5, 10 and 15 iterations of the loop. The coefficient of variation (CV) of each design parameter is then computed using Equation 6.1, provided by Brown [35].

$$CV = \frac{\sigma}{\mu} \tag{6.1}$$

Here σ is the standard deviation and μ is the mean. The coefficient of variation is then averaged over all design parameters. The results of this are displayed in Table 6.1

Table 6.1: Mean coefficient of variation $\bar{CV}$ for inputs randomised by 1% at 5, 10, and 15 iterations for a random sample size of 50

Iteration	$\bar{CV}$
5	0.0059
10	0.0062
15	0.0066
20	0.0082

As can be seen from Table 6.1, as the number of iterations increases, the coefficient of variation increases as well. In addition, the rate of change increases as well with iterations. To check whether the results of the method diverge over the total amount of iterations, an analysis with 100 iterations is performed with a reduced sample size of 20 due to limited computational resources. After 100 iterations 90% of all samples converge to a final design. Inspection of the data shows that for 5, 10, and 15 iterations the coefficients of variation are

[2] www.ibm.com [cited 18 June 2024]

consistent between the experiment using 20 and the experiment using 50 samples. This indicates the random sample size is sufficient. The analysis is repeated for $X \sim U(0.95, 1.05)$, $X \sim U(0.9, 1.1)$, $X \sim U(0.8, 1.2)$. All results of this are documented in Figure 6.1.

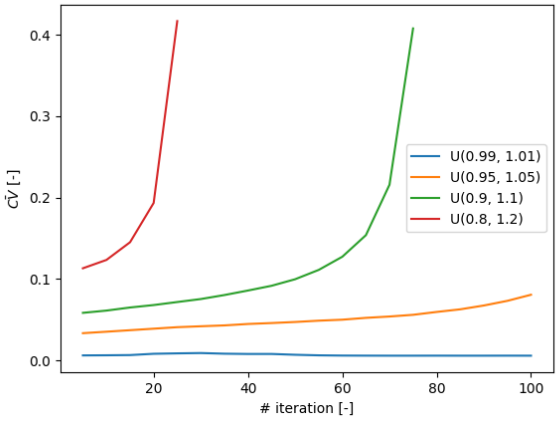

Figure 6.1: Coefficient of variation $\bar{CV}$ at different numbers of iteration, performed for uniform randomisations of inputs with sample sizes of 20.

From Figure 6.1 it can be observed that as the number of iterations increases beyond 25, the random samples stop diverging and start converging again, with the final coefficient of variation being close to the initial value. This demonstrates to a limited extent that the method is not overly sensitive to small deviations in input values within 1%.

For $X \sim U(0.95, 1.05)$ 55% of all samples converged after 50 iterations, and 75% of all samples converge after 100 iterations. However, as can be seen in Figure 6.1, a significantly higher coefficient of variation is observed at 100 iterations, as individual samples deviate more from each other. For $X \sim U(0.9, 1.1)$ only 30% of all samples converge after 50 iterations. As the number of iterations increases past that divergence of the design occurs in a sample. This yields a prominent increase in $\bar{CV}$ at 75 iterations visible in Figure 6.1 and causes the method to crash on the 78^{th} iteration. For $X \sim U(0.9, 1.1)$, divergence of designs occurs at the 26^{th} iteration, thus only up to the 25^{th} iteration is visible in Figure 6.1.

From this, it is concluded that the model produces very similar results for changes of inputs within 1%, and produces more significant variations in outputs for changes in inputs within 5%. For changes in inputs within 10%, samples, some of the the samples still converge, but some samples begin to diverge and the method becomes unreliable. For 20% percent the method becomes unusable.

6.6. Validation

by MianTao, Everyone

Minimal validation is performed at this stage of the design, as the resources of the team are limited. The airfield performance tools are verified by comparing results with data from existing aircraft, which found the tool to be consistent with real world data.

To ensure validity of the design method, the iteration loop should be applied using real world data as inputs and the outputs should be compared with existing craft. All methods that are not included within the iteration loop should also be validated in a similar manner. If real world data is not available, validation should be performed by comparing the results with existing validated models.

7

MARCUS-T: Technical Description

After the design of the sustainable glider tow craft, more specifics on *MARCUS-T* are presented in Chapter 7 until Chapter 11. These chapters include a 3D model, technical diagrams, operations and logistics, etc. This chapter functions as an introduction to Chapter 8 until Chapter 11. It includes a summary table of the most important values of *MARCUS-T* , and the 3D model created of *MARCUS-T*.

7.1. Summary Table

by Stan, Everyone

In Table 7.1 the summary table of the values of *MARCUS-T* can be seen. This table is separated into the five different departments.

Table 7.1: Summary table of the sustainable glider tow craft design.

Dep.	Name	Symbol	Value	Unit
PPP	Maximum Power Required	MaxP_{req}	61.5	kW
PPP	Maximum Climb Power	MaxP_{cl}	33.6	kW
PPP	Propeller Efficicieny	η_{pwr}	0.8	-
PPP	Nominal Mission Energy	$E_{\text{req}_{\text{nom}}}$	25.6	MJ
pp	Total Energy Available	$E_{tot_{avail}}$	35.8	MJ
PPP	Number of Motors	-	1.0	-
PP	Propeller Diameter	D_{prop}	1.54	m
PPP	Total Energy Recuperated	E_{recup}	6220.0	J
PP	Recuperation Efficiency	η_{recup}	0.1	-
PPP	Maximum Power Available	MaxP_{avail}	80.0	kW
PPP	Maximum Continuous Power	MaxP_{cont}	70.0	kW
PPP	Rotational Speed	n	1800-2400	rpm
APOL	Take-Off Distance	S_{TO}	472	m
APOL	Landing Distance	S_{LDG}	426	m
APOL	Stall Velocity Clean	$V_{\text{s,clean}}$	20.0	m/s
APOL	Stall Velocity LDG	$V_{\text{s,land}}$	17.6	m/s
APOL	Lift-Off Velocity	V_{LOF}	30.6	m/s
APOL	Climb Velocity	V_{C}	36.1	m/s
APOL	Dive Velocity	V_{D}	77.8	m/s
APOL	Approach Velocity	V_{APP}	22.9	m/s
APOL	Landing Velocity	V_{LDG}	19.3	m/s
AERO	Airfoil	-	DU15-160/15	-
AERO	Wing Span	b	8.65	m
AERO	Root Chord	c_{r}	0.75	m
AERO	Wing Area	S	4.72	m^2
AERO	Aspect ratio	AR	15.6	-
AERO	Taper Ratio	λ	0.45	-
AERO	Sweep at LE	Λ_{LE}	0.0	deg
AERO	Aircraft Maximum Lift Coeff.	$C_{\text{L}_{\text{max,ac}}}$	1.76	-

Continued on next page

Dep.	Name	Symbol	Value	Unit
SSC	Dihedral	Γ	6	$^\circ$
SSC	Tail Length	l_h, l_v	3.0	m
SSC	HTP Minimum Volume	V_h	0.471	-
SSC	VTP Minimum Volume	V_v	0.0265	-
SSC	HTP Minimum Surface Area	S_h	0.425	m^2
SSC	VTP Minimum Surface Area	S_v	0.361	m^2
SSC	HTP Aspect Ratio	$\mathrm{AR_h}$	5.0	-
SSC	VTP Aspect Ratio	$\mathrm{AR_v}$	2.0	-
SSC	Wing LEMAC Long. Location	x_LEMAC	1.7	m
SSC	Elevator Surface Area	S_e	0.11	m^2
SSC	Rudder Surface Area	S_r	0.088	m^2
SSC	Elevator Span	b_e	1.22	m
SSC	Rudder Span	b_r	0.68	m
SSC	Most Forward CG Location	$x_\mathrm{CG,fwd}$	1.8	m
SSC	Most Aft CG Location	$x_\mathrm{CG,aft}$	1.93	m
SSC	Most Forward NP Location	$x_\mathrm{NP,fwd}$	1.97	m
SSC	Most Aft NP Location	$x_\mathrm{NP,aft}$	2.0	m
SSC	Stability Margin	SM	5.0	-
SMM	Wing Box Height	h_wb	0.12	m
SMM	Wing Box Width	w_wb	0.38	m
SMM	Number of Stringers	N_str	16.0	-
SMM	Number of Ribs	N_rib	2.0	-
SMM	Wing Box Material	-	AL 6061 T6	-
SMM	Fuselage Lenght	l_f	6.1	m
SMM	Fuselage Material	-	AL 6061 T6	-
SMM	Landing Gear Height	h_lg	2.0	m
SMM	Landing Gear Material	-	AL 7075 T6	-
SMM	Tire Width	w_tr	0.10	m
SMM	Tire Diameter	D_tr	0.22	m
SMM	Max Take Off Mass	W_mto	209.7	kg
SMM	Wing Mass	W_w	39.7	kg
PPP	Electrical Motor Mass	W_em	30.0	kg
SMM	Empennage Mass	W_emp	6.6	kg
SMM	Landing Gear Mass	W_lg	11.6	kg
SMM	Fixed Equipment Mass	W_fe	65.4	kg
PPP	Battery Mass	W_bat	43.1	kg
SMM	Fuselage Mass	W_f	13.3	kg

7.2. 3D Model

by Andreas

Computer-aided design (CAD) is used in all stages of the design process. Throughout the process of making this report, CAD is used as a tool for dimensioning components, integrating systems, and as a 'sanity check', especially for the development of the aerodynamic and structural systems.

For a glider tow craft, CAD is particularly useful as it allows for direct comparisons between different gliders and the craft. At the start of this project, two gliders were modelled in CAD, the small 201 Libelle, and the large Arcus T. In earlier reports, they were used to size the 'Nose Plane' concept. In this report, CAD is largely used to size parts of the fuselage. By using known dimensions from both calculations and off the shelf parts

Figure 7.1: *MARCUS-T* Under an Arcus T.

like the electrical power system and avionics, minimum fuselage dimensions at several points along the length can be determined. Furthermore, a 3D model assists in determining possible battery placement locations, indicating which parts of the fuselage are both accessible and large enough for hot swapping batteries. For example, designing the fuselage and wings in CAD made it clear that the removable batteries could not be placed in the wing, as there is not enough accessible volume using the chosen wing-box design. Figure 7.1 shows a render of the 3D model next to an Arcus T.

Side View

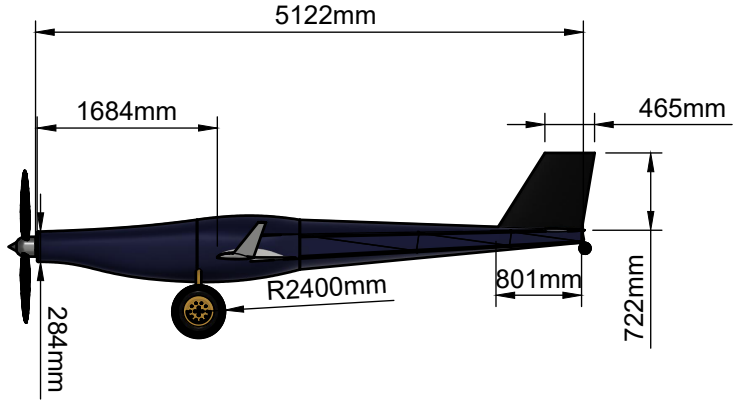

Front View

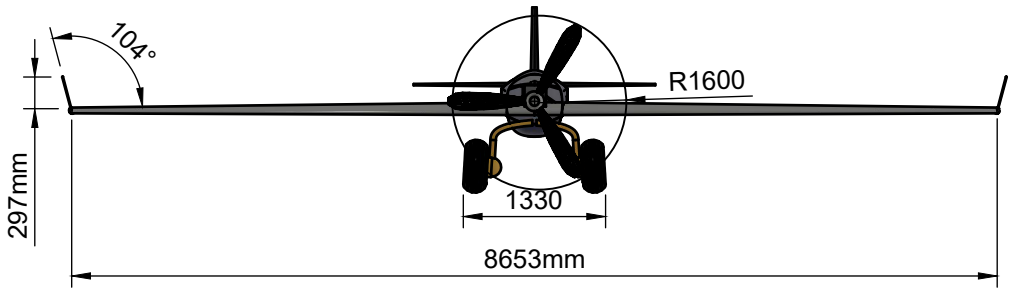

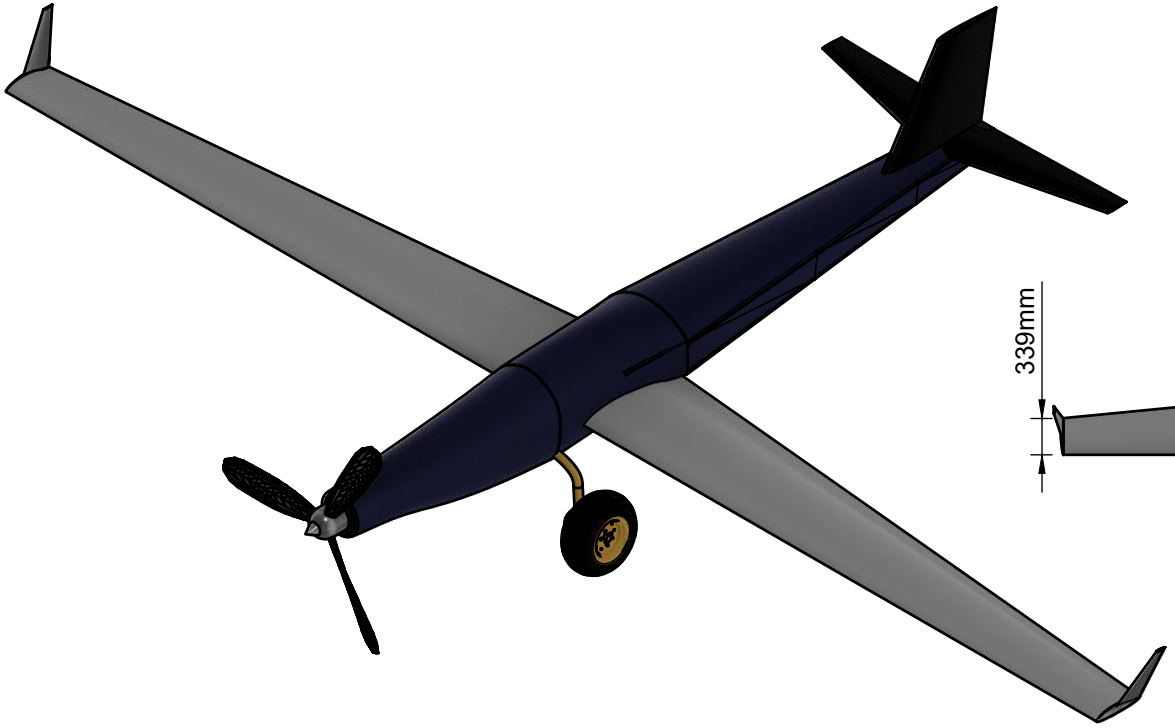

Top View

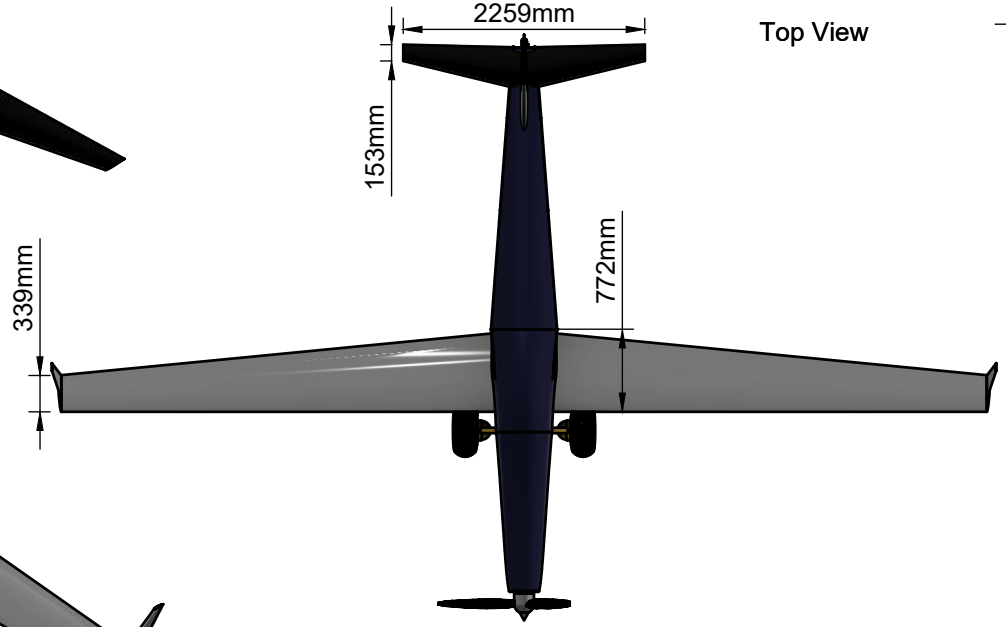

MARCUS-T Three View.
Units in mm

8

MARCUS-T: Logistics and Operations

by Mees, Tamara

The Logistics and Operations chapter gives an outline of the framework for operating and supporting *MARCUS-T*. Airfield logistics describes the systems that are required to support *MARCUS-T*. Moreover, ground, flight and emergency procedures are discussed in this chapter.

8.1. Logistics and Support

Logistics and support are crucial for *MARCUS-T* 's operation. This section covers the main logistical needs to keep the tow craft up and running. It starts with airfield logistics by setting up the support systems and then moves to inspection guidelines to maintain safety. Ensuring proper charging, storage, and control at the airfield is essential, and this section provides an overview of these needs.

8.1.1. Airfield Logistics

Airfield logistics are an important aspect, since they describe the support around *MARCUS-T*. This includes organising charging, storage, and support systems to keep the craft available and safe.

Charging Truck

During a nominal mission (which consists of the take-off, climb track, dive track and landing) the tow craft uses about 7,100 Wh (65% of the total battery capacity) within a block time of 15 minutes. On a busy day, approximately 30 tows are performed. Assuming all tows are conducted back to back, the total required flight time is 450 minutes. Using the values from Table 8.1, Figure 8.1 was generated.

Table 8.1: *MARCUS-T* battery parameters.

Parameter [Unit]	Value	Parameter [Unit]	Value
Max. battery range [%]	0-100	Ops. battery range [%]	15-85
Initial charge [%]	85	End of mission Charge [%]	20.8
Discharge time [min]	15	Charge time [min]	30

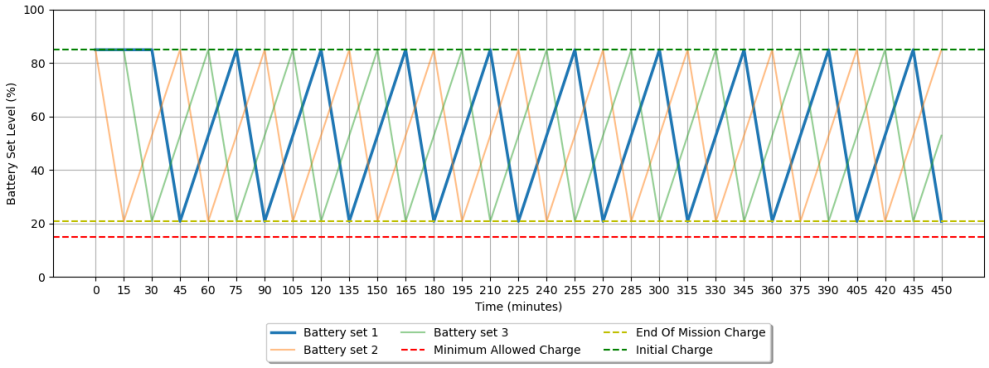

Figure 8.1: Battery levels per set throughout the day.

Figure 8.1 shows the battery set level throughout the day, demonstrating that there is always a charged battery set available for the next flight. Through iteration, it was determined that 3 battery sets are necessary to ensure continuous operations under these conditions. It is important to note, however, that it is unlikely the tow craft will be operated to this extent regularly. Typically, fewer tows are performed within this time frame. Furthermore, it is assumed that all towed gliders have a mass of 850 kg. During normal operations, the gliders

are usually in the range of 300-650 kg. Nevertheless, the capability to perform 30 tows in 450 minutes should be maintained, since the craft should not be a limiting factor in the flight operations according to the needs from the gliding clubs [36].

Three sets with four batteries each, hence twelve batteries in total are required. During the flight operations, 213,000 Wh is needed to perform all 30 flights. This is a large quantity of energy and therefore, the charging system will need two larger charging system batteries. A conceptual layout is shown in Figure 8.2. When the charging system is stored during the night, the dedicated system batteries and two *MARCUS-T* battery sets are charged. When the charging system is on the airfield during the day, the used battery sets are charged, while also being partially charged by solar energy. Each system battery will need to deliver 106,500 Wh of energy to the battery sets during the day. Assuming a depth of discharge of 70%, the total required capacity is 153,000 Wh per system battery. The design of the battery charging system shall be continued in a later design phase.

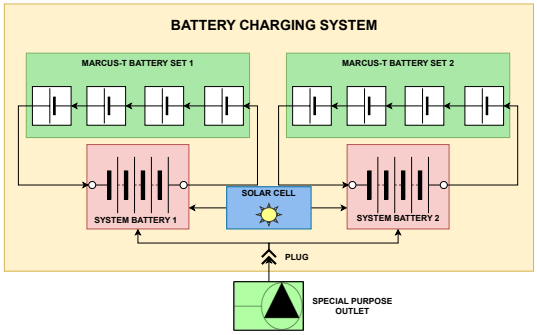

Figure 8.2: Conceptual layout of the battery charging system.

Hangar Layout

The gliders and ground equipment used for the gliding operations, are usually stored in a hangar. Here, all vehicles are charged for the next day of flying. As can be seen in Figure 8.3, the hangar is typically used to its fullest capacity, with many vehicles tightly packed together to optimise the usable space. Once again looking at Figure 8.3, the winch, control truck, transport carts and glider batteries are all charged inside the hangar. For this reason, it has been decided that the truck with the charging system and *MARCUS-T* will also be charged here. The electrical infrastructure in the hangar will need to be expanded to accommodate this. For the charging truck, a special purpose outlet is required. As determined previously, the energy used for 30 nominal tows per day is 213 kWh. This is a large quantity of energy which will need to be charged in about 12 hours, resulting into a required power of about 18 kW. Since the already existing heavy duty outlets will not deliver enough power, a special purpose outlet is required. However, *MARCUS-T* can and will be charged using a heavy duty outlet. The outlets and their specifications are also shown in Figure 8.3.

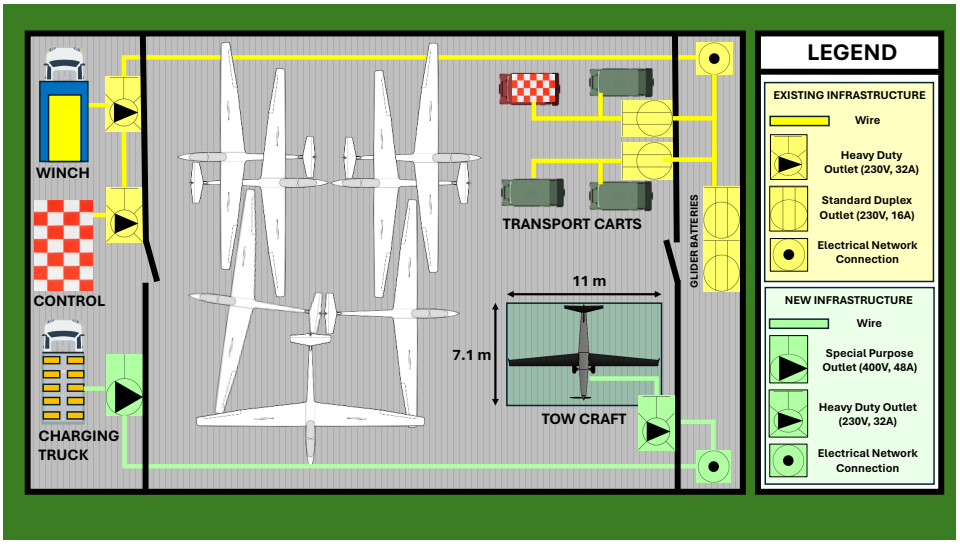

Figure 8.3: (Electrical) Lay-out of the hangar.

Control Truck

Most gliding clubs have a control truck. In this truck, signals are sent to the winch, the flight administration is performed and radios are installed here to communicate with people both on the ground and in the air. A small control station will be required for *MARCUS-T*. Since a dedicated control station vehicle would be too unnecessarily expensive, the remote control system will be designed such that it fits in these small control trucks. A Licensed UAV-pilot trained on the control and operations of *MARCUS-T* will monitor and control *MARCUS-T* from here.

8.1.2. MARCUS-T Inspections

Aircraft inspections are essential for ensuring safe operations, compliance with regulations and optimal performance. During inspections, potential issues like wear and tear, corrosion and other problems are identified, documented and if necessary repaired. Two types of inspections can be identified; regular and special inspections. Each of these will be briefly discussed.

Regular inspections are checks performed at predefined intervals to ensure the continued airworthiness of an aircraft. The most performed regular inspection is the daily inspection. Each day, all aircraft that will be flown are briefly inspected in the morning. During these so-called pre-flight inspections, the aircraft is visually checked for wear and damage, and the most important systems are tested. Since this is the most common inspection, a daily inspection procedure for *MARCUS-T* was created; to be seen hereafter.

DAILY INSPECTION PROCEDURE

(To be performed by authorised personnel)

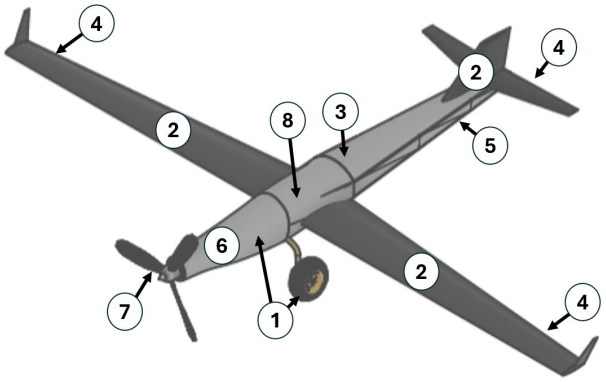

Figure 8.4: Locations of the daily inspection items.

1. **Fuselage and Gear:**
   (a) Fuselage: check for any visible damage, cracks, or abnormalities. Inspect the surface for any signs of wear.
   (b) Landing Gear: inspect the landing gear struts and tires. Check for any signs of damage or wear. Ensure that the tires are properly inflated.
   (c) Pitot and Static Ports: check for any obstructions, such as dirt or debris. Ensure that the ports are clear and free from blockages.
2. **Lifting Surfaces:**
   (a) Wings: ensure the wings are free from any damage. Check the leading and trailing edges for any dents or cracks. Apply a bending moment at the wing-tip to check the structural integrity. Check control surfaces for free movement.
   (b) Tail Section: inspect the horizontal and vertical stabilisers for any signs of damage or looseness. Check control surfaces for free movement.
3. **Electrical System:**
   (a) Battery: check the battery condition and ensure it is fully charged. Inspect for any corrosion or loose connections.

(b) Wiring: inspect all visible wiring for signs of wear or loose connections.
(c) Lighting: check all beacon and landing lights to ensure they are functioning properly.

4. **Control Systems:**
   (a) Control Surfaces: let the ailerons, rudder, and elevators move through their full range of motion. Check for extensive play.
   (b) Hydraulics: check the hydraulic pressure. Check actuators for proper operation. Ensure they extend and retract smoothly.
5. **Glider Coupling System:**
   (a) Inspect the glider coupling mechanism for any signs of wear or damage. Ensure that the coupling pins and hooks are free from deformation or excessive wear.
   (b) Check that the coupling mechanism engages anddisengages properly.
6. **Powerplant**:
   (a) Motor: check the electric motor for any visible signs of wear or damage. Ensure that the mounting bolts are secure.
   (b) Cooling System: ensure that the air cooling systems are not obstructed. Check the liquid cooling system for leaks.
7. **Propeller:**
   (a) Inspect the propeller blades for any cracks or other damage. Ensure the propeller is securely mounted.
8. **Safety Equipment:**
   (a) Fire Suppression System: ensure the fire suppression system is active and fully charged.
   (b) Ballistic Parachute Deployment System: inspect the parachute housing to ensure it is intact and secure. Check for any visible damage, corrosion, or signs of wear and tear on the canister and deployment mechanism.
9. **Hardware and Software:**
   (a) System Test: run the system test and verify if every system is active and functioning.
10. **Documentation:**
    (a) Ensure that all maintenance and inspection logs are up to date. Record any issues found during the inspection and report them to the maintenance team.

Other regular inspections are:

- **B-Check:** this check is conducted every 3 to 6 months. It is a more detailed inspection of the airframe, including the wings, fuselage, and empennage. System tests are performed on the electrical and hydraulic systems, and the engine's performance is checked. The landing gear and control surfaces are inspected for wear and proper operation.
- **C-Check:** this inspection is performed every 12 months. It covers an extensive inspection of the entire airframe, major systems and components. The inspection includes detailed checks of the fuselage, wings, empennage, and control surfaces. System overhauls, extensive functional tests and servicing of the engine and propeller are performed. All maintenance logs are to be reviewed and updated to ensure compliance with the safety standards and regulations.
- **D-check:** this inspection is also known as a heavy maintenance visit. The D-check is the most extensive inspection that an aircraft undergoes. It is performed approximately every 5-10 years, depending on the aircraft type and usage. The D-check involves a complete tear down and inspection of the entire aircraft, including all its systems and components [4, 37].

Special Inspections

Special inspections are additional checks required due to specific events occuring during the operations of the craft. These for instance include hard landing inspections, where the landing gear and airframe are checked, and bird strike inspections, where the aircraft's leading edges and engine are checked. Other examples are lightning strike inspections, where the craft is checked for electrical damage. In general, these are unscheduled maintenance inspections, which belong to unusual incidents or emergencies. Other special maintenance checks come from airworthiness directives or service bulletins[1].

[1] cla.aero [cited 14 June 2024]

8.2. Operations

This section describes the standard operating procedures (SOP's) for the UAV pilot and ground crew operating with *MARCUS-T*. Familiarity with these procedures is mandatory for all personnel involved. These procedures are preliminary and are intended to provide a brief overview of the operational aspects of *MARCUS-T*. Detailed procedures will be developed in a further stage. First the ground and flight operations are explained, supplemented with operational flow diagrams, based on the previously shown functional flow diagram in Section 2.3. After that, some emergency procedures are defined for when the system deviates from the nominal mission.

8.2.1. Ground Operations

Ground operations include everything from taking *MARCUS-T* out of storage to taxi to and from the battery swap area. The operational procedures are discussed in this section.

DEPLOYMENT

MARCUS-T will be removed from the hangar and the daily inspection shown in Subsection 8.1.2 will be performed. If the inspection is passed, *MARCUS-T* will be connected to one of the taxi vehicles. The taxi vehicle will tow *MARCUS-T* to the battery swap area on the airfield. This process is shown in Figure 8.5.

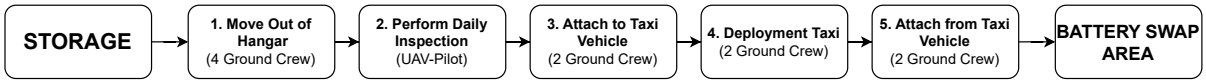

Figure 8.5: Operational flow of the storage removal and deployment taxi.

BATTERY SWAP AREA - PRE-LAUNCH

When *MARCUS-T* is at the battery swap area, the following operational flows presented in Figure 8.6 are initiated.

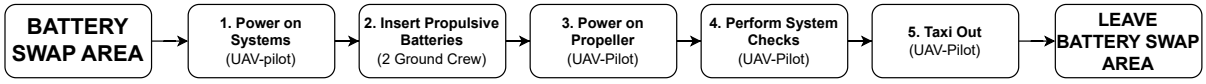

Figure 8.6: Operational flows in the battery swap area pre-launch.

MARCUS-T will be parked at the battery swap station. Here the dedicated ground crew will take over. The UAV-pilot will power on the systems while two ground crew get the four propulsion batteries and insert them. A visual representation is shown in Figure 8.7 When the ground crew is clear of *MARCUS-T* , the UAV-pilot will power on the propeller and perform the system checks. When everything is okay, *MARCUS-T* will taxi out to the tow launch area.

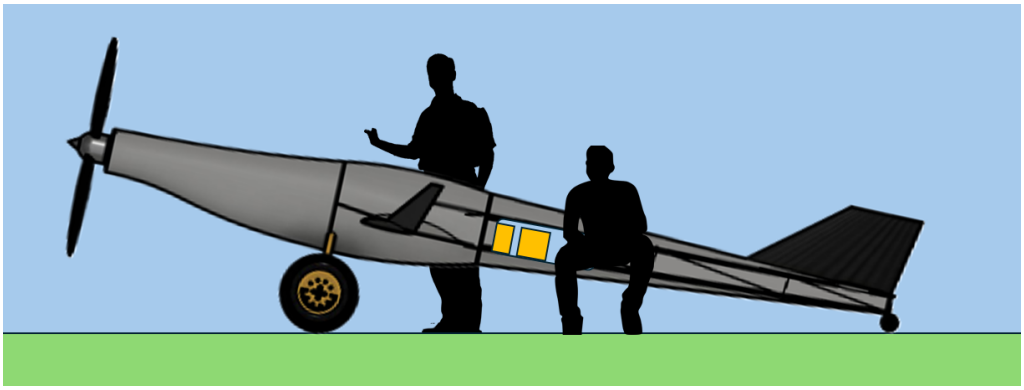

Figure 8.7: The *MARCUS-T* batteries are inserted.

PRE-LAUNCH

When a glider is ready to be towed, the pre-launch phase will be initiated. The operational flow can be seen in Figure 8.8.

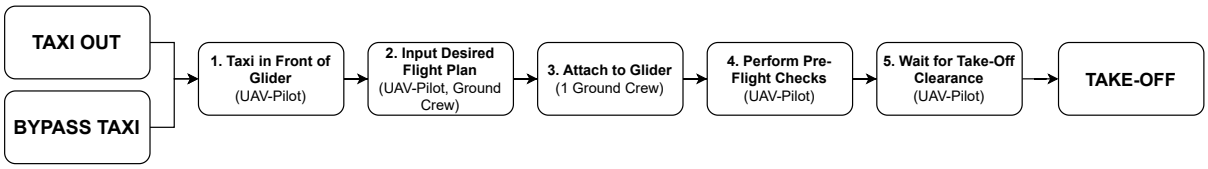

Figure 8.8: Operational flow before the launch of a glider.

MARCUS-T will taxi remotely to the tow launch area, following the taxi out path previously shown in Figure 2.3. A ground crew member will pull the cable from the Glider Coupling System to the glider and connect it to the nose hook. Pre-flight checks will be performed there. When both the glider pilots and *MARCUS-T* are ready, the launch can be initiated.

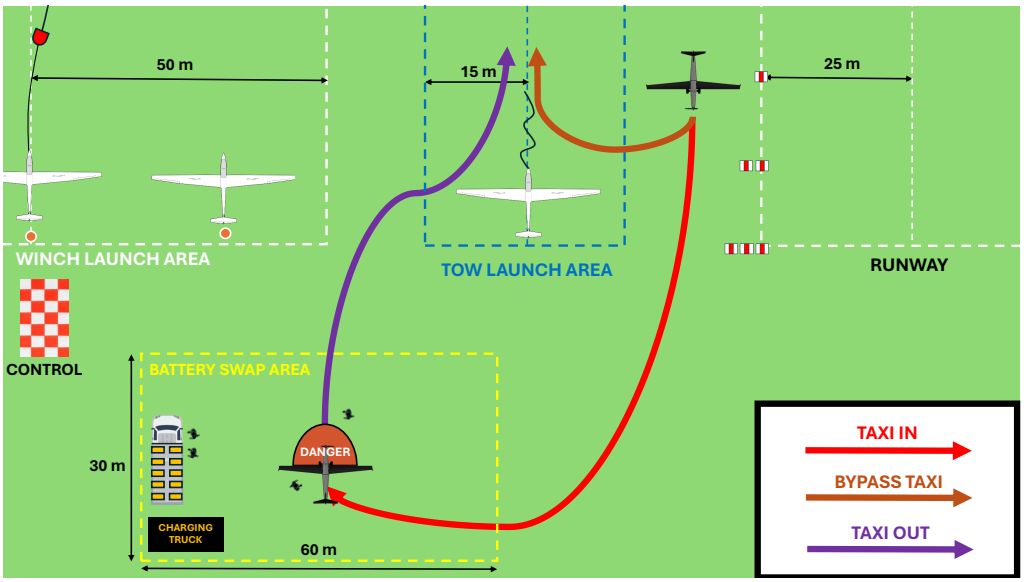

Figure 8.9: Taxi lay-out at the launch area.

BATTERY SWAP AREA - POST-LAUNCH

When *MARCUS-T* has landed, it will either bypass taxi and tow the next glider or taxi back to the battery swap area remotely. If the latter is the case, its systems will be checked and the batteries will be swapped. The operational flow diagram is visible in Figure 8.10. This operational flow diagram does overlap with the pre-launch operational flow diagram.

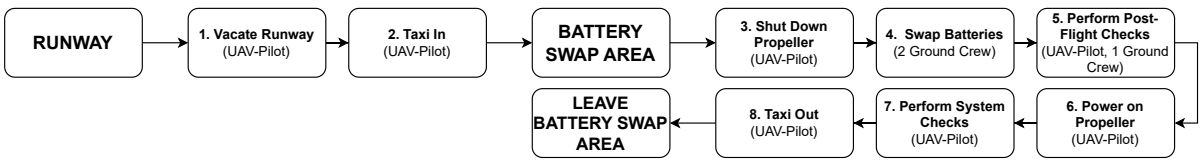

Figure 8.10: Operational flow in the battery swap area, post launch.

If the battery needs to be swapped, two crew members are required. One crew member will remove the empty batteries from the right side of the craft and the other crew member will insert the fully charged batteries from the left side. This is shown schematically in Figure 8.11. If available, more crew members should assist with carrying the batteries to and from the craft. The area around the propeller is a dangerous area and crew members are advised to not come in the vicinity of the propeller when the propulsive systems are active.

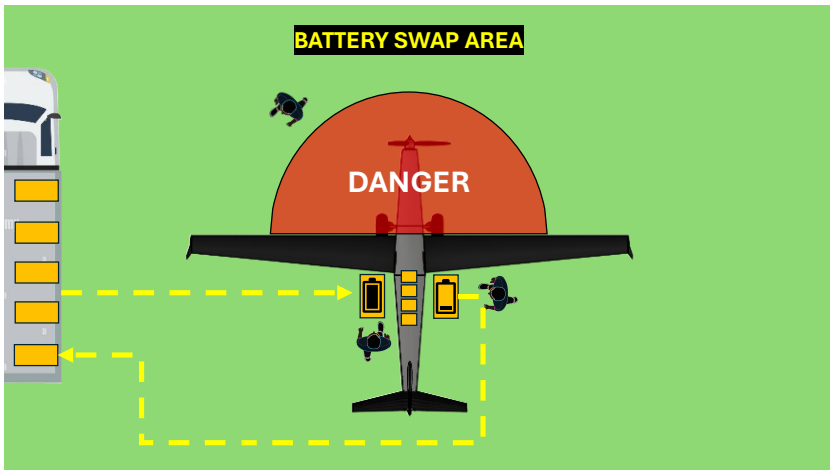

Figure 8.11: Battery swapping of *MARCUS-T*.

8.2.2. Flight Operations

The flight operations will follow the mission profile described in Section 2.2.

TOW LAUNCH

When clearance is given by the ground crew and pilots, the launch phase will initiate. The operational flow of the launch phase is shown in Figure 8.12.

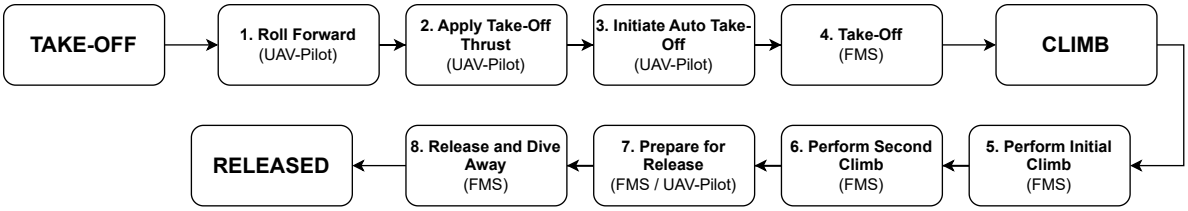

Figure 8.12: Operational flow of the tow launch.

The tow craft will remotely taxi forward until there is tension in the cable. When the GCS detects this tension, full throttle will be applied and the combination will start the take-off. The ground crew will notify over the radio that the tow combination is taking off. This will let all people listening on that frequency know that a tow launch is taking place. The glider and *MARCUS-T* will continue with the take-off. When the combination passes the screen height of 15 m, the climb phase will start. The combination will fly the predefined climb track as described in Section 2.2. During this phase the ground crew will closely monitor the tow crafts system and communicate with the glider pilot(s) if required. When the desired altitude is reached, the glider pilot(s) will disconnect from the tow craft according to the usual detachment procedures [38]. The tow craft diving down to the left and the glider pulling up to the right, as shown in Figure 8.13.

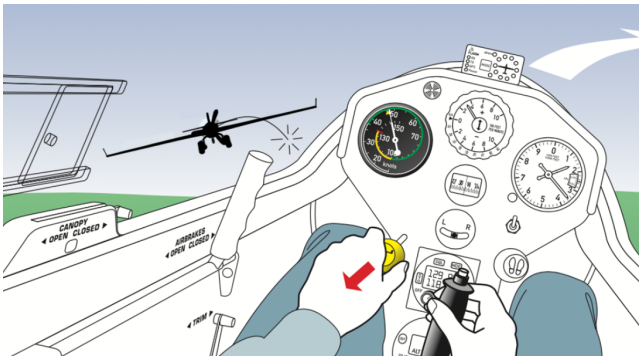

Figure 8.13: The glider releases from the tow craft.

DESCENT

When the glider has successfully released, *MARCUS-T* will initiate its descent. The operational flow of the descent can be seen in Figure 8.14.

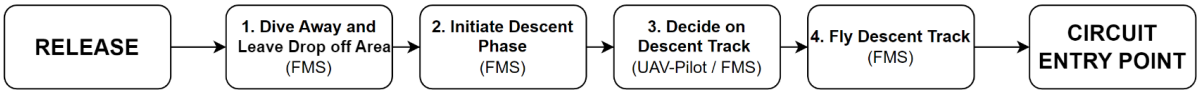

Figure 8.14: Operational flow of the descent.

Depending on the location of *MARCUS-T* or the aerial situation, it will fly one of the programmed descent tracks, specified in Section 2.2. One influence on the type of descent is the desired block time. The block time is heavily dependant on the descent track. A suitable track will be initiated by the ground crew, based on the tow schedule, the location with respect to the circuit entry point and the current airspace activity. The total block time per chosen descent profile is stated in Table 8.2. It has to be kept in mind that these are estimates. The airspeed and vertical speed are assumed to be constant during each individual flight phase, although in practice they will vary.

Table 8.2: Block times per descent profile. ($m_{glider} = 850\,\text{kg}$)

Descent Profile	Take-Off Time [s]	Climb Time [s]	Descent Time [s]	Circuit Time [s]	Total Time [s]	Total Time [min]
Special Case (Glide Profile)	45	383	**210**	140	**778**	**13.0**
Descent Track	45	383	**132**	140	**700**	**11.7**
Dive Track	45	383	**67**	140	**635**	**10.6**
Steep Dive Track	45	383	**19**	140	**587**	**9.8**

During the descent, the ground crew will closely monitor the crafts location and its surroundings. *MARCUS-T* will continue its descent towards the circuit entry point. Once *MARCUS-T* reaches the circuit entry point, the ground crew will give the necessary radio calls on the towers frequency. This will be done according to the VFR-RT[2] rules and operational procedures at the airfield, as defined in the AIP [3].

CIRCUIT AND LANDING

Once the ground crew have made the radio call and *MARCUS-T* has joined the downwind leg of the circuit, it will bleed off its excess speed and continue to fly the pre-programmed landing pattern. The operational flow is shown in Figure 8.15

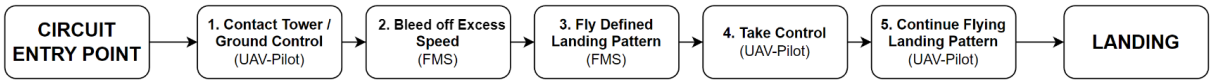

Figure 8.15: Operational flow of the landing phase.

The ground crew will closely monitor the crafts flight path and other traffic in the circuit. If *MARCUS-T* is below an altitude of 120 m, the ground crew could override the craft and remotely continue flying the landing pattern. They could decide to fly a tighter landing circuit to decrease the block time, and more importantly, the energy consumption. The landing is preferred to be piloted remotely. Currently, humans still have a better capability to recognise and respond to complex and dynamic situations that may occur on a small airfield, than automated systems[4]. These dynamic situations could involve unexpected obstacles on the runway, or other aircraft or vehicles on the runway. In this use case, human pilots can better assess the situation and react by aborting the landing and initiating a go-around. The craft will continue flying the pattern and land on the designated runway. If required, manual braking could be performed to decrease the total landing distance.

[2] www.easa.europa.eu [cited 17 June 2024]
[3] eaip.lvnl.nl [cited 15 June 2024]
[4] www.icao.int [cited 17 June 2024]

GO-AROUND

When a take-off is aborted and a go-around is initiated, the ground crew pilot will remotely fly the craft and fly the circuit pattern as shown in Section 2.2, Figure 8.15. *MARCUS-T* can then either be flown remotely the entire time or the automatic flight mode can be engaged again, since it is programmed to fly the entire circuit pattern.

8.2.3. Emergencies

This subsection describes the Emergency Operating Procedures (EOP's) for the tow operations. Familiarity with these procedures is mandatory for all personnel involved. These procedures are preliminary and are intended to provide a brief overview of potential emergencies that can occur during tow operations and what *MARCUS-T* should do in these situations. In the case of an emergency, *MARCUS-T* will be overridden and be piloted remotely.

Aborting Tow Launch During Ground Roll: If there is an issue with *MARCUS-T* during the ground roll phase, the UAV-Pilot should disconnect or cut the tow rope as quickly as possible. This creates more space between *MARCUS-T* and the glider. The glider pilot will see this and understand that the launch is being aborted.

When the tow launch is aborted due to a rope break or engine failure, the UAV-pilot will stop and steer to the left without braking, providing sufficient space for the glider, since the glider usually has less effective brakes. The glider pilot will disconnect and steer away to the right.

Engine Failure in the Air: In the event of an engine failure during the tow launch, *MARCUS-T* will roll its wings up and down and report the issue via the radio. The glider pilot must then immediately disconnect. For both the UAV-pilot and the glider pilot, the following applies:

- Below 100 meters: attempt a landing into the wind in a field or pasture. Low slow turns are undesirable. If no landing can be attempted, the Ballistic Parachute Deployment System shall be activated,
- Above 100 meters: assess whether *MARCUS-T* can reach the airfield. At an altitude of 100 meters, *MARCUS-T* can cover about three kilometers of horizontal distance. If it seems feasible, land *MARCUS-T* somewhere on the airfield. If the UAV-pilot is unsure about the distance and altitude, land outside the airfield into the wind. If this is not possible, the Ballistic Parachute Deployment System shall be activated.

Tow Release Failure: If the glider cannot release from *MARCUS-T* , the glider pilot should inform the UAV-Pilot over the radio. If the radio is malfunctioning, the glider should roll its wings up and down to attract the UAV-pilot's attention via the camera system. This is shown in Figure 8.16.

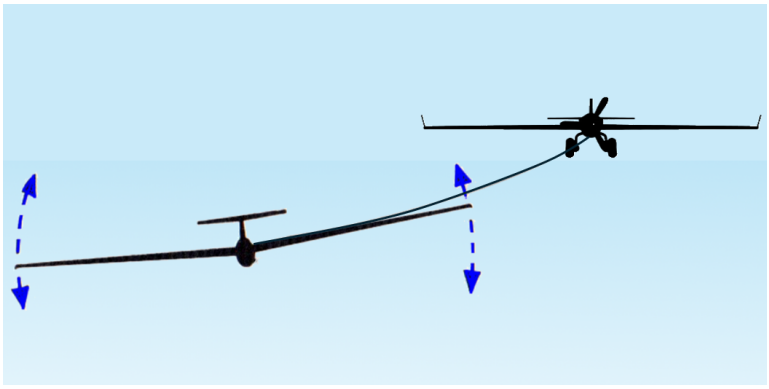

Figure 8.16: Glider will roll its wings in case of a radio failure.

Once the UAV-pilot realises that the glider is unable to release, they will tow the glider back to the airfield in a gradual descent. During the descent, no steep turns will be made. The UAV-pilot will choose a circuit that allows for a wide turn and gentle descent toward the runway. They will select a sufficiently long final approach. A few meters above the ground, the UAV-pilot will cut the rope, allowing the glider to land. If this fails, the combination will land together. *MARCUS-T* will not brake since this could lead to the glider hitting *MARCUS-T*.

Glider Lifting the Tow Craft: According to research conducted by the BGA[5], aerotow launches are significantly safer than winch launches. However, during an aerotow, a tow pilot is at the greatest risk. A life-threatening situation arises if the glider suddenly climbs above the tow plane during launch or at low altitude. While *MARCUS-T* is automatic and therefore does not have a tow pilot, this situation could still be catastrophic for people on the ground if *MARCUS-T* crashes.

If the glider, due to turbulence and the glider pilot's delayed reaction, gets towed so high above *MARCUS-T* that it is not visible anymore and lifts the tail, the glider pilot must immediately release. If this fails because the rope is too tight, they should try again after briefly descending.

As soon as the UAV-pilot notices the glider lifting the tail, causing *MARCUS-T* 's nose to pitch down, and if this cannot be corrected with the elevator, the UAV-pilot must immediately cut or release the rope to prevent an uncontrollable situation. Several factors can increase the risk of tail lifting:

- Towing from the centre of gravity hook,
- Light gliders,
- Short tow ropes,
- Glider pilots with little towing experience,
- Vintage gliders with high wings (further from the centre of gravity hook),
- Turbulent weather / Strong wind gradient.

The UAV-pilot can reduce the risk of this dangerous situation by:

- Assessing before the launch if multiple factors are present. If so, they may decide not to launch,
- Transitioning gradually from takeoff to the climbing phase. A rapid transition may cause the glider to momentarily descend below *MARCUS-T*. The glider pilot, seeing this, might initiate a climb too quickly and get slung upwards,
- Verifying the release from the GCS to ensure the rope has indeed released. If *MARCUS-T* dives too early and the rope has not released or is stuck, both aircraft could stall.

Loss of Control: In case of a full loss of flight controls, the Ballistic Parachute Deployment System shall be activated. An artistic impression of the deployed BPDS is shown in Figure 8.17. The descent rate of the craft with the chute deployed has been estimated to be 3.5 m/s considering a BRS Aerospace ballistic parachute[6].

Figure 8.17: *MARCUS-T* with a deployed parachute as seen from a glider.

[5] members.gliding.co.uk [cited 17 June 2024]
[6] brsaerospace.com [cited 19 June 2024]

9

MARCUS-T: System Description and Risk Analysis

In order to ensure that the design complies with all the requirements, especially the requirements set by EASA. The risk assessments and RAMS need to be completed. To complete this analysis, the required hardware and software needs to be selected and integrated.

9.1. Hardware, Software & Data

by Gerard, Andreas

After the design has been finalised, the craft has to be equipped with the necessary systems to make it airworthy. Stemming from requirements and engineering decisions, it has been decided that *MARCUS-T* would contain the following systems.

- Aerodynamic & Structural System (ASS),
- Electric Propulsion System (EPS),
- Flight Management System (FMS),
- Flight Navigation System (FNS),
- Glider Coupling System (GCS),
- Integrated Surveillance System (ISS),
- Power Provision System (PPS),
- Radio Transmission System (RTS),
- Emergency Descent System (EDS).

The boundaries of these systems are defined in Figure 9.1. Only the most relevant software and hardware elements are displayed; these are either hardware components that interact with each-other, or software applications within a computer that have very distinct functions.

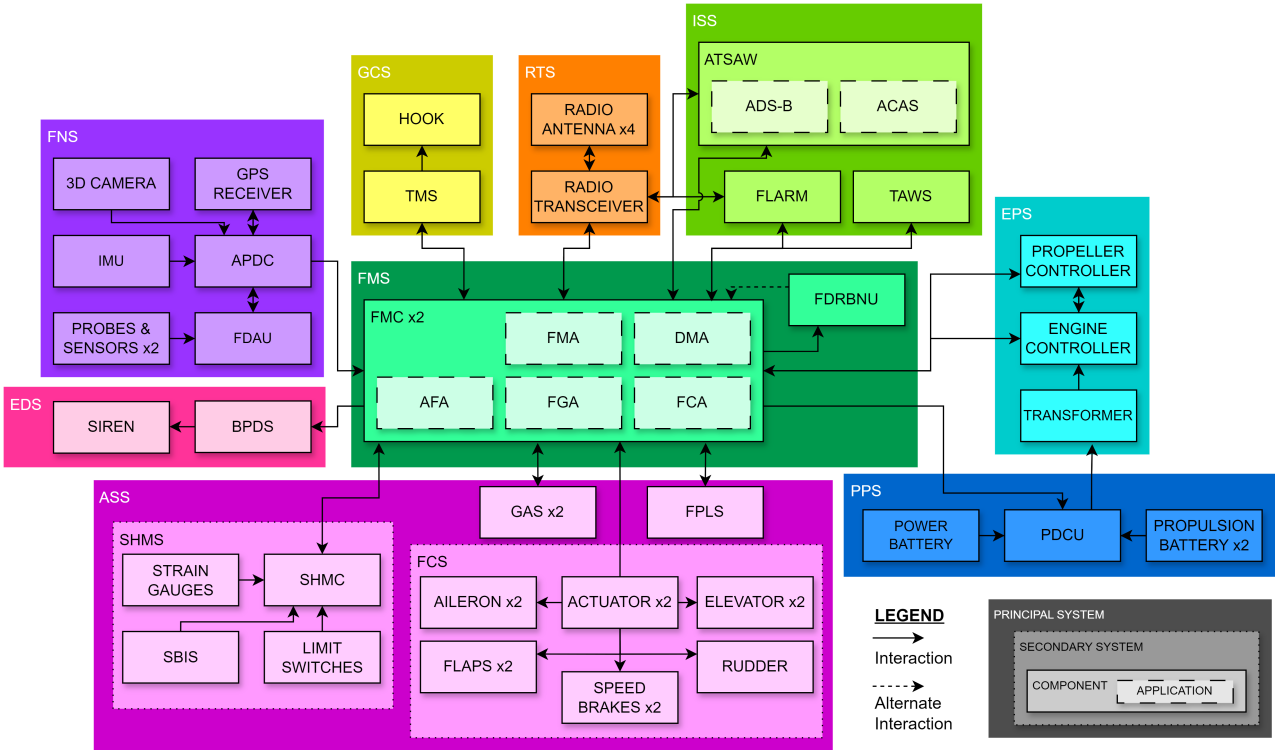

Figure 9.1: Hardware and software diagram with the components of *MARCUS-T*. Acronyms are explained later in the section.

Figure 9.1 shows the general boundaries and interactions. However, for a more detailed explanation of the data exchange between components and software applications, refer to Figure 9.2.

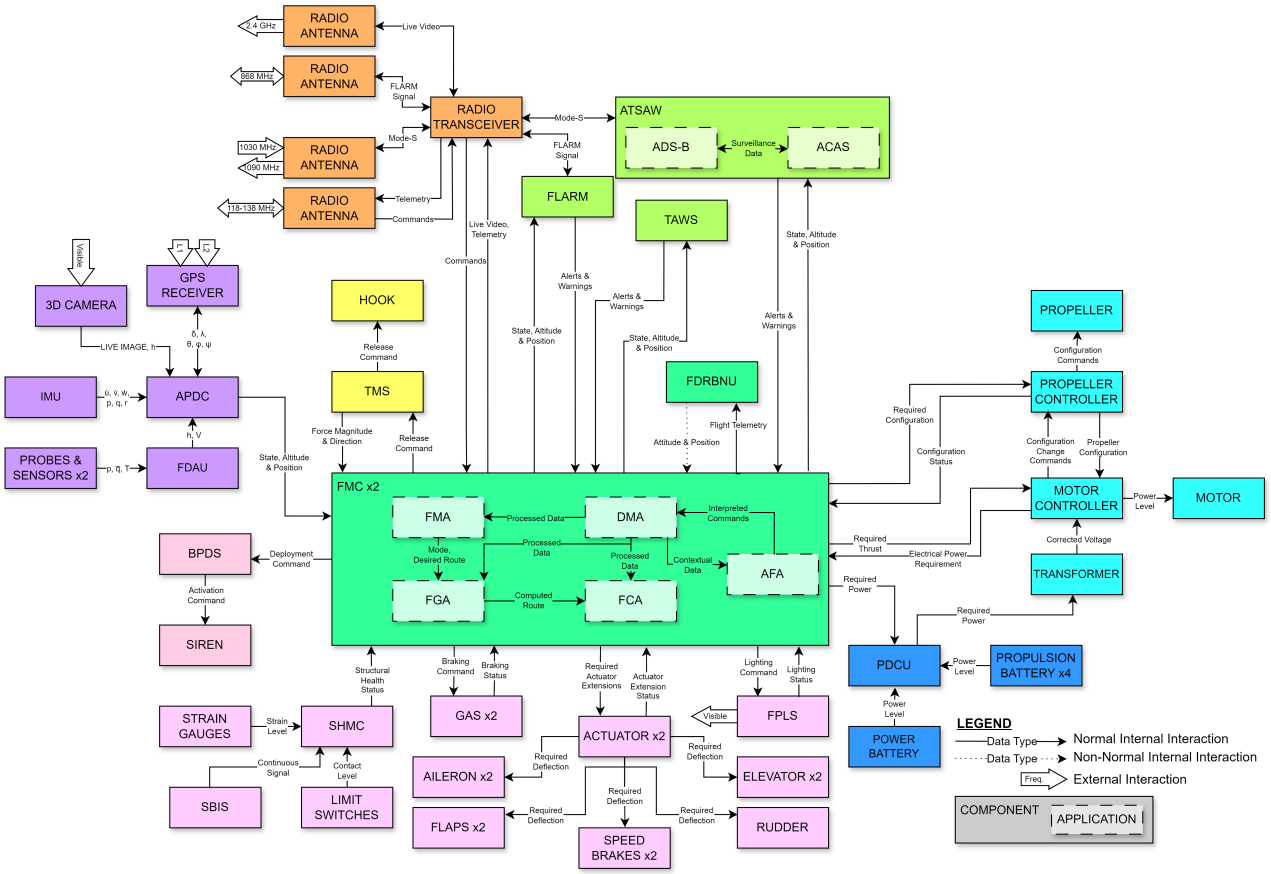

Figure 9.2: Data flow diagram showing exchange of information between components and software within *MARCUS-T* 's systems.

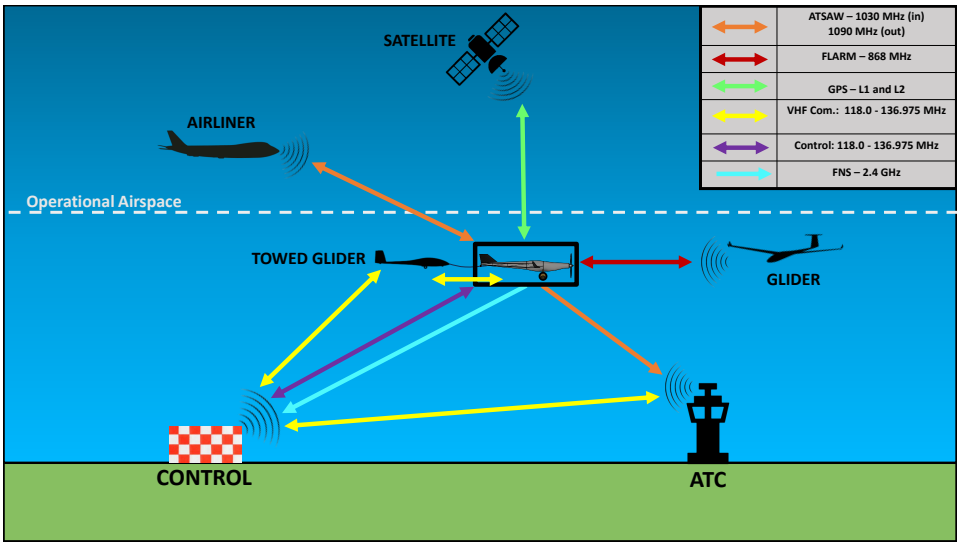

Figure 9.3: Communication diagram tow craft.

Figure 9.2 shows the components and software applications. Arrows show the direction of data flow. The data type or information is indicated in the arrow. Thick white arrows show the exchange of information with the environment, with the electromagnetic spectrum frequency or band used indicated. Dotted arrows show non-normal interactions. Figure 9.3 shows the interactions between *MARCUS-T* and other systems.

9.1.1. Aerodynamic & Structural System (ASS)

The ASS contains the Structural Health Monitoring System (SHMS), the Flight Control System (FCS), the Functional & Positional Lighting System (FPLS), and the Ground Arresting System (GAT).

The SHMS contains a computer that is able to determine the health status of the structure by processing data received from three types of sensors: strain gauges for critical parts, limit switches for critical joints, and a series of Structural Break-up Indication Sensors (SBIS). The SBIS are conducting cables running along the fuselage that indicate whether a severe structural break-up has occurred when a specific fraction of them stop drawing current. This system is mainly used to activate an immediate emergency response.

The FCS contains a series of redundant actuators that deflect the control surfaces. These control surfaces come in pairs, except for the rudder. As there are two actuators per surface, *MARCUS-T* contains a total of 14 actuators.

The GAS consists of the brakes in the main landing gear, and the FPLS consists of a series of lights to increase the visual situational awareness of other pilots.

9.1.2. Electric Propulsion System (EPS)

The EPS consists of an engine controller as well as a transformer that adapts the power supply for the engine, and a propeller controller, which allows for rotation of the blades. The controllers communicate with each other to attain the most efficient propeller-engine configuration.

9.1.3. Flight Management System (FMS)

The FMS consists of a pair of Flight Management Computers (FMC) and a Flight Data Recorder and Backup Navigational Unit (FDRBNU).

The FMS contains 5 main applications. The Flight Guidance Application (FGA) computes the route that must be flown given the target flightpath and the current position. The decisions taken by the FGA also highly depends on the mode engaged by the FMA. The Flight Control Application (FCA) computes the required control surface actuation needed to follow the required route. The Data Management Application (DMA) filters and processes the data received from all systems and distributes it between the necessary applications. The AI Flight Assistant (AFA) is powered by the custom Feature Identification and Language Interpretation Platform (FILIP) AI, and has two main functions: it processes input from the 3D camera to detect obstacles and the boundaries of the runway, and it processes any voice instructions and turns the information received into commands readable by the other FMC applications. This is an innovative application in the general aviation sector and thus the technology will need to be thoroughly verified and validated.

The Flight Management Application (FMA) monitors the state and performance of the flight, and engages the necessary modes programmed into the computer. Some preliminary example modes are listed here.

- “Climb Mode”: FMS strives for the optimal climb performance, while closely monitoring the TMS,
- “Landing Mode”: on approach, navigation through the 3D camera is prioritised to avoid possible runway incursions,
- “Override Mode”: the craft enables direct radio control,
- “Emergency Mode”: the craft broadcasts a distress call to activate an emergency response. The engine will be powered-off and will attempt to glide to safety. The glider, if coupled, will be released. If necessary, the ballistic parachute will be deployed.

During non-normal modes, the craft will is considered to be in “Alternate Law”. If the craft is performing on a normal mode, it will be in “Normal Law”. The FMS will offer flight envelope protection during Normal Law. However, this protection will be less limiting to allow for better emergency manoeuvrability during Alternate Law.

Finally, the FMS also consists of the FDRBNU. This FDRBNU has two main functions: it is both a flight data recorder, but also contains several backup navigation systems in case the FNS fails.

9.1.4. Flight Navigation System (FNS)

The FNS consists of four methods to obtain the state, position and attitude of the craft: visual through the 3D camera, digital through the use of the GPS receiver, inertial through the Inertial Measurement Unit (IMU) and

analogical through a series of probes and sensors. The analogical data is pre-processed by the Flight Data Acquisition Unit (FDAU), and then all of the methods are conglomerated and cross-checked inside the Attitude and Position Determination Computer (APDC).

9.1.5. Glider Coupling System (GCS)

The GCS consists of a Tension Monitoring System (TMS) and a hook where the towline is connected. If the TMS detects that the force magnitude or direction will bring the craft out of its design envelope and could cause a dangerous situation, it may release the tow-line by disengaging the hook if commanded by the FMS.

9.1.6. Integrated Surveillance System (ISS)

The ISS consists of three main surveillance systems: FLARM, the Terrain Alert and Warning System (TAWS), and the Airborne Traffic Situational AWareness (ATSAW) system. ATSAW is an Automatic Dependent Surveillance Broadcast (ADS-B) system that is integrated with an Airborne Collision and Avoidance System (ACAS). As per regulation, any traffic advisories and resolutions will have to be executed by a remote pilot override. TAWS strives to prevent collisions with terrain by also sending alert messages to the remote pilot. FLARM is also necessary as *MARCUS-T* will be operating mostly around gliders, and all of them are equipped with FLARM but not ADS-B. All of the surveillance systems communicate with or interrogate other systems through radio waves.

For redundancy, a passive system is also installed into *MARCUS-T* such that it can be detected even if powered-off: a radar reflector.

9.1.7. Power Provision System (PPS)

The PPS contains a Power Distribution and Control Unit (PDCU), and five batteries. Four batteries provide power to the EPS, while an additional independent battery provides power to all other systems. This battery will be fixed and thus charged overnight in the hangar.

9.1.8. Radio Transmission System (RTS)

The RTS contains a radio transceiver to provide the possibility of two-way communication. There are four antennas, as summarised in Table 9.1.

Table 9.1: Summary of RTS antennae.

Antenna	Frequency In	Frequency Out	Main System	Purpose
1	-	2.4 GHz	FNS	Send live footage to back-up remote pilot.
2	868 MHz	868 MHz	FLARM	Surveillance.
3	1030 MHz	1090 MHz	ATSAW	Surveillance.
4	118.00-136.975 MHz	118.00-136.975 MHz	FMS	Recieve direct/voice commands, send telemetry to back-up remote pilot.

9.1.9. Emergency Descent System (EDS)

The EDS is a system that will only engage in the worst case scenario during Emergency Mode. It consists of the Ballistic Parachute Deployment System (BPDS) and a siren.

The BPDS will deploy a ballistic parachute. If the BPDS is deployed, a distress signal is emitted by the craft including the location of the deployment. This location is also continuously broadcasted after the activation of the emergency response. A siren is also be engaged such that any possible collision with people on the ground is avoided.

9.2. System Location and Connection

by Mees, Niels

The placement of the systems along *MARCUS-T* is shown in Figure 9.4. It should be noted that the relative locations of the ISS, RTS, FMS, SHMC, ASS, PPS, and FNS are not completely accurate due to their 3D placement. The data flow directions between the systems in *MARCUS-T* are displayed in Figure 9.2. The relative dependencies of each subsystem, as well as those on outside information, can be deduced from this figure. Then, in Figure 9.5 the electrical wiring diagram can be found. There are two separate electrical circuits. One for the engine and the electric propulsion system which are powered off the larger propulsion batteries.

The other electrical circuit is powered off the fixed batteries that are located in the wings. These power the onboard computers, communication systems, actuators, and other systems that are not part of the propulsion unit.

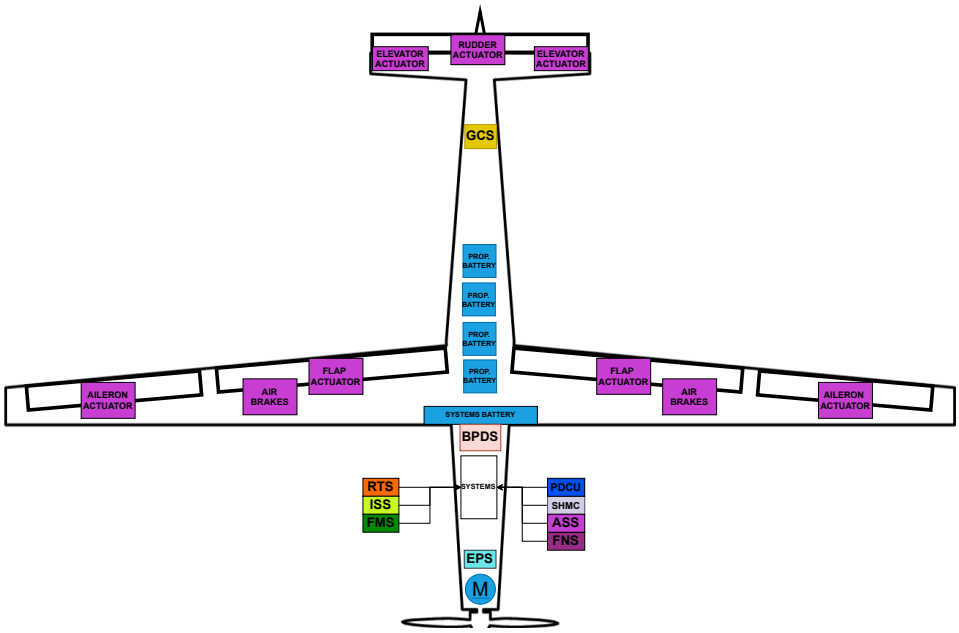

Figure 9.4: The locations of the systems.

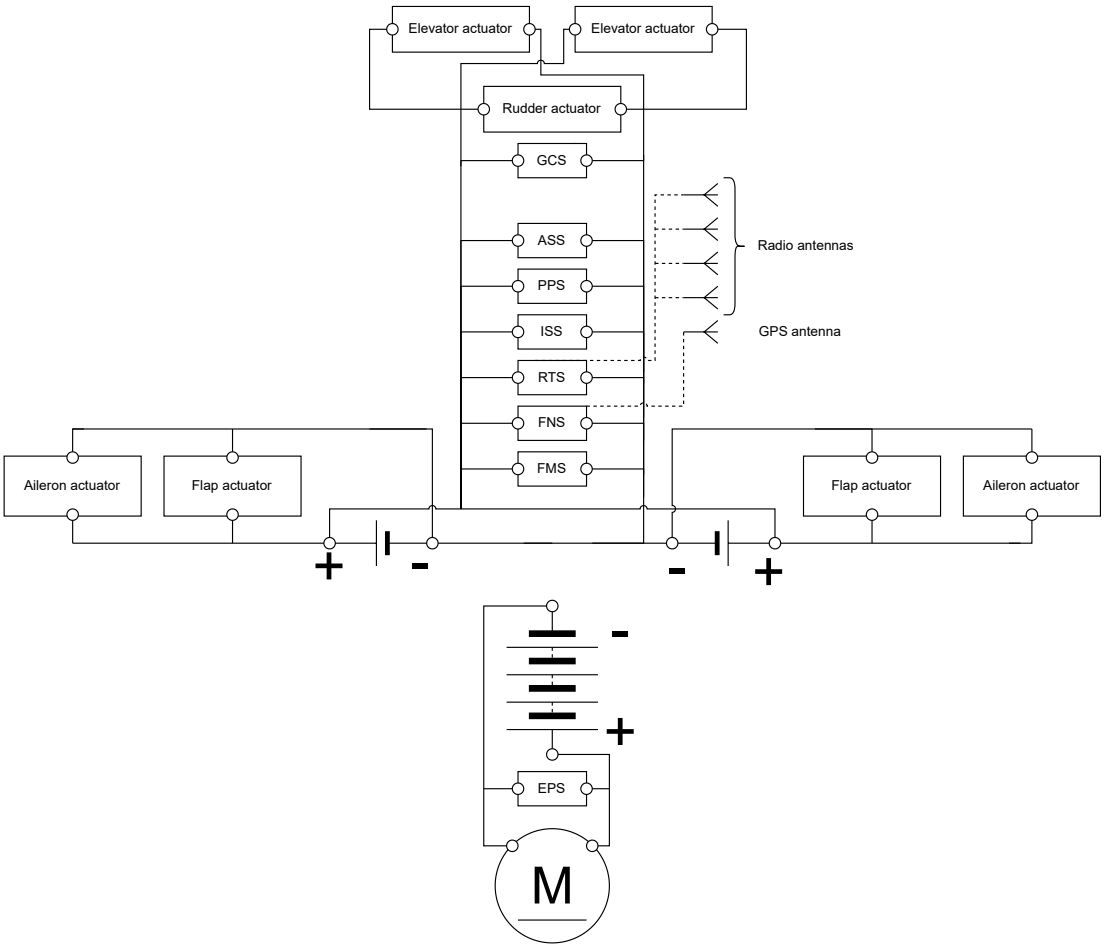

Figure 9.5: Electrical wiring diagram of *MARCUS-T*.

Centre of Gravity

The centre of gravity of *MARCUS-T* needs to be located such that it allows for stability and control-ability on the air and on the ground. From Table 5.9 the allowed centre of gravity range between 1.80 and 1.93 meters was calculated. All systems of the craft should be balanced such that this requirement is met during the flight condition. During ground operations, the batteries need to be replaced often. It would be very undesirable to have the craft tip on the nose when removed. Therefore the CG location must always remain behind the main landing gear when handling removable items (batteries). The centre of gravity is calculated with Equation 9.1.

$$X_{CG} = \frac{\sum_{i=1}^{i} X_{CG_i} \cdot W_i}{\sum_{i=1}^{i} W_i} \tag{9.1}$$

The positions of the subsystems are shown in Figure 9.6. With the exact values of the CG locations given in Table 9.2. The location of the battery, $X_{CG_{bat}}$, is represented as the combined CG of the 4 batteries together. In reality the 4 batteries are spaced 20 cm apart to allow for easy access during the swapping procedure. Furthermore, the FMS, ISS, RTS, SHMC, ASS, PDCU, FNS CG locations are grouped together under $X_{CG_{systems}}$. These systems consist of computers that are used for monitoring and regulating the craft. Therefore, it makes sense to group them together and place it into the craft as one larger computer consisting of smaller units combined.

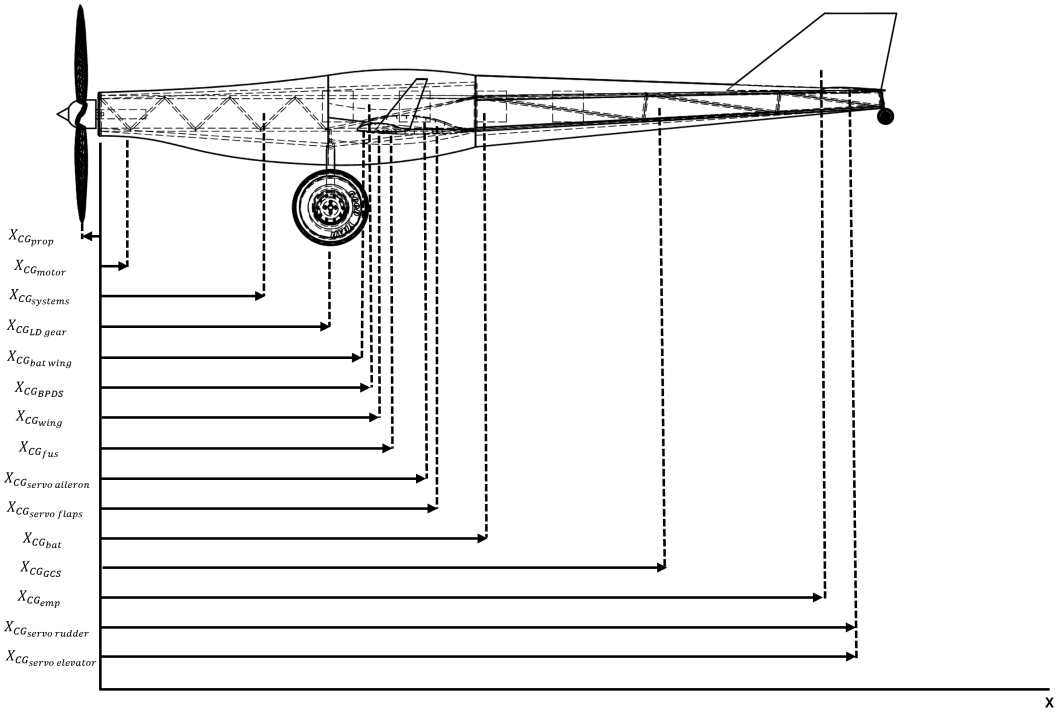

Figure 9.6: Definition of the CG locations of the major systems in the tow craft.

Table 9.2: CG locations of the major systems in the tow craft as defined by Figure 9.6.

Component	X position of the CG	Value [m]
Propeller	$X_{CG_{prop}}$	-0.1
Electric motor	$X_{CG_{motor}}$	0.3
FMS, ISS, RTS, SHMC, ASS, PDCU, FNS	$X_{CG_{systems}}$	1.4
Landing gear	$X_{CG_{LD\ gear}}$	1.5
Battery in the wing	$X_{CG_{bat\ wing}}$	1.81
BPDS	$X_{CG_{BPDS}}$	1.85
Wing	$X_{CG_{wing}}$	1.92
Fusulage	$X_{CG_{fus}}$	2.03
Servo for ailerons	$X_{CG_{servo\ aileron}}$	2.16
Servo for flaps	$X_{CG_{servo\ flaps}}$	2.22
Grouped battery location	$X_{CG_{bat}}$	3
GCS	$X_{CG_{GCS}}$	4.06
Empennage	$X_{CG_{emp}}$	4.7
Servo for rudder	$X_{CG_{servo\ rudder}}$	4.9
Servo for elevator	$X_{CG_{servo\ elevator}}$	4.9

9.3. Specific Operations Risk Assessment (SORA)

by Andreas, Gerard

In order to prove compliance with EU regulation, the Acceptable Means of Compliance (AMC) from EASA's Easy Access Rules for Unmanned Aircraft Systems (CS-UAS) has been used [5]. Article 11 of AMC 1 in CS-UAS requires that a specific operations risk assessment (SORA) is carried out on top of all other technical risk assessments. By following this AMC, compliance with EU regulation can be ensured.

9.3.1. Application

As defined by Section 1 of CS-UAS, there are certain limitations to the scope of the SORA analysis. SORA will mainly deal with the risk of collision between the unmanned aircraft (UA) and manned aircraft or people [5]. SORA will not deal with UA-UA collision risks, or risks associated with the craft or its information, such as security, financial, health, or privacy risks.

The SORA process consist of identifying risks and proposing mitigation strategies. Only risks that could cause immediate fatal injuries to third parties or damage to critical infrastructure must be analysed, thus chronic events, such as technical failures, are excluded. These mitigation strategies have to be evaluated to a level of integrity and assurance so that they can be assigned a level of robustness [5].

9.3.2. Ground Risk Classification (GRC)

The risks posed by *MARCUS-T* are determined to be fully covered by the SORA process, assuming no specific exclusions from relevant local authorities. This is determined using the following process,

- The craft does not fall within the 'open' category,
- The craft does not fall within a 'standard' scenario,
- The craft does not fall in a 'certified' category,
- The craft is not subject to any NO-GO from authorities.

The nature of operation is described in Chapter 8. A preliminary GRC value of 10 is assigned to *MARCUS-T* based on the operational profile, expected population density around glider clubs, and other SORA guidelines. According to the characteristics of *MARCUS-T* , in order to pass SORA, the GRC must be reduced to a maximum of 7.

The risks posed by this operation are broken down by level of control and structural integrity during failure. These modes are shown in Table 9.3. Each combination is qualitatively assessed for the probability of failure (PF), the probability of striking people or critical infrastructure (PH), and the probability that a strike causes

fatal injury or damage to the people and critical infrastructure respectively (PK). The product of PH and PK gives the severity (S). The product of P and S give the risk (R). This assessment is shown in Table 9.4. A lower number refers to lower risk, a higher number to higher risk.

For each operational failure mode, a risk mitigation strategy is developed. These strategies fall under one of three groups. M1 refers to 'strategic mitigation for ground risk'. M2 refers to strategies that reduce the ground impact effect. M3 covers the emergency response plans. Each strategy is then graded in terms of robustness. This comes from the product of the assurance level and the integrity level. These levels are determined from the tables in Annex B to AMC 1 to Article 11 of CS-UAS [5]. The mitigation strategies are summarised in Table 9.5. Each risk is assigned an appropriate mitigation strategy, which reduces their probabilities and severities (PF', PH', PK' S') into a reduced risk (R'). Then, the total GRC reduction due to the strategies is added linearly.

The total GRC reduction must not exceed -6 when applying M1 mitigation sequences, as per Section 2.3.2 (d) [5]. If a GRC reduction would be over the limit, it is marked with an asterisk.

The evolution of the identified risks is displayed in Figure 9.7. Risks in the red region must be reduced. Risks in the orange must be monitored monthly, while risks in the yellow region must be monitored weekly. Risks in the green region can be accepted, and will only need to be re-evaluated if they were to develop into their respective consequences.

Table 9.3: Operational failure mode identification matrix.

Integrity level / Controllability	Full Craft	Partial Detachment	Rapid Dissassembly
Full Speed + Control	SORA-FC-01	SORA-PD-01	SORA-RD-00
Full Speed + No Control	SORA-FC-02	SORA-PD-02	
No Speed + Control	SORA-FC-03	SORA-PD-03	
No Speed + No Control	SORA-FC-04	SORA-PD-04	

Table 9.4: Risk assessment of identified operational failure modes.

ID	PF	PH	PK	S	R	Mitigation	PF'	PH'	PK'	S'	R'	Total GRC Reduction
SORA-FC-01	4	1	4	1	4	1, 2, 3, 4	2	1	4	1	2	-3
SORA-FC-02	1	2	4	2	2	1, 2, 3, 4	1	2	1	1	1	-3
SORA-FC-03	2	2	4	2	4	1, 2, 3, 4	2	1	4	1	2	-3
SORA-FC-04	1	2	4	2	2	1, 2, 3, 4	1	2	1	1	1	-3
SORA-PD-01	4	2	4	2	8	1, 2, 4, 5, 6	1	2	1	1	1	-6
SORA-PD-02	1	3	4	3	3	3, 4, 5, 6	1	3	1	1	1	-5
SORA-PD-03	2	3	4	3	6	1, 2, 4, 5, 6	1	2	1	1	1	-6
SORA-PD-04	1	3	4	3	3	3, 4, 5, 6	1	3	1	1	1	-5
SORA-RD-00	1	4	2	2	2	4, 5, 6, 7, 8	1	4	2	2	2	-6*

Table 9.5: Mitigation strategies.

Mitigation ID	Mitigation Strategies	Mitigation Sequences	Assurance	Integrity	Robustness	GRC reduction factor
1	Ground crew override	M1	Low	Medium	Low	-1
2	Define dive zones	M1	Low	Medium	Low	-1
3	Flight termination system	M2	High	Medium	Medium	-1
4	Emergency response plan	M3	Medium	Medium	Medium	0
5	Quality inspections	M1	Medium	Medium	Medium	-2
6	Structural health monitoring system	M1	Medium	Medium	Medium	-2
7	Fire supression system	M1	High	High	High	-4
8	Speed envelope control	M1	Medium	Low	Low	-1

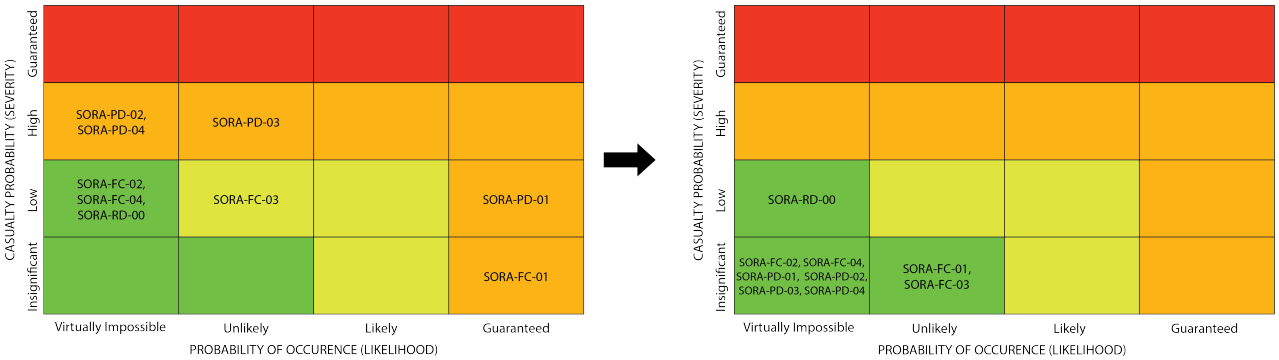

Figure 9.7: Preliminary and post-mitigation risk map with operational risks identified during SORA.

After mitigation all the ground risks are at an appropriate level and the GRC, in the most limiting case, is less than seven.

9.3.3. Air Risk Classification (ARC)

After GRC is reduced below seven, the ARC is calculated. Using Section 2.4.2 of AMC1 Article 11 of CS-UAS, the initial air risk class is determined to be ARC-C [5]. This is because *MARCUS-T* will not operate over FL600 or in Class B/C/D airspace. Strategic mitigations are outside of the scope at this stage of the design process, thus ARC-C is also the residual risk class. The tactical mitigation strategies must therefore meet the 'medium' level and 'medium' robustness. These strategies are prescribed in Annex D to AMC1 of Article 11. These include requiring systems such as FLARM and ADS-B as well as a warning for the UAS operator. To meet robustness, the mitigation system has to have a MTTR $>$ 1000 flight hours.

9.3.4. Specific Assurance Integrity Level (SAIL)

Finally, SORA establishes a synthesis between ARC and GRC. This value is the Specific Assurance Integrity Level (SAIL). According to Section 2.5.1 (d), *MARCUS-T* falls under SAIL VI. This SAIL level determines the recommended level of robustness for the Operational Safety Objectives (OSOs). In the case of SAIL VI, it is recommended that the level of robustness is "high" for all OSOs. These are given in Section 2.5.2 and Annex E [5].

9.3.5. Recommendations

After performing SORA, in order to fully comply with European Regulation, several actions need to be performed. Mainly, the mitigation strategies used to lower the GRC need to be implemented into *MARCUS-T* and its surrounding operations. Furthermore, in order to attain the specified levels of integrity and robustness for the mitigation strategies, third-party validation will be required.

It is recommended that a detailed analysis on the OSOs is performed to ensure that the required robustness levels are met. This was not performed as it is out-of-scope for the current development phase.

Both the FAA and EASA have identified the need for the implementation of Unmanned Traffic Management (UTM) systems. However, the timeline is still uncertain. Thus, it is recommended that, in the near future, the implementation of regulatory UTM is investigated. These changes may also come hand.in-hand with the future plans of EASA to develop actual Certification Specifications (CS) for unmanned aerial vehicles, as currently only Guidance Material (GM) and Acceptable Means of Compliance (AMC) to European Regulation are provided.

9.4. Technical Risk Assessment

by Andreas, Gerard

A failure mode effect analysis (FMEA) is performed on each component. A fault tree is created by analysing the possible failure effects of each component, and then the causes for the failure effects are analysed. The identified components, failure effects, and identified failure modes are shown in Table 9.6. The failure criticality is assessed and assigned a development assurance level (DAL), ranging from no safety effect (NSE), minor (MIN), major (MAJ), hazardous (HAZ), to catastrophic (CAT). These are quantified by numbers from one to

five. Five is is the most critical level, CAT, and one is the least critical, NSE.

Component failure probabilities are obtained by the MTBF values collected in the RAMS analysis. These are also quantified on a scale from one through five, again with five being the most critical, an MTBF less than 1,000 h, and one being the least critical, an MTBF greater than 1,000 h. Failure mode probabilities are estimated based on experience and intuition. Nominally, the failure mode probabilities of each component should add up to one, but due to the qualitative nature of the data, these failure mode probabilities are once again a scale from one to five. The overall failure probability is thus the product of the component failure rate and the failure mode rate divided by the sum of all the failure modes of that component. These probabilities are normalised and multiplied by the DAL to get the technical risk of each component failure mode. These are presented in Table 9.7.

The risks are divided into four color-coded categories. Green risks are acceptable, yellow risks require some additional monitoring, orange risks require significant monitoring, and red risks are unacceptable. To reduce the risks, mitigation strategies are presented in Table 9.8. Because the existing contingency and mitigation techniques from previous risks assessments are already implemented, and considered when assigning criticality, the number of unacceptable technical risks are low, and no new contingency strategies are needed.

Table 9.6: Failure mode discovery tree.

Component	Failure Effect	Failure Mode	ID
ELECTRIC MOTORS	Engine failure	Disconnection	EM-01
		Coolant loss at max power	EM-02
	Incomplete thrust	Partial electrical malfunction	EM-03
		Demagnetisation	EM-04
	Loss of efficiency	Partial electrical malfunction	EM-05
		Contamination	EM-06
		Corrosion	EM-07
MOTOR / PROPELLER CONTROLLER	Incorrect commands	Software error	CT-01
	No commands	Electrical short	CT-02
		Disconnection	CT-03
PROPELLER	Structural failure	Fatigue	PR-01
		Collision	PR-02
	Blade mechanism failure	Corrosion	PR-03
		Fatigue	PR-04
		Lubrication	PR-05
TRANSFORMER / PDCU	Stop	Disconnection	TF-01
		Burnout	TF-02
		Fire	TF-03
	Incorrect voltage	Software error	TF-04
	Loss of efficiency	Corrosion	TF-05
		Contamination	TF-06
MAIN WING / EMPENNAGE	Total loss of control	Control surface detachment	WE-01
		Actuator jamming	WE-02
	Partial loss of control	Partial breakage of surface	WE-03
		Actuator decalibrated	WE-04
	Total structural failure	Collision	WE-05
		Fatigue	WE-06
		Incorrect assembly	WE-07

Continued on next page

Component	Failure Effect	Failure Mode	ID
	Partial structural failure	Incorrect manufacturing	WE-08
		Fatigue	WE-09
LIGHTS	No light	Burnout	LT-01
		Disconnection	LT-02
		Breakage	LT-03
	Light dimming	Contamination	LT-04
		Partial disconnection	LT-05
	Excessive power draw	Electrical short	LT-06
COMPUTER / PROBE / SENSOR / ANTENNA	Total malfunction	Power Surge	CS-01
		Fire	CS-02
		Disconnection	CS-03
	Partial malfunction	Damaged electronics	CS-04
		Poor connection	CS-05
		Jamming	CS-06
		Spoofing	CS-07
	Software errors	Skill issue	CS-08
		Undiscovered error	CS-09
LANDING GEAR	Gear collapse	Fatigue	LG-01
		Hard landing	LG-02
	Low tire pressure	Puncture	LG-03
		Hard landing	LG-04
BALLISTIC PARACHUTE	No deployment	Hatch jamming	BP-01
		Entangled parachute	BP-02
		Degradation of charges	BP-03
		Incorrect maintenance	BP-04
	Incorrect deployment	Entangled parachute	BP-05
		Broken parachute	BP-06
	Unintentional deployment	Electrical short	BP-07
		Fire	BP-08
TAIL HOOK	Premature release	Fracture	TH-01
		Tear-out	TH-02
	No release	Corrosion	TH-03
		Impact	TH-04
BATTERY	Fire	Electrical short	BT-01
	Early power-down	Connection issue	BT-02
		Electrical short	BT-03
		Battery degradation	BT-04
	Leakage	Impact	BT-05
		Degradation	BT-06

Table 9.7: Failure mode risk assessment.

ID	Criticality	Component Failure Probability	Failure Mode Probability	Likelihood	Risk
EM-01	2	3	3	2	4
EM-02	2	3	3	2	4
EM-03	1	3	3	2	2
EM-04	1	3	3	2	2
EM-05	1	3	4	3	3
EM-06	1	3	4	3	3
EM-07	1	3	4	3	3
CT-01	2	2	3	5	10
CT-02	2	2	2	3	6
CT-03	2	2	2	3	6
PR-01	3	3	1	2	6
PR-02	3	3	1	2	6
PR-03	1	3	3	5	5
PR-04	1	3	3	5	5
PR-05	1	3	3	5	5
TF-01	3	2	2	2	6
TF-02	3	2	2	2	6
TF-03	3	2	2	2	6
TF-04	2	2	3	2	4
TF-05	1	2	4	3	3
TF-06	1	2	4	3	3
WE-01	2	3	2	2	4
WE-02	2	3	2	2	4
WE-03	1	3	3	3	3
WE-04	1	3	3	3	3
WE-05	2	3	1	1	2
WE-06	2	3	1	1	2
WE-07	2	3	1	1	2
WE-08	1	3	2	2	2
WE-09	1	3	2	2	2
LT-01	1	2	4	2	2
LT-02	1	2	4	2	2
LT-03	1	2	4	2	2
LT-04	1	2	5	2	2
LT-05	1	2	5	2	2
LT-06	1	2	3	2	2
CS-01	2	1	2	1	2
CS-02	2	1	2	1	2
CS-03	2	1	2	1	2
CS-04	2	1	3	1	2
CS-05	2	1	3	1	2
CS-06	2	1	3	1	2
CS-07	2	1	3	1	2
CS-08	2	1	3	1	2
CS-09	2	1	3	1	2

Continued on next page

ID	Criticality	Component Failure Probability	Failure Mode Probability	Likelihood	Risk
LG-01	2	3	2	3	6
LG-02	2	3	2	3	6
LG-03	1	3	4	5	5
LG-04	1	3	4	5	5
BP-01	4	4	1	2	8
BP-02	4	4	1	2	8
BP-03	4	4	1	2	8
BP-04	4	4	1	2	8
BP-05	4	4	1	2	8
BP-06	4	4	1	2	8
BP-07	3	4	3	5	15
BP-08	3	4	3	5	15
TH-01	2	1	4	2	4
TH-02	2	1	4	2	4
TH-03	1	1	3	2	2
TH-04	1	1	3	2	2
BT-01	4	5	2	4	16
BT-02	3	5	3	5	15
BT-03	3	5	3	5	15
BT-04	3	5	3	5	15
BT-05	4	5	2	4	16
BT-06	4	5	2	4	16

Table 9.8: Technical risk mitigation.

ID	Mitigation	New Criticality	New Likelihood	New Risk
CT-01	Additional integration tests	2	4	8
BP-01	Annual inspection	4	1	4
BP-02	Annual inspection	4	1	4
BP-03	Annual inspection	4	1	4
BP-04	Annual inspection	4	1	4
BP-05	Annual inspection	4	1	4
BP-06	Annual inspection	4	1	4
BP-07	Annual inspection	3	1	3
BP-08	Annual inspection	3	1	3
BT-01	Replacement of batteries after 300 cycles	4	2	8
BT-02	Replacement of batteries after 300 cycles	3	2	6
BT-03	Replacement of batteries after 300 cycles	3	2	6
BT-04	Replacement of batteries after 300 cycles	3	2	6
BT-05	Replacement of batteries after 300 cycles	4	2	8
BT-06	Replacement of batteries after 300 cycles	4	2	8

9.5. RAMS Analysis

by Andreas, Gerard

Once the final systems and its elements have been finalised, a Reliability, Availability, Maintainability, and Safety (RAMS) analysis is carried out. The components in Figure 9.1 are labelled with a logistics control number (LCN) as prescribed in MIL-STD-1388-2B and DEF-STAN-006. These are summarised in Figure 9.8.

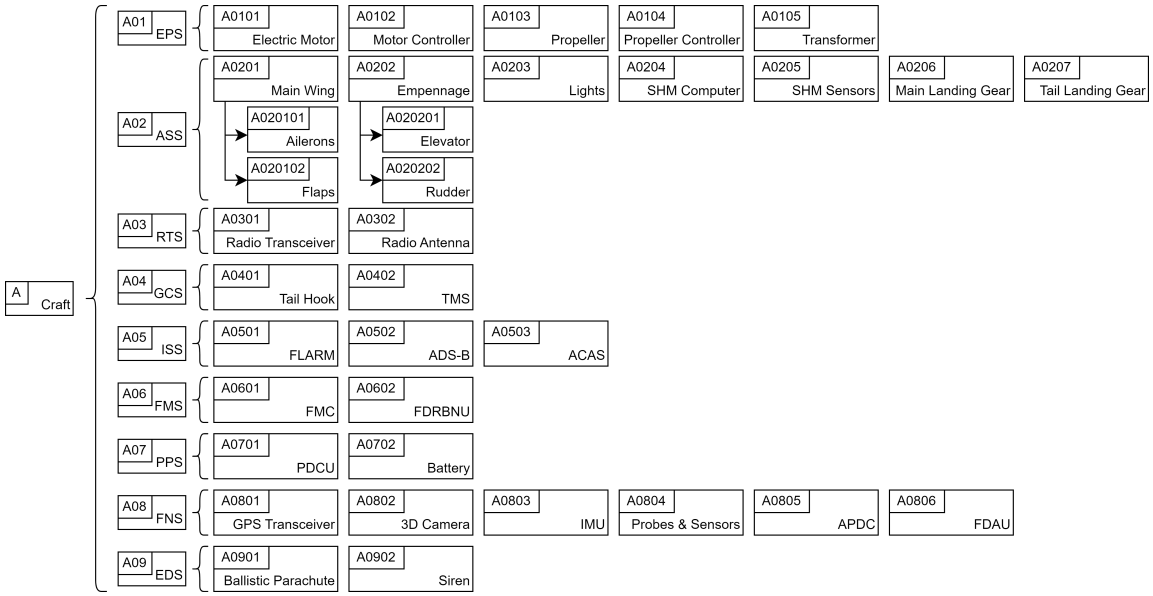

Figure 9.8: LCN numbers assigned to every component of all subsystems.

The safety analysis is informed from the aforementioned TRA. The most critical failure modes for each component are noted, and will drive the safety assessment. Their consequences are noted and labelled in a five-point scale: no safety effect (NSE), minor (MIN), major (MAJ), hazardous (HAZ), and catastrophic (CAT). Their likelihood was also estimated in a five-point scale: Very unlikely (VU), unlikely (U), medium (M), likely (L) and very likely (VL). It is important to note these likelihoods are not global, but the probability that if there is a failure of *that component*, the failure mode is the most critical one. The consequences are determined qualitatively using best judgement, this was done by assessing the likelihood that the failure would result in severe injury or death.

The consequence level estimates are used to define the safety targets for each component and system by using the development assurance level (DAL) system proposed by ARP4761A and the target failure likelihoods from CS 25. DAL-A will correspond to CAT, and DAL-E to NSE, respectively. In order, the target failure likelihood estimates are $<10^{-9}$, $<10^{-7}$, $<10^{-5}$, $<10^{-3}$, and no target.

To check for safety, the DALs of the failure modes have to be compared with the mean time between failures (MTBF) of the components. These MTBFs are adjusted using the failure mode likelihoods. For VU, the MTBF is taken as is, but for every level lower the MTBF is reduced by an order of magnitude, as failures for the reliability are modelled by an exponential function (Equation 9.3). If these fulfil the targets, the component or system will be considered safe. An individual component can be deemed not safe as long as the system as a whole is considered safe. This process is detailed in Figure 9.9.

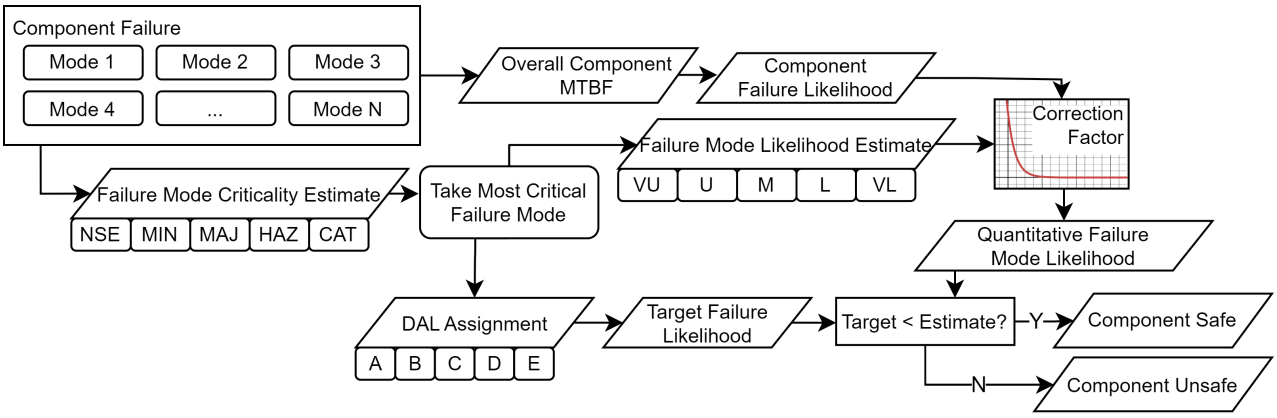

Figure 9.9: Safety assessment process for the RAMS analysis.

For every identified system, Mean Time Between Failure (MTBF) data has to be collected or calculated. As the design matures, these values need to continuously be updated. Due to the preliminary nature of the design,

many of these values cannot be calculated directly, but instead need to be estimated based on historical aircraft performance. The majority of the MTBF estimates are obtained from NASA's "General Aviation Aircraft Reliability Study" and the FAA's "Digital Systems Technical Analysis" [39, 40]. Other systems like the coupling hook are estimated based on fatigue cycles and material properties. Other components, such as the computer systems, FLARM, and ADS-B , are determined by selecting commercially available systems where the MTBF values are known. All MTBF values are converted and presented in flight hours. From MTBF the failure rate, λ, is calculated. Failure rates are assumed to be time invariate, indicating the probability of failure after infant mortality, but before age related failures. The MTBF of subsystems are calculated based on the values of its components. This depends on if components are redundant or in series. For the EPS, ASS, RNS, and GNS, all components are in series, meaning if one fails, the entire system is non-functional. The ISS and FDMS consist only of parallel units, the FNS and PPS are more complicated, and this described in Figure 9.10.

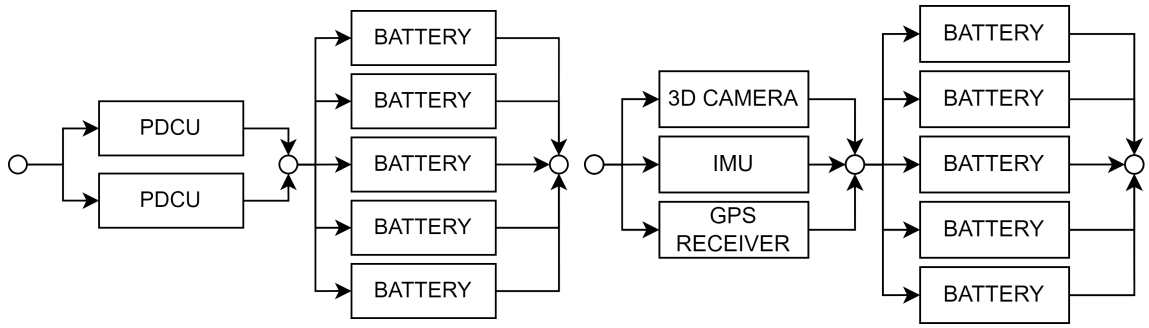

(a) Power provision system (PPS).

(b) Flight navigation system (FNS).

Figure 9.10: Example block diagrams used for the RAMS analysis.

The overall MTBF is calculated by summing the failure rates of series components and taking the product of parallel components. The reliability is then given by Equation 9.3.

$$\lambda = \frac{1}{MTBF} \tag{9.2}$$

$$R(t) = e^{-\lambda \cdot t} \tag{9.3}$$

Engineering judgement and experience is used to determine the Mean Time To Repair (MTTR). These values are summarised in Table 9.10. This represents the average time of any corrective or preventive maintenance, weighted to the failure rate of each failure mode. The inverse of MTTR gives μ, the repair rate. The repair rate gives the probability that a repair can be completed in a given time t, this is the maintainability value, calculated using Equation 9.4.

$$M(t) = 1 - e^{-\mu \cdot t} \tag{9.4}$$

Availability is the measure of the percentage of time that a system or component is in working order. This is given by Equation 9.5.

$$A = \frac{MTTR}{MTBF + MTTR} \tag{9.5}$$

The results of the top level system is calculated, giving a Reliability of 99.8%, an Availability of 97.7%, and a Maintainability of 100%. These values are all very positive, but come with the caveat that these are idealised values and will certainly be smaller in reality. Additionally, with every system added, even if they are fully redundant, the system availability will decrease, as the design matures, additional systems are likely.

Table 9.9: System functional hazard analysis showing only the failure modes that were deemed as the most critical.

LCN		Most Critical Failure Mode	Failure Mode Likelihood	Consequence	Consequence Level
	A				
EPS	A01				MAJ
	A0101	Motor burnout	M	Loss of propulsion, loss of control	MIN
	A0102	Total coltroller loss	U	Uncontrolled motor operation, loss of control	MIN
	A0103	Breakage	VU	Loss of propulsion, potential damage to surroundings/craft	MAJ
	A0104	Total controller loss	U	Uncontrolled propeller operation, loss of control	MIN
	A0105	Fire	U	Loss of life, loss of craft	MAJ
FCS	A02				MIN
	A0201	Structural failure	VU	Loss of lift	MIN
	A020101	Breakage	U	Loss of control, potential loss of craft	MIN
	A020102	Breakage	U	Loss of control, potential loss of craft	MIN
	A0202	Structural failure	VU	Loss of stability	MIN
	A020201	Breakage	U	Loss of control, potential loss of craft	MIN
	A020202	Breakage	U	Loss of control, potential loss of craft	MIN
	A0203	Burnout	L	Loss of situational awareness	NSE
	A0204	Total system failure	U	Inability to predict structural issues	MIN
	A0205	Total sensor loss	M	Inability to predict structural issues	MIN
	A0206	Collapse	U	Damage to craft on landing	MIN
	A0207	Collapse	U	Damage to craft on landing	NSE
RNS	A03				MAJ
	A0301	Total system failure	M	Partial surveillance loss, loss of communication	MAJ
GCS	A04				MIN
	A0401	Fracture	L	Premature release	MIN
	A0402	False reading	M	Inability to release, premature release	MIN
ISS	A05				HAZ
	A0501	Total system failure	M	Partial loss of surveillance	HAZ
	A0502	Total system failure	VU	Partial loss of surveillance	HAZ
	A0503	Total system failure	U	Partial loss of surveillance	HAZ
	A0504	Total system failure	U	Partial loss of surveillance	HAZ
EPS	A06				CAT
	A0601	Total system failure	VU	Loss of control	CAT
	A0602	Total system failure	M	Loss of telemetry storage, loss of backup navigation	MIN
FMS	A07				HAZ
	A0701	Fire	M	Loss of control	HAZ
	A0702	Fire	U	Loss of telemetry storage, loss of backup navigation	HAZ
PPS	A08				MAJ
	A0801	Total system failure	VU	Partial loss of positional awareness	MIN
	A0802	Total sensor loss	VU	Partial loss of positional awareness	MIN
	A0803	Total system failure	U	Partial loss of positional awareness	MIN
	A0804	Total sensor loss	VU	Partial loss of positional awareness	MIN
	A0805	Total system failure	M	Total loss of positional awareness	MAJ
	A0806	Total system failure	M	Partial loss of positional awareness	MIN
EDS	A09				HAZ
	A0901	No Deployment	VU	High-energy uncontrolled ground impact	HAZ
	A0902	No Activation	U	Silent descent	MIN

Table 9.10: Results of the RAMS analysis.

LCN	Likelihood Estimate [op.h^{-1}]	SAFETY	MTBF [h]	RELIABILITY	MTTR [h]	MAINTAINABILITY	AVAILABILITY
A			190	99.8%		100.0%	97.7%
A01	4.03E-06	TRUE	708	99.95%		49.44%	99.53%
A0101	3.20E-06	TRUE	3125	99.989%	5.00	6.387%	99.840%
A0102	2.28E-07	TRUE	4380	99.992%	3.00	10.417%	99.932%
A0103	2.90E-08	TRUE	3445	99.990%	1.00	28.108%	99.971%
A0104	3.45E-07	TRUE	2900	99.989%	3.00	10.417%	99.897%
A0105	2.28E-07	TRUE	4380	99.992%	5.00	6.387%	99.886%
A02	2.94E-05	TRUE	340	99.90%		74.99%	98.76%
A0201	2.69E-08	TRUE	3722	99.991%	10.0	3.246%	99.732%
A020101	2.44E-07	TRUE	4102	99.992%	5.0	6.387%	99.878%
A020102	2.78E-07	TRUE	3599	99.991%	5.0	6.387%	99.861%
A0202	2.29E-08	TRUE	4370	99.992%	10.0	3.246%	99.772%
A020201	2.39E-07	TRUE	4188	99.992%	5.0	6.387%	99.881%
A020202	1.93E-07	TRUE	5170	99.994%	5.0	6.387%	99.903%
A0203	2.03E-05	TRUE	4918	99.993%	1.0	28.108%	99.980%
A0204	2.50E-08	TRUE	40000	99.999%	2.0	15.211%	99.995%
A0205	7.49E-06	TRUE	1336	99.975%	1.0	28.108%	99.925%
A0206	2.55E-07	TRUE	3927	99.992%	5.0	6.387%	99.873%
A0207	2.55E-07	TRUE	3927	99.992%	2.0	15.211%	99.949%
A03	3.38E-06	TRUE	2961	99.99%		15.21%	99.93%
A0301	3.38E-06	TRUE	2961	99.989%	2.0	15.211%	99.933%
A04	1.08E-05	TRUE	9259	100.00%		39.04%	99.84%
A0401	1.08E-05	TRUE	9259	99.996%	1.0	28.108%	99.989%
A0402	7.49E-06	TRUE	1336	99.975%	2.0	15.211%	99.851%
A05	1.87E-29	TRUE	5.36E+16	100.00%		62.84%	99.96%
A0501	5.71E-08	TRUE	175200	100.000%	1.0	28.108%	99.999%
A0502	2.00E-09	TRUE	50000	99.999%	1.0	28.108%	99.998%
A0503	4.04E-07	FALSE	2474	99.987%	1.0	28.108%	99.960%
A0504	4.04E-07	FALSE	2474	99.987%	1.0	28.108%	99.960%
A06	3.50E-23	TRUE	2.86E+12	100.00%		39.04%	99.94%
A0601	2.50E-09	FALSE	40000	99.999%	2.0	15.211%	99.995%
A0602	5.60E-06	TRUE	1786	99.982%	1.0	28.108%	99.944%
A07	5.21E-12	TRUE	17253967	100.00%		96.55%	99.83%
A0701	2.28311E-06	FALSE	4380	99.992%	5.0	6.387%	99.886%
A0702	1.80E-06	FALSE	556	99.941%	0.1	96.312%	99.940%
A08	5.42E-07	TRUE	2128	99.98%		77.35%	99.87%
A0801	2.00E-11	TRUE	5000000	100.000%	1.0	28.108%	100.000%
A0802	2.50E-09	TRUE	40000	99.999%	1.0	28.108%	99.998%
A0803	3.91E-07	TRUE	2560	99.987%	2.0	15.211%	99.922%
A0804	4.20E-08	TRUE	2382	99.986%	1.0	28.108%	99.958%
A0805	2.50E-07	TRUE	40000	99.999%	2.0	15.211%	99.995%
A0806	2.50E-07	TRUE	40000	99.999%	2.0	15.211%	99.995%
A09	7.52E-08	TRUE	1348	99.98%		28.11%	99.93%
A0901	7.41E-08	TRUE	1350	99.976%	1.0	28.108%	99.926%
A0902	1.13E-09	TRUE	882000	100.000%	1.0	28.108%	100.000%

10

MARCUS-T: Budget Breakdown

With the characteristics of *MARCUS-T* set, a second market analysis and budget breakdown can be performed. In Section 10.1 the market analysis is presented, after which in Section 10.2 the budget breakdown is shown.

10.1. Market Analysis

by Christian, Niels

In the following section, a new market analysis is conducted. Where the final design is placed and audited in the current market. The return on investment and associated component cost will be presented based on researched data.

Market Share

According to the European Gliding Union, there are 80,000 pilots in Europe flying about 22,000 gliders [41]. Assuming there are on average 70 members per gliding club, this results in 1150 clubs spread around Europe. In the baseline report it was established that around 70% of the gliding clubs have a tow craft [2], meaning that there are approximately 800 aircraft used for aerotowing across Europe. This amount should be a representative number considering the amount of Robin DR400s (4500[1]), Piper Pawnees (5100[2]), Super Dimonas (900[3]), and Aviat Huskys (650[4]) produced, which are only a handful of the used tow planes.

From the baseline report, it was established that every 30 years a tow craft is replaced. This means that about 27 are replaced each year. *MARCUS-T* is supposed to replace these, but a market share of 100% is highly unrealistic for various reasons. After interviewing the aerotow pilots at the Dutch National Gliding Championships, it became clear they disliked the idea of being replaced by an automatic tow craft. The pilots stated that it was their hobby too, and that their planes are dual purpose for both leisure flights and aerotowing. Secondly, many aeroclubs will not have the budget to buy a €310,000 tow craft even if it is cheaper in the long run. However, as *MARCUS-T* is especially designed for aerotowing, it should still be attractive to some, wealthier, gliding clubs. Third, *MARCUS-T* uses advanced technology, which may be considered too novel or overly complicated to clubs. Fourth, currently existing operational working flows have to be adapted which can set the threshold for buying *MARCUS-T* higher than for conventional tow craft. Linked to that, fifth, is that there is not yet a proof of concept, while conventional aircraft have been almost around for 80 years. For those reasons, a target market share of 30% is assumed for the market analysis. This results in an average of 8 tow crafts sold each year. The craft will only be produced after it has been ordered, as pre-production is deemed to risky for the small amount of craft sold. As the series number is so low, supply chain enhancement is marginal. Hence, this is neglected in the price calculations. Furthermore, the total costs of the programme are highly dependent on the number of tow craft being produced in the first five years. The costs are estimated using statistical relationships, which are taken partially from Gudmundsson and partially from a source which adapted them for electric aircraft [42, 15]. Assuming a market share of 30%, a rounded estimate for the individual component cost is given in Table 10.1. This is the price at which *MARCUS-T* would have to be sold. However, the requirement stipulates a sell price of EUR 310,000.

[1] www.planeandpilotmag.com [cited 19 June 2024]
[2] www.vintagepiper.co.uk [cited 19 June 2024]
[3] scandinavianaircraft.com [cited 19 June 2024]
[4] www.aviataircraft.com [cited 19 June 2024]

Table 10.1: Cost break-down per craft for a market share of 30%.

Parameter	Value [EUR]
Engineering cost	102,000
Tooling cost	66,000
Development cost	11,000
Test operations cost	3,160
Certification cost	**182,000**
Manufacturing cost	173,000
Quality control cost	11,000
Material cost	13,000
Engine cost	11,000
Controller cost	7,000
Propeller cost	1,000
Avionics cost	30,000
Battery cost	9,000
Total Production Cost	**437,000**
Product liability insurance cost	77,000
Profit (10% of total cost to produce)	44,000
Sale Price	**558,000**

To clarify the certification cost, it can be seen that they are made up of the engineering cost, the tooling cost and the development cost, as well as the test operations cost. These numbers are calculated under the same assumptions as stated above and under the assumptions that three prototypes need to be built. This is because, it is expected that more crashes can occur due to the crafts complexity stemming from the automatic operations. The certification costs themselves are divided over the 40 craft that will be produced during the first five year of production. This means that the total programme volume itself lays in the region of EUR 7.28 million.

Investor, Customer & Manufacturer Perspective

The return on investment will be split into two perspectives: the first perspective is seen from the investor's point of view and the second one looks at the craft from a customer's point of view.

Investor Perspective

An investor, i.e. a party who puts money into an undertaking and expects a financial return after a certain amount of time, is interested in the break-even point. After this point in a production timeline, profit is made. Hence, from that point onwards, the investor can expect to start receiving a return on investment. Expending on the previous section, 40 tow craft are expected to be produced during the first five years, the return on investment chart is presented in Figure 10.1.

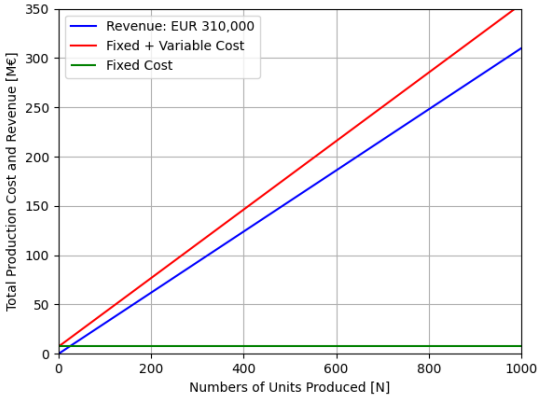

Figure 10.1: Return of investment outlook for 40 tow craft produced within the first five years.

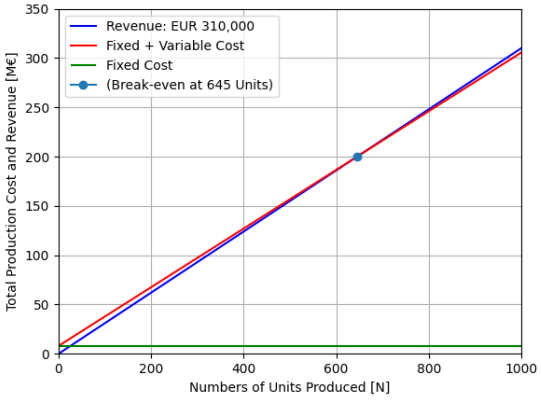

Figure 10.2: Return of investment outlook for 68 tow craft produced within the first five years.

It can be seen that the costs diverge (EUR 310,000 selling price required vs. EUR 560,000 actual selling price), meaning that under those conditions, a return of investment will never occur. In contrast, if the number of tow craft within the first five years can be brought up to 68, i.e. a market share of 50%, a return of investment is achieved after the production of the 645^{th} tow craft as seen in Figure 10.2.

Customer Perspective and Operating Cost

For the customer, the glider clubs, who are supposed to buy the craft, one of the first questions is whether it makes sense to buy *MARCUS-T* from a financial point of view. It is under no circumstance logical to buy a craft that will be more expensive during its whole lifetime than the current options. Hence, the operational costs are important for the customer. These are broken downin Table 10.2.

Table 10.2: Operational costs per flight of *MARCUS-T*.

Cost Factor	Value	Unit
Charging cost for energy (0-100%)	3.92	EUR
Maintenance cost	3.02	EUR
Airport landing fee	10.00	EUR
Inspection cost	0.67	EUR
Battery depreciation	9.64	EUR
Overhaul	1.76	EUR
TOTAL PER FLIGHT EXCL. CRAFT DEPRECIATION	**29.01**	**EUR**

This calculation is based on a set of batteries that lasts for 300 flights, the estimation that per year 700 flights are performed, and that the craft depreciates in value completely after 30 years. Using this data also the craft depreciation of EUR 310,000 over its entire number of flights is equal to EUR 15.

Combining the purchase price and the operational costs, the life time cost, or cost of ownership equates to approximately EUR 919,000 in total, or EUR 44 per flight. This means that for glider clubs it makes sense to buy the craft, due to its long term price advantage compared to conventional tow-craft. Looking at the price summary done earlier in the project, it can be seen that the craft lies above the average total life time cost, which is at EUR 838,000 [2]. However, *MARCUS-T* lies certainly under the most expensive craft, the GA aircraft Aviat Husky, having a total life time cost of EUR 1,100,000. There might be possibilities for subsidies that glider clubs can request for sustainability improvement. But the applicability of those funds is left for a later stage.

Manufacturer Perspective

From Figure 10.1 it can be deduced that under the current assumptions (selling price of EUR 310,000 and a market share of 30%) no return of investment is generated. There are two possibilities to still make the project feasible. The first possibility is to look for a higher number of tow craft that can be sold during the first five years, decreasing the total cost to produce a craft and hence increasing the profit margin to generate an (earlier) return of investment. A second possibility is to increase the selling price, such that the total life time cost matches the most expensive one of the tow craft analysed earlier during the project [2]. This would allow for a theoretical selling price of EUR 496,870, changing the brake-even analysis as presented in Figure 10.3.

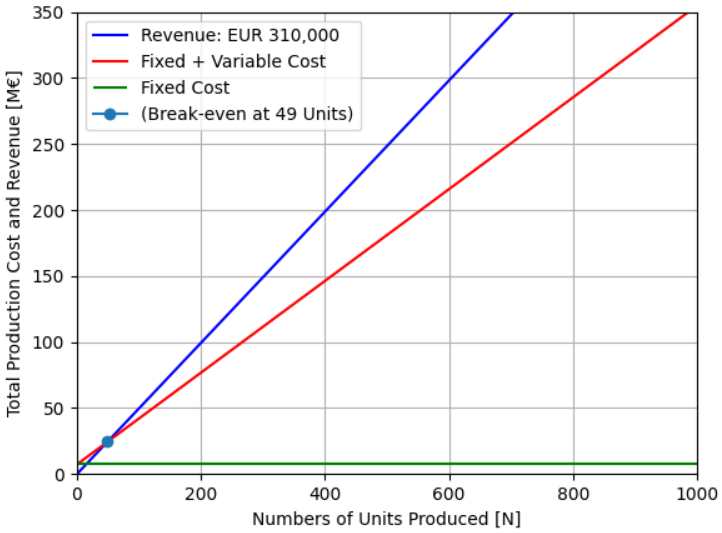

Figure 10.3: Return of investment with the updated tow craft selling price of EUR 496,870.

10.2. Budgets

by Filip, Stan, Christian, Mees

This section presents the budget breakdown developed after the design synthesis. First, non-technical budgets are presented, followed by technical budgets.

10.2.1. Non-Technical Budgets

This subsection presents the two non-technical budgets. It includes the team's schedule budget, detailing the timeframe allocated for project completion, and the non-technical portion of the cost budget. The latter encompasses the price the customer would be willing to pay for purchasing and maintaining the craft.

Schedule Budget The schedule budget outlines the distribution of work hours across various project phases. This allocation is based on an initial schedule created at the project's outset and regularly updated. The detailed breakdown of the schedule budget is presented in Table 10.3.

Table 10.3: Schedule budget of the entire team, as of 13 June 2024.

Phase		Meetings [h]	Lectures [h]	Extra Activities [h]	Report Revision [h]	Work Time [h]
PPP	**Used**	40	20	0	0	340
PDP	**Used**	40	20	0	40	300
DSP	**Used**	65	20	100	60	715
DDP	**Used**	20	0	0	0	1100
	Remaining	165	0	100	180	490
	TOTAL (used)	**20**	**60**	**100**	**100**	**2455**
	TOTAL (remain.)	**60**	**0**	**100**	**180**	**490**

Non-Technical Cost Budget This budget is presented in Table 10.2.

10.2.2. Technical Budgets

This subsection presents the technical budgets that can be specified after the preliminary design has been finalised. This includes the technical cost budget, mass budget, power budget, control and stability budget, and the size budget.

Technical Cost Budget This budget is shown in Table 10.1.

Mass Budget The mass budget flows from the Class II Weight estimation and multiple refined weight estimations. The mass breakdown is specified in Table 10.4.

Table 10.4: Mass breakdown.

Item	Mass [kg]	Mass fraction [%]
Wings	39.71	18.9
Fuselage	13.28	6.3
Empennage	6.66	3.2
Landing Gear	11.57	5.5
Battery	43.06	20.5
Engine	30.00	14.3
Fixed Equipment	65.39	31.2
MTOM	**209.67**	**100**

In this breakdown, the wing, fuselage, landing gear and battery mass are refined by calculating their masses manually, not relying on empirical methods. Empennage mass is based on empirical methods. Engine and fixed equipment mass have been defined by comparing them with off-the-shelf components.

Power Budget The power budget is derived from the performance calculations. The power budget details the energy capacity needed for each phase of the flight. It is specified in Table 10.5.

Table 10.5: Energy breakdown of the *MARCUS-T*

Item	Energy [Wh]	Energy Fraction [%]	Item	Energy [Wh]	Energy Fraction [%]
Taxi	135.37	1.21	Nominal Mission	7097.00	63.49
Take-off	1603.58	14.35	Mission Reserve	651.19	5.82
Initial Climb	834.44	7.47	Total Mission	7748.19	69.32
Continuous Climb	4232.18	37.86	Total Energy Propulsion	11087.95	99.19
Circuit	291.43	2.61	Total Energy Systems	90.00	0.81
-	-	-	**Total Energy**	11177.95	100

As can be seen, the continuous climb phase takes up the largest fraction of the total energy used by the craft, almost 60%. The stability and control budget consists of the CG excursion range. For stability and control reasons the CG must be kept between 1.8 m and 1.93 m from the nose of the tow craft. This range shall be kept in mind when fitting the fixed equipment components in the craft. The size budget specifies the dimensions of the main craft components. It follows from the iteration loop described in Chapter 5 and is shown in Table 10.6.

Table 10.6: Size budget breakdown.

Component	Dimension	Value	Unit
Fuselage	Length	5.08	m
	Nose height	0.3	m
	Max height	0.5	m
	Tail height	0.25	m
	Projected area	1.74	m^2
Wing	Span	8.65	m
	Area	4.73	m^2
Propeller	Diameter	1.54	m

Component	Dimension	Value	Unit
Landing gear	Height	1	m
Tire	Width	0.1	m
	Diameter	0.22	m
Horizontal tail	Span	1.46	m
	Area	0.43	m^2
Vertical tail	Height	0.85	m
	Area	0.36	m^2

11

MARCUS-T: Outlook to the Future

This chapter presents an outlook to the future of *MARCUS-T* , after the DSE is completed. First, in Section 11.1, the project development and design logic is shown, followed by a manufacturing plan in Section 11.2. The chapter ends with a description of the sustainability approach in Section 11.3.

11.1. Project Development and Design Logic

by Filip

This section presents the project development and design logic to be used in the future. As can be seen on Figure 11.1, the future stages are divided into five blocks, namely the design, certification, manufacturing, delivery and operation. During the DSE, a part of the design process is conducted.

Figure 11.1: Overview of future project development and design logic.

Design Phase (1)

The design phase is divided in three sub-phases: the preliminary design (1.1), the detailed design (1.2), and the production design (1.3). The flow of this phase can be seen on Figure 11.2. It is considered that the preliminary design phase is finalised during the DSE. Then, all subsystems are designed and every part of the craft is designed in the most detail possible. After this, a detailed manufacturing plan is made, including scheduling of the part production and of the assembly stages.

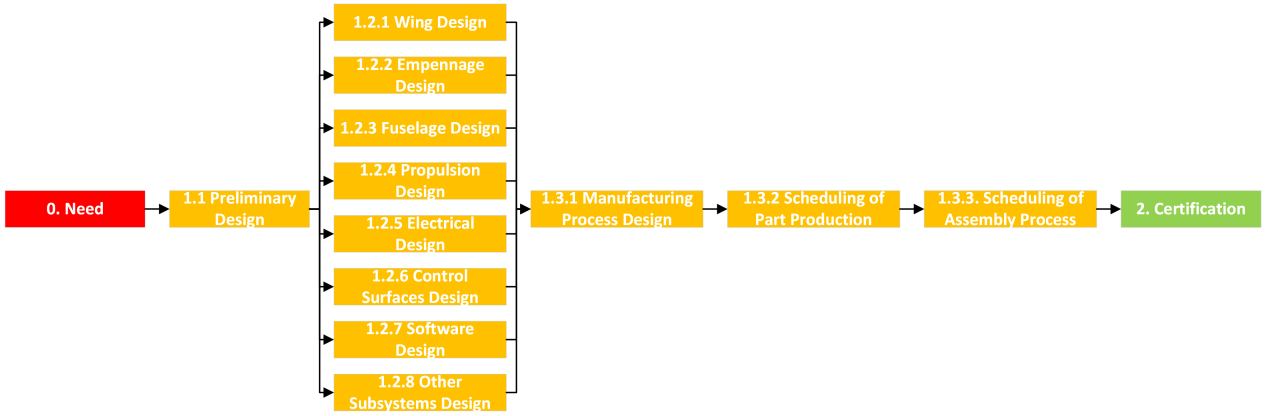

Figure 11.2: Design phase flow.

Certification Phase (2)

During the certification phase, authorities verify if the craft complies with all relevant certification and safety standards. The flow diagram of the certification phase, presented on Figure 11.3, is based on the tasks specified in the Airbus Test and Certification description[1]. The certification starts with pre-certification activities (2.1), where the certification plan is developed, along with an initial prorotype for the static tests. Then, the certification itself takes place (2.2), starting with static tests and followed by flight tests.

[1] www.airbus.com [cited 13 June 2024]

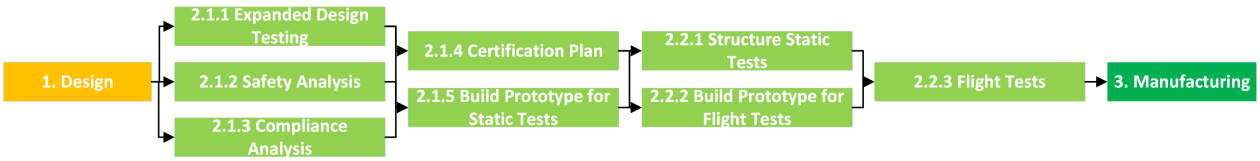

Figure 11.3: Certification phase flow.

Manufacturing Phase (3)

The manufacturing phase, presented on Figure 11.4, starts with sub-system production (3.1), where every component is produced and processed into sub-assemblies (wing, fuselage, tail, etc.). This phase also includes the purchase of off-the-shelf components used in the design. This phase is followed by a final assembly (3.2), where all the sub-assemblies are merged together into the final craft. This is also the phase where all quality inspections are made.

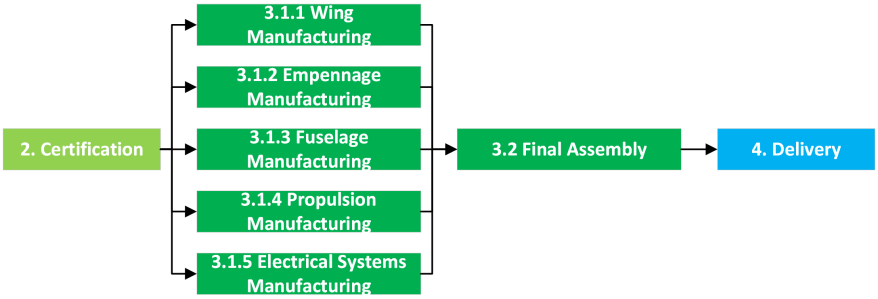

Figure 11.4: Manufacturing phase flow.

Delivery Phase (4)

During the delivery phase, final checks on the assembled craft are performed, including flight test to demonstrate the aircraft's airworthiness to the customer. Only then is the craft delivered to the customer. The flow of the delivery phase is presented on Figure 11.5.

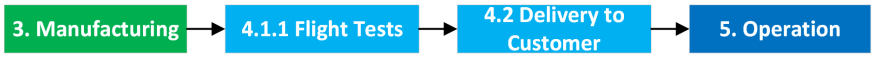

Figure 11.5: Delivery phase flow.

Post-DSE Gantt Chart

The Gantt chart based on the flow diagrams discussed in Section 11.1 is presented here. The Gantt chart can be seen in Figure 11.6.

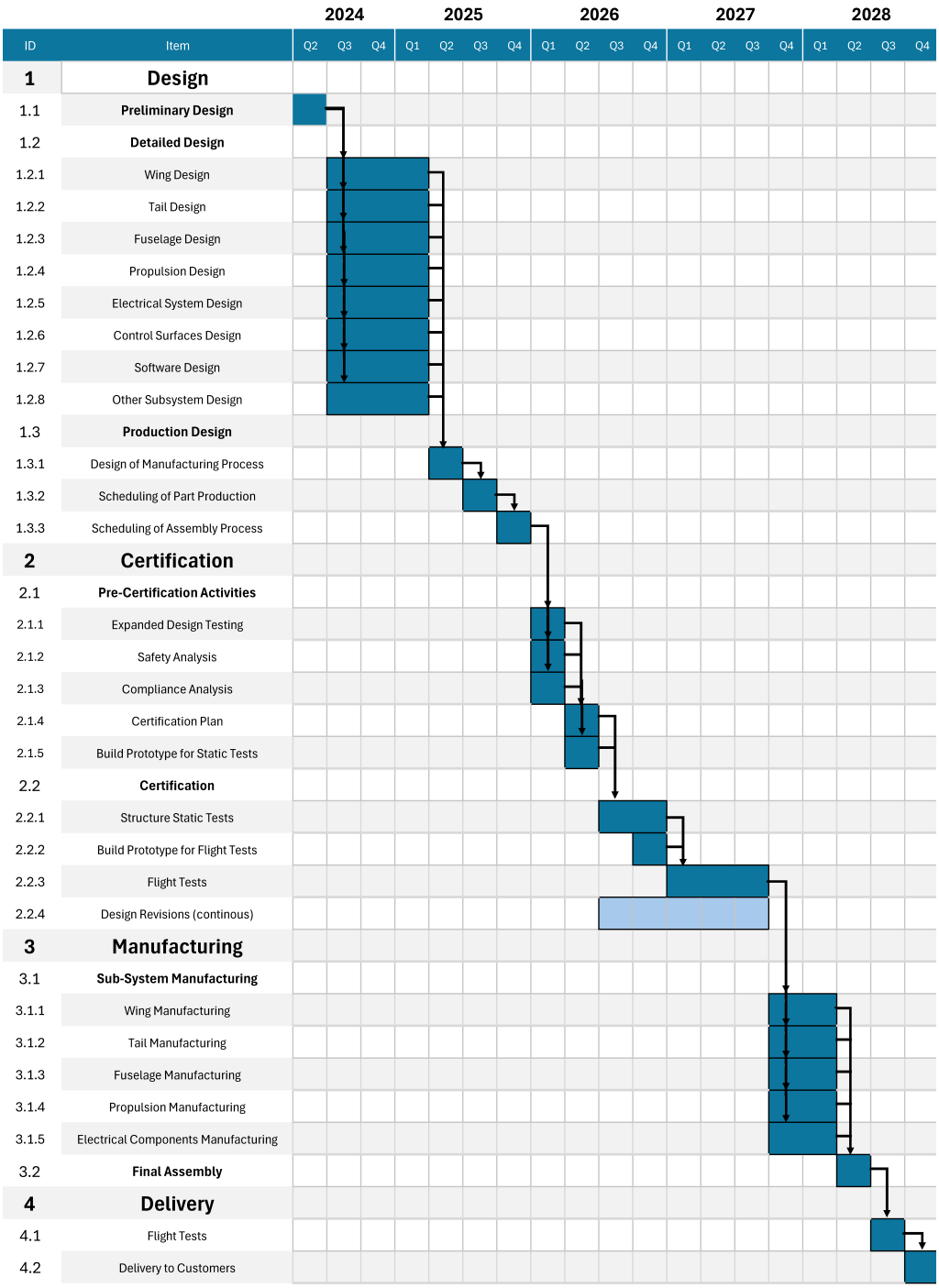

Figure 11.6: Post-DSE Gantt chart.

11.2. Manufacturing, Assembly, and Integration (MAI) Plan

by Andreas, Stan

Once the design is finalised, a prototype built, and the craft certified, scale production can begin. The initial production run planned is 50 aircraft, built over a span of five years. This small scale of production is primarily a result of the craft's small market, resulting in higher production costs. Manufacturing will have to be done with significant amounts of handwork, as the high initial costs of automation will probably not be recuperated with such a small production run. This approach does allow for an agile manufacturing plan. The structure of the craft can be built on order, and deliveries can be quick with a small stockpile of all off-the-shelf components, such as the motor, avionics, wheels, and actuators.

A detailed manufacturing plan will have to be developed, though it is recommended to approach this before the prototype is built. The prototype can be a test of the manufacturing process as well as a test of the system as a

whole, as any issues in the manufacturing plan will be identified in this process and inform changes to be made before full production. This will also be an opportunity to train the manufacturing personnel to kick-start the learning curve process.

11.2.1. Manufacturing Plan

A preliminary manufacturing plan is shown in Figure 11.7. The tasks are broken down by the required skills of manufacturing personnel. Tasks that require different personnel and those that can be done at the same time are shown in parallel. The manufacturing and assembly is performed by 4 kinds of personnel: welding, electrical, forming and machining, and general workers. For this manufacturing plan, it is assumed that the "general workers" section consists of enough personnel for two simultaneous tasks, the expert groups are limited to one block at a time. Further study needs to be done to determine if this plan will be fast enough to meet the requirement of one airframe per month, but scaling up to make multiple aircraft at once should be possible with this plan.

The height of the blocks in Figure 11.7 shows the relative estimated time of a manufacturing task. The tasks are also split up into their relative craft columns, namely the fuselage, wing, empennage, electrical propulsion system, avionics, and landing gear. An assembly column is included to show the integration of the full craft.

11.2.2. Maintenance and Battery Swapping

To accommodate any maintenance or battery swapping, ample access hatches need to be fitted to the internal systems on the craft. For the battery swapping, two hatches are installed, both being behind the trailing edge of the wing on either sides of the fuselage. The skin of the aircraft should be assembled such that removal is straightforward.

Figure 11.7: Manufacturing plan of *MARCUS-T*.

11.3. Sustainability

by Tamara

The goal of the design of *MARCUS-T* was to create a sustainable glider tow craft. This has been done by making an automatic and electric tow craft. In this chapter the sustainability of *MARCUS-T* is assessed, as well as how sustainability is taken into account in the development strategy. First all aspects that make the craft sustainable are discussed in Subsection 11.3.1. This is followed by an analysis of the CO_2 emissions of the craft, and how they compare to existing tow craft as well as theoretical smaller tow craft in Subsection 11.3.2.

11.3.1. Main Considerations

Sustainability is commonly considered to be divisible into three pillars: economic, social, and environmental sustainability [43]. Each of these pillars is used as a basis for analysis of the sustainability of the craft. In this analysis the potential contribution to global sustainability of the craft is assessed as well as what considerations were made during its design.

Economic Sustainability

In the context of *MARCUS-T* , the economic pillar of sustainability represents the ability for the craft to be economically viable in the long-term. This implies aiming for economic growth long-term. More specifically, it entails not incurring large long-term costs for the parties involved, as this could impact the social and environmental aspects of sustainability in a negative way[2].

Local Repairing Following constraint CON-SUS-04, 70% of all repairs should be performed locally. This will not only be more environmentally sustainable due to decreased transportion. It will also support the local economic business which gives local economic growth. In addition, ability to repair locally will also decrease individual repair costs, which are important long term.

Replacing Similar to the constraint that most of the repairs should be performed locally, there is also constraint CON-SUS-05 which states that at least 70% of the parts should be replaceable. This lowers repair costs and reduces the chance that the whole craft needs to be replaced. This is likely to reduce long term costs for glider clubs, as they are less likely to have to replace an entire tow craft in case of failure, instead only having to replace singular parts.

Lower Recurring Costs Although the initial cost of *MARCUS-T* is higher than other tow crafts. The operating and maintenance costs are lower. This means recurring costs for glider clubs are reduced, which may decrease total lifetime costs.

Development The development of *MARCUS-T* contributes to sustainability by exploring new use cases for electric unmanned aerial vehicles. In this way it may provide new knowledge and insight in the development of such technologies and further global research into general sustainable technologies such as batteries. In addition *MARCUS-T* may enable and drive the development for the usage of gliders for non-recreational purposes, replacing more polluting counterparts.

Social Sustainability

Social sustainability is to secure people's social needs both in the short and long term. [44].

Safety During the towing process, the tow pilot is at the biggest risk[3]. By replacing the tow pilot with an automatic system, there is one less person at risk, making the craft immediately safer. This therefore makes *MARCUS-T* more socially sustainable. To ensure safety in case of emergencies that the automatic system can not handle, the craft can still be overridden by ground crew. *MARCUS-T* has sufficient avoidance and emergency procedures to also be safe for people surrounding it.

[2] www.sustainability.umw.edu [cited 17 June 2024]
[3] www.members.gliding.co.uk [cited 18 June 2024]

Learning to Fly Not including the launch, gliding does not produce any pollutants. Therefore, it can be a good sustainable solution for people wanting to learn how to fly. With *MARCUS-T* more people can potentially learn and enjoy this way of flying which makes it more socially sustainable.

Environmental Sustainability

Arguably the most important pillar of sustainability is environmental sustainability. This pillar emphasizes the responsible use of natural resources as to enable their continued use in the future. It also includes limiting the harm done to the environment through emissions of toxic pollutants and greenhouse gases.

Reduced Mass As a consequence of developing a craft that is automatic and optimised for towing, the mass of *MARCUS-T* is significantly reduced with respect existing tow craft. The reduced mass means it consumes less energy during operation. This energy consumption can be minimised further through optimisation of the flight path and trim settings by the automatic system. In addition the reduced mass means less resources are consumed during the manufacturing process and less pollutants are produced.

Electric As the craft is powered through batteries, the energy it uses can be derived from environmentally sustainable sources such as solar or wind energy. The batteries of *MARCUS-T* have also been selected carefully to have a lower environmental impact compared to other batteries[4]. This means that *MARCUS-T* performs better than to other electrical options.

Material Use As stated in constraints CON-SUS-06 and CON-SUS-07 respectively, 60% of the parts and 60% of the mass of the craft should be recyclable. Therefore aluminium 6061-T6 has been selected as the material for the main structure of *MARCUS-T*. This material is 100% recyclable with no degradation in its material properties[5].

The main material used for the skin of the craft is ceconite. This material is repairable, whcih makes it a good material to use from a sustainability mindset.

11.3.2. Comparison

A key measure of the sustainability is the amount equivalent carbon dioxide (CO_2) emissions. This measure allows the sustainability of *MARCUS-T* to be compared with existing and alternative UAV tow craft. For this comparison it is assumed that the manufacturing of airframe and common subsystems of different craft produce similar emissions. Thus only operational emissions and emissions from battery production are assessed.

To compare, the fuel consumption of the Bristlell b23 is used. It has a consumption rate of 30 L/h with CO_2 emissions coefficients of 2,195 g/L. This gives an emission rate of 65.8 kg/h[6] [45]. *MARCUS-T* has a constant power required of 35 kW during the climb. It is found that the average CO_2 emissions of using electric energy produced by solar energy is 36 g/kWh[7]. This gives an emission rate of 1.3 kg/h for *MARCUS-T*. Here it can already be seen that *MARCUS-T* has a far lower emission rate than other tow craft currently on the market. Now the CO_2 emission rates may be compared to those of a UAV tow craft powered by fuel. It is assumed that this craft would have the same mass and power required as *MARCUS-T*. Assuming an energy density of aviation gasoline of 31 kWh/L, the emission rate of this craft would be around 8.9 kg/h. This is almost 7 times as high.

Now, the production of batteries for *MARCUS-T* need to be taken into account. It is assumed that each launch will take 15 minutes and that the battery pack needs to be charged after this. The assumed lifetime of lithium polymer batteries has been found to be around 675 cycles for a depth of discharge of 80% [8]. It was determined that the batteries could last for 169 flight hours, with 4 recharges every hour. The carbon dioxide emissions during the production of batteries is around 91.2 kg/kWh. One battery pack has 11.1 kWh, which means one produced battery creates 1,012.3 kg of CO_2 during manufacturing. With the 169 flight hours per battery pack that is 6.0 kg/h[46].

[4] www.datacenterknowledge.com [cited 17 June 2024]
[5] www.copperloy.com [cited 19 June 2024]
[6] www.eia.gov [cited 13 June 2024]
[7] iopscience.iop.org [cited 13 June 2024]
[8] www.renata.com [cited 25 June 2024]

An overview of the CO_2 emissions can be seen in Table 11.1. Here, the emissions due to the energy used by *MARCUS-T* are by far the lowest. Even with taking the production of the batteries into account *MARCUS-T* has the lowest CO_2 emissions. This means that *MARCUS-T* is a viable sustainable option with lower carbon dioxide emissions compared to the current available tow craft.

Table 11.1: CO_2 emissions rates for operating tow craft.

Current tow craft	UAV fuel tow craft	*MARCUS-T*	Energy of *MARCUS-T*	Battery production of *MARCUS-T*
65.8 kg/h	8.9 kg/h	7.3 kg/h	1.3 kg/h	6.0 kg/h

12

Design Verification and Validation

by MianTao, Everyone

In this chapter the design verification and design validation is discussed. Design verification is performed by determining its compliance with the requirements discussed in Chapter 3. This verification process is discussed in Section 12.1. Design validation is discussed in Section 12.2

12.1. Requirement Compliance

Compliance of the design to the requirements is crucial for a successful design. To check this, the design is inspected and calculations are performed to determine the characteristics of the design. The results of this analysis is compiled in a compliance matrix given in Table 12.1.

As the design is currently only in the conceptual design phase, compliance to all passed requirements needs to be checked as the design develops in more detail. In addition, there are several requirements that are not evaluated during this stage of the design. This is due to the limited detail the system has been designed in and the complexity of the system. For further development of the design it is of high importance to check these requirements, as they may present issues if not complied with.

More in depth tests using either physical measurements or detailed design parameters as mentioned in the previous report is not possible during this stage of design [3]. These tests should be performed once the design has been finalised.

Table 12.1: Compliance matrix of all system requirements of *MARCUS-T*.

Requirement Code	Requirement Description	Department	STATUS
SYS-PWR-01	The power system shall have a maximum power of 80kW.	PPP	Compliant
SYS-PWR-02	The power system shall have a maximum voltage of 800V.	PPP	Compliant
SYS-PWR-03	The power system shall have a minimum power of 62W.	PPP	Not evaluated
SYS-PWR-04	The power system shall have a minimum voltage of 400V.	PPP	Compliant
SYS-PWR-05	The power system shall be battery powered.	PPP	Compliant
SYS-PWR-06	The battery shall have a minimum capacity of 10kWh.	PPP	Compliant
SYS-PRO-01	The propulsion system shall provide a thrust of 2500 N.	PPP	Compliant
SYS-PRO-02	The propulsion system shall be electric.	PPP	Compliant
SYS-GHS-01	The maximum outer main gear wheel span shall be smaller than 15m	SMM	Compliant
SYS-STR-01	The structure shall have a maximum length of 7.10 m when disassembled.	SMM	Compliant
SYS-STR-02	The structure shall have a maximum width of 11.0 m when disassembled.	SMM	Compliant
SYS-STR-03	The structure shall have a maximum height of 2.30 m when disassembled.	SMM	Compliant
SYS-STR-04	The structure shall be manufacturable using existing techniques.	SMM	Not evaluated
SYS-STR-05	The structure shall have lights according to relevant regulation.	SMM	Compliant
SYS-STR-07	The wingspan shall be smaller than 80 m.	AERO	Compliant

Continued on next page

Requirement Code	Requirement Description	Department	STATUS
SYS-STR-08	The structure shall be able to withstand a maximum load factor of 5.	SMM	Compliant
SYS-STR-09	The structure shall be able to withstand a minimum load factor of -2.5.	SMM	Compliant
SYS-GCS-01	The coupling system shall couple to the glider.	SMM	Compliant
SYS-GCS-02	The coupling system shall resist a force of 16260 N.	SMM	Compliant
SYS-GCS-03	The pilot shall be able to directly decouple at all stages of the operations.	SMM	Compliant
SYS-GCS-04	The glider coupling system shall detect a decouple.	SMM	Compliant
SYS-GCS-05	The glider coupling system shall communicate its status to the FMS.	SMM	Compliant
SYS-FMS-01	The flight management system shall be programmed with an automatic mode.	SSC	Compliant
SYS-FMS-02	The flight management system shall react to pilot input.	SSC	Compliant
SYS-FMS-03	The flight management system shall have a database of the terrain.	SSC	Compliant
SYS-FMS-04	The flight management system shall have a database with the locations of airfields.	SSC	Compliant
SYS-FMS-05	The flight management system shall have two way communication with the communication system.	SSC	Compliant
SYS-FMS-06	The flight management system shall have two way communication with the ground handling system.	SSC	Compliant
SYS-FMS-07	The flight management system shall have two way communication with the guidance system.	SSC	Compliant
SYS-FMS-08	The flight management system shall have two way communication with the navigation system.	SSC	Compliant
SYS-FMS-09	The flight management system shall have two way communication with the flight control system.	SSC	Compliant
SYS-FMS-10	The flight management system shall have two way communication with the power system.	SSC	Compliant
SYS-FMS-11	The flight management system shall have two way communication with the propulsion system.	SSC	Compliant
SYS-FMS-12	The flight management system shall have two way communication with the data monitoring system.	SSC	Compliant
SYS-FMS-13	The flight management system shall have two way communication with the glider coupling system.	SSC	Compliant
SYS-FMS-15	The flight management system shall be programmed with an emergency mode.	SSC	Compliant
SYS-FMS-16	The flight management system shall provide flight envelope protection in Normal Law.	SSC	Compliant
SYS-FMS-17	The flight management system shall be programmed with Alternate Law.	SSC	Compliant
SYS-FMS-18	The flight management system shall have a database of the airspace.	SSC	Compliant
SYS-FMS-19	The craft shall be equipped with ACAS.	SSC	Compliant
SYS-FMS-20	The craft shall be equipped with FLARM.	SSC	Compliant
SYS-FMS-22	The flight management system shall have a total system error of (18 - OMGWS)/2 m	SSC	Not evaluated

Continued on next page

Requirement Code	Requirement Description	Department	STATUS
SYS-COM-01	The craft shall have 2-way communication with the glider pilot with a bandwidth of 100 kbps.	APOL	Compliant
SYS-COM-02	The craft shall have 2-way communication with the ground station with a bandwidth of 100 kbps.	APOL	Compliant
SYS-COM-03	The craft shall have 2-way communication with the ATC.	APOL	Compliant
SYS-COM-04	The craft shall have 2-way communication with other aircraft.	APOL	Compliant
SYS-COM-05	The craft shall be equipped with ADS-B.	APOL	Compliant
SYS-COM-06	The craft shall be equipped with a radio reflector.	SSC	Compliant
SYS-GDC-02	The guidance system shall compute the flight path to the airfield.	SSC	Compliant
SYS-NAV-03	The navigation system shall obtain the height above ground with an accuracy of at least 0.9 m.	SSC	Not evaluated
SYS-NAV-04	The navigation system shall trace the glider's position.	SSC	Compliant
SYS-FCS-01	The flight control system shall allow for external input.	SSC	Compliant
SYS-FCS-02	The craft shall be stable.	SSC	Compliant
CON-CST-05-R	The craft shall be insured for shipping.	APOL	Not evaluated
CON-OPS-07-R	The users of the craft shall be trained on emergency procedures.	APOL	Compliant
CON-OPS-08-R	The users of the craft shall be trained on SOP.	APOL	Compliant
CON-OPS-09-R	The emergency procedures shall be documented.	APOL	Compliant
CON-OPS-10-R	The SOPs shall be documented.	APOL	Compliant
CON-OPS-11-R	The manufacturing plan shall be fool-proof.	SMM	Not evaluated
CON-OPS-12-R	Batteries shall be replaced when their capacity drops below 80% of the initial capacity.	APOL	Compliant
CON-OPS-13-R	Battery charging station shall have a fire suppression system.	APOL	Compliant
CON-TEC-06-R	The craft shall have certified components of the shelf (COTS).	SMM	Not evaluated
SYS-PWR-12-R	The craft shall contain an independent power source for avionics.	PPP	Compliant
SYS-GHS-01-R	The landing gear shall be able to withstand the loads generated during landing at MTOW.	SMM	Compliant
SYS-DMS-01-R	The craft shall have a display to show system errors.	SSC	Compliant
SYS-DMS-02-R	The DMS shall be designed to prioritise false negatives.	SSC	Not evaluated
SYS-DMS-03-R	The DMS shall be designed under fail-safe philosophy (redundancy).	SSC	Compliant
SYS-DMS-04-R	The DMS shall keep track of maintenance tasks.	SSC	Not evaluated
SYS-DMS-05-R	The DMS shall inform the operator of maintenance tasks that need to be performed.	SSC	Not evaluated
SYS-FCS-05-R	The FCS shall be designed under fail-safe philosophy (redundancy).	SSC	Compliant
SYS-FMS-21-R	The FMS shall be designed under fail-safe philosophy (redundancy).	SSC	Compliant
SYS-GCS-06-R	The GCS shall use certified latches.	SMM	Compliant

Continued on next page

Requirement Code	Requirement Description	Department	STATUS
SYS-GCS-07-R	The GCS shall have release capabilities by both pilot and tow craft.	SMM	Compliant
SYS-GCS-08-R	The GCS shall have a redundant release mechanism.	SMM	Compliant
SYS-GCS-09-R	The GCS shall have an alternate independent quick-release mechanism.	SMM	Compliant
SYS-NAV-05-R	The navigation system shall be designed under fail-safe philosophy (redundancy).	SSC	Compliant
SYS-PWR-07-R	The batteries shall be contained in protective housing with at least an IP56W rating.	SMM	Not evaluated
SYS-PWR-08-R	The power system shall be equipped with a fire suppression system.	APOL	Compliant
SYS-PWR-09-R	The battery shall have a power indicator.	PPP	Compliant
SYS-PWR-10-R	The battery shall charge from 20% to 85% in 0.5 h.	PPP	Not evaluated
SYS-PWR-11-R	The batteries shall be certified according to MIL-STD-810G drop-test standard.	SMM	Not evaluated
SYS-STR-07-R	The craft shall have access hatches to all maintainable systems.	SMM	Not evaluated
CON-REG-01	The craft shall meet CS-Drone requirements.	APOL	Compliant
CON-REG-02	The craft shall meet relevant EASA operational requirements.	APOL	Compliant
CON-SUS-01	The peak noise emitted by the craft shall not exceed 100 dB when measured from 50 m.	PPP	Compliant
CON-SUS-02	The batteries used by the craft shall be rechargeable.	PPP	Compliant
CON-SUS-03	The lifetime equivalent CO2 emission of the craft shall be less than that of all existing tow craft normalised by the number of launches per lifetime.	APOL	Compliant
CON-SUS-04	At least 70% of repairs preformed on the craft shall be locally	APOL	Not evaluated
CON-SUS-05	At least 70% of components of the craft shall be replaceable	SMM	Not evaluated
CON-SUS-06	At least 60% of the components of the craft shall be reusable/recyclable	SMM	Not evaluated
CON-SUS-07	At least 60% by mass, of the craft, shall be recyclable.	SMM	Not evaluated
CON-CST-01	The craft shall cost less than EUR 310,000 to purchase.	APOL	Compliant
CON-CST-02	The total operational cost of the craft shall be less than EUR 252,000	APOL	Compliant
CON-CST-03	The craft shall cost less than EUR 562,000 to EOL.	SMM	Compliant
CON-CST-04	The craft shall cost less than EUR 310,000 to manufacture.	SMM	Compliant
CON-OPS-01	The craft shall have swappable batteries.	SMM	Compliant
CON-OPS-02	The craft shall have a turn-around time less than 20 minutes.	APOL	Compliant
CON-OPS-03	The craft shall have a block time of less than 30 minutes.	APOL	Compliant
CON-OPS-04	The craft shall have a deploy time of less than 40 minutes.	APOL	Compliant

Continued on next page

Requirement Code	Requirement Description	Department	STATUS
CON-OPS-05	The craft shall be connected to the glider in less than 5 minutes.	APOL	Compliant
CON-OPS-06	The craft shall have a delivery time of less than 14 days.	APOL	Not evaluated
CON-TEC-01	The craft shall have a total mission range of 30 km with a glider attached of 850 kg.	PPP	Compliant
CON-TEC-02	The craft shall have an endurance of 30 minutes.	PPP	Not evaluated
CON-TEC-03	The craft shall be able to tow a glider of 850 kg.	PPP	Compliant
CON-TEC-04	The craft shall be compatible with current gliders.	APOL	Compliant
CON-TEC-05	The craft shall have a minimum vertical tow speed of 2.5 m/s with a glider of 850 kg.	PPP	Compliant
CON-TEC-06	The maximum take-off distance of the combination (MTOW) to clear a 15 m obstacle shall be 500 m.	APOL	Compliant

As can be seen in Table 12.1, most requirements have been evaluated and all evaluated requirements are complied with. Therefore the design is mostly verified and determined to be feasible for future development. The not currently evaluated requirements will be analysed once the design is developed in more detail.

12.2. Design Validation

To validate whether the design complies to the needs of the stakeholders, reviews were conducted of the results from both the preliminary design phase and design selection phase. In these reviews the clients are updated on the parameters of the design and voice any concerns or objections they have with the design. Changes are then made to the design based upon these objections. This ensures that the clients agree with the design concept used in this stage.

To check the compliance of the current design, a final review of the design was conducted on 24 June 2024. In this review both the characteristics and design method of the craft were presented to the clients. From this review it was concluded that the clients were satisfied with the current design. For future development, these reviews must also be conducted to ensure all stakeholder requirements are fulfilled.

As reported previously, a field study was also conducted [3]. In this field study discussions were conducted with other stakeholders besides the client. This allowed the requirements to be formulated according to their needs. A second field study is recommended where the craft is presented to glider clubs, their members, and ground crew to assess their views on the design.

13

Conclusion & Recommendations

by Annika

The aim of this report was to design a craft capable of towing a glider sustainably, thereby minimising the environmental impact of the gliding sport. With the concept of an electric and automatic tow craft, *MARCUS-T* , a mission profile could be compiled. The starting steps of this mission profile concern *MARCUS-T* taxiing from the hangar to the runway, taking off, and climbing until the drop-off location and altitude are reached. Then, the glider is released from the tow craft. Hereafter, the descent process is initiated via one of the four descent profiles present, entailing two dive profiles at different slopes from one another, a descent profile at a relatively small flight path angle, and a profile considering an unpowered glide. A go-around may be initiated during this process, after which eventually the landing takes place.

To comply with the mission objective, several design choices were made very early on in the design process. Firstly, the structure of the craft consists of a truss-type fuselage and a taildragger configuration due to their simple, light, and cheap design. In addition, its maximum take-off mass is substantially lower than conventional tow craft at a value of 210 kg, mainly due to the automatic nature of the craft. Furthermore, a thick airfoil was selected, with the aim of optimising climb performance. High-lift devices are also added in order to reduce the stall speed in landing configuration, as are airbrakes. Additionally, a conventional tail was sized for tow-force and cross-wind disturbances, as well as to ensure longitudinal and lateral stability. Next, the electric propulsion system consists of a single engine along with one propeller with three blades. The batteries used for the engine are hot-swappable and made of lithium-ion polymer, weighing approximately 43 kg with specific energy of the battery at 257.5 Wh/kg.

Most batteries will be removable from the craft, with the exception of one, which will only be charged overnight in the hangar. During the daytime, the other batteries will be routinely swapped for charged ones in between aerotows. These batteries are charged on-site in a truck with on-board batteries to minimise the turnaround time. The airfield logistics describe the systems required to support these procedures, including the operation of *MARCUS-T* in its airborne stage. During a mission, the craft uses approximately 7,100 W·h (65% of its battery capacity) in 15 minutes time, necessitating three battery sets to be charged throughout the day. In order to charge the battery system and *MARCUS-T* overnight, a new electrical infrastructure is laid out in the hangar. A control station integrated into existing gliding club trucks allows a licensed UAV pilot to monitor and control *MARCUS-T* and its systems remotely. Operations ensuring all systems are checked for towing and emergency procedures are described. Important hardware and software of *MARCUS-T* are hereafter compiled, and their technical risks analysed. Out of all of these, none necessarily stand out.

A market analysis then concluded that a break-even point is estimated to be reached after selling the 49^{th} aircraft. This is a little over six years from the moment production of *MARCUS-T* starts. The total lifetime cost is estimated to be EUR 912,000. This price is calculated assuming the craft operates for 30 years, where 700 flights are performed each year. The total cost per tow lies significantly low at a value of approximately EUR 29.

Looking towards the future of the design, more work needs to be done. This report gives the following recommendations before the craft can enter the market.

- A critical material analysis needs to be done for the structures of the craft. The fuselage structure can be further optimised for additional efficiency gains. The landing gear requires a re-design using springs and dampeners.
- At high speeds, a positive flap deflection causes issues on the lower side of the airfoil since the transition point moves forward rapidly when the angle of attack decreases. This leads to the formation of a laminar separation bubble at the leading edge. Observations show the transition point shifting from approximately 0.68c to 0.21c as the angle of attack decreases. To address this, further investigation is needed. A potential solution could be using a 0° flap deflection for the return flight and increasing the size of the airbrake. In this case, the flaps are only used for takeoff, climb, and landing.
- A more in depth analysis of the dynamic stability parameters should be conducted, including computing C_{X_u}, analysing the effects of dihedral, wing twist, fuselage length, and wing tips. It is also recommended to develop model of the coupled dynamics of the glider and tow craft. A more in depth analysis and sizing of the control surfaces is also recommended to ensure they allow for the desired manoeuvrability. In addition, an analysis can be performed to take into account the effect of a freely dangling towline.

- Currently, there are no real safety factors used for take-off and landing distances; it is advised to use safety factors in the take-off distance calculation. Additionally, future designs iterations should include precise calculations for stall, lift-off, approach and landing velocities, integrate taxi energy calculations to reduce battery mass, and determine take-off power through calculated rather than estimated take-off times.
- Ensuring a more dynamic mission profile will allow for more accurate values with less overdesigning of *MARCUS-T* , for instance by considering different weather conditions. Combined analyses of the flight phases analysed are also relevant, especially when considering the turning, climbing flight phases. More information on novel battery types and the effect of the P-factor will also improve the overdesigning tendencies of the early stages of design. Certification regarding the Lithium polymer batteries should also be looked into, with especially specification DO-311 from the Radio Technical Commission for Aeronautics being relevant. Furthermore, the configuration of the propeller should be investigated further in light of improving recuperation efficacy, even if this means some performance is lost during climb. Additionally, a comparison to fuel-powered tow craft would be in place once the design reaches a more finalised stage of design.
- The validation of the calculations has to be improved on, more validation data has to be used. Furthermore, the requirements which are not validated yet should be validated.
- It is recommended that a detailed analysis on the operational safety objectives is performed to ensure that the required robustness levels are met. Both the FAA and EASA have identified the need for the implementation of Unmanned Traffic Management (UTM) systems. It is recommended that the implementation of regulatory UTM is investigated.
- In the future, it is advised to look into further improvements of battery systems. Cheaper systems can bring down the production cost of the craft. Better energy densities can lead to less battery mass required. Apart from that, it is assumed that electric energy prices drop, while fuel costs for conventional tow craft increase. This can increase interest in *MARCUS-T*. As technology is a rapidly-changing market, this should be closely monitored, such that a higher profit can be achieved, making a break even possible.

Bibliography

[1] D.S. Lee et al. "The contribution of global aviation to anthropogenic climate forcing for 2000 to 2018". In: *Atmospheric Environment* 244 (Jan. 2021), p. 117834. ISSN: 13522310. DOI: 10.1016/j.atmosenv.2020.117834.

[2] Group 08. *Sustainable Glider Tow Craft-Baseline Report*. Tech. rep. Delft: Delft University of Technology, May 2024.

[3] Group 08. *Sustainable Glider Tow Craft Midterm Report*. Tech. rep. 2024.

[4] EASA. *Certification Specifications, Acceptable Means of Compliance and Guidance Material for Sailplanes and Powered Sailplanes (CS-22)*. Tech. rep. 2021.

[5] EASA. "Easy Access Rules for Unmanned Aircraft Systems (Regulations (EU) 2019/947 and 2019/945)". In: (Apr. 2024), pp. 1–463.

[6] EASA. "TYPE-CERTIFICATE DATA SHEET ASW 28-18 E". In: (2022).

[7] Jan Roskam. *Airplane Design Part I: Preliminary Sizing of Airplanes*. 2003.

[8] THG Megson. *Aircraft Structures for engineering students*. Fourth Edition. Elsevier, 2007. ISBN: 978-0-75066-7395.

[9] EASA. "Certification Specifications and Acceptable Means of Compliance for Normal, Utility, Aerobatic, and Commuter Category Aeroplanes CS-23". In: (2015).

[10] Russell C. Hibbeler. *Engineering Mechanics: Statics*. 14th ed. Pearson, July 2020, pp. 1–400.

[11] Francis J Janik Junior. "AFFDL-TR-69-42 Stress Manual". In: (1986).

[12] Daniel P. Raymer. *Aircraft Design: A Conceptual Approach*. 2018.

[13] Wortmann. "Einige Laminarprofile für Segelflugzeuge". In: (1963).

[14] J. H. M. Gooden. "Experimental Low-Speed Aerodynamic Characteristics of the Wortmann FX 66-S-196 V1 Airfoil ". In: 1978.

[15] Snorri Gudmundsson. *General Aviation Aircraft Design: Applied Methods and Procedures*. 1st Edition. 2013.

[16] D. Scholz. "Estimating the Oswald Factor from Basic Aircraft Geometrical Parameters". In: 2012.

[17] B.T.C. Zandbergen R. Vos M.F.M. Hoogreef. *A/C Preliminary Sizing (T/W-W/S diagram)*. 2020.

[18] Sighard F Hoerner and Henry V Borst. *Practical Information on Aerodynamic and Hydrodynamic Lift*. 2nd ed. Mrs. Liselotte A. Hoerner, 1985.

[19] Jan Roskam. *Airplane Design Part VI: Preliminary Calculation of Aerodynamic Thrust and Power Characteristics*. Sixth. 2022.

[20] D. Maughmer. "Design of Winglets for High-Performance Sailplanes". In: *JOURNAL OF AIRCRAFT* (2003).

[21] Egbert Torenbeek. *Synthesis of Subsonic Airplane Design*. Dordrecht: Springer Netherlands, 1982. ISBN: 978-90-481-8273-2. DOI: 10.1007/978-94-017-3202-4.

[22] Fabrizio Oliviero. *AE3211-I - Systems Engineering and Aerospace Design: Requirement Analysis and Design principles for A/C stability & control*. Delft, Apr. 2024.

[23] W B Klemperer and NACA. *MEASUREMENT OF THE FORCES ACTING ON GLIDERS IN TOWED FLIGHT*. Tech. rep. 1940.

[24] Alexander in 't Veld. *AE3202 - Flight Dynamics Lecture Notes*. Delft, Mar. 2013.

[25] Pasquale M. Sforza. "Propellers". In: *Theory of Aerospace Propulsion* (Jan. 2017), pp. 487–524. DOI: 10.1016/B978-0-12-809326-9.00010-5.

[26] David Eržen et al. "D 1.1 Energy Recuperation". In: (2017).

[27] D.G. Simons and M. Snellen. *Aircraft Noise and Emissions (part A)*. Delft, July 2020.

[28] Kazutaka Suzuki et al. "Recycling of 6061 aluminum alloy cutting chips using hot extrusion and hot rolling". In: *Materials science forum* 544 (2007), pp. 443–446.

[29] Diamond Aircraft. *Diamond Dimona HK36 - Flight Manual*. 2002.

[30] Fred Thomas. *Fundamentals of Sailplane Design*. 1999.

[31] Aviat Aircraft. *Aviat Husky - Flight Manual*. 1987.

[32] Gabriela Benveniste et al. "Comparative life cycle assessment of Li-Sulphur and Li-ion batteries for electric vehicles". In: *Resources, Conservation & Recycling Advances* 15 (Nov. 2022), p. 200086. ISSN: 26673789. DOI: 10.1016/j.rcradv.2022.200086.

[33] European Union Aviation Safety Agency. *E-811-Certificate Data Sheet*. Tech. rep. 2020.

[34] Guido H. Tillema et al. "Perceptual Eigenmode Distortion Analysis for Motion Cueing Evaluation in Fixed-Wing Aircraft Simulators". In: *AIAA Scitech 2021 Forum*. Reston, Virginia: American Institute of Aeronautics and Astronautics, Jan. 2021. ISBN: 978-1-62410-609-5. DOI: 10.2514/6.2021-1012.

[35] Charles E. Brown. "Coefficient of Variation". In: *Applied Multivariate Statistics in Geohydrology and Related Sciences*. Berlin, Heidelberg: Springer Berlin Heidelberg, 1998, pp. 155–157. DOI: 10.1007/978-3-642-80328-4{_}13.

[36] Group 08. *Sustainable Glider Tow Craft Project Plan*. Apr. 2024.

[37] EASA. *European Union Aviation Safety Agency User Aircraft maintenance*. Tech. rep. 2022.

[38] Quinten Ooms and Mees Werners. *GoZC Operations Manual Versie: V2.2*. Tech. rep. 2021.

[39] Duane Pettit, Andrew Turnbull, and Henk A. Roelant. *General Aviation Aircraft Reliability Study*. 2001.

[40] L.H. Hogle and P.D. Blythe. *Digital Systems Technical Analysis*. Tech. rep. Atlantic City, N.J.: FAA, Feb. 1983.

[41] David Roberts Roland Stuck. "HOW TO (DE)-REGULATE GLIDING IN EUROPE ?" In: *EGU* (2006).

[42] Carsten Braun et al. *Cost Estimation Methods for Hybrid-Electric General Aviation Aircraft*. Tech. rep. 2019. URL: https://www.researchgate.net/publication/337757069.

[43] Ben Purvis, Yong Mao, and Darren Robinson. "Three pillars of sustainability: in search of conceptual origins". In: *Sustainability Science* 14.3 (Sept. 2018), pp. 681–695. ISSN: 1862-4057. DOI: 10.1007/s11625-018-0627-5. URL: http://dx.doi.org/10.1007/s11625-018-0627-5.

[44] Edward B. Barbier. "The Concept of Sustainable Economic Development". In: *Environmental Conservation* 14.2 (1987), pp. 101–110. ISSN: 14694387. DOI: 10.1017/S0376892900011449.

[45] BRMAERO. *BRISTELL B23 AIRCRAFT FLIGHT MANUAL*. Tech. rep. 2021.

[46] Quanwei Chen et al. "Investigating carbon footprint and carbon reduction potential using a cradle-to-cradle LCA approach on lithium-ion batteries for electric vehicles in China". In: *Journal of Cleaner Production* 369 (Oct. 2022), p. 133342. ISSN: 0959-6526. DOI: 10.1016/J.JCLEPRO.2022.133342.

[47] R. D. Finck. *USAF (United States Air Force) Stability and Control DATCOM (Data Compendium)*. Tech. rep. St. Louis: USAF, 1978, pp. 1–3134.

A

Linearised Non-Dimensional State Space Model

by Gerard, MianTao

The state space model $\dot{\vec{x}} = \mathbb{A} \cdot \vec{x} + \mathbb{B} \cdot \vec{u}$ was assembled from $\mathbb{P} \cdot \dot{\vec{x}} = \mathbb{Q} \cdot \vec{x} + \mathbb{R} \cdot \vec{u}$ using Equation A.1.

$$\mathbb{A} = \mathbb{P}^{-1} \cdot \mathbb{Q} \tag{A.1a}$$

$$\mathbb{B} = \mathbb{P}^{-1} \cdot \mathbb{R} \tag{A.1b}$$

For simplicity, the $\mathbb{P}$, $\mathbb{Q}$, $\mathbb{R}$ matrices are provided, rather than the $\mathbb{A}$ and $\mathbb{B}$ matrices.

A.1. Symmetrical State Space Model

The state vector is given by $\vec{x} = \begin{bmatrix} \hat{u} & \alpha & \theta & \frac{q \cdot \bar{c}}{V} \end{bmatrix}^T$, and the input vector is given by $\vec{u} = [\delta_e \quad \delta_t]^T$.

$$\mathbb{P} = \begin{bmatrix} -2\mu_c \cdot \frac{\bar{c}}{V} & 0 & 0 & 0 \\ 0 & (C_{Z_{\dot{\alpha}}} - 2\mu_c) \cdot \frac{\bar{c}}{V} & 0 & 0 \\ 0 & 0 & -\frac{\bar{c}}{V} & 0 \\ 0 & C_{m_{\dot{\alpha}}} & 0 & -2\mu_c \cdot K_Y^2 \cdot \frac{\bar{c}}{V} \end{bmatrix} \tag{A.2a}$$

$$\mathbb{Q} = \begin{bmatrix} -C_{X_u} & -C_{X_\alpha} & -C_{Z_0} - C_{f_0} \cdot \sin(\theta_0) & 0 \\ -C_{Z_u} & -C_{Z_\alpha} & C_{X_0} + C_{f_0} \cdot \cos(\theta_0) & -2\mu_c - C_{Z_q} \\ 0 & 0 & 0 & -1 \\ -C_{m_u} & -C_{m_\alpha} & C_{f_0} \cdot \cos(\theta_0) \cdot \frac{l_h}{\bar{c}} & -C_{m_q} \end{bmatrix} \tag{A.2b}$$

$$\mathbb{R} = \begin{bmatrix} -C_{X_{\delta_e}} & -C_{X_{\delta_t}} \\ -C_{Z_{\delta_e}} & -C_{Z_{\delta_t}} \\ 0 & 0 \\ -C_{m_{\delta_e}} & -C_{m_{\delta_t}} \end{bmatrix} \tag{A.2c}$$

A.2. Asymmetrical State Space Model

The state vector is given by $\vec{x} = \begin{bmatrix} \beta & \varphi & \frac{p \cdot b}{2V} & \frac{r \cdot b}{2V} & \psi \end{bmatrix}^T$, and the input vector is given by $\vec{u} = [\delta_a \quad \delta_r]^T$.

$$\mathbb{P} = \begin{bmatrix} \left(C_{Y_{\dot{\beta}}} - 2\mu_b\right) \cdot \frac{b}{V} & 0 & 0 & 0 & 0 \\ 0 & -\frac{1}{2} \cdot \frac{b}{V} & 0 & 0 & 0 \\ 0 & 0 & -4\mu_b \cdot K_X^2 \cdot \frac{b}{V} & 4\mu_b \cdot K_{XZ} \cdot \frac{b}{V} & 0 \\ C_{n_{\dot{\beta}}} \cdot \frac{b}{V} & 0 & 4\mu_b \cdot K_{XZ} \cdot \frac{b}{V} & -4\mu_b \cdot K_Z^2 \cdot \frac{b}{V} & 0 \\ 0 & 0 & 0 & 0 & -\frac{1}{2} \cdot \frac{b}{V} \end{bmatrix} \tag{A.3a}$$

$$\mathbb{Q} = \begin{bmatrix} -C_{Y_\beta} & -C_L + C_{f_0} \cdot \sin(\theta_0) & -C_{Y_p} & -C_{Y_r} + 4\mu_b & -C_{f_0} \\ 0 & 0 & -1 & 0 & 0 \\ -C_{l_\beta} & 0 & -C_{l_p} & -C_{l_r} & 0 \\ -C_{n_\beta} & -C_{f_0} \cdot \sin(\theta_0) \cdot \frac{l_h}{b} & -C_{n_p} & -C_{n_r} & C_{f_0} \cdot \frac{l_h}{b} \\ 0 & 0 & 0 & -1 & 0 \end{bmatrix} \tag{A.3b}$$

$$\mathbb{R} = \begin{bmatrix} -C_{Y_{\delta_a}} & -C_{Y_{\delta_r}} \\ 0 & 0 \\ -C_{l_{\delta_a}} & -C_{l_{\delta_r}} \\ -C_{n_{\delta_a}} & -C_{n_{\delta_r}} \\ 0 & 0 \end{bmatrix} \tag{A.3c}$$

B

DATCOM Method

by Gerard

This appendix presents the DATCOM method used to obtain the stability derivatives [47]. The methods have been adapted by Roskam [19]. Some simplifications that have been made by the team are also presented here, as well as any non-DATCOM estimation.

B.1. C_X Derivatives

According to DATCOM, $C_{X_{\dot{\alpha}}}$ and C_{X_q} are usually zero. C_{X_0} was defined as seen in Equation B.1a. C_{X_u} is provided by DATCOM, as seen in Equation B.1b, but was not calculated as it is usually very small. C_{X_α} is computed from the fact that $C_X \approx -C_T = -\left(C_D \cdot \cos(\alpha) - C_L \cdot \sin(\alpha)\right)$. Taking the derivative of C_X with respect to α and simplifying for small angles results in Equation B.1c. This assumption is not always true. However, as the stability derivatives are assumed to be constant and are computed at a very low angle of attack, it is a good first-order estimation.

$$C_{X_0} = \frac{W \cdot \sin(\theta_0)}{0.5\rho \cdot V^2 \cdot S} \tag{B.1a}$$

$$C_{X_u} = C_{D_M} \cdot M \tag{B.1b}$$

$$C_{X_\alpha} = C_L - C_{D_\alpha} \tag{B.1c}$$

B.2. C_Z Derivatives

C_{Z_0} was defined as seen in Equation B.2a. Similarly, it was assumed that $C_Z \approx -C_N = -\left(C_L \cdot \cos(\alpha) + C_D \cdot \sin(\alpha)\right)$. At small angles, it is to be assumed that $C_Z \approx -C_L$. Thus, most of the derivatives provided by DATCOM had to be inverted in sign.

$$C_{Z_0} = \frac{-W \cdot \cos(\theta_0)}{0.5\rho \cdot V^2 \cdot S} \tag{B.2a}$$

$$C_{Z_u} = -C_{L_u} = -\frac{M^2 \cdot C_L \cdot (\cos(\Lambda_{25c}))^2}{1 - M^2 \cdot (\cos(\Lambda_{25c}))^2} \tag{B.2b}$$

$$C_{Z_\alpha} = -C_{L_\alpha} \tag{B.2c}$$

$$C_{Z_{\dot{\alpha}}} = -C_{L_{\dot{\alpha}}} = -2\left(C_{L_h}\right)_\alpha \cdot \left(\frac{V_h}{V}\right)^2 \cdot \bar{V}_h \cdot \frac{\mathrm{d}\varepsilon}{\mathrm{d}\alpha} \tag{B.2d}$$

$$C_{Z_q} = -C_{L_q} = -\left(C_{l_q}\right)_{w,M=0} \cdot \left(\frac{A + 2\cos(\Lambda_{25c})}{A \cdot B + 2\cos(\Lambda_{25c})}\right) - 2 \cdot \left(C_{L_h}\right)_\alpha \cdot \left(\frac{V_h}{V}\right)^2 \cdot \bar{V}_h \tag{B.2e}$$

B.3. C_m Derivatives

C_{m_u} is assumed to be negligible. C_{m_α} was determined by the aerodynamics department. $C_{m_{\dot{\alpha}}}$ and C_{m_q} were given by DATCOM.

$$C_{m_{\dot{\alpha}}} = -2 \cdot \left(C_{L_h}\right)_\alpha \cdot \left(\frac{V_h}{V}\right)^2 \cdot \bar{V}_h \cdot \left(\frac{x_{\mathrm{ac}_h} - x_{\mathrm{ac}}}{\bar{c}}\right) \cdot \frac{\mathrm{d}\varepsilon}{\mathrm{d}\alpha} \tag{B.3a}$$

$$C_{m_q} = \left(C_{m_q}\right)_{w,M=0} \cdot \left(\frac{A^3 \cdot (\tan(\Lambda_{25c}))^2}{A \cdot B + 6 \cdot \cos(\Lambda_{25c})} + \frac{3}{B}\right) \Bigg/ \left(\frac{A^3 \cdot (\tan(\Lambda_{25c}))^2}{A + 6 \cdot \cos(\Lambda_{25c})} + 3\right) \tag{B.3b}$$

$$\left(C_{m_q}\right)_{w,M=0} = -0.9\left(C_{L_w}\right)_\alpha \cdot \cos(\Lambda_{25c}) \cdot \left(\frac{A\left(2\left(\frac{x_w}{c}\right)^2 + 0.5\frac{x_w}{c}\right)}{A + 2\cos(\Lambda_{25c})} + \frac{A^3 \cdot (\tan(\Lambda_{25c})^2)}{24(A + 6\cos(\Lambda_{25c}))} + \frac{1}{8}\right) \tag{B.3c}$$

B.4. C_Y Derivatives

According to DATCOM, C_{Y_β} has contributions from the wing, fuselage, and vertical tail. However, the main contribution to C_{Y_p}, C_{Y_r}, and $C_{Y_{\dot\beta}}$ is from the vertical tail. C_{Y_p} also has a contribution from the wing.

$$C_{Y_\beta} = \left(C_{Y_\beta}\right)_w + \left(C_{Y_\beta}\right)_f + \left(C_{Y_\beta}\right)_v \tag{B.4a}$$

$$C_{Y_p} = 2\left(C_{Y_\beta}\right)_v \cdot \left(\frac{z_v \cdot \cos(\alpha_0) - l_v \cdot \sin(\alpha_0) - z_v}{b}\right) + 3\sin(\Gamma) \cdot \left(1 - \sin(\Gamma) \cdot \frac{4z_v}{b}\right) \cdot \left(C_{l_p}\right)_{\Gamma=0, C_L=0} \tag{B.4b}$$

$$C_{Y_r} = -2\left(C_{Y_\beta}\right)_v \cdot \left(\frac{l_v \cdot \cos(\alpha_0) + z_v \cdot \sin(\alpha_0)}{b}\right) \tag{B.4c}$$

$$C_{Y_{\dot\beta}} = 2\left(C_{L_v}\right)_\alpha \cdot \frac{\mathrm{d}\sigma}{\mathrm{d}\beta} \cdot \frac{Sv}{S} \cdot \left(\frac{lp \cdot \cos(\alpha_0) + z_p \cdot \sin(\alpha_0)}{b}\right) \tag{B.4d}$$

Terms that need further explanation are expressed as a function of the variables they depend on. For the full equations, as well as the meaning of the symbols, please refer to Roskam Part VI [19].

$$\left(C_{Y_\beta}\right)_w = f\left(S_0, S, z_w, d_f\right) \tag{B.5a}$$

$$\left(C_{Y_\beta}\right)_f = f\left(\Gamma\right) \tag{B.5b}$$

$$\left(C_{Y_\beta}\right)_v = f\left(S_v, b_v, z_{w_v}, \mathrm{AR}_v, z_f, d_f, S, \Lambda_{25c}, \left(C_{L_v}\right)_\alpha\right) \tag{B.5c}$$

$$\left(C_{l_p}\right)_{\Gamma=0, C_L=0} = f\left(M, \left(C_{l_\alpha}\right)_{\text{airfoil}}, \mathrm{AR}_v, \Lambda_{25c}, \lambda\right) \tag{B.5d}$$

$$\frac{\mathrm{d}\sigma}{\mathrm{d}\beta} = f\left(M, \lambda, \Lambda_{\mathrm{LE}}, \mathrm{AR}_w, d_f, b\right) \tag{B.5e}$$

B.5. C_l Derivatives

According to DATCOM, both C_{l_β} and C_{l_p} have contributions from the tailless aircraft and the empennage. However, C_{l_r} does not have a contribution by the horizontal stabiliser.

$$C_{l_\beta} = \left(C_{l_\beta}\right)_{wf} + \left(C_{l_\beta}\right)_h + \left(C_{l_\beta}\right)_v \tag{B.6a}$$

$$C_{l_p} = \left(C_{l_p}\right)_w + \left(C_{l_p}\right)_h + \left(C_{l_p}\right)_v \tag{B.6b}$$

$$C_{l_r} = \left(C_{l_r}\right)_w + \left(C_{l_r}\right)_v \tag{B.6c}$$

Terms that need further explanation are expressed as a function of the variables they depend on. Simplified relations are expressed with an approximation sign ($\approx$). For the full equations, as well as the meaning of the symbols, please refer to Roskam Part VI [19].

$$\left(C_{l_\beta}\right)_{wf} \approx f\left(C_{L_{wf}}\right) \tag{B.7a}$$

$$\left(C_{l_\beta}\right)_h = f\left(\left(C_{l_\beta}\right)_{wf}, \bar{V}_h\right) \tag{B.7b}$$

$$\left(C_{l_\beta}\right)_v = f\left(\left(C_{Y_\beta}\right)_v, z_v, l_v, b, \alpha_0\right) \tag{B.7c}$$

$$\left(C_{l_p}\right)_w \approx f\left(M, \left(C_{l_\alpha}\right)_{\text{airfoil}}, \Lambda_{25c}, \lambda, \mathrm{AR}_v\right) \tag{B.7d}$$

$$\left(C_{l_p}\right)_h = f\left(\left(C_{l_p}\right)_w, S_h, S, b_h, b\right) \tag{B.7e}$$

$$\left(C_{l_p}\right)_v = f\left(\left(C_{Y_\beta}\right)_v, b, z_v, l_v, \alpha_0\right) \tag{B.7f}$$

$$\left(C_{l_r}\right)_w \approx f\left(C_L, \mathrm{AR}, \lambda, \Lambda_{25c}, M\right) \tag{B.7g}$$

$$\left(C_{l_r}\right)_v = f\left(\left(C_{Y_\beta}\right)_v, b, l_v, z_v, \alpha_0\right) \tag{B.7h}$$

B.6. C_n Derivatives

According to DATCOM, all yawing stabilities have the contribution of the vertical stabiliser. Additionally, C_{n_β} also has a big contribution by the fuselage, and C_{n_p} and C_{n_r} have a big contribution by the wing. $C_{n_{\dot\beta}}$ is proportional to $C_{Y_{\dot\beta}}$.

$$C_{n_\beta} = \left(C_{n_\beta}\right)_f + \left(C_{n_\beta}\right)_v \tag{B.8a}$$

$$C_{n_p} = \left(C_{n_p}\right)_w + \left(C_{n_p}\right)_v \tag{B.8b}$$

$$C_{n_r} = \left(C_{n_r}\right)_w + \left(C_{n_r}\right)_v \tag{B.8c}$$

$$C_{n_{\dot\beta}} = C_{Y_{\dot\beta}} \cdot \left(\frac{l_p \cdot \cos(\alpha_0) + z_p \cdot \sin(\alpha_0)}{b}\right) \tag{B.8d}$$

Terms that need further explanation are expressed as a function of the variables they depend on. For the full equations, as well as the meaning of the symbols, please refer to Roskam Part VI [19].

$$\left(C_{n_\beta}\right)_f = f\left(S_{f,\text{side}}, l_f, d_f, x_{\text{cg}}, S, b, \text{Re}\right) \tag{B.9a}$$

$$\left(C_{n_\beta}\right)_v = f\left(\left(C_{Y_\beta}\right)_v, l_v, z_v, b, \alpha_0\right) \tag{B.9b}$$

$$\left(C_{n_p}\right)_w = f\left(C_L, \text{AR}, \Lambda_{25c}, M\right) \tag{B.9c}$$

$$\left(C_{n_p}\right)_v = f\left(\left(C_{Y_\beta}\right)_v, l_v, z_v, b, \alpha_0\right) \tag{B.9d}$$

$$\left(C_{n_r}\right)_w = f\left(C_L, C_{D_0}, \text{AR}, \frac{\bar{x}}{c}, \Lambda_{25c}, \lambda\right) \tag{B.9e}$$

$$\left(C_{n_r}\right)_v = f\left(\left(C_{Y_\beta}\right)_v, l_v, z_v, b, \alpha_0\right) \tag{B.9f}$$

C

Selected Components

For this report, commercially available avionics have been selected in order to comply with CS22, CS-UAS, SORA and risk requirements. These avionics have been selected as an indicator for potential cost, mass, and power consumption. There has been no analysis to verify that these avionics are compatible, only that they cover the requirements.

Table C.1: Avionics datasheet.

System	Component	MASS [kg]	COST [EUR]	REQUIRED POWER [W]	REQUIRED VOLTAGE [V]	Manufacturer
FDAU	Air data computer	0.5	3000	10	10	[1]
FMC	High performance rugged computer	8.2	4500	70	No Data	[2]
RTS	VHF Antenna	0.22	180	30	No Data	[3]
RTS	GPS antenna	0.1	80	No Data	5	[4]
ATSAW	ADS-B	0.1	450	1.4	14	[5]
RTS	Transponder	3.6	2000	250	No Data	[6]
ATSAW	FLARM	0.25	2200	1.5	20	[7]
RTS	FLARM ANTENNA	0.05	40	No Data	No Data	[8]
FDRBNU	backup gps adsb, dr	0.28	1200	No Data	No Data	[9]
3D Camera	3D camera	0.9	12000	28	No Data	[10]
IMU	UAV IMU	0.003	40	No Data	3	[11]

Table C.2: EDS component selection.

System	Component	
EDS	Ballistic Parachute	[12]
EDS	Siren	[13]

[1] allavionics.com/product/sandia-sac-7-35-air-data-computer/
[2] www.onlogic.com/store/k804/
[3] allavionics.com/product/rami-av-10-vhf-antenna/
[4] allavionics.com/product/trig-ta50-compact-gps-antenna-39/
[5] allavionics.com/product/trig-tn72-ads-b-gps-position-source/
[6] allavionics.comproduct/trig-tt22-mode-s-class-1-transponder-remote-unit-certified-copy/
[7] millenair.eu/product/powerflarm-fusion/
[8] millenair.eu/product/flarm-dipole-antenna-flarm-sma-connector/
[9] allavionics.com/product/ilevil-3-sw-wireless-module/
[10] www.dslrpros.com/dji-zenmuse-l2-with-care-enterprise-basic-2-year.html
[11] eu.robotshop.com/products/bno055-9-dof-absolute-orientation-imu-fusion-breakout-board
[12] www.brs-vertrieb.de/wp-content/owners-manual.pdf
[13] www.e2s.com/product/13459-a121-alarm-horn-sounder

D

Unit Tests

by MianTao, Everyone

All performed unit tests are presented in Table D.1, in which they are sorted by department. These tests are intended to verify individual functions of the design method code. Tests can be performed either by hand calculations (HC), comparison and cross checking with alternative methods (CC), or visual inspection (VI).

Table D.1: Unit tests performed on design method code.

Tested File	Test ID	Function Name	Test Type	Test Description	Ex. Err.	Pass /Fail
classII.py	U-SMM-01	wing_weight	HC	Rewrote eq. in Excel. Based on Roskam GA aircraft Cessna 210J	Low	Pass
classII.py	U-SMM-02	empennage_weight	HC	Rewrote in Excel tested with 210J	Low	Pass
classII.py	U-SMM-03	instrumentation_ avionics_electronics_ weigth_estimate	HC	Value from off-the-shelf component	Low	Pass
classII.py	U-SMM-04	electrical_weight_ estimate	HC	Hand calculated with the maximum take-off weight of 1500 pounds	Low	Pass
classII.py	U-SMM-05	fixed_empty_weight	HC	Hand calculated with fixed flight control and electronics weight	Low	Pass
classII.py	U-SMM-06	main_landing_gear_ weight_estimate	HC	Hand calculated with 210J data in Excel	Low	Pass
classII.py	U-SMM-07	nose_landing_gear_ weight_estimate	HC	Hand calculated with 210J data in Excel	Low	Pass
classII.py	U-SMM-08	battery_weight_ estimate	HC	Hand calculated with arbitrary values	Low	Pass
classII.py	U-SMM-09	flight_control_ weight_estimate	HC	Hand calculated with maximum take-off weight of 1500 pounds	Low	Pass
classII.py	U-SMM-10	fuselage_weight_ estimate	HC	Hand calculated estimate of the craft	Low	Pass
wingbox_ geometry.py	U-SMM-11	centroid	HC	Hand calculated two different rectangles with different areas	Low	Pass
wingbox_ geometry.py	U-SMM-12	local_moments_of_ inertia	HC	Hand calculated on rectangle of 20 by 100 meters	Low	Pass
wingbox_ geometry.py	U-SMM-13	global_moments_of_ inertia	HC	Hand calculated for two different rectangles with different areas	Low	Pass
shear_ bending.py	U-SMM-14	required_moment_ of_inertia_bending	HC	Hand calculated with arbitrary rectangles	Low	Pass
shear_ bending.py	U-SMM-15	shear_flow	HC	Hand calculated using simplified version of example 21.2 in Aircraft structures for engineering students [8]	Low	Pass
shear_ bending.py	U-SMM-16	wing_box_thickness_ sizing_for_bending	HC	Hand calculated stress for a wing box with certain dimensions. Putting this stress with these dimensions into the function will result in the correct thickness	Med.	Pass

Continued on next page

Tested File	Test ID	Function Name	Test Type	Test Description	Ex. Err.	Pass /Fail
shear_ bending.py	U-SMM-17	wing_box_moment_ of_inertia_xx	HC	Hand calculated moment of inertia for a certain size of the wing box	Low	Pass
loads.py	U-SMM-18	calculate_gust_ loading_factor	HC	Hand calculated moment of inertia for a certain size of the wing box	Low	Pass
wingbox_ geometry.py	U-SMM-19	wing_structure_mass	HC	Hand calculated total craft mass for arbitrary values	Low	Pass
shear_ bending.py	U-SMM-20	buckling_force	HC	Hand calculated for arbitrary values	Low	Pass
landing_ gear.py	U-SMM-21	buckling_force_ cylinder	HC	Hand calculated for arbitrary values	Low	Pass
landing_ gear.py	U-SMM-22	force_on_landing_ gear	HC	Hand calculated for arbitrary values	Low	Pass
landing_ gear.py	U-SMM-23	thickness_required_ buckling	HC	Hand calculated for arbitrary values	Med.	Pass
landing_ gear.py	U-SMM-24	thickness_required_ bending	HC	Hand calculated for arbitrary values	Med.	Pass
fuselage.py	U-SMM-25	moment_of_inertia_ main_fuselage	HC	Hand calculated for arbitrary values	Low	Pass
fuselage.py	U-SMM-26	moment_of_inertia_ tail_fuselage	HC	Hand calculated for arbitrary values	Low	Pass
fuselage.py	U-SMM-27	cylinder_distances_ to_central_line	HC	Hand calculated for arbitrary values	Med.	Pass
fuselage.py	U-SMM-28	plot_fuselage	VI	Visual check for the plots created	Low	Pass
fuselage.py	U-SMM-29	experienced_moment	HC	Hand calculated for arbitrary values	Med.	Pass
fuselage.py	U-SMM-30	plot_moment_ diagram	VI	Visual check for the plots created	Low	Pass
fuselage.py	U-SMM-31	thickness_needed_ for_cylinders	HC	Hand calculated for arbitrary values	High	Pass
fuselage.py	U-SMM-32	plot_required_ thickness_needed	VI	Visual check for the plots created	Low	Pass
lift.py	U-AERO-01	calculate_wing_ zero_lift_AoA	HC	Hand calculation with arbitrary values	Low	Pass
lift.py	U-AERO-02	calculate_wing_lift_ curve_slope	HC	Hand calculation using theoritical lift slope of 2π and arbitrary wing parameters	Low	Pass
lift.py	U-AERO-03	calculate_wing_ linear_range	HC	Hand calculation using arbitrary value	None	Pass
lift.py	U-AERO-04	calculate_wing_ maximum_lift_coeff	HC	Hand calculation using arbitrary values	None	Pass
lift.py	U-AERO-05	calculate_airplane_ lift_curve_slope	HC	Hand calculation using arbitrary values	Low	Pass

Continued on next page

Tested File	Test ID	Function Name	Test Type	Test Description	Ex. Err.	Pass /Fail
lift.py	U-AERO-06	calculate_airplane_linear_range_AoA	HC	Hand calculation using arbitrary values	None	Pass
lift.py	U-AERO-07	calculate_airplane_zero_AoA_lift_coefficient	HC	Hand calculation using arbitrary values	Low	Pass
lift.py	U-AERO-08	calculate_airplane_zero_lift_AoA	HC	Hand calculation using arbitrary values	Low	Pass
lift.py	U-AERO-09	calculate_airplane_maximum_lift_coefficient	HC	Hand calculation using arbitrary values	Low	Pass
lift.py	U-AERO-10	make_lift_curve	VI	Check if the resulting plot matches the shape expectation and if all important points are present	Med.	Pass
horizontal.py	U-SSC-01	horizontal_downwash_gradient_SSC	HC	Calculated in Excel using simplified values	Low	Pass
horizontal.py	U-SSC-02	x_cg_mid_normal_SSC	CC	Cross checking with alternative method	Low	Pass
horizontal.py	U-SSC-03	tail_volume_ratio_controllability	CC	Cross checking with alternative method	Low	Pass
horizontal.py	U-SSC-04	tail_volume_ratio_stability	CC	Cross checking with alternative method	Low	Pass
horizontal.py	U-SSC-05	x_cg_fwd_normal_controllability	CC	Cross checking with alternative method	Low	Pass
horizontal.py	U-SSC-06	x_cg_aft_normal_stability	CC	Cross checking with alternative method	Low	Pass
horizontal.py	U-SSC-07	calc_xcg_normal_mass_fwd_aft	CC	Cross checking with alternative method	Low	Pass
vertical.py	U-SSC-08	vertical_tail_volume_ratio	HC	Calculated in Excel using simplified values	Low	Pass
vertical.py	U-SSC-09	calc_K_beta	HC	Calculated in Excel using simplified values	Low	Pass
vertical.py	U-SSC-10	calc_Cnb_f	HC	Calculated in Excel using simplified values	Low	Pass
vertical.py	U-SSC-11	calc_Cnb_p	HC	Calculated in Excel using simplified values	Low	Pass
vertical.py	U-SSC-12	calc_tail_volume_engine_failure	HC	Calculated in Excel using simplified values	Low	Pass
asymmetrical_ss.py	U-SSC-13	calc_asym_ss_mod	CC	Compare the state space system obtained for zero tow force with a state space model that does not account for tow force	None	Pass
asymmetrical_ss.py	U-SSC-14	calc_asym_ss_mod	CC	Verify a single entry of the A-matrix of the state space model	None	Pass
performance.py	U-PPP-01	propellor_sizing	HC	Hand calculation using arbitrary values	Low	Pass

Continued on next page

Tested File	Test ID	Function Name	Test Type	Test Description	Ex. Err.	Pass /Fail
performance.py	U-PPP-02	calculate_battery_mass_fraction_climb	HC	Hand calculation using arbitrary values in both Python and Excel	Low	Pass
performance.py	U-PPP-03	calculate_battery_mass_fraction_steady_flight	HC	Hand calculation using arbitrary values in both Python and Excel	Low	Pass
performance.py	U-PPP-04	turn_time	HC	Hand calculation using arbitrary values	Low	Pass
performance.py	U-PPP-05	v_tas_alt	HC	Hand calculation using arbitrary values	Low	Pass
performance.py	U-PPP-06	power_static	HC	Hand calculation using arbitrary values	Low	Pass
performance.py	U-PPP-07	calc_power	HC	Hand calculation using arbitrary values	Low	Pass
performance.py	U-PPP-07	propulsion_2	CC	Compare results of the function to each other and look if values are in a certain range	Med.	Pass
take_off_landing_functions.py	U-APOL_01	calculate_total_weigt	HC	Hand calculation using arbitrary values	Low	Pass
take_off_landing_functions.py	U-APOL_02	calculate_thrust	HC	Hand calculation using arbitrary values	Low	Pass
take_off_landing_functions.py	U-APOL_03	calculate_k_1	HC	Hand calculation using arbitrary values	Low	Pass
take_off_landing_functions.py	U-APOL_04	calculate_drag_coeficent	HC	Hand calculation using arbitrary values	Low	Pass
take_off_landing_functions.py	U-APOL_05	calculate_aero_forces	HC	Hand calculation using arbitrary values	Low	Pass
take_off_landing_functions.py	U-APOL_06	calculate_ground_friction	HC	Hand calculation using arbitrary values	Low	Pass
take_off_landing_functions.py	U-APOL_07	calculate_velocity_from_lift	HC	Hand calculation using arbitrary values	Low	Pass
take_off_landing_functions.py	U-APOL_08	calculate_thrust_climb	HC	Hand calculation using arbitrary values	Low	Pass
take_off_landing_functions.py	U-APOL_09	calculate_transition_radius	HC	Hand calculation using arbitrary values	Low	Pass
take_off_landing_functions.py	U-APOL_10	calculate_transition_height	HC	Hand calculation using arbitrary values	Low	Pass

Continued on next page

Tested File	Test ID	Function Name	Test Type	Test Description	Ex. Err.	Pass /Fail
take_off_ landing_ functions.py	U-APOL_ 11	calculate_transition_ distance_limit	HC	Hand calculation using arbitrary values	Low	Pass
take_off_ landing_ functions.py	U-APOL_ 12	calculate_transition_ distance	HC	Hand calculation using arbitrary values	Low	Pass
take_off_ landing_ functions.py	U-APOL_ 13	calculate_climb_ distance	HC	Hand calculation using arbitrary values	Low	Pass
take_off_ landing_ functions.py	U-APOL_ 14	calculate_transition_ climb_distance	HC	Hand calculation using arbitrary values	Low	Pass
landing.py	U-APOL_ 15	calculate_velocity_ over_acceleration_ landing	HC	Hand calculation using arbitrary values	Med.	Pass
landing.py	U-APOL_ 16	calculate_ground_ roll_distance_landing	HC	Hand calculation using arbitrary values	Med.	Pass
take_off.py	U-APOL_ 17	calculate_velocity_ over_acceleration_ take_off	HC	Hand calculation using arbitrary values	Med.	Pass
ops.py	U-APOL_ 18	ground_operations	CC	Testing if the return values are correct, by combaring them to the results of other functions	Low	Pass